Novel Adaptive Array Algorithms and Their Impact on Cellular System Capacity

by

Paul Petrus

Dissertation submitted to the Faculty
of the Virginia Polytechnic Institute and State
University in partial fulfillment of the requirements for the degree of

Doctor of Philosophy
in
Electrical Engineering

Approved:

Dr. Jeffrey H. Reed (Chairman)
Dr. Brian D. Woerner
Dr. Theodore S. Rappaport
Dr. Louis A. Beex
Dr. Christopher Beattie

18, March 1997
Blacksburg, Virginia

Keywords: Adaptive arrays, Smart Antennas, AMPS, CDMA, GBSBM, Cellular Overlay, Cellular Capacity

Novel Adaptive Array Algorithms and Their Impact on Cellular System Capacity

by

Paul Petrus

Committee Chairman: Dr. Jeffrey H. Reed

Electrical Engineering

Abstract

This report focuses on the application of adaptive arrays to the Advanced Mobile Phone Service (AMPS) and Code Division Multiple Access (CDMA) cellular systems. Adaptive arrays have been proposed as early as in the 1960s to improve the signal quality, but most of its applications were restricted to defense purposes. Recently, there has been a surge in interest of applying adaptive arrays for cellular systems. This work introduces new blind adaptive array algorithms for AMPS and CDMA signals. The theoretical capacity limit using an adaptive array at the base station for an AMPS cellular system is derived in this work. One of the significant contributions in this research is a macrocell channel model which provides angle-of-arrival (AOA) statistics of the multipath components. Practical issues involved in the implementation of an adaptive array are addressed and the author's implementation of an 8-element adaptive array operating at 2.05 GHz is explained. This research also analyzes the capacity that can be offered by an adaptive array in a system where CDMA users co-exist with existing AMPS users. A novel cellular CDMA system which exploits adaptive arrays is introduced and the capacity offered by this system is compared with existing and other systems exploiting spatial dimension.

Dedicated to Devadasse and Xaverine Petrus

Acknowledgments

A long journey has come to an end and I wish to thank all the people who crossed my path of life, who influenced me in ways I realized and in ways I did not. My stay at MPRG has been technically very satisfying and I have the pleasure of working with some of the best brains in the business.

In my thank-list, Dr. Jeffrey H. Reed, my advisor, comes first. I wish to thank Dr. Reed for all his technical and financial support during the course of my stay at Virginia Tech. I sincerely feel that I have not seen anyone as accommodative as Dr. Reed. Thank you Dr. Reed for giving me the wonderful opportunity to work in MPRG! Dr. Reed gave me a free hand in my research and encouraged me to be innovative.

My sincere thanks to Dr. Ted Rappaport for not only serving in my committee but also for the keen interest he showed in the development of the GBSBM channel model. Thank you Dr. Rappaport for doing an excellent job presenting the GBSBM model at Globecom '96! My thanks to Drs. Brian Woerner, Christopher Beattie, and Louis Beex for serving in my committee and for all their useful comments.

My gratitude goes to my roomies Rias Muhamed and Francis Dominique. You guys have been great and thank you both for all the wonderful technical and philosophical discussions we had. I thank Nitin Mangalvedhe for being a great friend throughout my stay at Tech. I also thank Joe Liberti for helping me in the channel model development and Rich Ertel in the capacity calculations. My sincere thanks to Steve Nicholoso for helping me develop assembly codes for the Analog Devices DSP. Thank you very much Steve!

My sincere thanks to Tom Biedka for all discussions we had on adaptive arrays. It was truly a great experience working with Zhigang Rong in the development of the array algorithms for CDMA. Special thanks to Annie Wade for her love and for all the administrative help.

I thank the following people (in no particular order) who have directly or indirectly contributed to this dissertation:

Rong He	Volker Aue
Don Breslin	Mike Buehrer
Carl Dietrich	Rick Cameron
T. P. Subramanian	Nishith Tripathi
Kevin Saldanha	Neiyer Correal
Ashish Kaul	Anil Doradla

I will be failing if I don't thank my Parents, Devadasse and Xaverine Petrus. Thank you Mom and Dad for all your support and love. My dreams would have never become a reality without you folks. I also thank my brothers (Joseph, Gerard, and Christian) for all the great times we had growing up together.

Above all I thank my creator for the abilities he has entrusted me with.

Contents

List of Figures

List of Tables

Chapter 1

Introduction

"By the year 2050, wired links will be obsolete, while spatial filters will be ubiquitous"

Current cellular technology is driven by the need for better grade of service and the need for serving increased number of subscribers. Service providers keep in mind both these factors when they design a cellular system. In the current billion dollar cellular market, better grade of service is a key factor to keep the customers happy. To get increased revenue, the service provider would like to serve more people in their service area. Multiple access techniques are effectively used to accommodate parallel transmissions by subscribers and these techniques are key in designing a high capacity and high quality cellular system. Unfortunately, there is a limit to the maximum number of users a system can accommodate. The limitation may be *bandwidth* as in a Frequency Division Multiple Access (FDMA) (e.g., AMPS)[1] system or *time* as in a Time Division Multiple Access (TDMA) (e.g., IS-136)[2] system or the *number of good codes* as in a Code Division Multiple Access (CDMA) (e.g., IS-95)[3] system.

Frequency reuse is a technique to increase the capacity of a cellular system and is also the key in designing a high capacity and high quality cellular system. Frequency reuse involves reusing the same frequency in two different cells which are spaced far enough apart so that users in one cell do not significantly interfere with the users in the other cell (cochannel users).

[1] AMPS - Advanced Mobile Phone Service is the analog standard for FDMA in the U.S. and many regions of the world.

[2] IS-136 is the latest interim standard for TDMA in the U.S.

[3] IS-95 is the interim standard for CDMA in the U.S. and was proposed by Qualcomm Inc.

Grade of service is not only determined by the interference from the cochannel users but also by natural impairment such as additive white Gaussian Noise (AWGN) and fading. Any researcher who dreams about increasing the cell capacity is faced with two major problems:

- cochannel or multiple access interference
- multipath fading.

Noise is not a significant factor in determining the capacity, but limits the range of cellular systems.

FDMA and TDMA systems have no inherent resistance to fading, while CDMA systems can mitigate multipath fading because of its processing gain property. To increase the capacity there is need to implement techniques that can combat both fading and interference. Multiple Access Interference and MUltipath Rejection (MAIMUR) techniques vary from one multiple access technique to the other. MAIMUR techniques can be classified as *single* and *multi-channel* techniques. Single channel techniques do not use multiple antennas, as opposed to multiple channel techniques. Adaptive antenna array is a Multi-channel MAIMUR technique that promises to enhance the capacity of a cell significantly. The focus of this research is to investigate capacity enhancement provided by adaptive arrays for FDMA and CDMA systems. The research presented in this report is segmented into four phases as explained below.

The first phase of the research focuses on the investigation of adaptive arrays for the AMPS system. Here we develop a blind[4] adaptive array algorithm which exploits the cyclostationary property exhibited by the AMPS signal. This phase also involves the development of a theoretical framework to calculate the capacity of a cell when using a beamformer at the base station for an AMPS system. This blind algorithm possesses the ability to distinguish the desired user from the interference even when the power of the interference is higher than the desired user.

The second phase of the research involves the development of a statistical channel model that provides all the parameters that characterize a channel. This new statistically based channel model, called the Geometrically Based statistical Single Bounce Macrocell (GBSBM) channel model, provides angle-of arrival (AOA), time-of-arrival (TOA), and the power of the multipath components. This channel model

[4]Blind adaptation is an adaptation method that does not require a training signal.

is one of the first channel models that provides AOA statistics which is an important factor to be taken into account when spatial filtering is applied. The channel model can be used to predict the reduction in Doppler spread when directional antennas are used at the base station.

The third phase of the research focuses on investigation of adaptive arrays for CDMA systems. The CDMA system under investigation here differs significantly from IS-95 CDMA system. The CDMA parameters used in this dissertation are the GloMo parameters, GloMo[5] is a DARPA[6] sponsored project whose parameters are explained in Chapter 6. This phase includes development of new blind adaptive array algorithms for CDMA signals and building an 8-element adaptive array for the GloMo specifications. This work presents the design and implementation of an adaptive array.

The next phase of the research involves forward and reverse link analysis of a CDMA over AMPS overlay system when the base station employs a beamformer. The presence of CDMA users degrade the performance of the AMPS system depending on the number and the power of the users. But when a beamformer is employed at the base station, the interference power is reduced and hence more number of CDMA users can be accommodated in the system.

In the final phase, a new cellular system called the Spatial Code Division Multiple Access (SCDMA) is introduced. SCDMA is a hybrid cellular system which exploits Spatial Division Multiple Access (SDMA) and CDMA. Capacity offered by this new system is compared to the existing and other proposed systems.

Figure 1.1 illustrates the overview of the research presented in this report. The research report is organized as follows: Chapter 2 provides the motivation for this research and also includes fundamental principles of adaptive arrays. A new blind adaptive array algorithm for AMPS signals called the Spectral Correlation Discriminator Array (SCDA) is introduced and its performance is analyzed in Chapter 3. In Chapter 4, a general framework to evaluate the outage probability for an AMPS system which uses a beamformer at the base station is presented. Chapter 5 presents the true capacity improvements that can be achieved using physically realizable antenna arrays. The GBSBM model is introduced in Chapter 6, followed by Chapter 7, which

[5]GloMo - Global Mobile Information Systems
[6]DARPA - Defense Advanced Research Project Agency

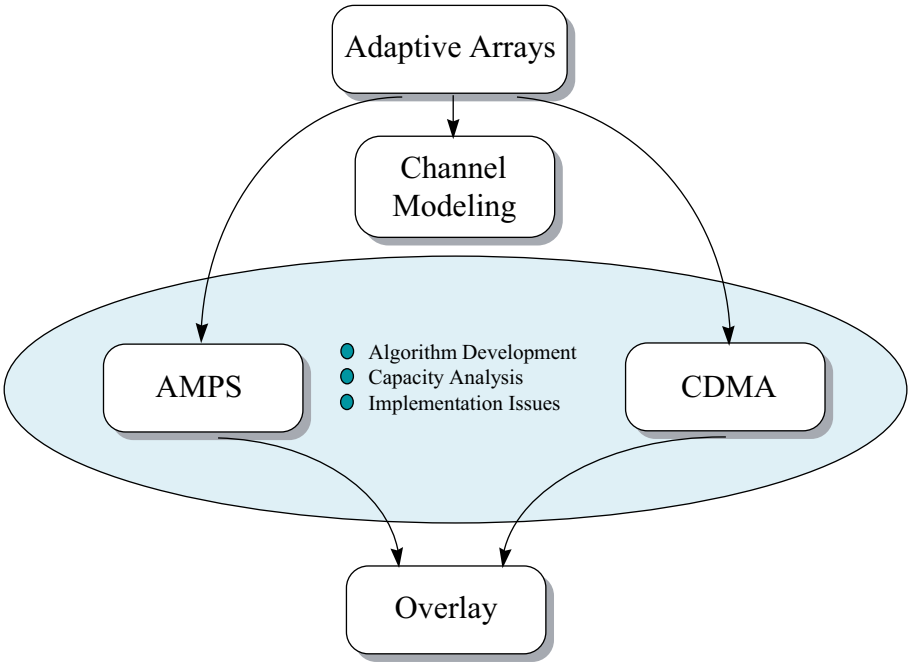

Figure 1.1: Overview of the research presented in this report.

discusses the adaptive array algorithms for CDMA. Chapter 8 examines the issues involved in the implementation of an adaptive array for CDMA systems. Forward and reverse link analysis for a CDMA over AMPS overlay system employing a beamformer is presented in Chapter 9. Chapter 10 introduces the SCDMA system. The conclusions of the research and suggestions for future work are presented in Chapter 11.

Chapter 2

Adaptive Arrays: Fundamental Concepts

2.1 Fundamentals of antenna arrays

An antenna array has spatially separated sensors whose output are fed into a weighting network or a beamforming network as shown in Figure 2.1. The antenna array can be implemented as a transmitting or a receiving array. Our application is focussed on applying the antenna array for the reverse link of a cellular systems and hence the antenna array is a passive receiving device. There are many assumptions made in analyzing an antenna array, they are as follows:

- All signals incident on the receiving antenna array are composed of finite number of plane waves. These plane waves result from the direct as well as the multipath components.
- The transmitter and the objects that cause multipaths are in the far-field of the antenna array.
- The sensors are placed closely so that the amplitudes of the signals received at any two elements of the antenna array do not differ significantly. Also the angle-of-arrival of the signals at two elements do not differ significantly.
- Each sensor is assumed to have the same radiation pattern and the same orientation.

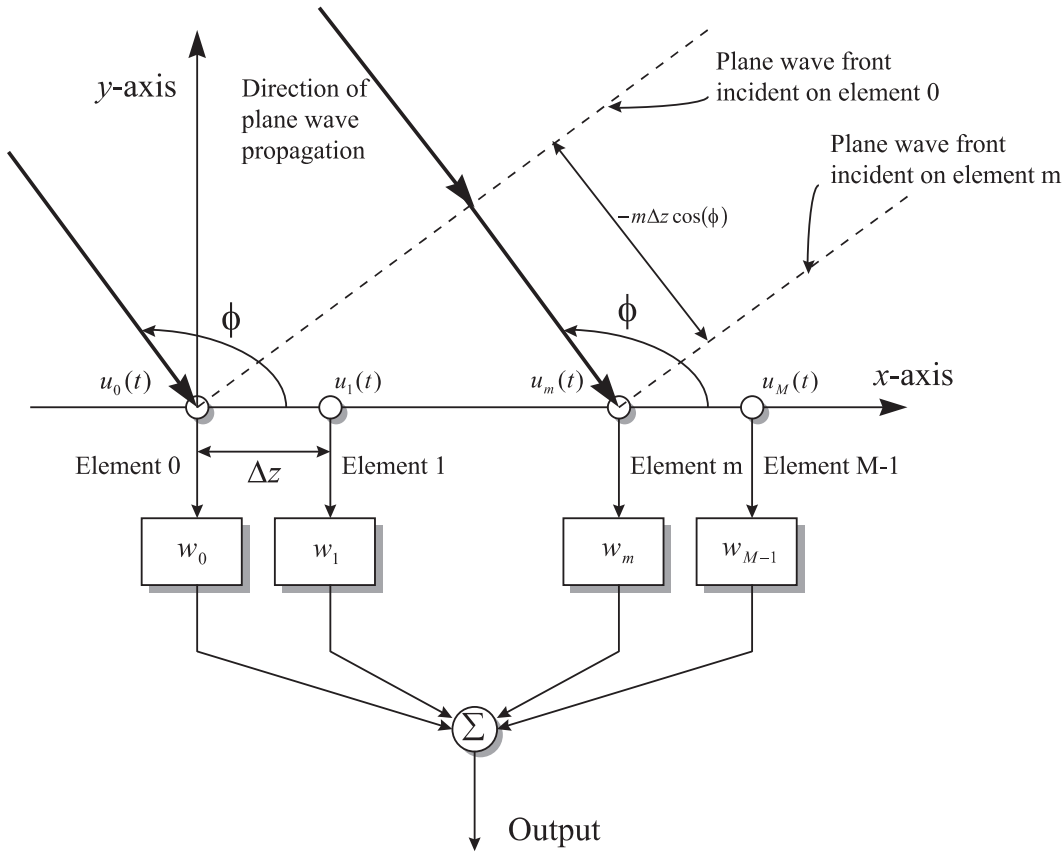

Figure 2.1: Illustration of plane wave incident from an angle of ϕ on an uniform linear array (ULA) with inter-element spacing of Δz.

- The mutual coupling between the antenna elements is assumed to be negligible.

An antenna array with its coordinates are illustrated in Figure 2.2.

2.1.1 Theoretical model for an antenna array

An antenna array can be arranged in any arbitrary fashion, but the most preferred geometries are linear and circular geometries. Linear geometry is simpler to implement than the circular geometry, but the disadvantage is the symmetry (ambiguity) of the radiation pattern about the axis along the endfire[1], which is not the case in a circular array. Linear array with uniformly spaced sensors is the most commonly used structure.

[1]Endfire is the direction that is parallel to the line joining the antenna elements in a linear array.

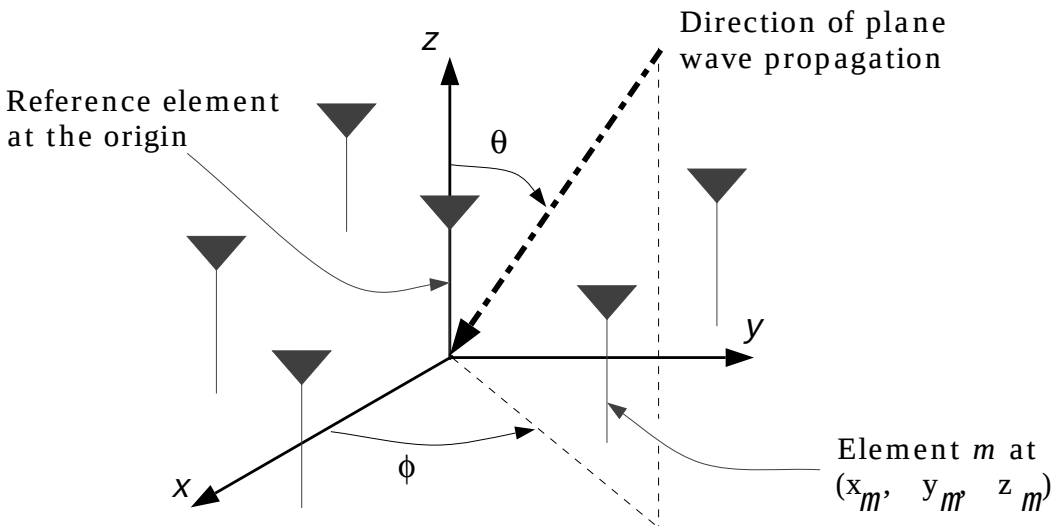

Figure 2.2: Illustration of the coordinates of an antenna array.

The array as shown in Figure 2.2 has a reference element at the origin and the coordinates of the mth antenna element is marked as (x_m, y_m, z_m). The signal as it travels across the array undergoes a phase shift, the phase shift between the signal received at the reference element and the signal received at the element m is given by

$$\Delta\gamma_m = \gamma_m(t) - \gamma_0(t) = -\beta x_m cos\phi sin\theta - \beta y_m sin\phi sin\theta - \beta z_m cos\theta, \tag{2.1}$$

where $\beta = 2\pi/\lambda$. The ground plane is assumed to lie on the $x - y$ plane. Since the distance between the transmitter-receiver is larger than the difference in the distance between the heights of the receiver and the transmitter antenna, a wave reaching the antenna array can be assumed to come along the horizon or $\theta = 90^o$. Therefore,we will describe the direction-of-arrival (DOA) of each plane wave using only azimuthal coordinate, ϕ. From Eqn. 2.1, it can be seen that any variation in the array element height z_m does not affect the phase difference between the reference element and element m. Therefore, we may consider only x and y offsets from the reference element.

It is convenient to represent the signal at each antenna element as a complex envelope representation and is given by

$$u_m(t) = A_m(t)e^{j\gamma_m(t)}, \tag{2.2}$$

where $A_m(t)$ is the magnitude and $\gamma_m(t)$ is the phase of the signal. The vector containing these signals is called the *data* or the *illumination factor*:

$$\mathbf{u}(t) = [u_0(t) \quad u_1(t) \quad u_2(t) \cdots u_{M-1}(t)]. \tag{2.3}$$

A complex quantity $a_m(\phi)$ is defined as the ratio between the signal received at the antenna element m and the signal received at the reference element when a plane wave is incident on the array. $a_m(\phi)$ is given by

$$a_m(\phi) = e^{-j\beta(x_m cos\phi + y_m sin\phi)}. \tag{2.4}$$

If a single plane wave is incident on the antenna array, then

$$u_m(t) = u_0(t)a_m(\phi). \tag{2.5}$$

The response of an antenna array to a traveling single plane wave coming at an angle ϕ is defined as the *steering vector* which is given by

$$\mathbf{a}(\phi) = \begin{bmatrix} 1 \\ a_1(\phi) \\ \cdots \\ a_{M-1}(\phi) \end{bmatrix} = \begin{bmatrix} 1 \\ e^{-j\beta(x_1 cos\phi + y_1 sin\phi)} \\ \cdots \\ e^{-j\beta(x_{M-1} cos\phi + y_{M-1} sin\phi)} \end{bmatrix} \tag{2.6}$$

Note that the $0th$ element is the reference element and its response is defined as 1. The response of the array with the weighting network shown in Figure 2.1 is called the *array factor*. The array factor $f(\phi)$ is defined as

$$f(\phi) = \frac{f_u(\phi)}{max\,[f_u(\phi)]}, \tag{2.7}$$

where $f_u(\phi)$ is the unnormalized response of the array which is given by

$$f_u(\phi) = \sum_{m=0}^{M-1} w_m e^{-j\beta(x_m cos\phi + y_m sin\phi)} = \mathbf{w}^H \mathbf{a}(\phi). \tag{2.8}$$

The weighting network in an antenna array can be fixed or varying. In an adaptive array, the weights are adapted by minimizing a certain criterion to maximize the signal-to-interference plus noise ratio (SINR)[2] at the output of the array. Hence the weighting network is very similar to an finite-impulse response (FIR) filter, where the time samples are replaced by spatial samples. The weighting network is hence called spatial filter.

[2]In the following chapters, signal-to-interference ratio (SIR) and carrier-to-interference ratio (CIR) will be interchangeably used. Both the terms are equivalent.

2.1.2 Array geometry and element spacing

The inter-element spacing between the antenna elements is an important factor in the design of an antenna array. *Grating lobes* appears in the antenna pattern if the elements are more than $\lambda/2$ apart, where λ is the wavelength of the signal which is given by $3 \times 10^8/f_c$, f_c is the carrier frequency. For an array oriented along the x-axis, this means that for every array factor lobe that the array forms for $0 \leq \phi < \pi$, another lobe may also appear in $0 \leq \phi < \pi$. Similarly for every null formed, a *grating null* may appear for element spacings greater than $\lambda/2$. The appearance of grating lobes and nulls are not desirable [1].

Mutual coupling is an effect that limits the inter-element spacings of an array. If the elements are spaced closely, the coupling effects will be larger and generally tends to decrease with increase in the spacing. The mutual coupling effect depends on the array geometry and the radiation pattern of element in the array. It was shown in [1], for two parallel resonant dipoles, the mutual impedance, defined as the voltage induced on one element by a current in the other element, is present over a broad range of element spacings, d; however, for $d < \lambda/2$ the mutual impedance tends to increase considerably. Therefore it is generally advisable to maintain at least $\lambda/2$ spacing between arrays of dipoles.

Directivity is another desired feature of an array, the maximum directivity[3] of an array is proportional to the length of the array in wavelengths. For a uniform linear array (ULA) with identical isotropic elements, in which the weighting factors are identical, the directivity of the array is approximately $2L/\lambda$, when the phases are adjusted to form a broadside pattern for Δz, the spacing between antenna elements, $\leq 0.8\lambda$, where L is the total length of the ULA. For the endfire case, the directivity is approximately $4L/\lambda$. In either case, if $L = (M-1)\Delta z$ is small compared with the wavelength, λ, the array cannot exhibit a high directivity. Therefore the elements have to far enough to avoid mutual coupling and the spacings have to be smaller than $\lambda/2$ to avoid grating lobes. For all practical purposes, a spacing of $\lambda/2$ is preferred.

[3]Directivity is defined as the ratio of maximum to average value of radiation intensity.

2.1.3 Channel impulse response and spatial signature

The propagation channel in a mobile radio channel is very complex. The channel is characterized by multiple signal propagation paths (called *multipaths*) from the transmitter to the receiver. These multipaths arise due to scattering, reflection and diffraction. Each multipath is characterized by a complex amplitude $\alpha_{k,i}$, a delay $\tau_{k,i}$, and an azimuthal directional-of-arrival, $\phi_{k,i}$, as well as a direction-of-departure, $\theta_{k,i}$. The multipath response between the transmitter for user k and the reference element is given by

$$h_{0,k}(t) = \sum_{i=0}^{L_k-1} \alpha_{k,i}\delta(t - \tau_{k,i}), \tag{2.9}$$

where L_k is the number of multipaths for user k. The complex quantity $\alpha_{k,i}$ models the attenuation and the phase shift the channel introduces to the signal. This model assumes an omnidirectional antenna at the transmitter and at the receiver and it does not take into account polarization mismatch or losses in the transmitter and in the receiver.

The channel impulse response between the transmitter of user k and the nth element of the receiver array is given by

$$h_{n,k}(t) = a_n(\phi) \sum_{i=0}^{L_k-1} \alpha_{k,i}\delta(t - \tau_{k,i}), \tag{2.10}$$

where $a_n(\phi)$ is given by Eqn. 2.4, and $\alpha_{k,i}$ and $\tau_{k,i}$ are independent of n. The vector impulse response, $\mathbf{h}_k(t)$, for a particular user is defined as

$$\mathbf{h}_{n,k}(t) = \sum_{i=0}^{L_k-1} \mathbf{a}(\phi_{k,i})\alpha_{k,i}\delta(t - \tau_{k,i}), \tag{2.11}$$

where $\mathbf{a}(\phi_{k,i})$ is the steering vector defined in Eqn. 2.6. This channel impulse response is a snapshot of the time-varying channel. If the users are moving then $\alpha_{k,i}$ varies with time. If all the multipaths arrive within a time window which is less than the channel symbol period for that user, then it is convenient to model the channel as a narrowband channel. In this case, we assume that all the delays for user k are approximately equal, i.e., $\tau_{k,i} = \tau_k$, therefore

$$\mathbf{h}_{n,k}(t) = \delta(t - \tau_k) \sum_{i=0}^{L_k-1} \mathbf{a}(\phi_{k,i})\alpha_{k,i} = \delta(t - \tau_{k,i})\mathbf{b}_k, \tag{2.12}$$

where $\mathbf{b}_k$ is called the spatial signature for user k which is given by

$$\mathbf{b}_k = \sum_{i=0}^{L_k-1} \mathbf{a}(\phi_{k,i})\alpha_{k,i}. \tag{2.13}$$

In general, the received data vector is given by

$$\begin{aligned} \mathbf{u}(t) &= \sum_{k=0}^{K-1} s_k(t) * \mathbf{h}_k(t) + \mathbf{n}(t), & (2.14) \\ &= \sum_{k=0}^{K-1} \sum_{i=0}^{L_k-1} \mathbf{a}(\phi_{k,i})\alpha_{k,i} s_k(t-\tau_k) + \mathbf{n}(t). & (2.15) \end{aligned}$$

For narrowband channels, the data vector may be expressed as

$$\mathbf{u}(t) = \sum_{k=0}^{K-1} s_k(t-\tau_k) \sum_{i=0}^{L_k-1} \mathbf{a}(\phi_{k,i})\alpha_{k,i} + \mathbf{n}(t) = \sum_{k=0}^{K-1} s_k(t-\tau_k)\mathbf{b}_k + \mathbf{n}(t) \tag{2.16}$$

2.2 Beamforming

Beamforming signal processing is used in conjunction with an array of sensors to provide a versatile form of spatial filtering. The sensor array collects spatial samples of propagating wave fields, which are processed by the beamformer. A beamformer does spatial filtering to separate signals that have overlapping frequency content but originate from different spatial locations.

Systems designed to receive spatially propagating signals often encounter the presence of interfering signals. If the desired signal and the interfering signals occupy the same temporal frequency band, then linear time-invariant temporal filtering cannot be used to completely separate the signal from the interferers. However, the desired and interfering signals usually originate from different locations. This spatial separation can be exploited to separate the desired signal from the interferers using spatial filtering at the receiver. Implementing a temporal filter requires processing of data collected over a temporal aperture. Similarly, implementing a spatial filter requires processing of data collected over a spatial aperture. The beamformer linearly combines the spatially sampled time series from each sensor to obtain a scalar output time series in the same manner that an FIR filter linearly combines temporally sampled data.

Two important characteristics of spatial sampling with an array of sensors are:

1. Spatial discrimination capability depends on the size of the spatial aperture; as the aperture increases, discrimination improves. The absolute aperture size is not important, rather its size relative to wavelength is the critical parameter. A single physical antenna (continuous spatial aperture) capable of providing the requisite discrimination is often practical for high frequency signals because the wavelength is short. However, when low frequency signals are of interest, an array of sensors can often synthesize a much larger spatial aperture than that practical with a single physical antenna.

2. A significant advantage of using an array of sensors, relevant at any wavelength, is the versatility. In many applications, it is necessary to change the spatial filtering function in real time to maintain effective suppression of interfering signals. This change is easily implemented in a discretely sampled system by changing the way in which the beamformer linearly combines the sensor data.

2.2.1 Narrowband beamforming

A signal is considered to be *narrowband* if all the frequency components of the signal as they travel across the array undergo only a phase shift and not a change in the magnitude. This is illustrated in Figure 2.3. In other words, the signal bandwidth is very small compared to the carrier frequency. The signal has a spectrum centered around f_c and the solid line represents the phase shift the signal undergoes as the signal travels across the array as a function of frequency. If the signal bandwidth is very small compared to the carrier frequency then the phase shifts undergone by the frequency components at the two edges of the band are almost equal. Therefore the phase shift line appears as a flat line across the bandwidth of interest. For a narrowband signal, narrowband array processing is the appropriate choice. A narrowband array is shown in Figure 2.4. A narrowband array has one weight per element followed by a linear combiner.

2.2.2 Wideband beamforming

A signal is considered to be *wideband* if all the frequency components of the signal as they travel across the array undergo not only a phase shift but also a change in the magnitude. This is illustrated in Figure 2.5. In other words, the signal bandwidth is

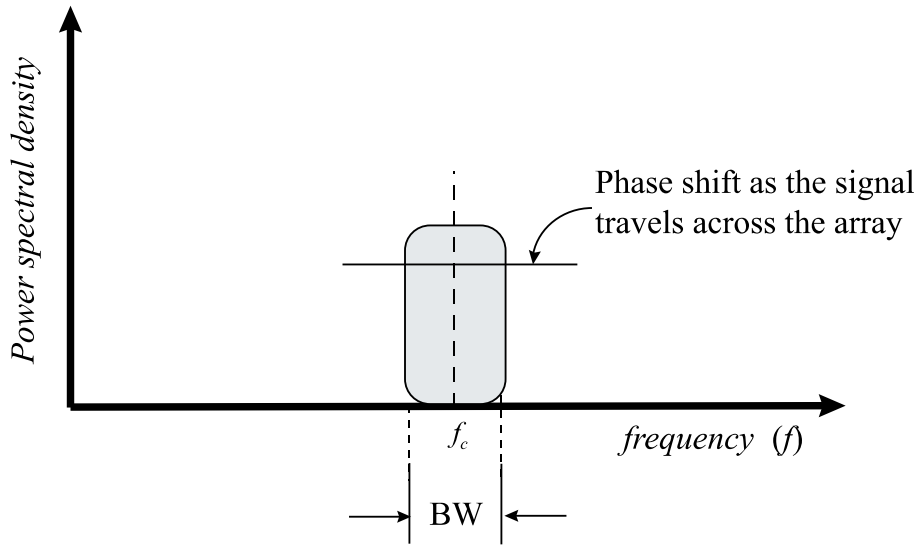

Figure 2.3: Figure illustrating a narrowband signal.

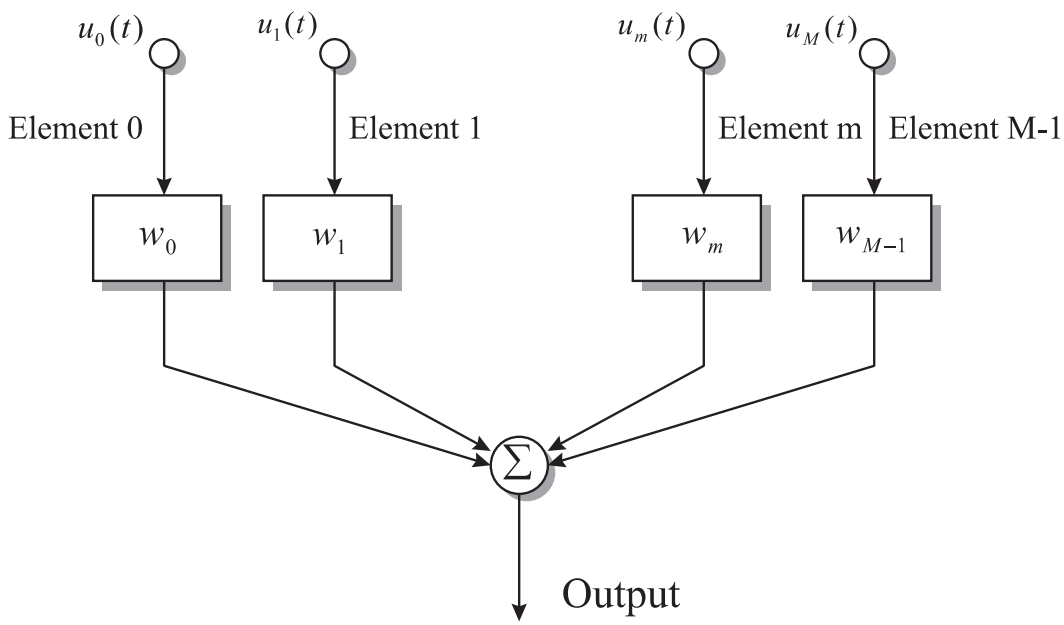

Figure 2.4: Block digram of a narrowband array.

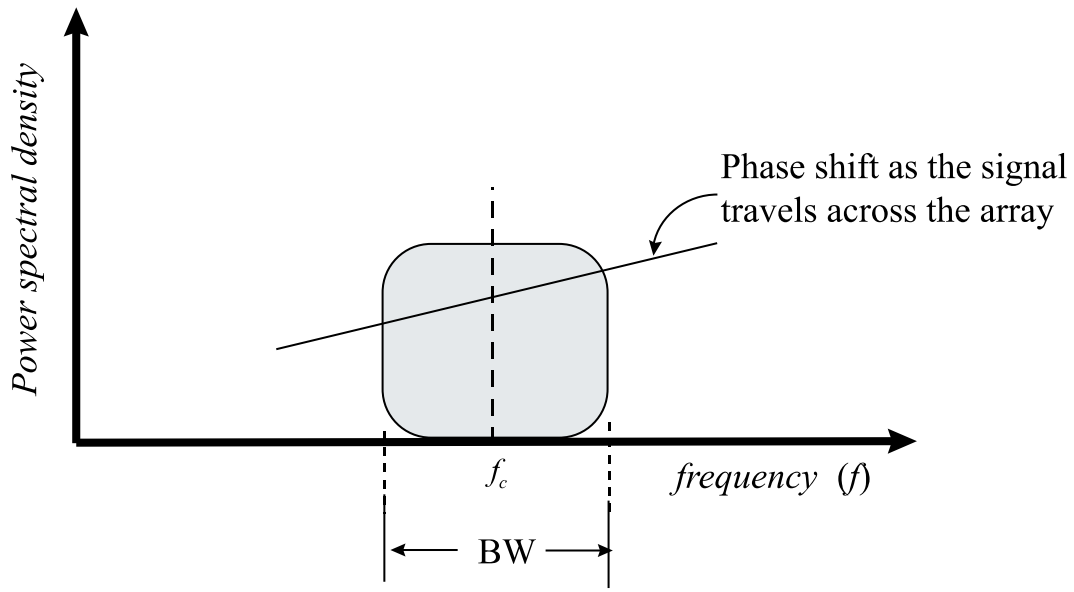

Figure 2.5: Figure illustrating a wideband signal.

not very small compared to the carrier frequency. The signal has a spectrum centered around f_c and the solid line represents the phase shift the signal undergoes as the signal travels across the array as a function of frequency. If the signal bandwidth is not very small compared to the carrier frequency then the phase shifts undergone by the frequency components at the two edges of the band are not equal. Therefore the phase shift line appears not to be flat across the bandwidth. For a wideband signal, wideband array processing is the appropriate choice. A wideband array is shown in Figure 2.6. A wideband array has an FIR filter of length T in each of its element. Different frequency components of a wideband signal as it travels across the array undergo different phase shifts and hence an array should have the ability to compensate for the frequency dependent distortion. The array has to be *frequency-selective*, i.e., it has to perform temporal processing in addition to spatial processing. This type of processing is also called Space Time Array Processing (STAP).

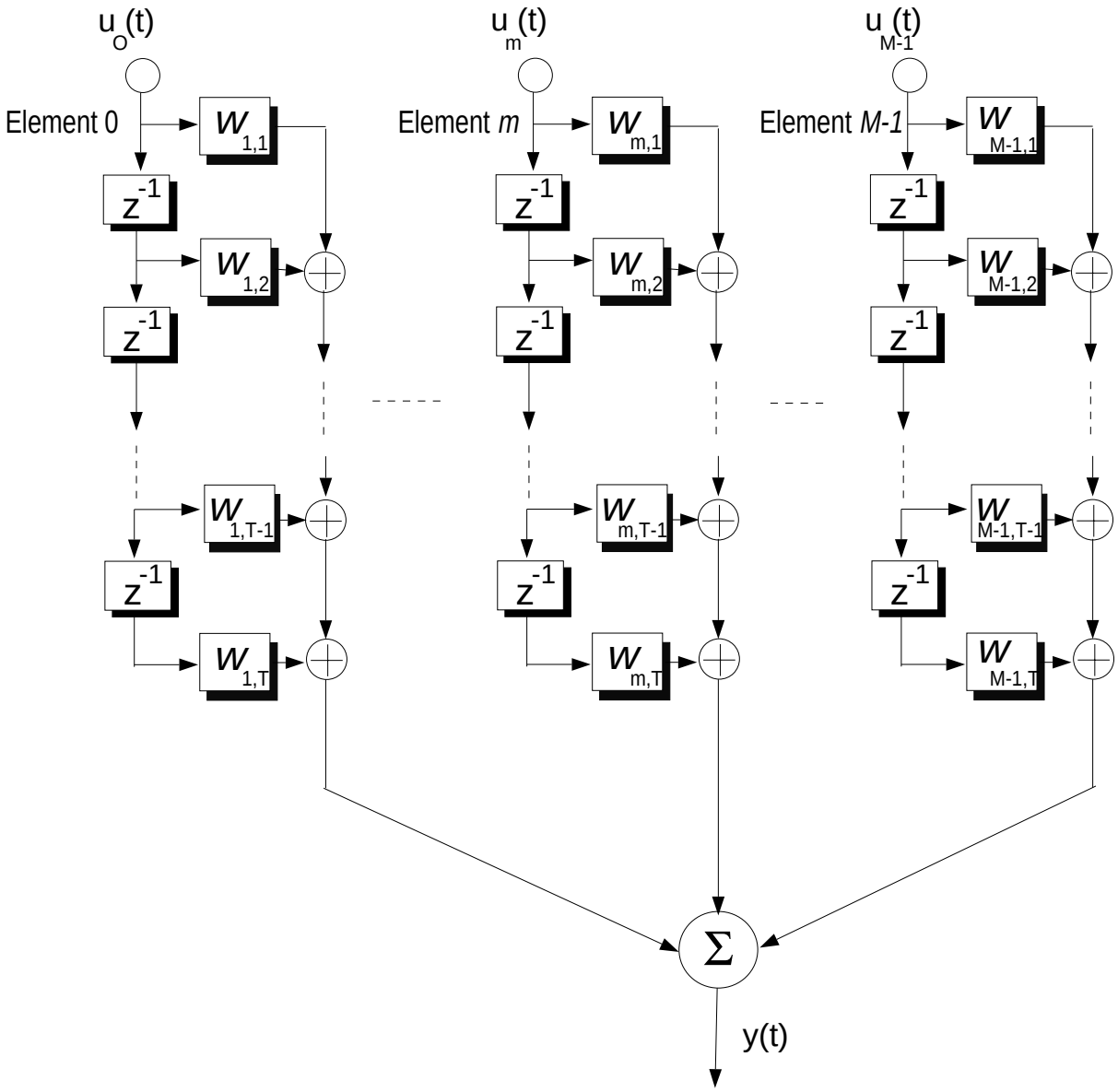

Figure 2.6: Block diagram of a wideband array.

2.3 Elementspace and beamspace beamforming

The arrays that perform beamforming based on the input directly from the antenna is called *elementspace beamforming*. The arrays discussed so far fall under this category. In *beamspace beamforming*, the outputs from the antenna elements are preprocessed by a *beamforming network* as shown in Figure 2.7 before being converted to baseband. This beamforming network acts as though the antennas are directional. This network forms beams in orthogonal directions and hence provides directionality to omnidirectional antennas. By using the beamforming network, beams with increased CIR can be achieved and in the digital combining network (i.e., the weight vector $\mathbf{w} = [w_0 \quad w_1 \quad \cdots \quad w_{M-1}]$) beams with high CIRs are given high gain and beams with low CIRs are given low gain. The beamforming network can be used before the A/D (Analog-to-digital) converter or after it. The beamforming network is implemented at RF using a *Butler matrix*. The beamforming networks at the RF helps in enhancing the dynamic range of the system.

2.4 Classification of adaptive array algorithms

In this section, a brief description of the classification of adaptive array algorithms is presented. Many of the adaptive array algorithms were derived from equalization[4] algorithms and they have been later adapted to suit spatial processing. In spatial processing, *spatial samples* are the input samples as opposed to *temporal samples* in equalization. The broad classification of adaptive array algorithms is shown in Figure 2.8.

2.4.1 Trained algorithms

The adaptive array algorithms are broadly classified as: trained and blind algorithms. Trained algorithms use a finite set of training symbols to adapt the weights of the array and maximize the SINR. The processor in the adaptive array has a pre-stored training sequence and the array adapts its weights when the training signal is transmitted by the transmitter. This technique requires synchronization. These algorithms work very well, but the only cost paid is the excess transmission time or wastage of

[4]Equalization is a technique to compensate for multipath distortions.

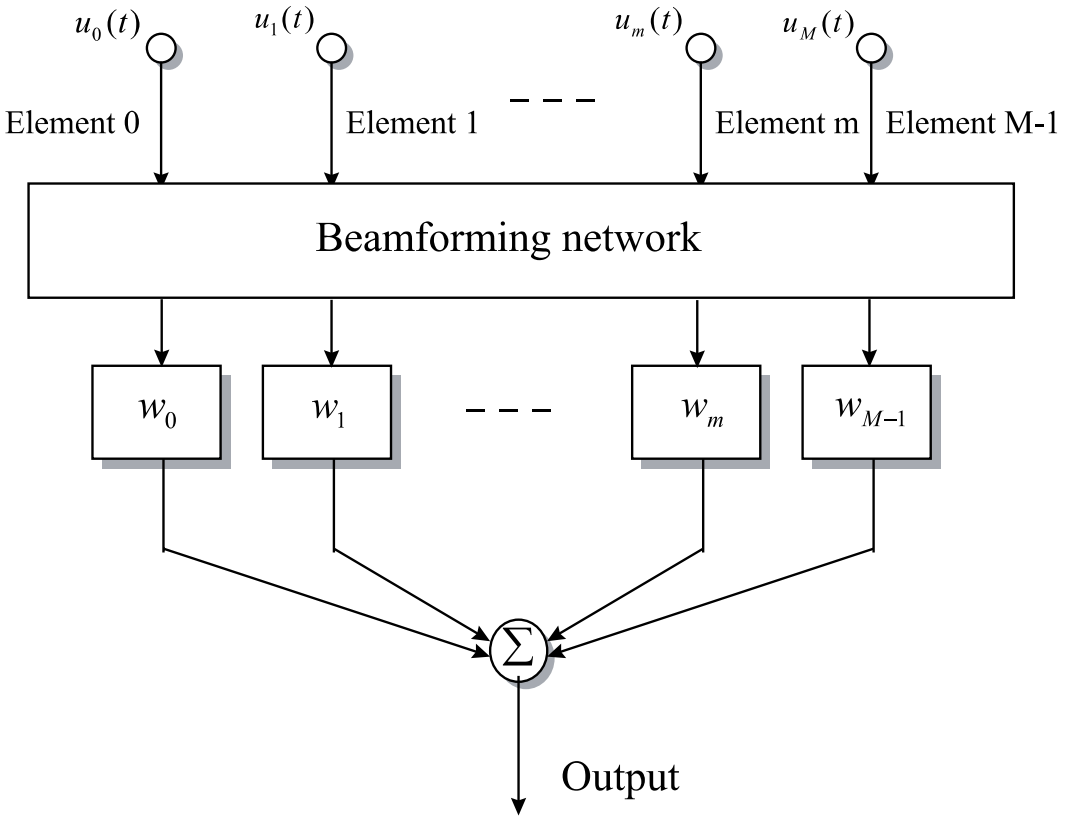

Figure 2.7: Block digram of a narrowband beamspace array.

bandwidth. The trained algorithms are classified based on their adaptation criteria and they are *least-mean squares* method (LMS), *sample matrix inversion* (SMI) or *least-squares* method (LS), and *recursive least-squares* method (RLS). All these techniques minimizes the squared error or the L_2-norm of the error vector, $\mathbf{e}$, whose length is N. The fundamental assumptions behind these minimization techniques is that the error vector follows a Gaussian probability density function. It is well known from estimation theory that the L_2 norm is the *maximum likelihood* (ML) estimator for a Gaussian signal [2].

The LMS algorithm is a steepest-descent based approach and hence it is computationally least intensive and also suffers from slow convergence [3]. The computation requirements for the implementation of an LMS algorithm, if narrowband processing is employed, is of the order of M, where M is the number of elements. LMS is sample-by-sample based algorithm. The LS algorithm is a direct weight estimation technique which operates on a block of data. The convergence of the LS algorithms is faster than LMS but it requires computations of the order of M^3. LS method requires inversion of a matrix and this operation is not desirable from a numerical stability point of view. Instead of inverting the matrix, one can solve the linear system of equations using techniques like Gaussian elimination. RLS is a recursive version of the LS approach, where the inversion of the matrix is carried out using a recursion. RLS requires computations of the order of M^2. It is a *popular misconception* that RLS is cheaper than LS approach. This is *not true*. Let us consider an example to prove this point. Let us assume that the signal is real and real processing is employed.

- RLS operates on a sample-by-sample basis and hence to process N samples, RLS requires computations on the order of $M^2 \times N$ operations.

- LS to process the same block size requires computation so the order of $M^3 + N \times M$ operations, where M^3 and $N \times M$ correspond to the computations required to perform weight calculation and output calculation, respectively.

Therefore as long as M is smaller than N which is true in the array processing case, RLS is computationally comparable with LS and it is also well known that LS approach and RLS approach yields the same solution asymptotically.

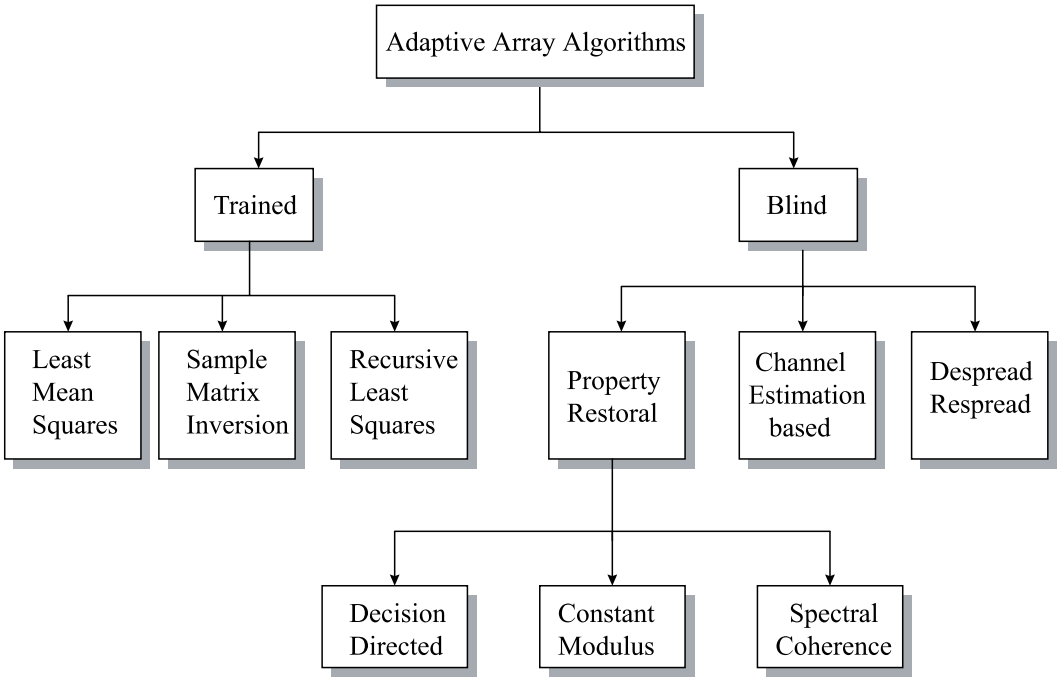

Figure 2.8: Classification of adaptive array algorithms.

2.4.2 Blind algorithms

Blind algorithms do not require training signals to adapt their weights[5]. Therefore these algorithms save transmission bandwidth. Blind algorithms can be classified as *property restoral* algorithms, *channel estimation algorithms*, and *despread and respread* algorithms. Property restoral algorithms restore certain properties of the desired signal and hence enhance the SINR. The property that is being restored may be the modulus or the spectral coherence. Blind property restoral algorithms can be classified as Constant Modulus (CM) algorithm, Spectral self-COherence REstoral (SCORE) algorithms, and decision directed (DD) algorithms.

The CM algorithm [4] [5] is applicable to constant modulus signals and the algorithm tries to undo the distortion introduced by the channel and the interference by forcing the output magnitude of the array to be constant, but preserving the phase of the input signal. The CM algorithms can use steepest-descent approach or least-squares based approach to minimize the CM cost function. CM algorithms using the

[5]The classification presented here does not include higher-order techniques

LS adaptation converges very fast and can perform very similar to a trained algorithm. The only disadvantage of using a CM type algorithm is that it lacks the property of *signal-selectivity*, i.e., the algorithm cannot distinguish one constant modulus signal from the other. The CM algorithm always has a tendency to capture the strongest signal.

SCORE [6] and related algorithms [7, 8] exploit the property of cyclostationarity, which most digital and some analog signals exhibit. Most man-made signals encountered in communication, telemetry, radar and sonar systems, have some parameters that vary periodically with time. In some cases even some multiple incommensurate (not harmonically related) periodicities are involved. Examples include sinusoidal carriers in amplitude, phase, and frequency modulation systems, periodic keying of amplitude, phase and frequency in digital modulation systems. In most cases, the underlying periodicities can be neglected, but an increased improvement in performance can be obtained by recognizing and exploiting these underlying periodicities. This leads to the to the treatment of random signals as *cyclostationary*, in which the signal parameters vary in time with single or multiple periodicities [9].

The existence of correlation between widely separated spectral components (separation equal to a *cycle frequency*) can be interpreted as *spectral redundancy*. The meaning of the term *redundancy* that is intended here is essentially the same as that used in the field of information theory and coding. Specifically, multiple randomly fluctuating quantities (random variables) exhibit some redundancy if they are statistically dependent, for example, correlated. In speech coding theory, undesired redundancy is removed from the data to increase the efficiency with which it represents information. In the case of error correcting codes, redundancy is introduced to insure reliable transmission of information. Here spectral redundancy is inherently introduced into signals by the modulation process and this be exploited to enhance the corrupted signals. The performance of a signal processor can be substantially improved if it exploits cyclostationarity in its decision making process. The degree of improvement, relative to conventional processors, depends on both the severity of the signal corruption (noise, interference, distortion) and the degree of spectral redundancy in the signal. The degree of improvement also depends on the available data for processing (the collect time). The performance can also be improved by designing the signal to exhibit a sufficient amount of spectral redundancy.

Decision directed algorithm [10] demodulates the array output and a binary decision is made. These decisions are fed back as the reference signal. This algorithm works well if the eye pattern of the input signal is "open", otherwise the algorithm fails.

Channel estimation techniques [11, 12, 13, 14] use the knowledge of the special code properties of the spread spectrum signals to obtain estimates of the channel parameters. These techniques first estimate the channel parameters and then use the channel estimates to form beams in the direction of the desired signals. These techniques are applicable only for CDMA signals.

Despread-respread techniques for CDMA belong to the family of *demod-remod* techniques, which is common in FM interference rejection. A despread-respread technique works on the principle of despreading the signal at the output of the ith user and then making a bit decision. Then the ith user's PN code C_i *re*spreads the data bit. Then the error between the respread data and the output of the array is minimized using a least-squares or a steepest descent approach. The assumption behind the despread-respread based adaptation is that the synchronization has been achieved prior to beamforming, since despreading requires synchronization.

2.5 Cochannel interference problem: A major capacity limiting factor

Cochannel interference is a major factor that limits the capacity of a cellular system. In a cellular system to increase the capacity, frequencies are *reused*, i.e., a frequency band is used in two different cells belonging to different clusters, sufficiently separated so that they don't interfere significantly with each other. But when a mobile travels at a high speed, the received signal undergoes fading. Therefore at times, the SIR can be below 0 dB resulting in the loss of the desired signal. A typical cochannel scenario is shown in Figure 2.9. Cells that are marked by the same shades are cochannel cells. The base stations are marked by rectangular boxes. The mobile unit, marked by a diamond, receives signal from the desired base station and the interfering base station. For the current AMPS system and the TDMA (IS-136) system, to maintain toll quality speech the CIR has to be greater than 18 dB and hence each cluster has seven cells or a reuse factor of 7 is used. In a CDMA system (IS-95), many users in a

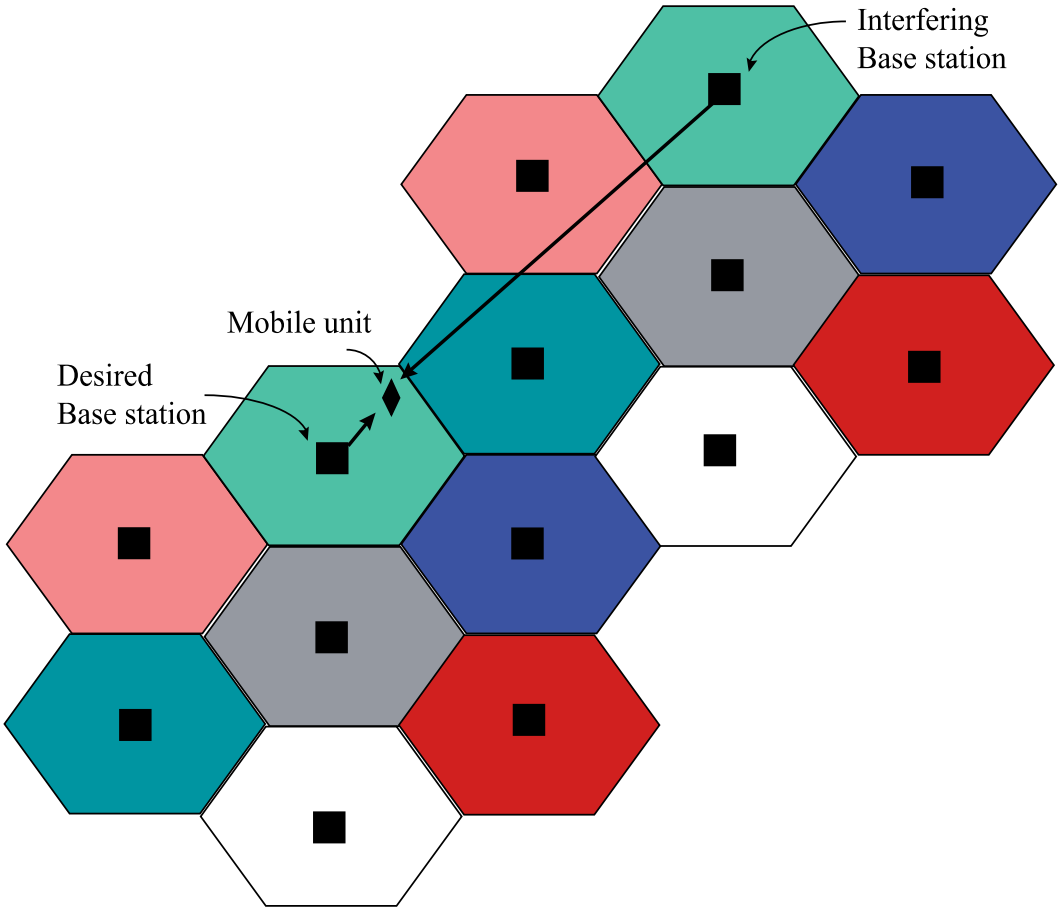

Figure 2.9: Illustration of the cochannel problem in a cellular environment (AMPS and TDMA systems).

cell use the same frequency band and frequencies are reused in every cell, and hence theoretically CDMA systems have a reuse factor of 1. The number of users that can occupy the same frequency depends on the processing gain of the spread spectrum signal.

The level of the interference dictates how close the cochannel users can be located in AMPS and TDMA systems and the number of users/cell in a CDMA system. In order to achieve increase in capacity, the level of the interference has to be reduced and this can be achieved using signal processing techniques. In this research, the focus is on using adaptive arrays at the base station to reduce the interference level and hence enhance capacity. The focus is on the reverse link, i.e., the link from

the mobile to the base station, because the reverse link is the weak link since there is a limitation to the radiated power from the mobile unit. Moreover, the base station can be the only place to support an adaptive array in a cellular system in terms of the availability of space and the processing power.

2.6 Adaptive array algorithms: A survey

Widrow et al. [15] were the first to introduce an LMS adaptive antenna array. They showed that the array can adapt to reject interference without the knowledge of the interference and noise. After the pioneering work on blind equalization by Sato [16], blind equalization for one- and two-dimensional communication systems has become an area of great interest for research and industry applications. Blind equalizers converge without resorting to a known training sequence. For some blind equalizers phase recovery is not necessary. A new self-recovering equalization algorithm was introduced by Godard [17] for application to phase and amplitude-modulated signals. Both blind adaptive equalization and adaptive antennas continued to be developed in parallel for many years before these signal processing operations were combined.

2.6.1 CM-based algorithms

In the 1980's, many blind adaptive algorithms were developed and eventually applied to train adaptive arrays. The Constant Modulus Algorithm (CMA), introduced by Treichler and Agee [18] in 1983 has become one of the most commonly applied blind algorithms. They showed that this adaptive digital filtering algorithm can compensate for both frequency-selective multipath and interference on constant modulus signals. The first application of CMA to arrays is attributed to Gooch and Lundell [4]. The performance of this algorithm for an FM signal with a tonal interference and for a QPSK data signal with intersymbol interference was presented in this paper. They used the LMS algorithm to train the weights of the FIR filter.

Thereafter extensive studies of this algorithm have been carried out. Treichler and Larimore [19] analyzed the asymptotic convergence behavior of the weight vector when the norm of the initial weight vector is very large. They also analyzed the convergence behavior of the output modulus to investigate the tone capture effects [20]. In addition, the abnormal phenomena in the CMA, such as the tone capture

and noise capture effects, were studied [21, 22]. Recently, Agee proposed a least-squares CMA to improve the convergence speed, but his algorithm is computationally intensive [23].

As a new application, Ferrara proposed a CMA structure that can reject strong constant envelope interference from a weak desired signal with known modulus [24]. In this application, the *a priori* knowledge of the absolute value of the transmitted signal modulus is used. Also, to prevent the CMA from locking to an interference signal, the tap weights of the interference-canceler are constrained such that its filter weights be symmetric about the center weight with the unity constraint. More recently, Kammeyer et al. modified the CMA in order to be used in a commercial FM stereo broadcasting system for multipath echo cancelation [25]. Recently, several researchers have tried to analyze the performance of CMA. Chan and Shynk analyzed the stationary-point performance of the CMA when the equalizer input signal is a zero-mean, real Gaussian signal [26]. Bershad and Roy analyzed the performance of the 2-2 CMA for Rayleigh fading sinusoids in Gaussian noise assuming Gaussian input signals [27]. Takeo Ohgane [28] analyzed the characteristics of the CMA adaptive array for frequency selective fading compensation in digital land mobile radio communications. It was shown that there is great improvement in BER by employing an adaptive array. The channel was modeled using two-ray model. It was also shown that the error rate is improved better when the delay difference between the two arriving waves is large. Takeo Ohgane et al. [29] implemented a CMA adaptive array for a high speed GMSK transmission in mobile communications. They implemented a 4-element adaptive array based on the digital beamforming concept to reduce the multipath fading effect in high-speed communications.

Gooch and Lundell [4] were the first to apply the CMA to the adaptive array to reject interference. Simulation results were presented showing the beampattern adapting to the desired signal and placing nulls in the direction of the interferers. Capture analysis was also presented in this paper. Performance of constant modulus adaptive filter for interference cancelation was analyzed by Kwon et al [30]. They investigated the optimum weight vector that minimizes the performance index of the CMA which is defined as the mean-square difference between the estimated and true modulus. The convergence behavior of the squared output modulus and the performance index was analyzed in this work.

Tugnait et al. [31] came up with a way to improve the convergence of CMA adaptive filters. They used higher-order statistics to estimate the channel and then compute the channel inverse of a specified length to initialize a CMA equalizer. Kikuma et al. [32] used non-steepest descent algorithms (Marquardt method), in contrast to the conventional steepest descent algorithms, to speed up the convergence. The fast convergence of this algorithm makes it useful in a highly dynamic environment like the mobile channel. It was shown that the Marquardt method, a nonlinear least squares method, can reduce the convergence time by a factor of 10 to 100 compared to the steepest descent method. Agee [33] also examined the convergence behavior of the CMA arrays in Gaussian interference environments. Simulation results of the performance of the least-squares CMA (LSCMA) array for a mobile channel was presented by Agee et al. [34]. Spatial equalization without beamforming using the CMA for a mobile channel was analyzed by Sylvie [35], the equalization was performed without temporal processing i.e., acting upon a single snapshot.

In [36], Talwar et al introduced the Iterative Least Squares Projection technique (ILSP). ILSP is a property restoral based algorithm which can jointly detect the spatial signatures and the waveforms associated with the multiple sources incident on the receiver array. ILSP uses the knowledge of the finite alphabet structure of the digital signals. In [37], the ILSP technique was extended for constant modulus signals and was called the Iterative Least Squares Projection Constant Modulus Algorithm (ILSP-CMA). In [38], Van der Veen and Paulraj have shown that the underlying constant modulus factorization problem in the blind separation of constant modulus signals, is a generalized eigenvalue problem and may be solved using a simultaneous diagonalization of a set of matrices. This new analytic approach was shown to be robust to noise.

Recently, Li and Liu [39] introduced two new blind algorithms, *second order statistics based algorithm* (SOSA) and *modified second order statistics based algorithm* (MSOSA), for spatial-temporal equalization using antenna arrays. Through computer simulations, it was demonstrated that the performance of these two new algorithms is better than Orthogonal Fractionally Spaced CMA (OFS-CMA).

2.6.2 Cyclostationary-based algorithms

Agee, Gardner and Schell [33, 40, 41] were the first to use the property of cyclostationarity to help mitigate interference and fading in a mobile environment. They presented three different adaptive array processors least-squares SCORE, auto-SCORE and cross-SCORE processors. Cross-SCORE performs better than the least-squares SCORE, because of its ability to separate signals with same cyclic periodicities. Simulation results show the superior performance of this algorithm in rejecting narrow band and wideband interferers. Gardner et al. [42] discussed the increase in the capacity of a cellular radio by applying blind adaptive spatial filtering. Space/time/frequency division multiplexing access (STFDMA) was proposed in this paper and simulation results show that the cell capacity is increased by a factor of 128 compared to FDMA. This system can accommodate five times as many users as the proposed CDMA scheme using the same bandwidth. Schell and Gardner [43] analyzed the maximum likelihood and common factor-analysis based adaptive spatial filtering for cyclostationary signals. They derived a blind adaptive spatio-temporal filtering for unknown cyclostationary signals in noise in two ways, one by maximizing a constrained conditional likelihood function and by solving a common factor analysis problem. It was shown that the specific choice of free constraint-parameters within the resulting beamformer structure yield the existing cross-SCORE and conjugate cross-SCORE algorithms which blindly adapt an antenna array to extract signals having specified cyclostationary properties from the interference and noise.

A new cost function for adaptive beamformers which uses cyclostationary signal properties was developed by Castedo et al. [44]. This new approach exploits the property of higher order cyclostationarity to generate spectral lines by use of a particular class of nonlinear transformations. They demonstrated that the beamformer can extract the desired signal using only the information from the spectral lines. It was also shown that the interferences can be eliminated even when they exhibit the same cyclostationary properties as the desired signal.

Shamsunder [45] proposed new bearing and range estimation algorithms which uses cyclostationary of the underlying processes. Direction finding algorithms were proposed for narrowband non-Gaussian signals by exploiting the higher order temporal properties of communication signals. Schell et al. [46] presented a blind adaptive

spatiotemporal filtering for wide-band cyclostationary signals. Schell et al [47] applied SCORE algorithm and SCORE extensions to sorting in the rank-L spectral self-coherence environment. This paper investigated the ability of the SCORE algorithm to separate cyclostationary signals from a rank L spectral self-coherence environment where L signals exhibit spectral self-coherence at the same value of frequency separation. It was shown that the signals with spectral self-coherence at the same frequency separation can be separated if their relative self-coherence strengths are different. Agee et al. [48] analyzed a blind capture and geolocation of general spatially self-coherent waveforms using multiplatform SCORE. This approach can simultaneously estimate the time difference-of-arrival of multiple temporally-uncorrelated SOIs impinging on multiple receiver platforms, and blindly separate those signals with maximum-attainable SINR at each platform.

2.6.3 Decision directed-based algorithms

Decision-directed algorithms was also investigated by many in the 1980's. Gooch and Sublett [49] described joint spatial and temporal equalization using a decision directed adaptive algorithm. They presented two methods for jointly optimizing the weights of a single-weight per channel adaptive diversity combiner followed by a fractionally-spaced equalizer and showed that this system can reject multipath distortion and co-channel interference for a variety of digital communication system. "Stop and Go" decision directed algorithm for blind equalization and carrier recovery was presented by Picchi and Pratti [50]. They showed that the standard decision-directed estimated gradient adaptation algorithm for joint MSE equalization and carrier recovery, normally utilized in the open-eye condition, can be used for closed-eye start-up condition with no need of a training sequence. They used a simple flag to tell the synchronizer and the equalizer whether the current output error with respect to the decided symbol is sufficiently reliable to be used.

2.7 Conclusions

The fundamentals of adaptive array processing are explained in this chapter. Modeling and classification of adaptive antenna systems based on their structure are addressed here. Adaptive array algorithms have been broadly classified as trained and

blind algorithms. A brief survey of existing adaptive array algorithms has been provided in this chapter.

Chapter 3

A Blind Adaptive Array Algorithm for AMPS Signals

3.1 Introduction

The drastic growth in cellular communications has resulted in crowding of the spectrum. As the number of users per cell increases, the level of interference seen by any user also increases. To accommodate more users in a cell, cell splitting is usually employed, where bigger cells are split into smaller cells. An adaptive antenna array in the base station can significantly reduce cochannel interference and hence increase the capacity of the cell. A beamformer for cochannel interference cancelation of AMPS signals is proposed and analyzed for improving the performance of the reverse link (link from the mobile to the base station). AMPS is the analog frequency modulation (FM) cellular standard used in North and South America and the bandwidth of each channel is 30 kHz. AMPS uses a seven-cell reuse pattern and thus the carrier-to-interference ratio (CIR) is typically above 17 dB [51].

The number of cells per cluster determines the level of cochannel interference power. For simplicity let us consider here the cells to be hexagonal in shape though it is not the case in practice. The frequency reuse factor determines the spacing between the cochannel cells and hence the power of the cochannel interference. The mean distance between cells using the same frequency set is called the *mean reuse distance* D. Because of the hexagonal geometry of the cells D is related to the cell radius R, and the ratio (D/R) is called the *reuse ratio*. D and R are related to

the cluster size, N_1, by $\frac{D}{R} = \sqrt{3N_1}$. Assuming the path-loss exponent to be 4, an approximate value for carrier-to-interference ratio (CIR) for a 7-cell cluster [51] is $CIR = \frac{C}{\sum_{i=1}^{6} I_i} \approx \frac{R^{-4}}{6D^{-4}}$, where C is the carrier power and I_i is the power of the ith interferer, assuming the interferers contribute equally[1]. From $\frac{D}{R} = \sqrt{3N_1}$, then CIR $\approx 1.5N_1^2$, i.e., the CIR is a function of cluster size[2]. If the cluster size is reduced to 3, the CIR is maintained around 11 dB, but for reliable communication a CIR of at least 18 dB is required [51]. Therefore if the beamformer can reduce the interference power by 7 dB, reliable communication can be accomplished even if there are 3 cells per cluster.

Several single channel FM interference rejection techniques have been proposed in the past. Cassara *et al* [52] proposed a detector which consists of two phase-locked loop demodulators interconnected to permit one phase locked loop (PLL) to lock on to the strongest FM signal while the other loop tracks and demodulates the weaker FM signal. Stojanovic *et al* [53] proposed a modified FM demodulation technique which is concerned with the reduction of residual demodulated interference of the stronger signal. This reduction is achieved by the generation of further demodulation products and subsequent subtraction of these from the main product to reduce unwanted components. Bar-Ness *et al* [54] suggested a method for estimating the parasitic phase introduced by the FM interference and subtracting the parasitic phase from the composite FM signal to obtain the desired strong signal's phase information. The weak signal is then obtained by suitable subtraction from the composite signal after limiting. Hawkes reviews other adjacent and cochannel interference rejection techniques for FM signals in [55]. Rich *et al* [56] address the cochannel FM interference rejection using adaptive notch filters. They proposed a cross-coupled notch filter interference suppressor in which one of the PLL tracks the stronger signal and the other the weaker signal. The estimated strong signal is then notched out from the path that leads to the PLL which tracks the weak signal. Similarly the estimated weaker signal is notched out from the path that leads to the PLL which tracks the strong signal. Most of these techniques work well for adjacent channel interference cancelation and to a certain extent for cochannel interference cancelation. Rong *et al* [57] proposed a technique based on cyclostationarity to reject cochannel interference rejection for

[1]This calculation is the average CIR at the base station for a mobile at the cell boundary.

[2]Note that the result is an approximation for values other than $N_1 = 7$, these values give us an approximate relationship between the CIR and N_1.

AMPS signals. This was the first paper that applied cyclostationary-based filtering technique to the AMPS cochannel interference problem.

Blind multi-channel adaptive filtering techniques have been proposed to reject FM cochannel interference. Interference rejection using adaptive filters for FM signals must be blind because a training signal is not applicable for analog FM signals. Gooch *et al* [4] proposed a beamformer (constant modulus array) that minimizes the modulus variation at the beamformer output. The main disadvantage of this beamformer is that it can capture interference with a constant-modulus. Agee [5] proposed a multi-target constant modulus array (MT-LSCMA) which can blindly capture and separate multiple signals coming onto the array. This blind adaptive array has multiple ports and signals arriving from different directions appear at different ports. If there are n signals coming onto the array, then the MT-LSCMA requires adaptation of n beamformers. This array has the disadvantage of *port-shuffling*, where the signals may jump from one port to the other. For AMPS signals, port shuffling can be partially solved by detecting the signals based on their SAT frequency. However, for a rapidly varying channel the port-shuffling may be too fast to identify the signal based on the SAT since there is only 30 Hz separation between the SATs.

Agee *et al* [6] proposed a family of SCORE (spectral self-coherence restoral) algorithms which exploit the cyclostationary feature of the signals impinging the array. The aim of the SCORE methods is to restore the spectral self-coherence of the signal-of-interest (SOI) at a particular cycle frequency and therefore separate the SOI from the rest of the signals in the environment. Least-squares SCORE suffers from slow convergence, while Cross-SCORE speeds up convergence, it requires the adaptation of two beamformers at the same time. Auto-SCORE and phase-SCORE require solving the generalized eigenvalue problem which involves high computational cost.

Recently Castedo *et al* [58] proposed a beamformer that is based on the property of cyclostationary signals of generating spectral lines by using a class of nonlinear transformations. The beamformer output is passed through the non-linearity, and its weights are adjusted to minimize the mean squared error between the output of the non-linearity and a complex exponential reference. For AMPS signals, we have found that this beamformer captures the interference while operating in negative carrier-to-interference ratio (CIR) environments when the array is initialized with an

omni-directional radiation pattern. This is due to the cyclic frequencies of the SOI and the signal-not-of-interest (SNOI) being very close to each other for AMPS signals.

This chapter proposes and analyzes a new method of adaptive beamforming introduced in [7] which exploits the cyclostationary nature of the desired signal. The basic idea behind this beamformer is derived from the least-squares SCORE. This array exploits spatial, temporal and spectral diversities to separate the SOI from the SNOI. This beamformer has a tapped delay line following each array element, and it shapes the input signal to combine coherently the SOI components and combine incoherently the SNOI components. This beamformer can be included in the family of *time dependent adaptive arrays* introduced in [8]. This chapter is organized as follows: Section 3.2 explains the spectral features of AMPS signals and Section 3.3 describes the Spectral Correlation Discriminator Array (SCDA) algorithm. The mean squared error (MSE) analysis of the SCDA is presented in Section 3.4. Section 3.5 discusses the simulation results and the conclusions are presented in Section 3.6.

3.2 Spectral features of AMPS signals

Supervision in a mobile communication system involves the dual task of detecting the presence of the signal and monitoring the strength of the signal. Supervisory audio and the signaling tones are used to avoid a false supervisory indication caused by the cochannel interference. Three frequencies are allocated for SAT signaling: 5970, 6000 and 6030 Hz. The base station sends out a SAT and the mobile sends back a SAT, if the SATs are the same then the loop is connected. If not, the base station decides the signal to be interference. One of the three SAT frequencies is assigned to each cell-cluster and thus the SAT scheme provides supervision and reduces the chance of misinterpreting an interferer as the desired signal.

An AMPS FM signal can be modeled as

$$x(t) = \Re\left[e^{j\left[\omega_c t + \beta f_m \int_{-\infty}^{t} v(u)du + k\sin(2\pi f_{sat} t)\right]}\right]. \tag{3.1}$$

where ω_c is the carrier frequency, β is the voice modulation index[3], $v(u)$ is the band-limited speech signal, f_m is the maximum frequency of the speech signal, k is the modulation index for SAT (1/3 for AMPS), and f_{sat} is the frequency of the SAT.

[3] $\beta \leq 3$ for AMPS and hence the frequency deviation of the baseband FM signal $\leq$ 12 kHz.

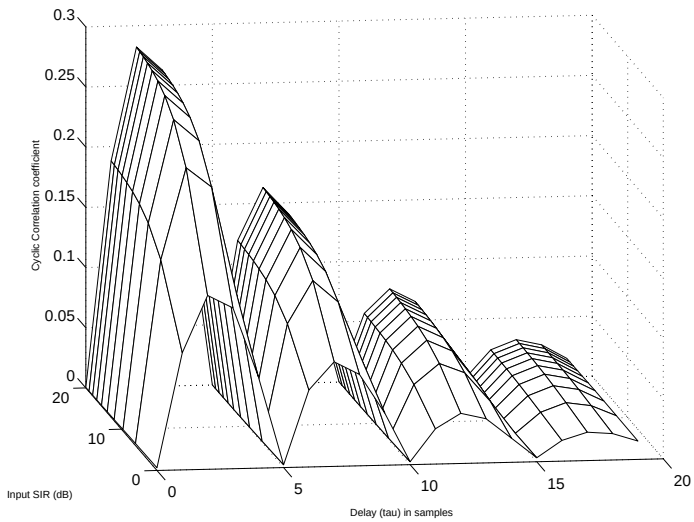

Figure 3.1: Plot of cyclic correlation coefficient in cochannel interference environment (SAT frequency of the SOI is 6.00 kHz and that of SNOI is 6.03 kHz).

AMPS signals exhibit cyclostationarity due to the presence of the SAT and the beamformer analyzed here exploits this property to distinguish the SOI from the SNOI. Cyclostationary signals exhibit spectral redundancy, that is the spectral components separated by the cycle frequencies are correlated with each other [9]. The cyclostationary feature of a signal is measured by the cyclic autocorrelation function in the time domain and the spectral correlation density function in the frequency domain. It was shown in [57] that the spectral correlation density function (SCD) of the AMPS signal (the Fourier transform of the cyclic autocorrelation) is given by,

$$\begin{aligned} S_{xx}^{\alpha}(f) &= \int_{-\infty}^{\infty} R_{xx}^{\alpha}(t) e^{-j2\pi f t} dt, \qquad (3.2) \\ &= \sum_{n=-\infty}^{\infty} \sum_{m=-\infty}^{\infty} J_n(k) J_m(k) S_{xx}\left(f + \frac{(n-m)}{2} f_{sat}\right), \end{aligned}$$

where $S_{xx}(f)$ is the power spectral density (PSD) of the AMPS signal and the terms J_n and J_m are Bessel functions. It was also shown in [57] that $S_{xx}^{\alpha}(f)$ is nonzero when $(n-m)/2$ is an integer. So the cyclic spectrum consists of replicated versions of the FM spectrum at multiples of the SAT frequencies which are weighted by the Bessel functions.

Cyclic correlation coefficient ($\rho_{xx}^{\alpha}(\tau) = R_{xx}^{\alpha}(\tau)/R_{xx}(0)$) is a measure of the strength of the cyclostationary feature and $\rho_{xx}^{\alpha}(\tau)$ is maximum for a particular value

of τ. The τ that maximizes the $\rho_{xx}^{\alpha}(\tau)$ for AMPS signal is equal to $1/(2f_{sat})$. The cyclic correlation coefficient of an AMPS signal (which has a SAT frequency of 6 kHz) is measured and listed in Table 3.1. It can be seen there is a strong cyclic feature at 6 kHz and a weak feature at 12 kHz. The cyclic feature of the SOI in the presence of an interference signal is measured for different levels of CIR as shown in Figure 3.1. The SATs of the SOI and the SNOI are 6.00 and 6.03 kHz, respectively. The AMPS signal was sampled at 30 kHz and the time-bandwidth product for this measurement was 10,000. It can be seen that the cyclic correlation coefficient has deep nulls at multiples of 5 samples ($30kHz/6kHz$), and therefore there is a strong feature at 6 kHz in the cyclic spectrum. To exploit the maximum cyclic feature, the sampling rate should be chosen to be an integer multiple of the SAT frequency of the desired user. $\beta = 3$ is used in all the simulations presented in this chapter.

3.3 Spectral correlation discriminator array

Here we consider a uniform linear array (ULA) with M elements and L signals impinging onto the array. The signals are assumed to be narrowband and in the far-field of the ULA. The received signal can be modeled as

$$\mathbf{x}(t) = \sum_{i=1}^{L} d_i(t)\mathbf{a}_i(\theta_i) + \mathbf{n}(t), \tag{3.3}$$

where $\mathbf{x}$ is the input vector of size (M x 1), $d_i(t)$ is the ith signal, $\mathbf{a}_i(\theta_i)$ is the steering vector corresponding to the angle-of-arrival (θ_i), and $\mathbf{n}$(t) is the background Gaussian noise. The SATs of each signal $d_i(t)$ are assumed to be different and hence a *rank*-1 spectral self-coherence environment is assumed here. The signal $d_1(t)$ is the desired user's signal. The SCDA has finite impulse response (FIR) filters with N taps per antenna element and the output of the array is the combination of all the outputs from the FIR filters. The SCDA exploits the redundancy or the correlation between

Table 3.1: Cyclic correlation coefficient for an AMPS signal

Cycle frequency (α)	Cyclic correlation coefficient
$\alpha = 6$kHz	0.28
$\alpha = 12$kHz	0.05

spectral components. The basic idea behind the SCDA is derived from the SCORE algorithm [6]. The block diagram of the SCDA is shown in Figure 3.2. A reference signal is derived form one of the elements by

$$r(t) = \mathbf{c}^H \mathbf{x}(t-\tau) e^{j2\pi\alpha t}, \tag{3.4}$$

where H is Hermitian transpose and $\mathbf{c}$ is referred to as the control vector. If $\mathbf{c} = [0 \;\; 0 \;\; \cdots \;\; 1]$, then the reference signal is created from the output of the last antenna element. The cost function of the SCDA is

$$J = \left\langle |y(t) - r(t)|^2 \right\rangle, \tag{3.5}$$

where $\langle . \rangle$ is the time-average operation. The output of the SCDA is $y(t) = \mathbf{w}^H \mathbf{x}_1$, where $\mathbf{w}$ is the weight vector which is formed by stacking the weights of M FIR filters and hence $\mathbf{w}$ is of size $MN \times 1$. $\mathbf{x}_1$ is also formed by cascading the input signals which appear across the input to all the FIR filters and is of size $MN \times 1$. Though the SCDA cost function is very similar to the SCORE cost function, the mechanism of operation of the SCDA is very different from that of SCORE. The SCDA has frequency selective capability and it shapes the spectrum of the input signal using FIR filters. The SCDA cost function is based on minimizing an error between the frequency shifted input signal, i.e. reference signal, and the shaped input signal. The reference signal is generated by frequency shifting the input signal by the cycle frequency, i.e. the SAT frequency of the desired signal. Thus to match the output of the array to the reference signal, the FIR filters extract the sidelobes of the AMPS signal to create an AMPS signal centered around the SAT frequency.

Figure 3.3 illustrates the working principle of the SCDA. The observed signal has the SOI and the SNOI at the same carrier frequency (f_c) (corresponds to the worst case interference) and the reference signal has a spectrum centered around $f_c + f_{sat}$, where f_{sat} is the SAT frequency of the SOI. The filters $w_i(t)$, $(i = 1, .., M)$ are the FIR filters attached to M antenna elements, each w_i is of size $N \times 1$, and $\mathbf{w} = [w_1(t) \;\; w_2(t) \;\; \cdots \;\; w_M(t)]$. These filters shape the input signal to match the reference signal. The error between the output of the array and the reference signal is minimized when the estimated SOI is centered around $f_c + f_{sat}$. The error will not go to zero in the presence of the interference, but will be a distorted version of the SNOI. Since the reconstructed spectrum is centered around the SAT frequency,

the demodulated speech signal has a DC component. This DC component does not affect the speech signal. This beamformer works well for AMPS signals but will not necessarily work for digital signals. For digital signals with different cycle frequencies, the SCDA can be tuned to track the SNOI and then adaptively cancel the SNOI from the input to produce an estimate of the SOI. This approach distorts the SNOI, but the quality of the SOI at the error output is improved. The recursive least squares version of the SCDA is described below.

Algorithm description

The following is the recursive least squares implementation of SCDA.

Algorithm:

M is the number of elements in the array,
N is the number of taps in each tapped delay line,
$\mathbf{P}$ is the inverse of the correlation matrix of size [MN x MN],
$\mathbf{x}$ is the input data vector of size [MN x 1] at any time instant n,
$\mathbf{w}$ is the weight vector of size [MN x 1],
λ is the forgetting factor ≤ 1,
d is the reference signal,
and y is the output signal.

Initialize the algorithm by setting
$\mathbf{P} = \delta^{-\mathbf{1}}\mathbf{I}$, $\delta =$ small positive constant,
$\mathbf{w} = \mathbf{0}$, initial weights are set to zero.
For each instant of time, $n = 0, 1, 2, \cdots$, compute

$$\begin{aligned}
\mathbf{m} &= \mathbf{x}^H\mathbf{P} \quad \text{(Intermediate result)} \\
\mathbf{k} &= \lambda + \mathbf{m}^T.\mathbf{x} \quad \text{(Intermediate result)} \\
\mathbf{k}_1 &= \mathbf{m}^H./\mathbf{k} \quad \text{(Intermediate result)} \\
d(n) &= \mathbf{x}((L-1)N + N/2)e^{j2\pi\alpha n} \quad \text{(Desired signal creation by extracting the signal} \\
&\quad \text{from the center tap of the FIR filter corresponding to the } Lth \text{ antenna} \\
&\quad \text{and frequency shifting by the cyclic frequency)} \\
e(n) &= d(n) - y(n-1) \quad \text{(Error signal)}
\end{aligned}$$

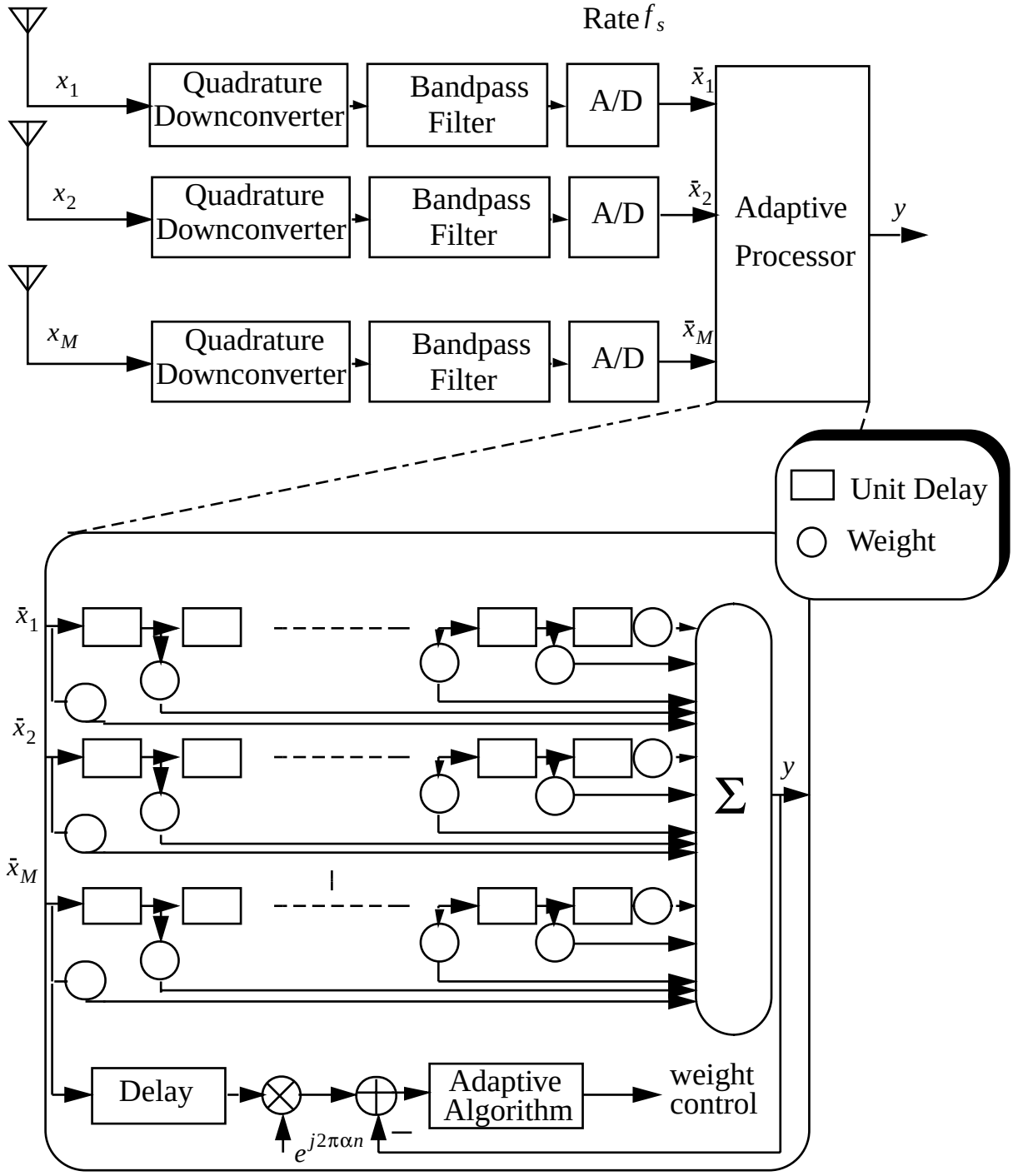

Figure 3.2: Block diagram of a M-sensor SCDA ($\alpha = f_{sat}/f_s$).

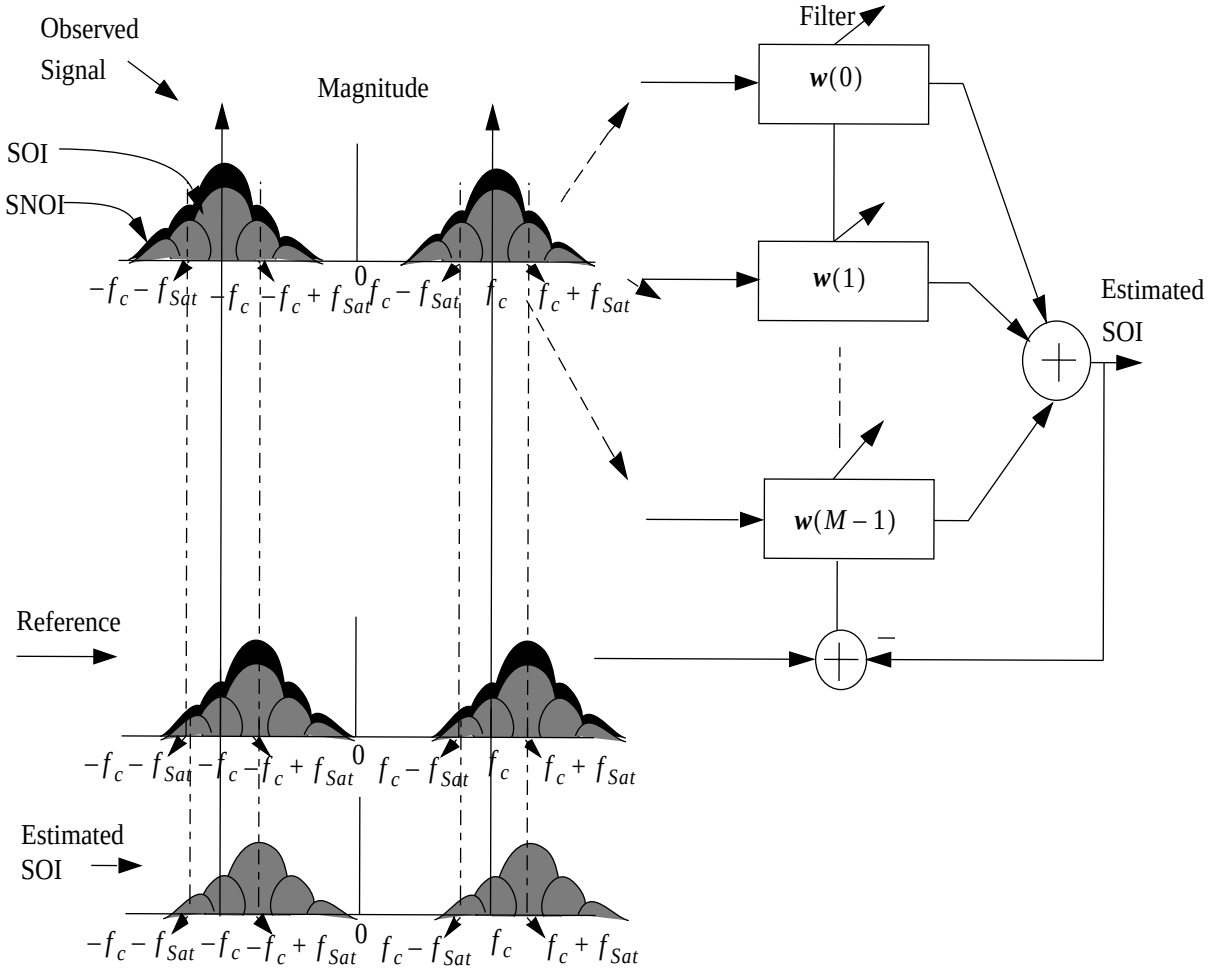

Figure 3.3: Illustration of the SCDA operation, where f_c is the carrier frequency and f_{Sat} is the frequency of the SAT of the SOI.

$$\begin{aligned}
\mathbf{P} &= \frac{1}{\lambda}(\mathbf{P} - \mathbf{k}_1\mathbf{m}) \quad \text{(Inverse correlation matrix update)} \\
\mathbf{w}_n &= \mathbf{w}_{n-1} + \mathbf{k}_1 e(n) \quad \text{(Weight update)} \\
y(n) &= \mathbf{w}^H\mathbf{x} \quad \text{(Output of the array)}
\end{aligned}$$

---

where $(.)^T$ is the transpose, $(.)^H$ is the hermitian transpose, . is the element-by-element multiplier, and ./ is the element-by-element divisor.

3.4 Asymptotic MSE analysis of the SCDA

The objective is to find $h(t,u)$, the impulse response of the filter that minimizes the mean-squared error. The asymptotic mean squared error (MSE) is defined as

$$MSE = \lim_{z\to\infty} \frac{1}{z} \int_{-z/2}^{z/2} (d_1(t) - y(t))^2 dt. \tag{3.6}$$

where $y(t)$ is the output of the array and is given by $y(t) = \int_{-\infty}^{\infty} h(t,u)x(u)du$, $x(t)$ is the input to the array, $d_1(t)$ is the SOI, and the MSE is the mean-squared error based on time averaging as opposed to an ensemble averaging. The optimal filter $h(t,u)$ contains the weights which make the gradient of the MSE with respect to the filter weights equal to zero,

$$\nabla(MSE) = 0. \tag{3.7}$$

In the SCDA the time-varying filter can be approximated as,

$$h(t,u) = [w_1(t-u), w_2(t-u), \cdots, w_M(t-u)]. \tag{3.8}$$

where $w_i(t-u)$ represents the weight vector corresponding to the element i at output time t and input time u. Considering the signal to be in the far-field of the antenna array, the output of the array is then given by

$$\begin{aligned}
y(t) &= \int_{-\infty}^{\infty} w_1(t-u)[d_1(u) + d_2(u) + \cdots + d_L(u)]du + \int_{-\infty}^{\infty} w_2(t-u)[b_{21}(u) \\
&\quad *d_1(u) + b_{22} * d_2(u) + \cdots + b_{2N} * d_L(u)]du + \cdots \int_{-\infty}^{\infty} w_M(t-u)[b_{M1}(u) * d_1(u) + \\
&\quad b_{M2} * d_2(u) + \cdots + b_{MN} * d_L(u)]du.
\end{aligned} \tag{3.9}$$

where b_{ji} is the impulse response of the channel seen by the ith signal traveling to the jth element and $*$ is the convolution operator. Let us consider the signal

undergoes only a phase shift traveling from one element to the other and therefore $b_{ji}(t) = \delta(t - \tau_i)$, where τ_i is the delay undergone by the ith signal traveling from one element to the next. The estimate of the SOI can be written as

$$\begin{aligned} y(t) &= w_1(t) * \left[\sum_{i=1}^{L} d_i(t)\right] + w_2(t) * \left[\sum_{i=1}^{L} d_i(t-\tau_i)\right] + \cdots \\ &\quad + \cdots + w_M(t) * \left[\sum_{i=1}^{L} d_i(t-(M-1)\tau_i)\right], \end{aligned} \tag{3.10}$$

or can be written as

$$y(t) = w_1(t) * x_1(t) + w_2(t) * x_2(t) + \cdots + w_M(t) * x_M(t), \tag{3.11}$$

where $x_1(t) = \sum_{i=1}^{L} d_i(t)$, and $x_2(t) = \sum_{i=1}^{L} d_i(t - \tau_i)$, and so on. Because of the narrowband assumption, the weights at each element differ by a complex constant, i.e., $w_2(t) = C_2 w_1(t)$, $w_3(t) = C_3 w_1(t), \cdots$, $w_M(t) = C_M w_1(t)$, where $C_2, C_3, \cdots, C_M$ are complex constants ($C_1 = 1$). The estimate can be written as

$$y(t) = \sum_{j=1}^{M} C_j \left[w_1(t) * x_j(t)\right]. \tag{3.12}$$

The gradient of the error for a particular coefficient of the time-varying filter is given by

$$\nabla = \int_{-\infty}^{\infty} \lim_{z\to\infty} \frac{-2}{z} \int_{-z/2}^{z/2} (d_1(t) - y(t))x^*(t-u)dtdu. \tag{3.13}$$

Setting the gradient to zero,

$$\lim_{z\to\infty} \frac{1}{z} \int_{-z/2}^{z/2} (d_1(t) - y(t))x^*(t-u)dt = 0, \text{for all } u. \tag{3.14}$$

Therefore,

$$\lim_{z\to\infty} \frac{1}{z} \int_{-z/2}^{z/2} (d_1(t)x^*(t-u))dt = \lim_{z\to\infty} \frac{1}{z} \int_{-z/2}^{z/2} (y(t)x^*(t-u))dt. \tag{3.15}$$

The right-hand side of Eqn. 3.15 can be written as

$$\sum_{j=1}^{M} C_j \left[w_1(u) * R_{x_j}(u)\right], \tag{3.16}$$

where $R_{x_j}(u) = \lim_{z\to\infty} \frac{1}{z} \int_{-z/2}^{z/2} (x(t)x^*(t-u))dt$. The left-hand side of Eqn. 3.15 is $R_{d_1 x}(u)$, therefore Eqn. 3.15 becomes

$$R_{d_1 x}(u) = \sum_{j=1}^{M} C_j \left[w_1(u) * R_{x_j}(u)\right]. \tag{3.17}$$

Transforming the above equation to the frequency domain,

$$S_{d_1x}(f) = \sum_{j=1}^{M} C_j W_1(f) S_{x_j}(f), \tag{3.18}$$

where $S_{d_1x}(f)$ is the *cross power spectral density function* of d_1 and x, $W_1(f)$ is the Fourier transform of $w_1(u)$, and $S_{x_j}(f)$ is the power spectral density (PSD) of the signal x_j.

Eqns. 3.17, 3.18 are the *design equations* in the time and the frequency domains, respectively.

The asymptotic mean-squared error is obtained by substituting Eqn. 3.14 in Eqn. 3.6,

$$MSE = \lim_{z\to\infty} \frac{1}{z} \int_{-z/2}^{z/2} (d_1(t) - y(t)) d_1^*(t) dt. \tag{3.19}$$

Substituting Eqn. 3.12 in Eqn. 3.19, MSE is given by

$$MSE = R_{d_1}(0) - \int_{-\infty}^{\infty} \left[\sum_{j=1}^{M} C_j w_1(u) * R_{d_1x_j}(u) \right] du. \tag{3.20}$$

where $R_{d_1}(0)$ is power of the desired signal, $R_{d_1x_j}(u)$ is the crosscorrelation function of the desired signal and x_j. Eqn. 3.19 can be reduced to

$$\begin{aligned} MSE &= R_{d_1}(0) - \int_{-\infty}^{\infty} \left[\sum_{j=1}^{M} C_j \right] w_1(u) * R_{d_1x_1}(u) du & (3.21) \\ &= R_{d_1}(0) - K \int_{-\infty}^{\infty} w_1(u) * R_{d_1x_1}(u) du, & (3.22) \end{aligned}$$

where $K = \sum_{j=1}^{M} C_j$. In the frequency domain, MSE is given by

$$MSE = \int_{-\infty}^{\infty} \left[S_{d_1}(f) - K W_1(f) S_{d_1x_1}(f) \right] df, \tag{3.23}$$

where $S_{d_1}(f)$ is the PSD of the desired signal and $S_{d_1x_j}(f)$ is the cross power spectral density function of d_1 with x_j. The asymptotic optimal MSE can be calculated using Eqn. 3.22 or 3.23 by substituting the vector $C = \mathbf{a_1}(\theta_\mathbf{1})$, i.e., the steering vector of the SOI. The weight vector can be computed from the design equations 3.17, 3.18. In Section 3.5, we evaluate the optimal MSE and compare with the simulation results. To compute the theoretical MSE, we use a measured quantity for $R_{d_1x_1}(u)$.

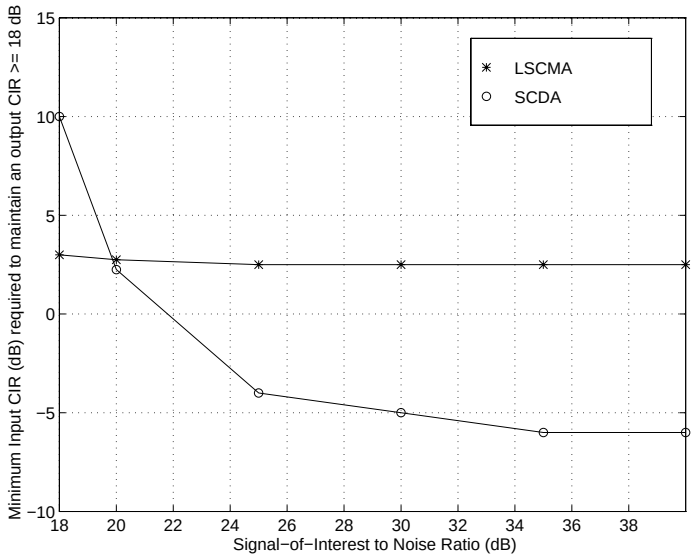

Figure 3.4: Minimum input carrier to interference ratio (CIR) required to maintain an output CIR $\geq$ 18 dB as a function of input signal-of-interest to noise ratio.

3.5 Numerical results

Simulations results are presented in this Section. Complex baseband AMPS signals are simulated and sampled at 30 kHz. The SOI has a SAT at 6.00 kHz and the SNOI's SAT is at 6.03 kHz. A ULA with two elements and a spacing of $\lambda/2$ is used in all the simulations. All sensors are assumed to be ideal and have an omnidirectional radiation pattern. The SCDA has 10 taps (to include two lobes of the cyclic autocorrelation function) in each of its antenna elements and is implemented as explained in Section 3.3. The reference signal for the SCDA is created by frequency shifting *one* of the antenna outputs. The performance of the SCDA is tested in static and dynamic multipath channels. The enhanced signal selectivity feature of the SCDA is demonstrated by comparing the performance of the SCDA with the least-squares constant modulus array (LSCMA) [34].

Table 3.2: AOAs of the Two Ray Multipath Channel

Multipath component	AOA in degrees
SOI component 1	120
SOI component 2	130
SNOI component 1	30
SNOI component 2	20

3.5.1 Interference rejection performance comparison of the SCDA with the LSCMA

In this Section, the interference rejection capability of the SCDA and the LSCMA is compared for different input noise conditions. The interference rejection capability of the SCDA is dependent on the input signal-to-noise ratio (SNR). This is because the lower the noise level the higher the sidelobes of the signal with respect to the noise floor and hence reconstruction of the signal is improved. In this test case, the angle-of-arrival (AOA) of the SOI is 120° and the SNOI is 30°. The signal-of-interest to noise ratio is varied from 18 to 40 dB. The minimum input CIR (MIC) required to maintain the output CIR of 18 dB is calculated for the SCDA and the LSCMA. Results for both the SCDA and the LSCMA arrays are depicted in Figure 3.4. It can be seen that as the input SNR increases the MIC required by the SCDA improves and drops to a minimum of -6 dB, but for a LSCMA the MIC remains around 2.5 dB irrespective of the SNR. This is because the LSCMA will capture the interferer when operated in the negative input CIR conditions as illustrated in Section 3.5.4.

3.5.2 Performance of SCDA in static multipath channels

The SCDA is tested in four different multipath channel conditions. The static channels investigated include two ray and four ray channels with and without delay between the multipath components. The average power of the multipath components are equal to the average power of the direct component. The AOA of the multipath components are assumed to be fixed.

Table 3.3: AOAs of the Four Ray Multipath Channel

Multipath component	AOA in degrees
SOI component 1	120
SOI component 2	110
SOI component 3	100
SOI component 4	90
SNOI component 1	30
SNOI component 2	35
SNOI component 3	40
SNOI component 4	10

Two ray multipath channel

In the first test case there is no delay between the multipath components. The AOAs of the two rays are listed in Table 3.2. The cumulative distribution function[4] (CDF) of the output SINR at the output of the array is used as the performance measure. Three different SINR conditions are considered and the performance curves comparing a single omnidirectional antenna with the SCDA are shown in Figure 3.5. The solid curves from left to right are the CDF curves obtained using a single omnidirectional antenna corresponding to three different input SINR conditions and the dotted curves are the SCDA results. A two-element SCDA provides approximately 25 to 30 dB improvement in the output SINR compared to a single omnidirectional antenna. The next test case involves a two ray channel with the multipath component delayed by $33\mu s$ with respect to the main component and the AOAs are the same as above. The performance improvement in this case is approximately 18 to 23 dB. The results are depicted in Figure 3.6. Based on these simulations, there is degradation of approximately 5 dB in a delay spread environment.

Four ray multipath channel

The channel is modeled to have four multipath components in the third test case and there is zero delay between the multipaths. The AOAs of the four rays are listed in

[4]The output SINR is measured for short segments of the signal (say 100 samples) after the algorithm has converged and the cumulative distribution function of the SINR is used as the performance measure.

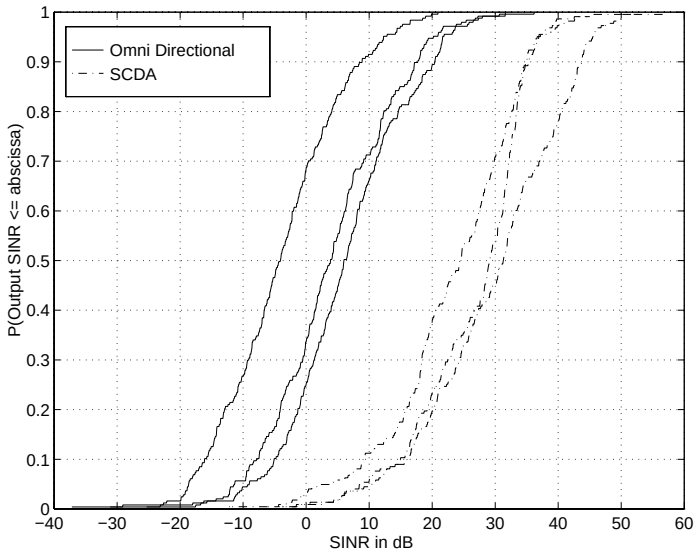

Figure 3.5: Cumulative probability density function of the output SINR in a two ray static multipath channel with zero delay between the multipaths. From left to right the solid curves correspond to the CDF curves of a single omni-directional antenna with mean input SINRs of -5, 4, and 6 dB. The dotted lines from left to right are the CDF curves of the output SINR of the SCDA.

Table 3.3. The output SINR CDF curve for this test case is plotted in Figure 3.7. The two-element SCDA provides 25 to 30 dB SINR improvement over an omnidirectional antenna. In a delay spread environment the channel is modeled to have four rays and the multipath components have relative delays of 33, 66, and 99 μs with respect to the main component. The average power of the delayed components are the same as the direct component. The output SINR CDF curves are shown in Figure 3.8 and the improvement varies from 15 to 25 dB depending on the input SINR. The performance of a two-element SCDA has degraded significantly in the presence of delayed multipath components.

3.5.3 Performance of the SCDA in dynamic multipath channels

In this Section the performance of the two-element SCDA in a dynamic mobile channel is discussed. The channel is modeled to have four rays with delays of 33, 66, and 99 μs with respect to the main component. Each ray is modeled as having independent

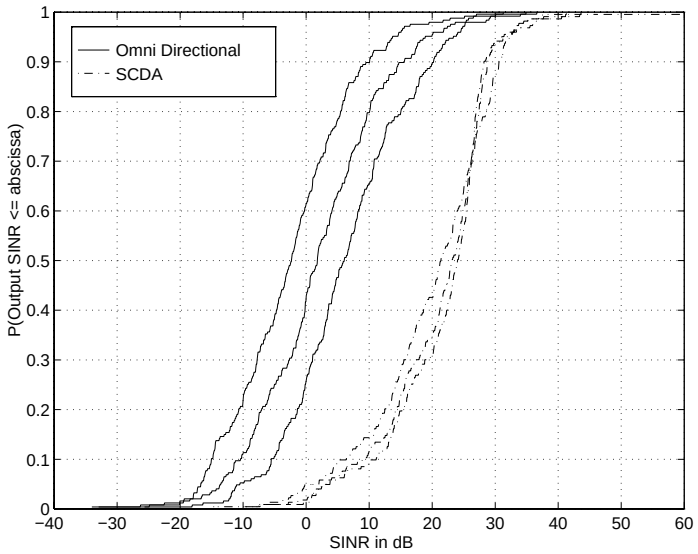

Figure 3.6: Cumulative probability density function of the output SINR in a two ray static multipath channel with $33\mu s$ delay with respect to the direct component. From left to right the solid curves correspond to the CDF curves of a single omni-directional antenna with mean input SINRs of -2, 2, and 6 dB. The dotted lines from left to right are the CDF curves of the output SINR of the SCDA.

Rayleigh fading with Doppler frequency of 10 Hz. The Doppler spectrum is obtained using Clarke's model [59]. The channel is said to be *frequency-selective* in nature. The average power of the delayed components are the same as the direct component. The two-element SCDA in a frequency selective Rayleigh fading channel gives an improvement of only 5 dB over a single omni-directional antenna. This is because, if the output signal of the antenna element from which the reference signal is created is in a deep fade, then the quality of the estimated signal is poor. A modified SCDA is proposed in Figure 3.9 for the fading environments. The modified SCDA has an equal gain combiner in its reference path. The signals from the output of the antenna elements are combined and the output of the combiner is frequency shifted by the cycle frequency and used as the reference signal. The modified SCDA performs 7 dB better than the SCDA. The output SINR CDF curves for both these structures are shown in Figure 3.10. The reason behind this improvement is due to the following: if one of the element is in a deep fade, then the probability that the other element is also in a fade is very small (if the correlation coefficient of the signals at different antenna elements is low). Thus the modified SCDA provides resistance towards multipath and

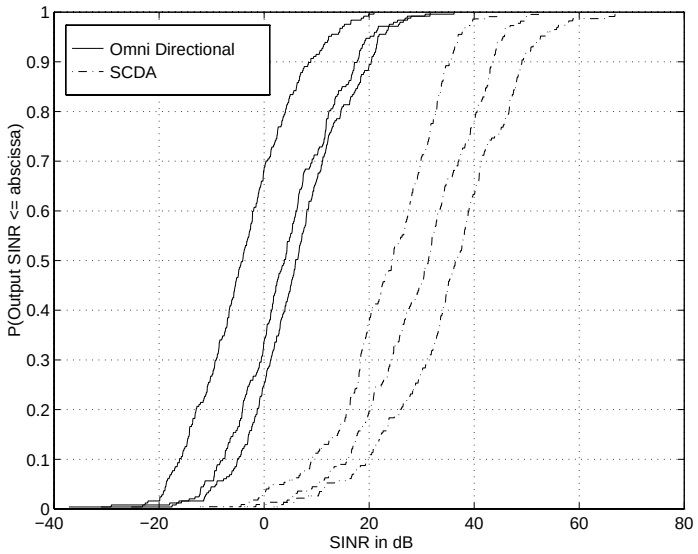

Figure 3.7: Cumulative probability density function of the output SINR in a four ray static multipath channel with zero delay between the mutipaths. From left to right the solid curves correspond to the CDF curves of a single omni-directional antenna with mean input SINRs of -5, 4, and 6 dB. The dotted lines from left to right are the CDF curves of the output SINR of the SCDA.

interference.

3.5.4 Signal selectivity performance comparison of the SCDA with the LSCMA

In this section the enhanced signal selectivity of the SCDA is demonstrated and compared to the LSCMA [34]. The performance of a two-element LSCMA is compared with that of a two-element SCDA in a negative CIR environment.The channel is modeled as a static multipath channel having four rays and the multipath components have delays of 33, 66, and 99 μs with respect to the main component. The average power of the delayed components are the same as the direct component. The mean input SINR is -3 dB and the output SINR performance curves for the SCDA, the LSCMA and a single omnidirectional antenna are plotted in Figure 3.11. It can be seen that the LSCMA is captured by the interferer and the mean output SINR of the LSCMA is -10 dB, while the SCDA selects the SOI with the SAT at 6.00 kHz. The SCDA provides an improvement of nearly 30 dB over a single omnidirectional

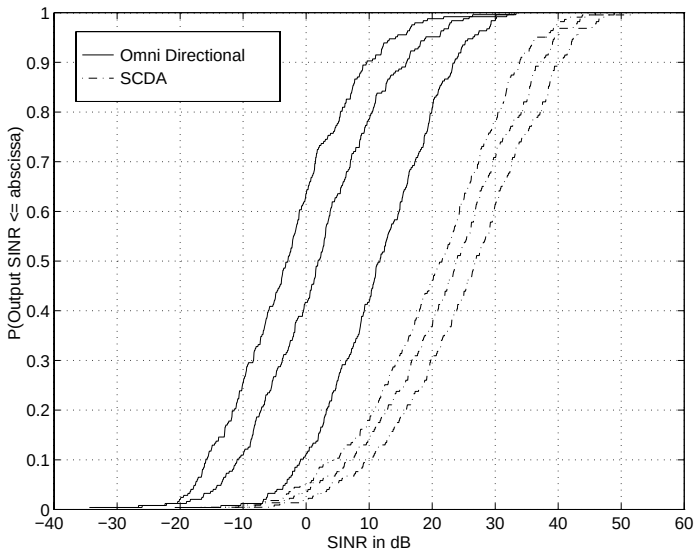

Figure 3.8: Cumulative probability density function of the output SINR in a four ray static multipath channel with relative delays of $33\mu s$, $66\mu s$, and $99\mu s$ with respect to the direct component. From left to right the solid curves correspond to the CDF curves of a single omni-directional antenna with mean input SINRs of -3, 2, and 11 dB. The dotted lines from left to right are the CDF curves of the output SINR of the SCDA.

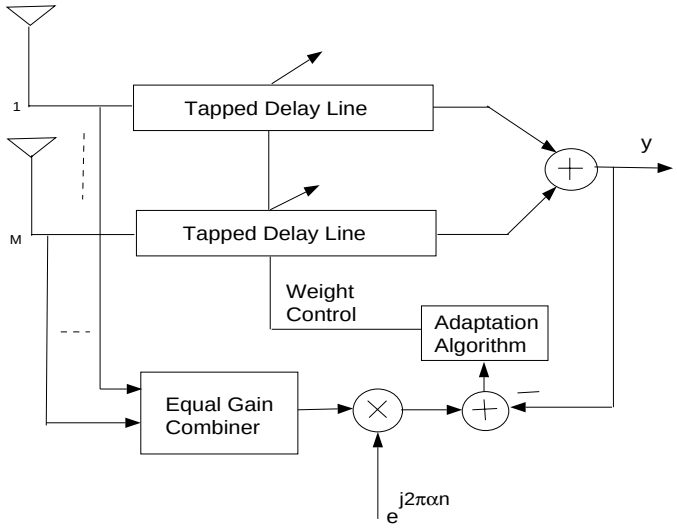

Figure 3.9: Modified SCDA to combat fading.

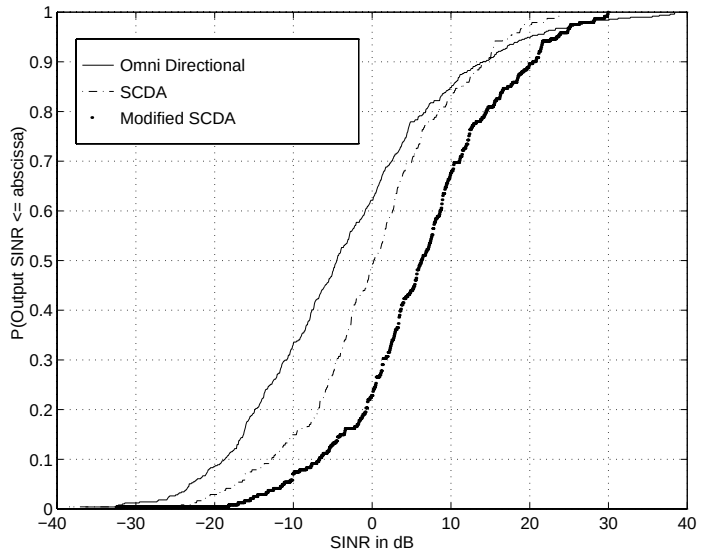

Figure 3.10: Cumulative probability density function of the output SINR in a four ray dynamic multipath channel with relative delays of $33\mu s$, $66\mu s$, and $99\mu s$ with respect to the direct component. Each multipath has independent Rayleigh fading on it.

antenna. But by using the MT-LSCMA, the SOI and the SNOI can be separated, but the MT-LSCMA requires adaptation of two beamformers at the same time.

3.5.5 Performance of SCDA in the presence of two interferers and in a two ray multipath channel

In this subsection, we study the performance of the SCDA in the presence of two interferers. The SATs of the two interferers are different from the desired user's SAT. Consider four test cases where the AOAs of the signals are varied. In all test cases and for all of the signals, a two ray static multipath channel is assumed and the second component arrives 5 μsecs after the direct component. The AOAs for these test cases are listed in Tables 3.4, 3.5, 3.6, and 3.7. The average power of the direct component is assumed to be the same as the delayed component and the power of all interfering direct components are equal. The desired signal has the SAT at 6.00 kHz, and the interferers # 1 and # 2 have SATs at 6.03 kHz and 5.97 kHz, respectively. The output SINR CDF curves for the test cases # 1 and # 2 are plotted in Figure 3.12. The solid line is the output SINR CDF curve using an omnidirectional antenna

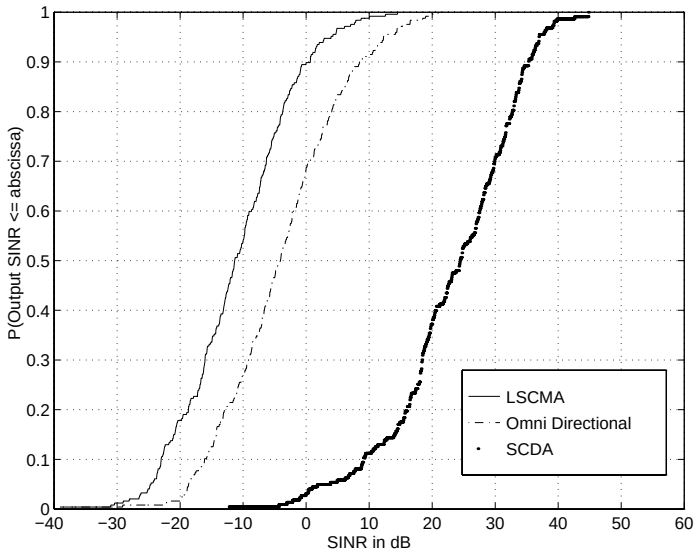

Figure 3.11: Comparison of cumulative probability density function of the output SINR for LSCMA, SCDA, and omni-directional antenna. Input mean SINR is -3dB and the channel has four multipaths with relative delays of $33\mu s$, $66\mu s$, and $99\mu s$.

Table 3.4: AOAs of the signals in degrees from 3 users in a Two Ray Multipath Channel (Test Case # 1)

Component	SOI	SNOI # 1	SNOI # 2
Direct	90	92	88
Delayed	91	93	89

Table 3.5: AOAs of the signals in degrees from 3 users in a Two Ray Multipath Channel (Test Case # 2)

Component	SOI	SNOI # 1	SNOI # 2
Direct	90	95	100
Delayed	91	96	101

Table 3.6: AOAs of the signals in degrees from 3 users in a Two Ray Multipath Channel (Test Case # 3)

Component	SOI	SNOI # 1	SNOI # 2
Direct	0	5	-5
Delayed	1	6	-6

Table 3.7: AOAs of the signals in degrees from 3 users in a Two Ray Multipath Channel (Test Case # 4)

Component	SOI	SNOI # 1	SNOI # 2
Direct	0	5	10
Delayed	1	6	12

for these two cases. The dotted line is the output SINR CDF curve for test case # 1 and the line with crosses is the output SINR CDF curve for test case # 2. The cochannel users are located within an angular separation of 4 degrees in test case #1, while in the second test case, the cochannel users are located within an angular separation of 10 degrees. The performance gain of the SCDA decreases as the angular separation between the desired signal and the interferers is reduced and there is a 12 dB difference in performance between test cases # 1 and # 2. In the third and the fourth test cases, different set of AOAs are considered for the cochannel users. The results for these test cases are plotted in Figure 3.13. The maximum angular separation between the cochannel users is the same in both the test cases. In test case # 3, the interferers are spatially separated from the desired user by 5 degrees, while in the test case # 4, the second interferer is moved 10 degrees away from the desired user's AOA. The output SINR improves approximately 6 dB due to the change in the SNOI's AOA.

3.5.6 Convergence characteristics of the SCDA

In this subsection, we discuss the convergence characteristics of the SCDA and compare the theoretical MSE developed in Section 3.4 with the simulated MSE. A two element ULA is used and only one interferer is considered. The AOAs of the SOI

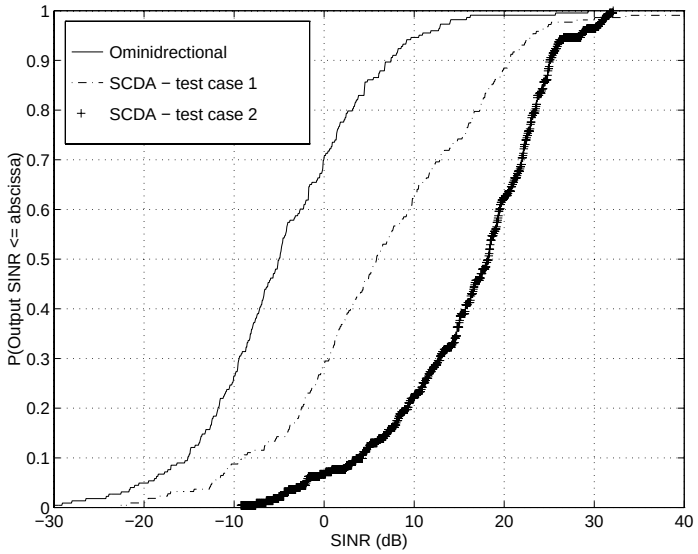

Figure 3.12: Cumulative probability density function of the output SINR in a two ray static multipath channel with a delay of 5 μsecs between the mutipaths.

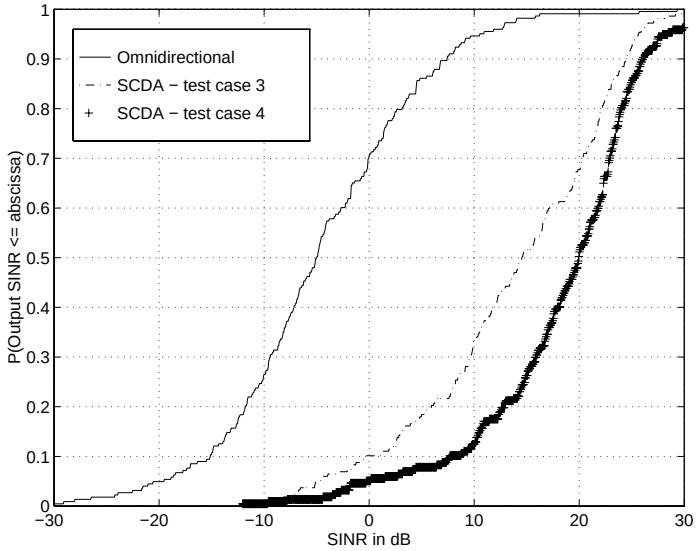

Figure 3.13: Cumulative probability density function of the output SINR in a two ray static multipath channel with a delay of 5 μsecs between the mutipaths.

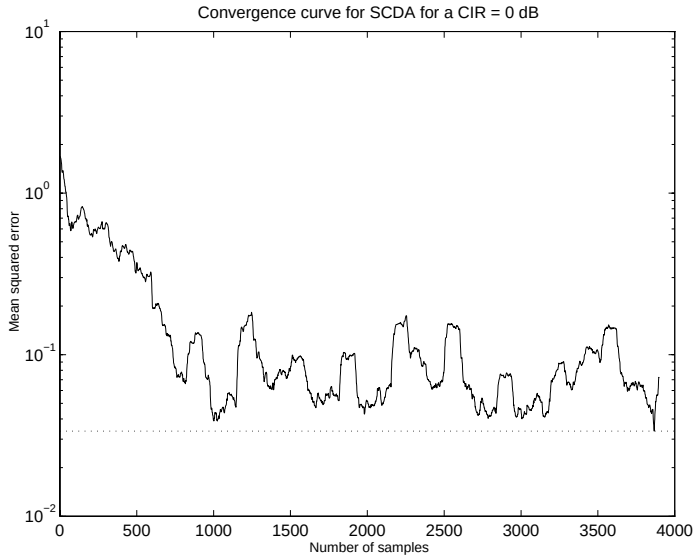

Figure 3.14: Convergence curves for the SCDA for CIR = 0.

and the SNOI are 120 and 30 degrees, respectively. The noise is 20 dB below the power of the SOI and two cases for the CIR are considered (CIR=0, 6 dB). The MSE convergence curve for CIR = 0dB is shown in Figure 3.14 and for CIR = 6 dB in Figure 3.15. The dotted line shows the minimum MSE that can be achieved based on Eqn. 3.22. As expected, the SCDA for the CIR=6 dB case achieves an MSE lower than the CIR=0 dB case. Also the convergence is slightly faster than the CIR=6 dB case. The MSE performance of the SCDA approaches the optimum MSE by 2.5 dB.

3.6 Conclusion

In this chapter we analyzed the performance of the spectral correlation discrimination array (SCDA) introduced in [7]. The SCDA is a blind adaptive array technique applicable to mitigating interference in the AMPS signal environment. The mean square error analysis for the SCDA is presented. Cochannel interference rejection for AMPS signals using this novel array has been tested in different mobile radio channel conditions. The interference rejection capability of the SCDA improves as the power of the noise decreases. It was shown that the SCDA can provide 20-30 dB improvement in SINR under static channel conditions and 10-15 dB under dynamic

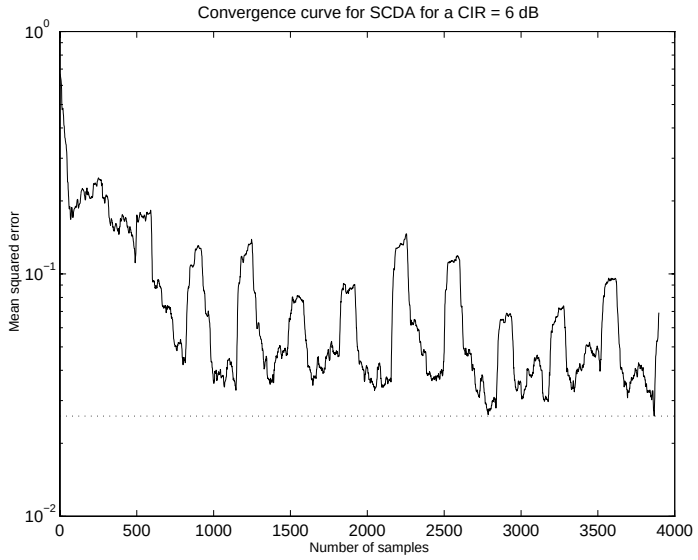

Figure 3.15: Convergence curves for the SCDA for CIR = 6 dB.

fading channel conditions. A modified SCDA has been proposed in this chapter to combat fading. The SCDA has been shown to have better signal selectivity properties as compared to the LSCMA and can maintain toll quality speech at the output of the demodulator even if the input CIR is -6 dB.

Chapter 4

Evaluation of Outage Probability Due to Cochannel Interference in Fading for an AMPS System With a Beamformer

4.1 Introduction

Outage probability calculation for an AMPS system when using an omnidirectional antenna at the base station has been adequately addressed in the literature. Muammar and Gupta [60] have derived the probability of cochannel interference in Rayleigh and log-normal fading. Based on these results, they calculated the reuse distance and the cluster size. Yeh and Schwartz [61] calculated the outage probability due to multiple cochannel log-normal interferers for both the forward and the reverse links. An important result from this paper is that the outage probabilities for the forward and the reverse links do not differ significantly. Sowerby and Williamson [62] also calculated the outage probability for a Rayleigh fading channel, based on an analytical method using a recursive process. Heeralall and Hughes [63] proposed novel sectorized patterns for high capacity cellular systems and calculate the outage probability using directional antennas. The results in [63] are mostly simulation based.

The focus of this Chapter is to evaluate the outage probability due to cochannel interference for the existing AMPS cellular system when a beamformer is employed.

Two beamformers are considered, an ideal and a flat-top beamformer. The performance of the beamformers is compared with the performance obtained using an omnidirectional antenna. This chapter is organized as follows. In Section 4.2, an overview of the calculation of the outage probability for an ideal beamfomer is presented. In Section 4.3, we characterize the angle-of-arrival (AOA) for a cochannel interferer at the base station of the desired cell. Outage calculation for an ideal beamformer is discussed in Section 4.4. Outage probability calculation for a flat-top beamformer is discussed in Section 4.5. Section 4.6 examines numerical results for outage probability based on exploiting spatial diversity. The results take into account environmental conditions. Section 4.7 presents the conclusions.

4.2 Overview of carrier to interference ratio evaluation for an ideal beamformer at the base station

The main goal of this chapter is to evaluate the probability of outage due to cochannel interference using a beamformer at the base station. In Sections 2 through 4, the probability of outage is determined under the condition that the desired mobile's signal is received by an ideal beamformer. In Section 4.5, the results will be extended to a flat-top beamformer. An ideal beamformer is assumed to have a flat beam of beamwidth, $\Delta\theta$, with unity gain and with zero sidelobe gain. A flat-top beamformer, shown in Figure 4.1, has a flat main beam of beamwidth, $\Delta\theta$, with unity gain and a flat sidelobe with a gain of A, where $A < 1$. The probability of outage is defined as the probability that the carrier to interference ratio (CIR) is below a specified value. The outage probability depends on the following two factors when an ideal beamformer is used at the base station.

1. The probability that the desired user and the interferer lie within an angular separation of $\Delta\theta$, the beamwidth of the ideal beamformer.

2. The power ratio between the desired signal and the interference if the desired user and the interferer lie within the beam.

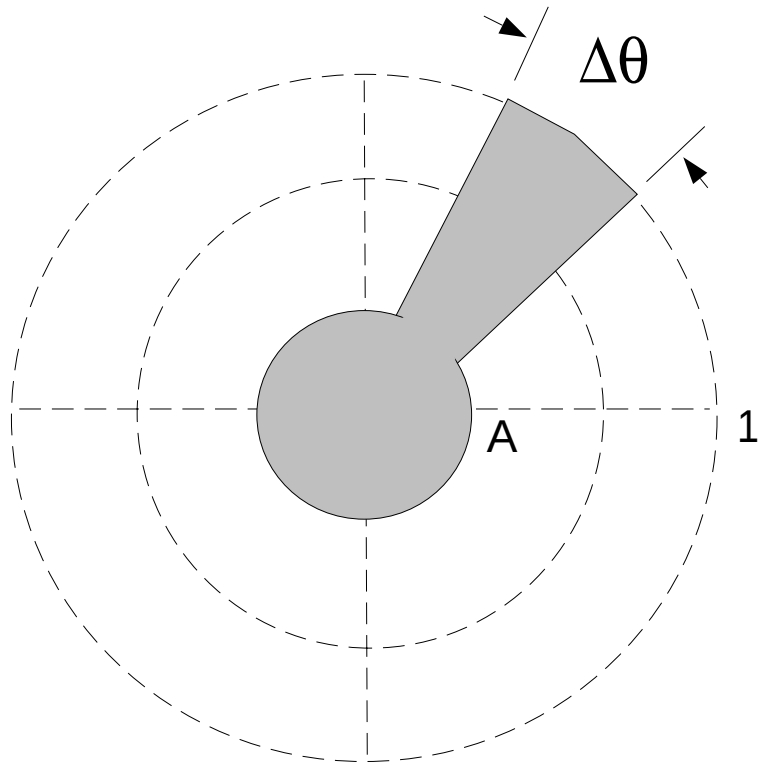

Figure 4.1: Beam pattern of a flat-top beamformer with a beamwidth of $\Delta\theta$ and a sidelobe level of A, where $0 < A \leq 1$. If $A = 0$, then an ideal beamformer results.

To compute (1), we need to calculate the probability density function (pdf) of the angle-of-arrival (AOA) for the interferer and the pdf of the AOA for the desired mobile unit. The AOA of the interferer will be characterized in Section 4.3.

4.3 Characterizing the angle-of-arrival for a cochannel interferer

In order to characterize the AOA of a cochannel interference at the base station of the desired cell, a statistical model is developed. The model is based on formulating the pdf for the AOA. For this derivation, a single line-of-sight signal path is assumed between the interferer and the base station of the desired cell. Figure 4.2 illustrates the cochannel interference condition. The desired base station is B_1 and the cochannel base station is B_2. The two base stations are separated by a distance D and the cells

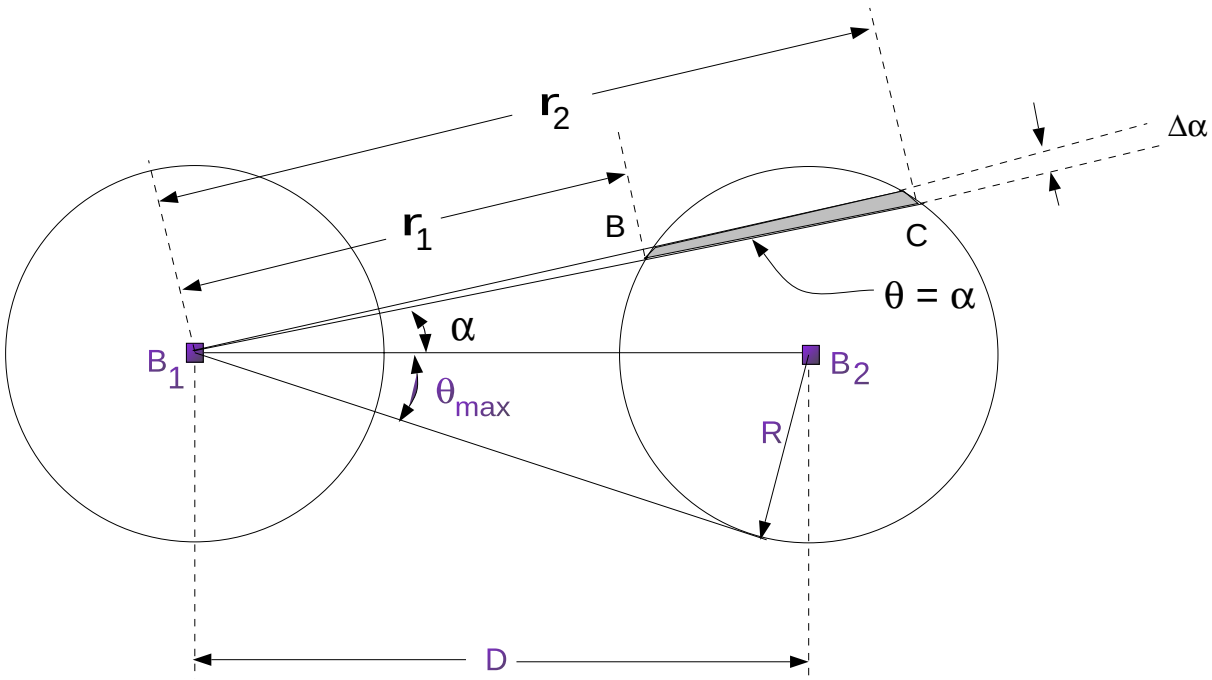

Figure 4.2: Illustration of the angle-of-arrival of the signal from the cochannel interference in an AMPS system. B_1 and B_2 are the desired and the interfering base stations, respectively.

are assumed to be circular with a radius R. The interfering mobile is equally likely to be at any location within the cell associated with the base station B_2. The goal of this derivation is to derive the pdf of θ, $f_\theta(\theta)$, where θ is the AOA of the interfering signal at the base station B_1. Since the mobile is confined within the circular cell, the AOA is restricted within a range and is specified by θ_{max}, the maximum AOA of the interfering signal, which is given by

$$\theta_{max} = sin^{-1}\left(\frac{R}{D}\right). \tag{4.1}$$

In Figure 4.2, let us consider the strip between $\theta = \alpha$ and $\theta = \alpha + \Delta\alpha$. Since the users are assumed to be uniformly distributed within the cell, the area within the strip is proportional to the probability of the AOA of the interfering signal. The AOA, $\theta = \alpha$, line meets the cell boundary around the base station, B_2, at B and at C. Let the length of the line segment $\overline{B_1B}$ be r_1 and $\overline{B_1C}$ be r_2.

The cell boundary around the base station B_2 can be expressed as

$$r^2 - 2Drcos(\theta) + D^2 - R^2 = 0. \tag{4.2}$$

From Eqn. 4.2, r can be expressed as

$$r = Dcos(\theta) \pm \sqrt{D^2cos^2(\theta) - D^2 + R^2}. \tag{4.3}$$

Therefore $r_2 = Dcos(\theta)+\sqrt{D^2cos^2(\theta) - D^2 + R^2}$ and $r_1 = Dcos(\theta)-\sqrt{D^2cos^2(\theta) - D^2 + R^2}$. Since the users are assumed to be uniformly distributed within the cell, the density of the area within the circle of radius R is given by

$$f_{area} = \frac{1}{\pi R^2}. \tag{4.4}$$

The area within the strip, A_1, formed by $\theta = \alpha$ and $\theta = \alpha + \Delta\alpha$ can be shown using calculus to be

$$A_1 = \int_{\alpha}^{\alpha+\Delta\alpha} \frac{1}{2}\left(r_2^2 - r_1^2\right) d\theta. \tag{4.5}$$

Using this result, the cumulative distribution function (cdf) of the AOA, $F_\theta(\theta)$, can be expressed as

$$\begin{aligned} F_\theta(\theta) &= \int_{-\infty}^{\theta} \frac{1}{2\pi R^2}\left(\left[Dcos(\beta) + \sqrt{D^2cos^2(\beta) - D^2 + R^2}\right]^2 - \right. \\ &\quad \left.\left[Dcos(\beta) - \sqrt{D^2cos^2(\beta) - D^2 + R^2}\right]^2\right) d\beta. \end{aligned} \tag{4.6}$$

The probability density function (pdf) of the AOA, $f_\theta(\theta)$, is the derivative of the cdf with respect to θ and is given by

$$\begin{aligned} f_\theta(\theta) &= \frac{1}{2\pi R^2}\left(\left[Dcos(\theta) + \sqrt{D^2cos^2(\theta) - D^2 + R^2}\right]^2 - \right. \\ &\quad \left.\left[Dcos(\theta) - \sqrt{D^2cos^2(\theta) - D^2 + R^2}\right]^2\right), \end{aligned} \tag{4.7}$$

which can be reduced to

$$f_\theta(\theta) = \frac{2Dcos(\theta)\sqrt{D^2cos^2(\theta) - D^2 + R^2}}{\pi R^2}. \tag{4.8}$$

Therefore the pdf of the AOA of the interfering signal is given by

$$f_\theta(\theta) = \begin{cases} \frac{2Dcos(\theta)\sqrt{D^2cos^2(\theta)-D^2+R^2}}{\pi R^2} & , \quad -sin^{-1}\left(\frac{R}{D}\right) \leq \theta \leq sin^{-1}\left(\frac{R}{D}\right) \\ 0 & , \quad otherwise. \end{cases} \tag{4.9}$$

Now we will relate θ_{max} to the reuse factor, N_1. The reuse factor is related to D, the distance between the base stations and R, the radius of the cell, by the following relationship [64],

$$\frac{D}{R} = \sqrt{3N_1}, \tag{4.10}$$

(assuming hexagonal cell geometry). Therefore each reuse factor corresponds to a particular θ_{max}. Therefore using Eqns. 4.1 and 4.10, θ_{max} can be approximated as

$$\theta_{max} \approx sin^{-1}\left[\frac{1}{\sqrt{3N_1}}\right]. \tag{4.11}$$

The pdf of the AOA can be expressed in terms of the reuse factor, N_1, as

$$f_\theta(\theta) = \begin{cases} \frac{2}{\pi}cos(\theta)\sqrt{3N_1 - 9N_1^2 sin^2(\theta)} & , \quad -sin^{-1}\left(\frac{1}{\sqrt{3N_1}}\right) \leq \theta \leq sin^{-1}\left(\frac{1}{\sqrt{3N_1}}\right) \\ 0 & , \quad otherwise. \end{cases} \tag{4.12}$$

Figure 4.3 is a plot of the pdf of the AOA of the interference for reuse factors of 3, 4, and 7. It can be seen that as the reuse factor increases, θ_{max} also increases. The θ_{max} for reuse factors of 3, 4, and 7 are 19.47, 16.77, and 12.60 degrees, respectively.

4.4 Outage calculation due to cochannel interference when using an ideal beamformer at the base station

To avoid the complexity associated with simulating an actual beamforming algorithm, the beamformer model shown in Figure 4.2 is used to estimate it's performance. The model consists of a main beam that has a uniform gain of one over it's beamwidth of $\Delta\theta$, and a uniform side lobe gain of A, where $0 \leq A \leq 1$. This section considers the outage probability for an ideal beamformer, for which the side lobe gain, A, is zero. The ideal beamformer is a reasonable model when the number of antenna elements exceeds the number of interfering signals; hence, the beamformer has enough degrees of freedom to steer nulls towards the interferers.

The probability of outage may be defined as the probability that the desired signal power S does not exceed the cochannel interference Y by the protection ratio γ. Hence, $P(\text{outage}) = P(S \leq \gamma Y)$, which is equivalent to $P(\text{CIR} < \gamma)$, where $\text{CIR} = \frac{S}{Y}$

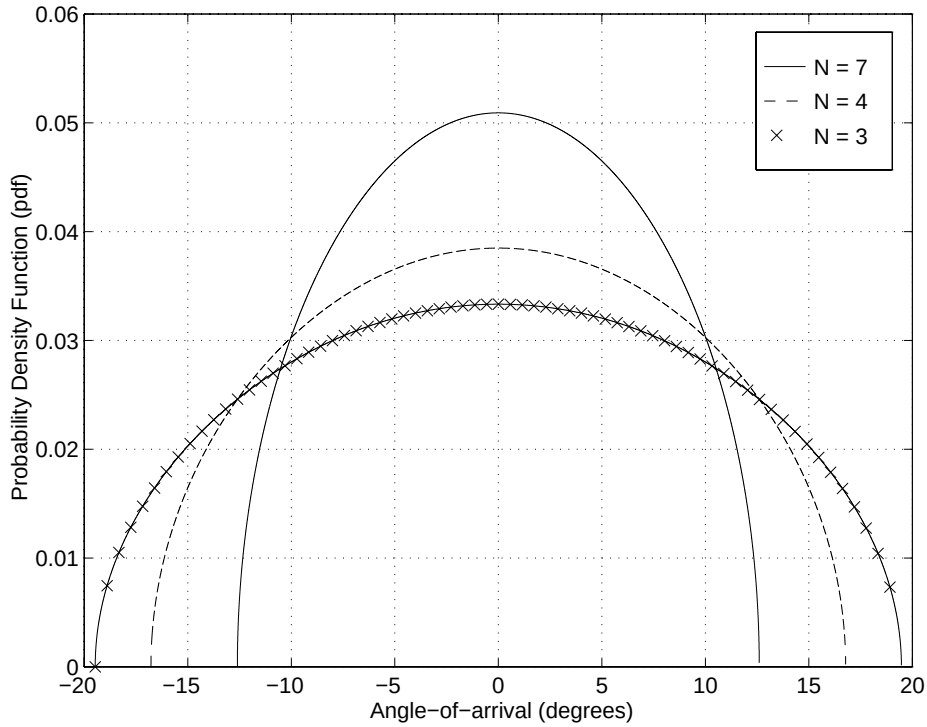

Figure 4.3: Probability of AOA of the interfering signal for reuse factors of 3, 4, and 7.

is the carrier to interference ratio [60]. For an AMPS system, the outage probability is a function of the direction the beamformer is pointing, θ, since the pointing direction determines the amount of overlap between the main beam and the cochannel cell regions. In this work, it is assumed that the beamformer is aimed directly towards the desired user which is uniformly distributed throughout the cell. To remove the dependence on pointing direction, the average probability of outage can be found by integrating the conditional probability of outage given θ times the probability that the desired user is in the direction of θ over the range $[0, 2\pi]$, i.e.,

$$P(\text{outage}) = P(\text{CIR} < \gamma) = \int_0^{2\pi} P(\text{CIR} < \gamma|\theta)P(\theta)d\theta = \frac{1}{2\pi}\int_0^{2\pi} P(\text{CIR} < \gamma|\theta)d\theta. \tag{4.13}$$

The conditional probability, $P(\text{CIR} < \gamma|\theta)$ is a function of the probability that n interferers are present. Clearly when the number of interferers increases, the interference power increases, which causes a corresponding increase in the outage probability.

Using total probability, the conditional probability of outage given θ may be expressed as,

$$P(\text{CIR} < \gamma|\theta) = \sum_{n=1}^{N} P(\text{CIR} < \gamma|n)P(n|\theta), \tag{4.14}$$

where $P(n|\theta)$ is the probability that n interference signals are present inside the main beam, when the beam is pointed in the direction of θ. Substituting Eqn. 5.1 into Eqn. 4.14, changing the order of integration and summation, and then taking the terms that do not depend upon θ outside of the integral gives,

$$P(\text{CIR} < \gamma) = \sum_{n=1}^{N} P(\text{CIR} < \gamma|n) \cdot \frac{1}{2\pi} \int_{0}^{2\pi} P(n|\theta) d\theta. \tag{4.15}$$

Finally, denoting the average probability of n interferers over θ as $P_{avg}(n)$, the outage probability may be expressed as,

$$P(\text{CIR} < \gamma) = \sum_{n=1}^{N} P(\text{CIR} < \gamma|n) \cdot P_{avg}(n), \tag{4.16}$$

where

$$P_{avg}(n) = \frac{1}{2\pi} \int_{0}^{2\pi} P(n|\theta) d\theta. \tag{4.17}$$

The conditional probability, $P(\text{CIR} < \gamma|n)$ was considered in [60] for the case when both the desired user and interference have Rayleigh fading envelopes. In [60], it was shown that when the total interference is given by $Y = \sum_{i=1}^{N} y_i$, where y_i are interference signals which are independent identically distributed with a mean m_y and variance σ_y^2, then the conditional probability of outage given n interferers can be approximated by,

$$P(\text{CIR} \leq \gamma|n) = \sqrt{\frac{\pi}{8\sigma_Y^2}} \int_{0}^{\infty} \int_{0}^{\gamma Y} \frac{S}{10^{M_d/10}} \exp\left(-\frac{\pi S^2}{4 \times 10^{M_d/10}}\right) exp\left(-\frac{(Y - M_Y)^2}{2\sigma_Y^2}\right) dS dY, \tag{4.18}$$

where σ_Y^2 is the variance of the total interference, M_d is the mean power of the desired user in dB, M_y is the mean power of the total interference in dB, and γ is the required protection ratio. The mean and variance of the total interference may be expressed in terms of the mean and variance of the individual interferers as,

$$M_Y = n \exp\left(\frac{m_y}{2C}\right)$$

and

$$\sigma_Y^2 = n \exp\left(\frac{m_y}{C}\left[\frac{4}{\pi} - 1\right]\right),$$

respectively, where $C = 10/log_e 10 = 4.343$.

The integral in Eqn. 4.18 over S is easily performed using variable substitution. The resulting single integral becomes,

$$P(CIR < \gamma|n) = \frac{1}{\sqrt{2\pi\sigma_Y^2}} \int_0^\infty \left[1 - \exp\left(\frac{-\pi\gamma^2 Y^2}{4 \times 10^{M_d/10}}\right)\right] \exp\left(-\frac{(Y - M_Y)^2}{2\sigma_Y^2}\right) dY \tag{4.19}$$

which may be expressed as

$$P(CIR < \gamma|n) = \frac{1}{2}\text{erfc}\left(\frac{-\lambda}{\sqrt{2}}\right) - \frac{1}{\sqrt{8a}} \exp\left(\frac{\lambda^2(1-2a)}{4a}\right) \text{erfc}\left(\frac{-\lambda}{2\sqrt{a}}\right) \tag{4.20}$$

where $\lambda = \frac{M_Y}{\sigma_Y}$, $a = \frac{\pi\gamma^2\sigma_Y^2}{4\times 10^{M_d/10}} + \frac{1}{2}$, and $\text{erfc}(x) = \frac{2}{\sqrt{\pi}} \int_x^\infty e^{-v^2} dv$ is the well known complementary error function.

Next, the average probability of n interferers, $P_{avg}(n)$ must be found. In this work, only the first tier of interferers is considered. Let N denote the number of interfering cells in the first tier. For a given value of θ the probability that a particular user is causing interference is equal to the product of the probability that the user is within the main beam and the probability that the user is active. The probability that the ith user is within the main beam is equal to

$$P(\theta - \Delta\theta/2 < \theta_i < \theta + \Delta\theta/2) = \int_{\theta-\Delta\theta/2}^{\theta+\Delta\theta/2} f_{\theta_i}(\alpha) d\alpha, \tag{4.21}$$

where θ is the angle to the center of the main beam, $\Delta\theta$ is the beamwidth, and $f_{\theta_i}(\alpha)$ is the AOA pdf for the ith interferer. Multiplying this quantity by the activity level p, the probability that a given user is active, gives the probability that the user is causing interference, i.e, the user is within the main beam and is active.

Let $P_i, i = 1, 2, \cdots, N$, denote the probability that the user in the ith cell is causing interference. The probability that n out of the possible N users are causing interference is given by the sum of all possible products of the probability that n users are interfering by the probability that the remaining $N - n$ users are not interfering. For example, for $N = 3$, the probability that there is only one interferer is given by $P(n = 1) = P_1(1 - P_2)(1 - P_3) + (1 - P_1)P_2(1 - P_3) + (1 - P_1)(1 - P_2)P_3$.

However, taking all possible combinations is not required since there is a maximum of four unique probabilities for a given value of θ, corresponding to the four different amounts of overlap of the main beam with the cells. At most, two cells will be partially contained within the beam, while the other cells are either completely inside the beam, or are entirely outside of the beam. Without loss of generality, let the order of the probabilities be such that $P_1 \leq P_2 \leq P_3 \cdots \leq P_N$. If there are K cells that are at least partially contained within the beam, then there will be K nonzero probabilities, $P_1, P_2, \cdots, P_K$, that correspond to the probability that the ith user is causing interference.

With the conditions set on P_i, if there are two partially overlapped cells, then P_1 and P_2 will be the corresponding probabilities. The remaining probabilities, $P_3, P_4, \cdots, P_K$ will be equal to the activity level, p, since for cells completely contained within the beam, the probability that the user is within the beam is one. For the case of three or less unique nonzero probabilities, the following relationships hold:

$$P(0) = \begin{cases} 1 - P_1 & : \quad K = 1 \\ (1-P_1)(1-P_2) & : \quad K = 2 \\ (1-P_1)(1-P_2)(1-P_3)^{K-2} & : \quad K \geq 3 \end{cases}$$

$$P(1) = \begin{cases} P_1 & : \quad K = 1 \\ P_1(1-P_2) + (1-P_1)P_2 & : \quad K = 2 \\ P_1(1-P_2)(1-P_3)^{K-2} + (1-P_1)P_2(1-P_3)^{K-2} + C_1(1-P_1)(1-P_2) & : \quad K \geq 3 \end{cases}$$

$$P(n) = \begin{cases} 0 & : \quad K = 1, n \geq 2 \\ P_1 P_2 & : \quad K = 2, n \geq 2 \\ C_2 P_1 P_2 + C_3[P_1(1-P_2) + (1-P_1)P_2] + C_4(1-P_1)(1-P_2) & : \quad K \geq 3, n \geq 2 \end{cases} \tag{4.22}$$

where,

$$C_1 = \begin{cases} P_3 & : \quad K = 3 \\ (K-2)P_3(1-P_3)^{K-3} & : \quad K \geq 4, \end{cases}$$

$$C_2 = \begin{cases} P_3^{n-2} & : \quad K = n \\ \frac{(K-2)!}{(n-2)!(K-n)!} P_3^{n-2}(1-P_3)^{K-n} & : \quad K \geq n, \end{cases}$$

$$C_3 = \begin{cases} 0 & : \quad K \leq n \\ P_3^{n-1} & : \quad K = n+1 \\ \frac{(K-2)!}{(n-1)!(K-n-1)!} P_3^{n-1}(1-P_3)^{K-n-1} & : \quad K \geq n+2, \end{cases}$$

$$C_4 = \begin{cases} 0 & : \quad K \leq n+1 \\ P_3^{n} & : \quad K = n+2 \\ \frac{(K-2)!}{n!(K-n-2)!} P_3^{n}(1-P_3)^{K-n-2} & : \quad K \geq n+3. \end{cases}$$

Eqn. 4.22 gives the probabilities $P(n)$ for $n = 1, 2, \cdots N$ for a particular value of θ. In order to determine $P_{avg}(n)$, the probabilities must be averaged over the range of θ. In this work, the probabilities are calculated for a particular value of θ and then the angle θ is incremented by a small value and the probabilities are recalculated. The increments in θ were chosen small enough to give four to five accurate significant digits in the estimates of the average probability. Substituting the values for $P_{avg}(n)$ calculated in Eqn. 4.17 and the value for $P(CIR < \gamma|n)$ calculated in Eqn. 4.20 into Eqn. 4.16 gives the desired average probability of outage.

4.5 Outage calculation due to the cochannel interference when using a flat-top antenna at the base station

When the number of antenna elements is less than the number of interferers, then it is not possible for the beamformer to steer nulls toward all of the interferers, and therefore a nonzero side lobe gain must be considered. The outage probability for the beamformer model shown in Figure 4.2 with $A > 0$ is considered in this section.

The calculation of the average probability of outage for the case of a flat-top beamformer, where $0 < A < 1$ is similar to the calculation in previous section for the ideal beamformer. However, in this case the probability of m interferers being present in the sidelobes is required in addition to the probability of n interferers being present in the main beam. Hence, the outage probability is a function of both n and m and may be expressed as,

$$P(\text{CIR} < \gamma) = \frac{1}{2\pi} \int_0^{2\pi} \sum_{m=1}^{N} \sum_{n=1}^{N} P(\text{CIR} < \gamma | m, n) P_s(m|\theta) P_b(n|\theta) d\theta \tag{4.23}$$

where $P_s(m|\theta)$ is the probability that m interferers are in the sidelobes, and $P_b(n|\theta)$ is the probability that n interferers are in the main beam. Eqn. 4.23 may be rearranged to give,

$$P(\text{CIR} < \gamma) = \sum_{m=1}^{N} \sum_{n=1}^{N} P(\text{CIR} < \gamma | m, n) \cdot P_{avg}(m, n), \tag{4.24}$$

where $P_{avg}(m, n) = \frac{1}{2\pi} \int_0^{2\pi} P(m|\theta) P(n|\theta) d\theta$ is the average over θ of the product of $P(m|\theta)P(n|\theta)$.

The probability that n interferers are in the main beam, $P(n|\theta)$ for the flat-top beamformer is exactly the same as for the ideal beamformer. Hence, $P(n|\theta)$ is calculated using Eqn. 4.22. Likewise, the probability that m interferers are in the side lobes is calculated using Eqn. 4.22, except that the probabilities P_i used in this case are calculated using a beamwidth of $2\pi - \Delta\theta$. The product of the resulting probabilities are then determined to obtain $P(m, n|\theta) = P(n|\theta)P(m|\theta)$ which is averaged over θ to give $P_{avg}(m, n)$.

The calculation of $P(CIR < \gamma | m, n)$ can be found using Eqn. 4.20. However, for the flat top beamformer the mean and variance of the total interference are calculated differently.

Let Y_{in} and Y_{out} denote the total interference inside and outside of the main beam, respectively. Since the gain of the antenna inside the main beam is unity, the mean and variance of Y_{in} is the same as that given for the ideal beam,

$$M_{Y_{in}} = n \exp\left(\frac{m_y}{2C}\right)$$

and

$$\sigma^2_{Y_{in}} = n \exp\left(\frac{m_y}{C}\left[\frac{4}{\pi} - 1\right]\right),$$

For the interference outside the main beam, the signal is multiplied by a factor of A. Therefore, the mean and variance will be,

$$M_{Y_{out}} = Am \exp\left(\frac{m_y}{2C}\right)$$

and

$$\sigma^2_{Y_{out}} = A^2 m \exp\left(\frac{m_y}{C}\left[\frac{4}{\pi} - 1\right]\right),$$

respectively.

Since both Y_{in} and Y_{out} have Gaussian distributions when expressed in dB, the total interference will also be Gaussian, with mean,

$$M_Y = M_{Y\,in} + M_{Y_{out}}$$

and variance,

$$\sigma^2_Y = \sigma^2_{Y_{in}} + \sigma^2_{Y_{out}}.$$

Substituting these values in Eqn. 4.20 gives the desired value for $P(CIR < \gamma | m, n)$.

4.6 Numerical results on outage probability due to the cochannel interference

4.6.1 Outage performance of an ideal beamformer at the base station

In this section we compare the outage probability performance for an ideal beamformer with a single omni-directional antenna. The ideal beamformer has a flat top beamformer with a beamwidth $\Delta\theta$ and gain of 0 dB. The sidelobes are assumed to be zero. Here the channel is modeled to be a Rayleigh fading channel. Figure 4.4 is a plot of the outage curves for ideal beamformers with beamwidths of 5, 20, and 120 degrees. The outage curves are compared to that obtained using an omnidirectional antenna. The users are assumed to be active only for 40% of the total time. The activity level depends on the blocking probability and the number of channels available in the cell. The carrier to interference ratio plus protection ratio (CIRP) is varied from -10 dB to 40 dB. A protection ratio of 8 dB is used in all simulations. Let us

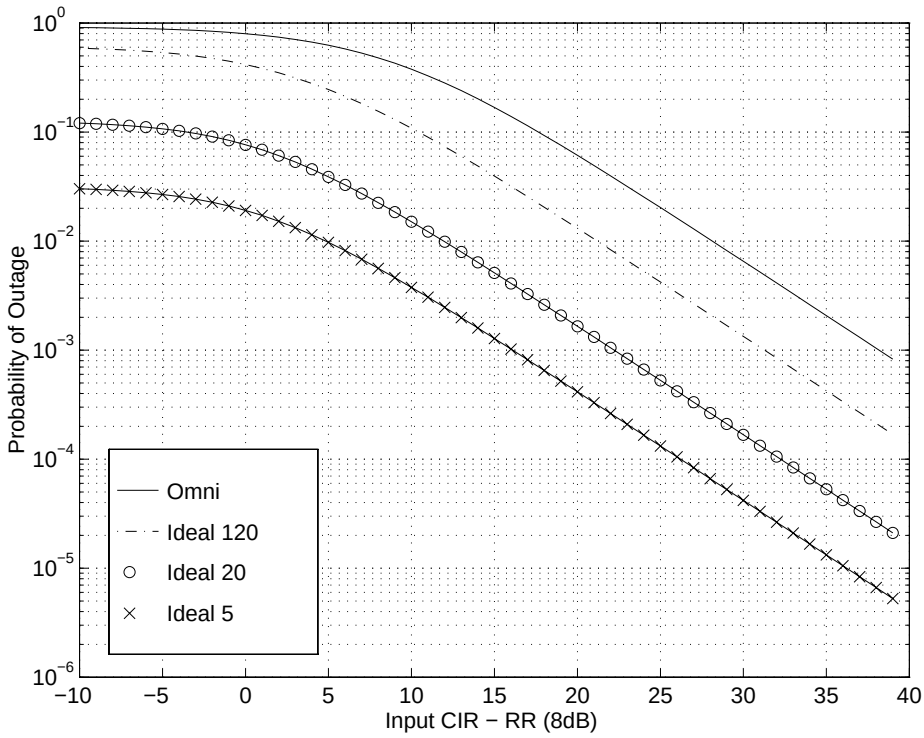

Figure 4.4: Plot of outage curves as a function of carrier to interference plus protection ratio (8 dB) for ideal beamformers of beamwidths 5, 20, 120 degrees. Also the outage curve of an omnidirectional antenna is compared with the ideal beamformer. Activity level of the users is set equal to 0.4.

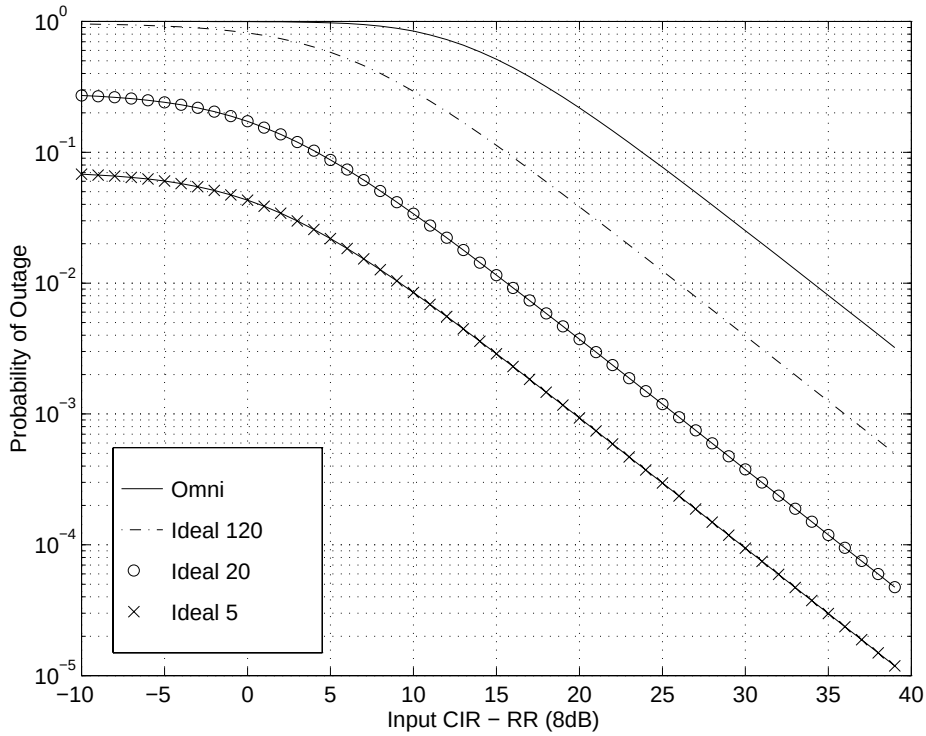

Figure 4.5: Plot of outage curves as a function of as a function of carrier to interference plus protection ratio (8 dB) for ideal beamformers of beamwidths 5, 20, 120 degrees. Also the outage curve of an omnidirectional antenna is compared with the ideal beamformer. Activity level of the users is set equal to 0.9.

define a term *outage improvement factor*, Γ_1, which is defined as

$$\Gamma_1 = 10 \times log_{10} \left[\frac{\text{Probability of outage using omnidirectional antenna at any given CIRP}}{\text{Probability of outage using a beamformer at any given CIRP}} \right].$$

For a CIRP of 20 dB, Γ_1 for 5, 20, and 120 degrees beamwidth ideal beamformers are 20.8, 14.5, 6.2 dB, respectively. A 10-element uniform linear array (ULA) with $\lambda/2$ spacings can achieve a beamwidth of 20 degrees along the broadside of the array and a beamwidth of 5 degrees requires an ULA with 44 elements and hence not practically feasible. From Figure 4.4, it is important to note that the outage curves for the ideal beamformer saturates at a certain value for lower CIRPs. The outage curves for low CIRPs do not reach an outage probability of 1 since the ideal beamformer has no sidelobes. Figure 4.5 shows the outage curves as a function of as a function of carrier to interference plus protection ratio for an activity level of 0.9. The outage probability has increased as expected. Figure 4.6 shows the outage curves as a function of activity

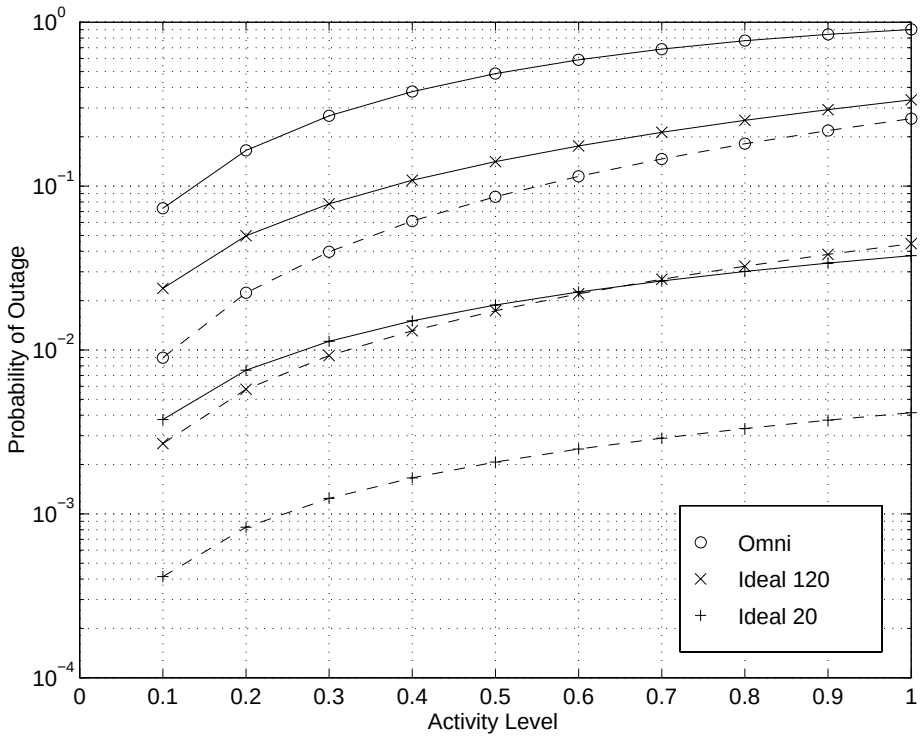

Figure 4.6: Plot of outage curves as a function of activity level for ideal beamformers of beamwidths 20 and 120 degrees are compared with the omnidirectional antenna. Two different carrier to interference plus protection ratios of 10 and 20 dB are considered. Solid curves correspond to 10 dB and the dashed curves correspond to 20 dB.

level. Two different CIRP conditions are considered here, 10 and 20 dB. Two different beamwidths, 20 and 120 degrees, for the ideal beamformer are considered. The outage curves are compared to that obtained using an omnidirectional antenna. The solid curves correspond to the CIRP of 10 dB and the dashed curves correspond to the CIRP of 20 dB. It can be seen that as the activity levels of the users increase, the probability of outage also increase. For a change in activity level from 0.4 to 0.9, the probability of outage degrades approximately by a factor of 2. The probability of outage degrades by an order of magnitude as the CIRP decreases from 20 to 10 dB for all the beamformers and the omnidirectional antenna.

4.6.2 Outage performance of a flat-top beamformer at the base station

Here we consider a flat-top beamformer at the base station and we study the effects of sidelobes on the probability of outage. In an ideal beamformer, there are no sidelobes and this beamformer is not practically feasible. Therefore, we consider a non-ideal implementation of a spatial filter whose beam pattern is closely related to the practical beam patterns. Figure 4.7 is a plot of the probability of outage as a function of CIRP for a flat-top beamformer with a sidelobe level of -6 dB. The activity level is maintained at 40%. Beamwidths of 5, 20, and 120 degrees are considered in this test case. For a CIRP of 20 dB, the outage improvement factors are 10, 8.6, 3.6 dB for beamwidths of 5, 20, and 120 degrees, respectively. The important point to be noted is that all the outage curves reach a probability of 1 at certain low CIRP. This behavior is attributed to the presence of sidelobe levels. The rate at which the outage curves reach a probability of 1 is dependent on the beamwidth and the sidelobe level of the beamformer. For a beamformer with high sidelobe level and large beamwidth, the outage curve reaches a probability of 1 faster than a beamformer with low sidelobe level and small beamwidth. Figure 4.8 shows the outage curves as a function of as a function of carrier to interference plus protection ratio for an activity level of 0.9. The outage probability has increased as expected.

Figure 4.9 shows the outage curves as a function of sidelobe level for flat-top beamformers of beamwidth, 20 and 120 degrees. The activity level of the users is 40% and the CIRP is 20 dB. It can be seen that the performance degrades as the

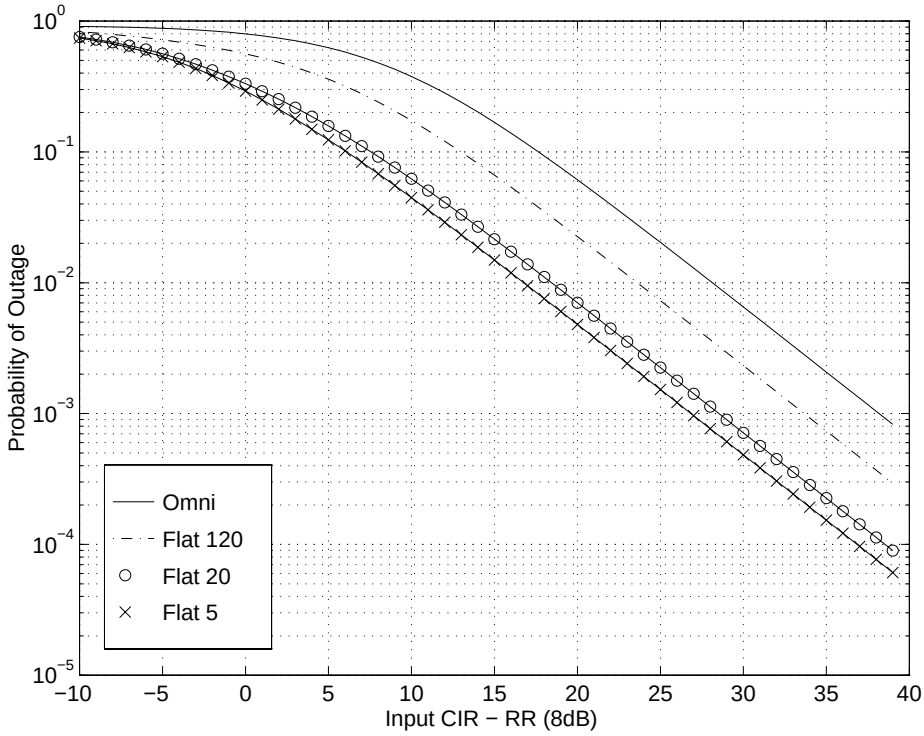

Figure 4.7: Plot of outage curves as a function of carrier to interference plus protection ratio (8 dB) for flat-top beamformers of beamwidths 5, 20, 120 degrees. Also the outage curve of an omnidirectional antenna is compared with the ideal beamformer. Activity level of the users is set equal to 0.4 and the sidelobe level is -6 dB.

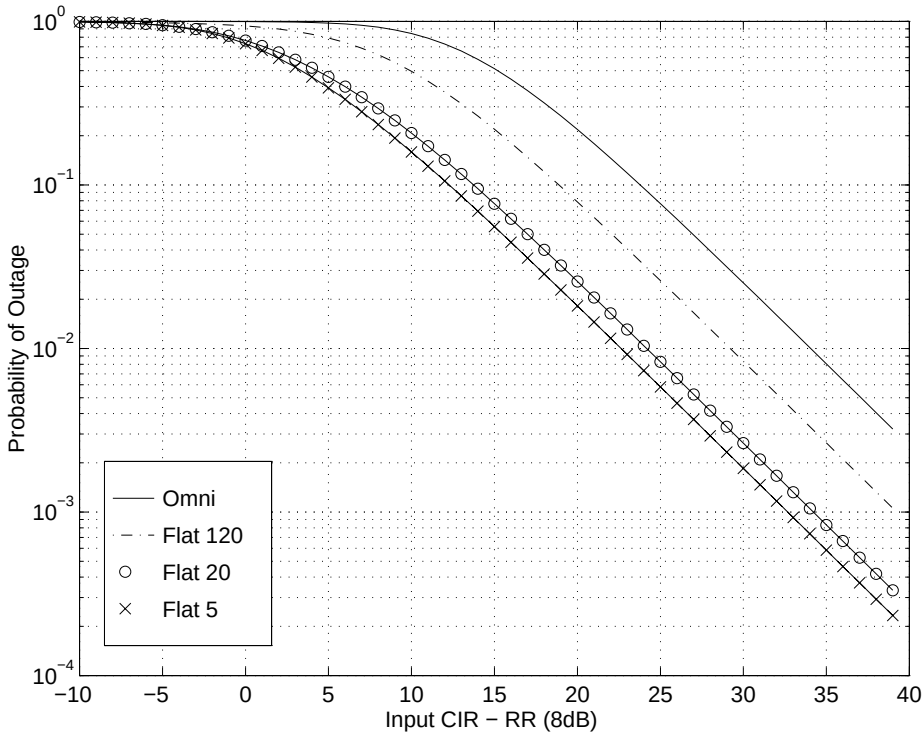

Figure 4.8: Plot of outage curves as a function of as a function of carrier to interference plus protection ratio (8 dB) for flat-top beamformers of beamwidths 5, 20, 120 degrees. Also the outage curve of an omnidirectional antenna is compared with the ideal beamformer. Activity level of the users is set equal to 0.9 and the sidelobe level is -6 dB.

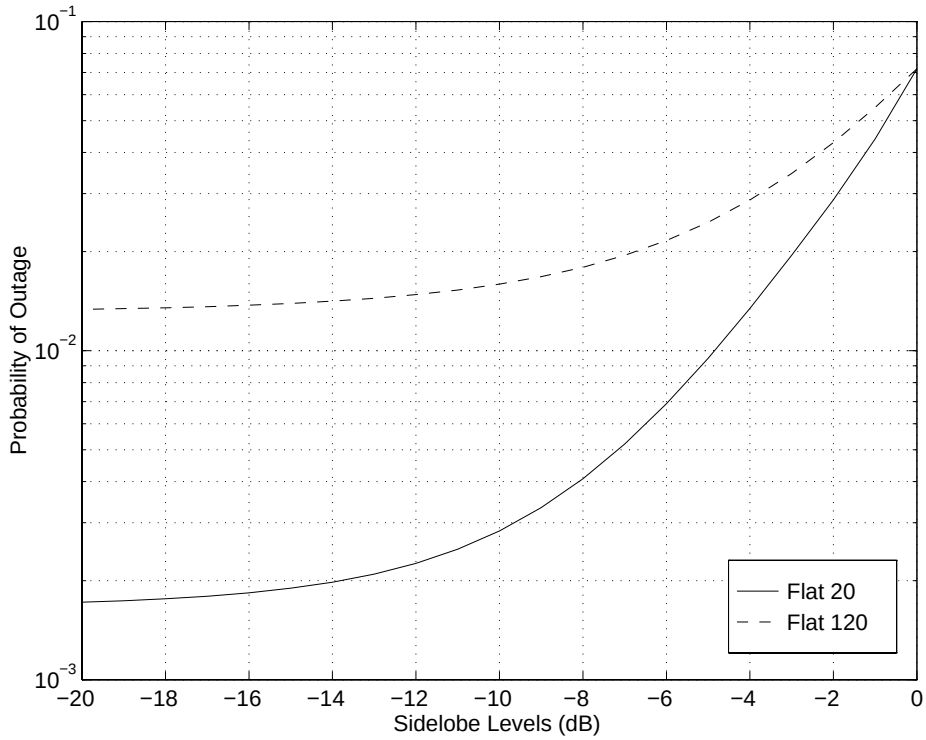

Figure 4.9: Plot of outage curves as a function of sidelobe levels for flat-top beamformers with beamwidths 20 and 120 degrees. Activity level of the users is set equal to 0.4 and the carrier to interference plus protection ratio (8 dB) is equal to 20 dB.

sidelobe levels increase. The performance degrades gracefully for the beamformer with beamwidth of 120 degrees than the beamformer whose beamwidth is 20 degrees. The outage performance of the flat-top beamformers with low sidelobe levels (e.g., -20 dB) is very close to the ideal beamformer with the same beamwidth. Figure 4.10 shows the outage curves as a function of activity level for the flat-top beamformers. Two different CIRP conditions are considered here, 10 and 20 dB. Two different beamwidths, 20 and 120 degrees, for the flat-top beamformer are considered. The outage curves are compared to that obtained using an omnidirectional antenna. The solid curves correspond to the CIRP of 10 dB and the dashed curves correspond to the CIRP of 20 dB. It can be seen that as the activity levels of the users increase, the probability of outage also increase. For a change in activity level from 0.4 to 0.9, the probability of outage degrades approximately by a factor of 2. The probability of outage degrades by an order of magnitude as the CIRP decreases from 20 to 10 dB

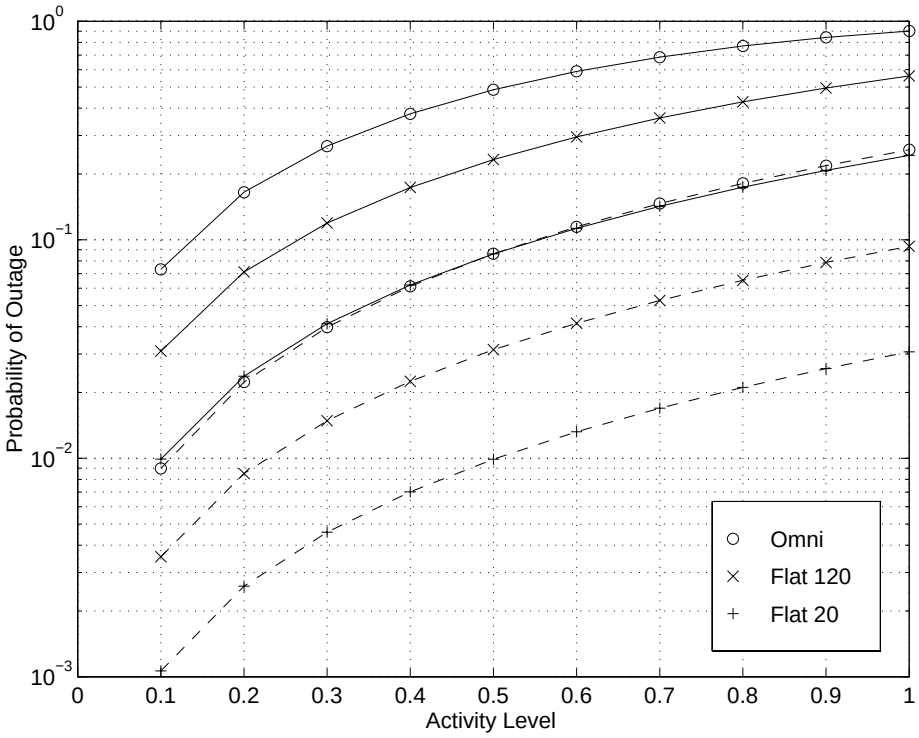

Figure 4.10: Plot of outage curves as a function of activity level for flat-top beamformers of beamwidths 20 and 120 degrees are compared with an omnidirectional antenna. The sidelobe level is set equal to -6 dB. Two different carrier to interference plus protection ratios of 10 and 20 dB are considered, the solid curves correspond to 10 dB and the dashed curve correspond to 20 dB.

for all the beamformers and the omnidirectional antenna.

4.6.3 Comparison of the outage performance of the ideal beamformer with the flat-top beam

Here we compare the performance of the ideal beamformer and the flat-top beamformer as a function of beamwidths of the beamformers. In this case, we define *implementation penalty factor*, Γ_2, as

$$\Gamma_2 = 10 \times log_{10} \left[\frac{\text{Probability of outage using a flat-top beamformer at any given CIRP}}{\text{Probability of outage using an ideal beamformer at any given CIRP}} \right].$$

The implementation penalty factor is plotted as a function of beamwidth in degrees in Figure 4.11. Four different sidelobe levels are considered here, -5, -10, -15, and -20

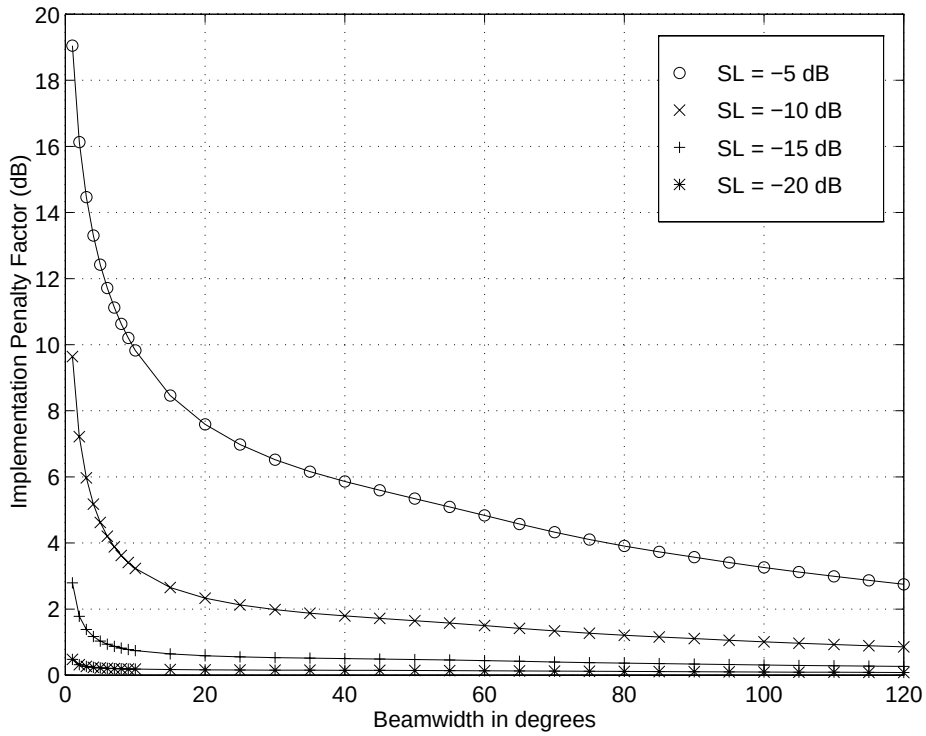

Figure 4.11: Plot of implementation penalty factor for flat-top beamformers with sidelobe levels (SL) of -5, -10, 15, and -20 dB as a function of beamwidth. Activity level of the users is set equal to 0.4 and the carrier to interference plus protection ratio (8 dB) is equal to 25 dB.

dB. The CIRP is set equal to 25 dB and the activity level is 40%. It can be seen that the implementation penalty factor reduces as the beamwidth increases in all the cases. The implementation penalty factor is higher for flat-top beamformers with high sidelobe levels. The curves clearly show the sidelobes can degrade performance. If adaptive beamforming is employed at the base station, the beampattern can have deep nulls in the directions of the interferers. But if the array is overloaded, i.e., the number of cochannel signals is greater than the number of elements, then the depth of the nulls decreases. This condition is very similar to having a flat-top beamformer with a high sidelobe level.

4.7 Conclusions

In this chapter, we derive the outage probability due to cochannel interference in fading at the base station of an AMPS system with an ideal beamformer. We derive a general framework to compute the outage probability when spatial filtering is applied at the base station of a cellular system. We consider two types of spatial filters, one a flat-top beamformer with no sidelobes and the other with the sidelobes. As a part of the outage calculation, we also derive an expression for the angle of arrival of the signal from a cochannel mobile unit. Results show that the ideal beamformer with 20 degrees beamwidth can provide 2 orders of magnitude improvement in outage probability over an omnidirectional antenna and 1 order of magnitude improvement in outage probability over a 120 degrees ideal beamformer. An ideal beamformer assumes the sidelobes to be non-existent, this is not true for any practical spatial filter. Therefore, we consider a flat-top beamformer with different sidelobe levels. As expected, the sidelobe levels play an important role in deciding the outage probability. For a flat-top beamformer with 20 degree beamwidth, the outage probability improves by nearly an order of magnitude as the sidelobe levels decreases from -4 to -20 dB. A 10-element ULA with inter-element spacing of $\lambda/2$ along the broadside can achieve a beamwidth of 20 degrees. The analysis presented in this chapter has been restricted to single AOA component for any user with Rayleigh fading, but future analysis can include multiple AOA components and gains that can be obtained from spatial diversity.

Chapter 5

Capacity Improvement Using Adaptive Arrays in an AMPS System

5.1 Introduction

In the previous chapter, we evaluated the performance of an AMPS system when a beamformer is employed at the base station. In this chapter, we will calculate the size of the array required to achieve reuse factors less than 7. In the literature, there is very little analysis on the capacity increase that can be achieved using adaptive arrays for AMPS systems. This motivated us to investigate the following issues:

1. Is SDMA possible in an AMPS system?

2. If adaptive arrays are used in an AMPS system, what is the minimum achievable reuse factor using a practically feasible antenna array?

To investigate the issue #2, we need to evaluate the probability of outage using a beamformer at the base station. Muammar and Gupta [60] have derived the probability of cochannel interference in Rayleigh and log-normal fading when an omnidirectional antenna is used at the base station. We extend their analysis to take into account the spatial filter used at the base station. In the analysis two types of spatial filters: an ideal and a non-ideal (flat-top) beamformers, are considered. The ideal beamformer has no sidelobes while the flat-top beamformer has a flat sidelobe. The

ideal beamformer models a practical beamformer when the array is *underloaded*, i.e., the number of interferers is less than the number of elements -1. When the array is underloaded, the array can form deep nulls in the direction of the interferers and hence closely modeled by an ideal beamformer. It will be shown later that the outage performance of a flat-top beamformer with -20 dB sidelobe level is very similar to the ideal beamformer. A flat-top beamformer models a beamformer when the array is *overloaded*, i.e., the number of interferers is greater than the number of elements -1. When the array is overloaded, the array cannot steer nulls in the direction of all the interferers and hence the array has higher sidelobe levels compared to an underloaded case.

The chapter is organized as follows: Section 5.2 presents the feasibility study of SDMA for an AMPS system. We use here the calculation of outage probability and the angle-of-arrival characterization of the signal from the interferer at the base station of the desired cell (for reuse factors ≥ 1) described in Chapter 4. Capacity enhancement due to the reduction in reuse factor that can be achieved using the ideal and the flat-top beamformers is discussed in Section 5.3 and Section 5.4 presents the conclusions.

5.2 SDMA for AMPS - A feasibility study

Here we study the possibility of SDMA for an AMPS system. The spatial filter considered here is the ideal beamformer (beamwidth $= \Delta\theta$) whose beampattern is shown in Figure 5.1. The probability of outage is defined as the probability that the desired signal power S does not exceed the cochannel interference Y by the protection ratio γ. Hence, $P(\text{outage}) = P(S \leq \gamma Y)$, which is equivalent to $P(\text{CIR} < \gamma)$, where $\text{CIR} = \frac{S}{Y}$ is the carrier to interference ratio [60].

For an AMPS system which employs SDMA, the outage probability is a function of only the beamwidth of the beamformer and not on the direction the beamformer is pointing, θ, since the desired and interfering users are assumed to be uniformly distributed within a cell. In this work, it is assumed that the beamformer is aimed directly towards the desired user. The outage probability, $P(\text{CIR} < \gamma)$, may be

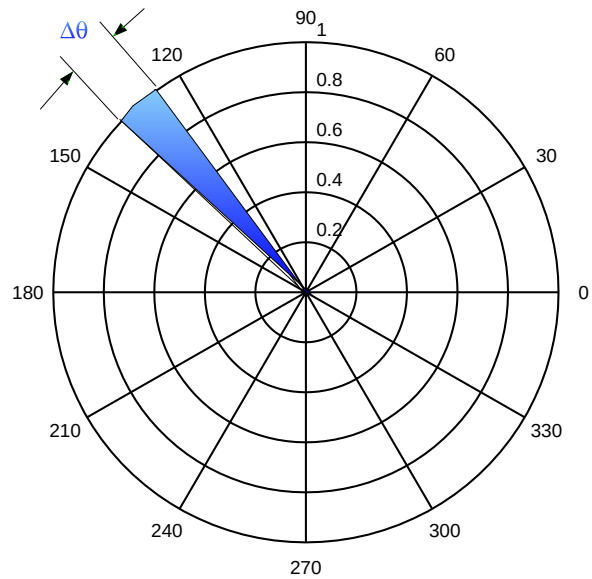

Figure 5.1: Beampattern of an ideal beamformer with beamwidth $\Delta\theta$.

expressed as,

$$P(\text{CIR} < \gamma) = \sum_{n=1}^{N} P(\text{CIR} < \gamma | n) P(n), \tag{5.1}$$

where $P(\text{CIR} < \gamma | n)$ is the probability that CIR $< \gamma$ when there are n interferers, $P(n)$ is the probability that n interferers are present inside the main beam, N is the number of interferers within the cell ($N + 1$ is the total number of users in the cell). Here we assume that perfect or coarse power control is implemented and hence if two users are within the beam then outage occurs, i.e., $P(\text{CIR} < \gamma | n) = 1$ for $n \geq 1$. Therefore the outage probability

$$P(\text{CIR} < \gamma) = \sum_{n=1}^{N} P(n). \tag{5.2}$$

The probability that n cochannel users are active is given by the binomial distribution as follows

$$P(n) = \binom{N}{n} \eta^n (1 - \eta)^{N-n}, \tag{5.3}$$

where

$$\eta = \frac{\text{Number of active channels in the beam}}{\text{Total number of channels}}$$

$$= \frac{\text{Number of active channels}}{\text{Total number of channels} \times m},$$

and

$$m = \frac{2\pi}{\Delta\theta}.$$

The number of active channels is divided by m, because only a fraction $(1/m)$ of the active users lie within the main beam and interfere with the desired user. Since SDMA is employed, the total number of channels is equal to 1 and the number of active channels is equal to 1 for $n \geq 1$. Therefore

$$\eta = \frac{\Delta\theta}{2\pi}. \tag{5.4}$$

Probability of outage can then be written as

$$P(\text{CIR} < \gamma) = \sum_{n=1}^{N} \binom{N}{n} \left(\frac{\Delta\theta}{2\pi}\right)^n \left(1 - \frac{\Delta\theta}{2\pi}\right)^{N-n} \tag{5.5}$$

Figure 5.2 is a plot of the outage probability as a function of number of users in the system for an AMPS system that employs ideal beamformers with beamwidths 5, 10, 20 and 120 degrees. If the acceptable probability of outage is 2%, only the beamformer with 5 degrees beamwidth can accommodate more than 1 user.

If an ULA with inter-element spacing of d is used at the base station, then the minimum achievable null-to-null beamwidth, Θ_B, along the broadside of the array is given by [1]

$$\Theta_B = 2 \cdot sin^{-1}\left(\frac{\lambda}{M \cdot d}\right),$$

where M is the number of elements and d is the inter-element spacing. For an ULA with inter-element spacing of $\lambda/2$, minimum achievable null-to-null beamwidth is given by

$$\Theta_B = 2 \cdot sin^{-1}\left(\frac{\lambda}{M \cdot \lambda/2}\right) = 2 \cdot sin^{-1}\left(\frac{2}{M}\right).$$

Figure 5.3 is a plot of the null-to-null minimum bandwidth of an ULA with inter-element spacing of $\lambda/2$ as a function of number of elements. A 44-element uniform linear array (ULA) with inter-element spacing of $\lambda/2$, where λ is the wavelength of the carrier frequency, can achieve a null-to-null beamwidth of 5 degrees along the broadside of the array. An array with 44 elements is difficult to implement. Since a 44-element adaptive array can provide acceptable probability of outage for only 3 users, SDMA is *not feasible* for an AMPS system.

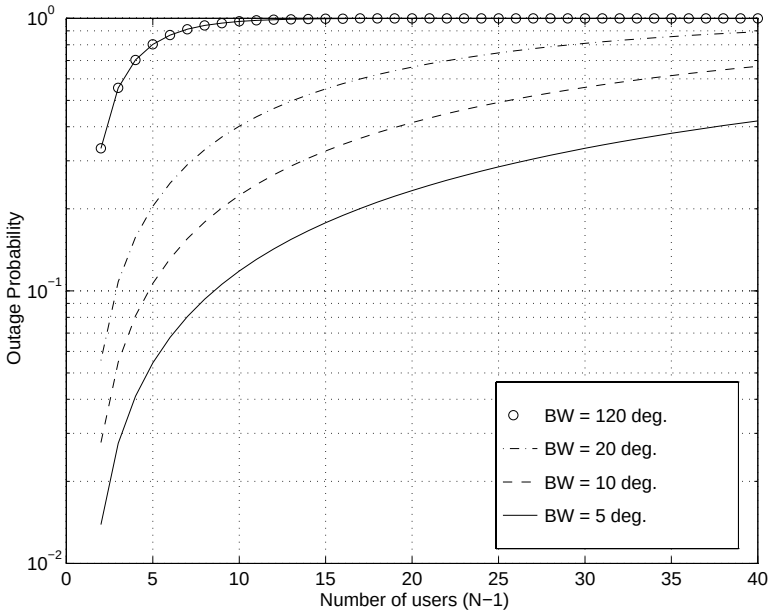

Figure 5.2: Outage probability curves as a function of number of users in an AMPS system that employs SDMA. Ideal beamformer with beamwidths of 5, 10, 20 and 120 degrees are considered.

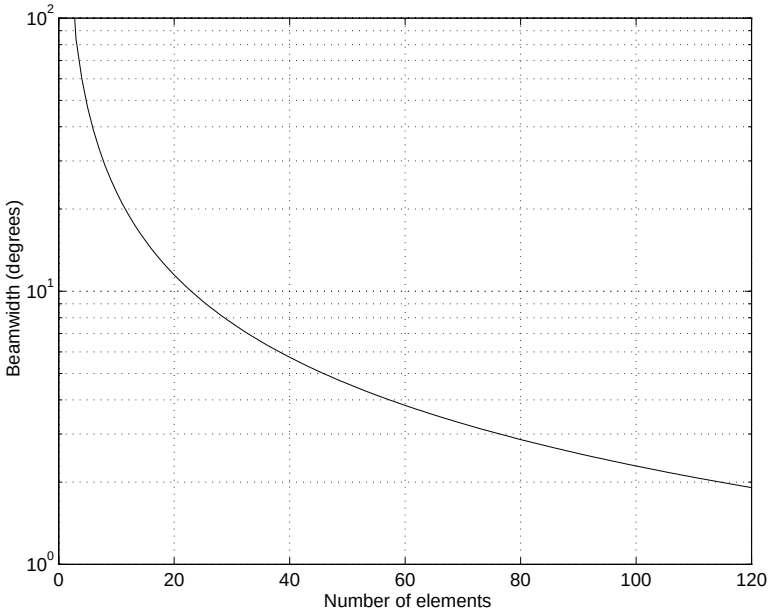

Figure 5.3: Plot relating minimum null-to-null beamwidth to the number of elements for a uniform linear array with inter-element spacing of $\lambda/2$.

5.3 Capacity enhancement calculation using a beamformer

In this section we present numerical results of outage when an ideal and a flat-top beamformer are employed at the base station. We then discuss the capacity increase that can be achieved using the beamformers. The frequency reuse factor can be reduced from 7 to a lower reuse factor due to the increase in CIR at the output of the beamformer. The calculation relates the number of elements required in an adaptive array to achievable reuse factors lower than 7.

5.3.1 Outage curves for ideal and the flat-top beamformer

Here we compare the outage probability performance of an ideal beamformer with a single omni-directional antenna. The ideal beamformer has a beamwidth $\Delta\theta$ and gain of 0 dB. Here the channel is modeled to be a Rayleigh fading channel. The numerical results presented here results from the analysis presented in the previous Chapter. Figure 4.4 is a plot of the outage curves for ideal beamformers with beamwidths of 5, 20, and 120 degrees. The outage curves are compared to that obtained using an omnidirectional antenna. The users are assumed to be active only for 40% of the total time. The activity level depends on the blocking probability and the number of channels available in the cell. The carrier to interference ratio plus protection ratio (CIRP) is varied from -10 dB to 40 dB. A protection ratio of 8 dB is used in all simulations. The outage curves for beamwidths less than 360 degrees saturates at an outage probability less than 1 for low CIRPs. This behavior is attributed to the absence of sidelobes in an ideal beamformer.

Figure 4.5 shows the outage curves for an activity level of 90%. As expected, the probability of outage is higher for 90% activity level than 40% activity level. Comparing Figures 4.4 and 4.5, if the acceptable level of probability of outage is 1%, then the improvement in CIRP achieved by the ideal beamformers over an omnidirectional antenna is independent of the activity level of the users.

The numerical results of outage for flat-top beamformers are presented in Figures 4.7 and 4.8 for activity levels of 40% and 90%. Irrespective of the beamwidths, the outage curves of the beamformers reaches an outage probability of 1 at certain low CIRPs. This behavior is attributed to the presence of sidelobes. As in the ideal

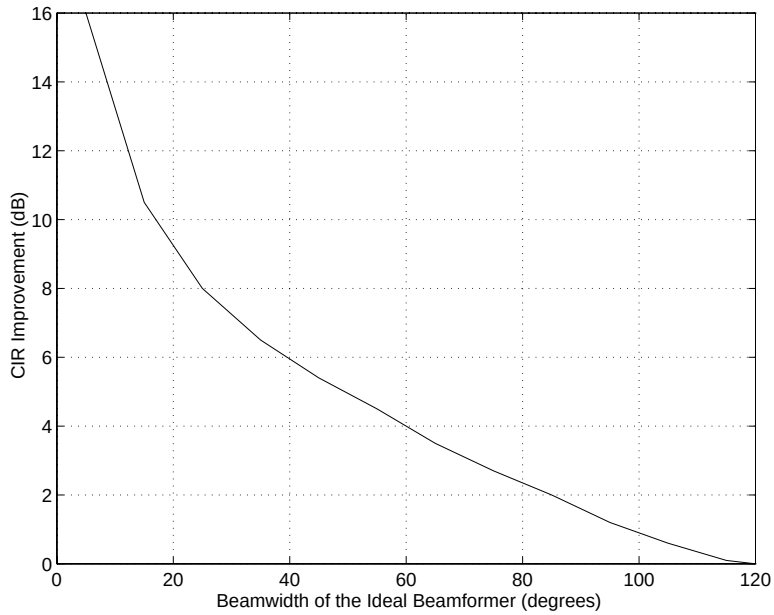

Figure 5.4: Improvement in CIR as a function of beamwidth ($\Delta\theta$) of an ideal beamformer over a 120 degrees ideal beamformer to maintain an outage probability of 10^{-2}.

beamformer case, the probability of outage is higher for 90% activity level than 40% activity level. If the acceptable level of probability of outage is 1%, then the improvement in CIRP achieved by the flat-top beamformers over an omnidirectional antenna at 40% activity level is approximately same as 90% activity level.

5.3.2 Reduction in reuse factor - Capacity increase

Ideal beamformer

Let us assume that an ideal beamformer with 120 degrees beamwidth is able to achieve an outage probability of 1% for a reuse factor of 7. This assumption is justifiable because current AMPS system uses 120 degrees sectorized antenna for a reuse factor of 7 and maintains toll quality speech. Figure 5.4 is plot of the CIR improvement that can be achieved by an ideal beamformer with beamwidth $\Delta\theta$ over an ideal beamformer with 120 degrees beamwidth. $\Delta\theta$ is varied from 5 degrees to 120 degrees.

If the transmit power of each base station is assumed to be equal and the path

Table 5.1: Degradation in input CIR relative to a reuse factor of 7.

Reuse Factor (N_1)	Degradation of CIR in dB
4	4.86
3	7.35
1	16.90

loss exponent is the same throughout the coverage area, then the CIR is given by [64]

$$CIR = \frac{R^{-l}}{\sum_{i=1}^{N} D_i^{-l}} \tag{5.6}$$

where l is the path-loss exponent. Considering only the first tier of interfering cells, if all the interfering base stations are equidistant from the desired base station then the CIR is given by

$$CIR = \frac{(\sqrt{3N_1})^l}{N}. \tag{5.7}$$

From the above Equation, we can calculate the degradation in CIR for any reuse factor lower than 7, relative to the reuse factor of 7. Table 5.1 lists the degradation in CIR for reuse factors of 1, 3, and 4 relative to 7 for $l = 4$.

If a beamformer can deliver a CIR improvement of 4.86 dB over a 120 degrees ideal beamformer, then a reuse factor of 4 can be achieved. From Figure 5.4, if the acceptable outage probability is 10^{-2}, a CIR improvement of 4.86 dB can be achieved using an ideal beamformer with beamwidth 50°. A null-to-null minimum beamwidth of 50° can be achieved by a 5-element ULA with $\lambda/2$ spacing (see Figure 5.3). Figure 5.5 is a bar chart of the number of elements required as a function of achievable reuse factors. A reuse factor of 3 can be achieved with a 8-element ULA and hence reuse factors of 3 and 4 are physically realizable. A reuse factor of 1 requires more than 46 elements and hence *not* practically feasible. By reducing the reuse factor from 7 to 4, a capacity increase of 75% can be achieved, while a reduction of reuse factor from 7 to 3 can enhance the capacity by 133%.

Flat-top beamformer

Similarly for the flat-top beamformer, the improvement in CIR offered by a flat-top beamformer over a 120 degrees ideal beamformer as a function of beamwidth and the

sidelobe level is plotted in Figure 5.6. It can be seen that the sidelobe level plays an important role in deciding the improvement in CIR. The flat-top beamformer is of particular interest in the practical situations when the array is operated in an overloaded condition. When the array is overloaded the array cannot null out all the interferers and hence the sidelobe level of the array increases as the number of interferers increases. This is very well modeled by a flat-top beamformer with high sidelobe levels. Figure 5.7 is a bar chart of the number of elements required to achieve reuse factors of 3 and 4 with flat-top beamformers of sidelobe levels -10, -15, and -20 dB. It is interesting to note that a flat-top beamformer with -10 dB sidelobe level can achieve a reuse factor of 4 and the main beam can be realized using a 7-element ULA. An ideal beamformer, on the other hand, can achieve a reuse factor of 4 and the main beam can be realized using a 5-element ULA. An ideal beamformer has no sidelobes, but the flat-top beamformer with a -10 dB sidelobe to achieve the same outage probability as the ideal beamformer, requires two more elements. By increasing the number of elements the array can form sharper beams to compensate for the high sidelobe level. A flat-top beamformer with a sidelobe level of -5 dB cannot achieve reuse factors of 3 and 4 with physically realizable arrays.

5.4 Conclusions

In this chapter, we analyze the capacity enhancement that can be achieved using an adaptive arrays for an AMPS system. We have developed a theoretical framework to evaluate the outage probability for an AMPS system which employs a spatial filter. An ideal and a non-ideal implementation of the spatial filter in considered here. An ideal beamformer models an underloaded beamformer, while a flat-top beamformer models an overloaded beamformer. As a part of theoretical framework, we have characterized the angle-of-arrival of the signal arriving from the co-channel interfering mobile at the desired base station. Numerical results for outage using the ideal and the non-ideal implementation of the beamformer are also presented. In this chapter we have shown that Spatial Division Multiple Access (SDMA), i.e., all the users in a cell occupy the same frequency, is *impossible* to achieve in an AMPS system. A cell reuse factor of 4 can be easily achieved with a 5-element uniform linear array

(ULA) with $\lambda/2$ spacings, but to achieve a reuse factor of 3, an ULA with 8 elements is required. It is also shown that a reuse factor of 1 is impossible to achieve with a physically realizable antenna array.

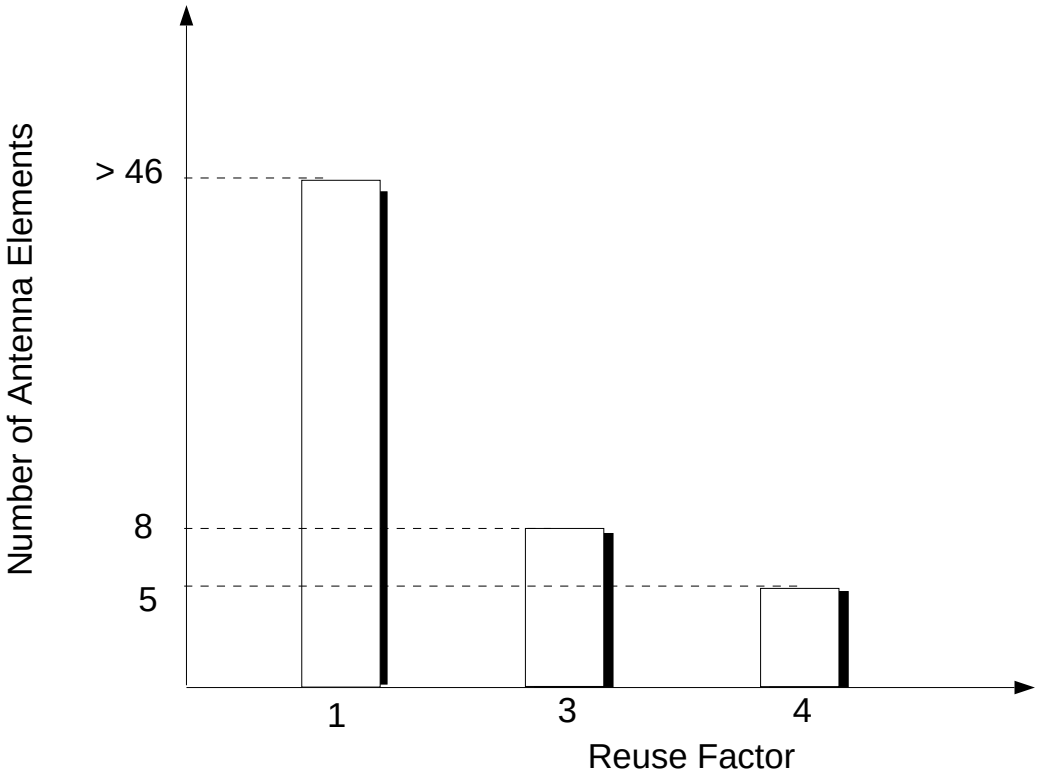

Figure 5.5: Bar chart showing number of elements required to realize an ULA versus reuse factor required to maintain an outage probability of 10^{-2} for an ideal beamformer.

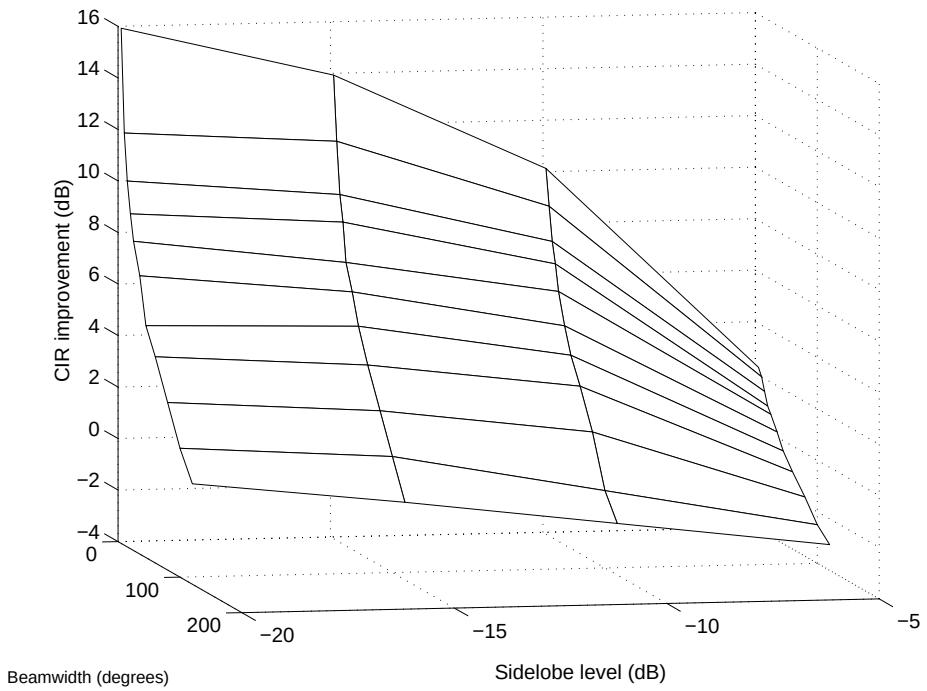

Figure 5.6: Improvement in CIR as a function of beamwidth and the sidelobe level of a flat-top beamformer over a 120 degrees ideal beamformer to maintain an outage probability of 10^{-2}.

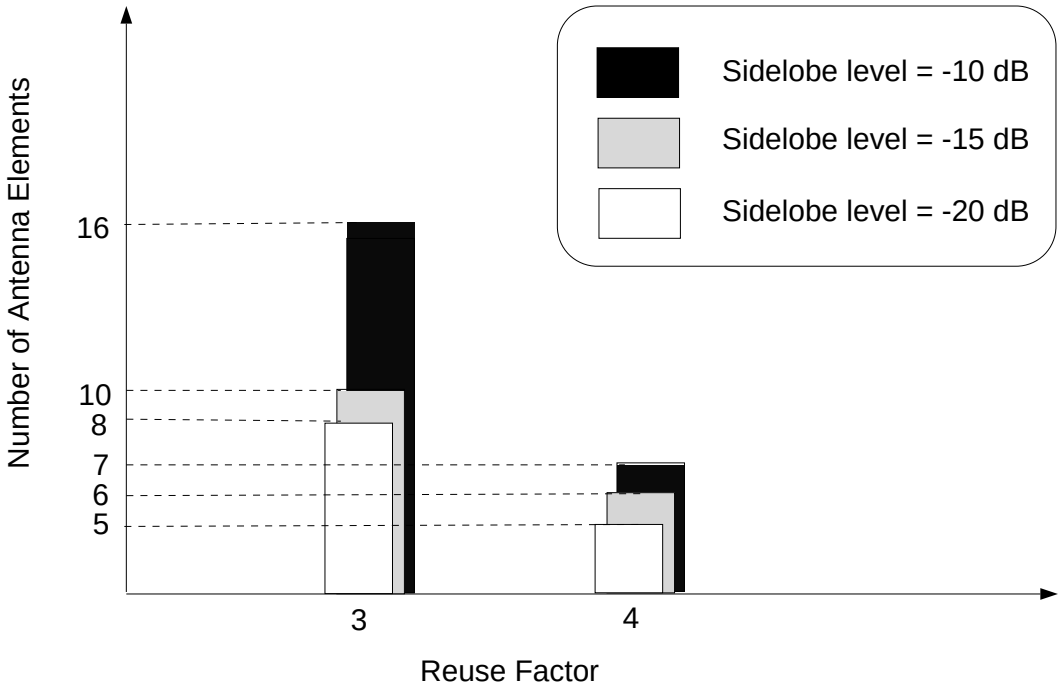

Figure 5.7: Bar chart showing number of elements required to realize an ULA versus reuse factor required to maintain an outage probability of 10^{-2} for a flat-top beamformer with sidelobe levels of -10, -15, and -20 dB.

Chapter 6

Geometrically Based Statistical Macrocell Channel Model for Mobile Environment

6.1 Introduction

To test adaptive array algorithms using simulation, statistical channel models that provide the angle-of-arrival (AOA) and time-of-arrival (TOA) of the multipath components are a must. Classically dense scattering is viewed as a Rayleigh fading phenomenon [59]. This model (Clarke's) assumes that the signals arrive horizontally at the receiver antenna and uniformly along the azimuth coordinates. Aulin proposed a channel model [65] which takes into account the elevation coordinates and which assumes uniform AOAs along the azimuth coordinates. Aulin's model is appropriate to model fading at a mobile unit, because scatterers are located closer to the mobile and are of different heights and therefore the assumption of plane waves arriving horizontally is not valid. Also the scatterers are uniformly located around the mobile and therefore the AOAs along the azimuth can be assumed to be uniform. But this model is not appropriate to model signals arriving at the base station. Liberti [66] developed a statistical channel model for microcells called the Geometrically Based Single Bounce model (GBSB). The GBSB model assumes that the scatterers lie in an ellipse which encompasses the transmitter and the receiver.

In this chapter, we develop a statistical channel model for macrocells called the Geometrically Based Single Bounce Macrocell (GBSBM)[1] channel model that assumes that the multipath reflection is caused by scatterers which are located closer to the mobile. The GBSBM model introduced here, is applicable for the reverse link of a cellular system, because it assumes that the plane waves reaching the base station travel horizontally and then it calculates the probability density function of the AOA along the azimuth. The assumption that the plane waves arrive horizontally is true because in a cellular environment, the separation of the mobile and the base station is larger than the difference in the height of the base station antenna and the mobile antenna.

The chapter is organized as follows: Section 6.2 discusses the GBSBM channel model and the derivation of the probability density function (pdf) of angle of arrival of the multipaths at the base station from a mobile surrounded by scatterers. Section 6.3 compares theoretical and simulation results of the pdf of the AOA of the multipath components. Section 6.4 discusses the generation of power-delay-angle (PDA) profile. Effects of directional antennas on the Doppler spectrum is discussed in Section 6.7 and Section 6.8 summarizes the results.

6.2 Geometrically Based Single Bounce Macrochannel (GBSBM) model and the probability density function of the angle of arrival of the multipaths at the base station in a macrocell

Here we introduce a geometrically based statistical macrocell channel model and derive the probability density function of the angle of arrival of the multipaths in a macrocell at the base station. The following are the assumptions made in developing the model:

- The signals received at the base station are assumed to be plane waves arriving from the horizon and hence the angle of arrival calculation include only azimuth

[1] The name GBSBM was derived from Liberti's channel model.

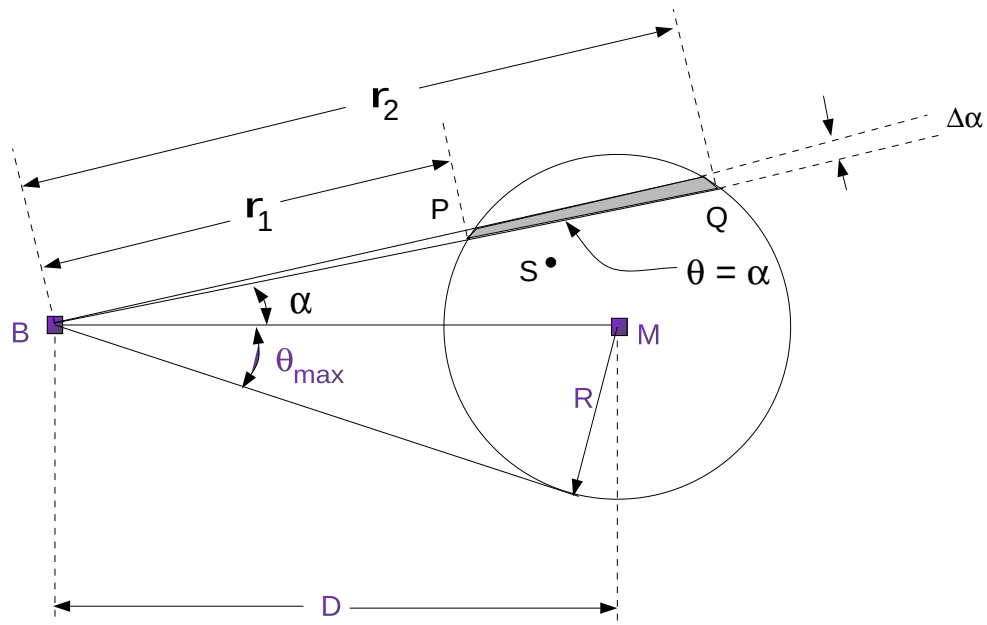

Figure 6.1: Illustration of the Geometrically Based Single Bounce Macrocell channel (GBSBM) model.

coordinates.

- The scatterers are assumed to be uniformly distributed within a circle around the mobile. Each scatterer is an omnidirectional re-radiating element whereby the plane wave, on arrival, is reflected directly to the mobile receiver antenna without the influence from other scatterers.

Figure 6.1 illustrates the GBSBM channel model. The base station is marked as B and M is the mobile unit. The base station and the mobile unit are separated by a distance D. The location of a scatterer is marked as S. The scatterers are assumed to be uniformly located around the mobile inside a circle of radius R. The goal of this derivation is to derive the pdf of θ, $f_\theta(\theta)$, where θ is the AOA of the multipath components at the base station B. Since the scatterers are confined within the circular region, the AOA of the multipath components is restricted to a narrow range and is specified by $2\theta_{max}$, where θ_{max} the maximum AOA of the multipath

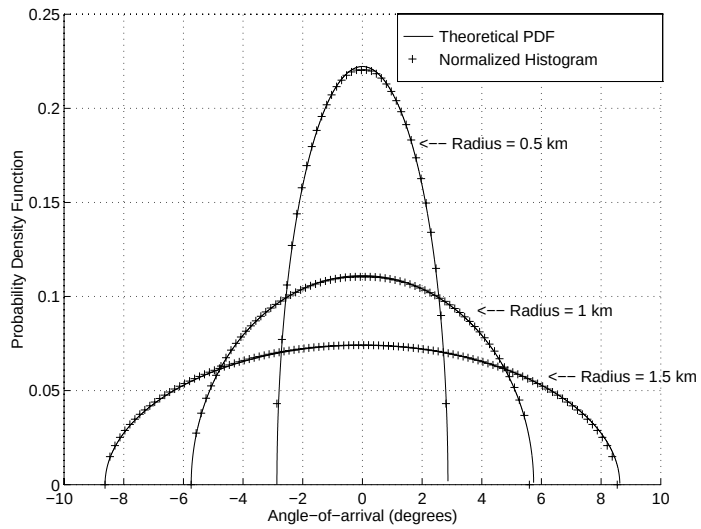

Figure 6.2: Probability density function for the angle of arrival of the multipaths at the base station from a mobile located 10 km away from the base station and the radius of the scatterers are 0.5, 1, and 1.5 kms.

components given by

$$\theta_{a_{max}} = sin^{-1}\left(\frac{R}{D}\right). \tag{6.1}$$

The multipath geometry in Figure 6.1 is exactly the same as the interference geometry in Figure 4.2. Therefore the pdf of the AOA of the multipath components is

$$f_\theta(\theta) = \begin{cases} \frac{2Dcos(\theta)\sqrt{D^2cos^2(\theta)-D^2+R^2}}{\pi R^2} & , \quad -sin^{-1}\left(\frac{R}{D}\right) \leq \theta \leq sin^{-1}\left(\frac{R}{D}\right) \\ 0 & , \quad otherwise. \end{cases} \tag{6.2}$$

6.3 Comparison of theoretical and simulation results

In this Section, we validate the theoretical model developed in the above section using simulation. The true probability density function in Eqn. 6.2 is evaluated for a test case where the distance of separation between the base station and the mobile unit is 10 km. The scatterers are uniformly located within a circle of radius 0.5, 1, and 1.5 kms. Simulated normalized histograms are generated by creating uniformly located

scatterers around the mobile and for each location of the scatterer, the angle-of-arrival of the signal at the base station B is calculated. The histogram for the AOA is then calculated by carrying out 10,000 Monte Carlo trials. The normalized histograms and the theoretical pdf are plotted in Figure 6.2. The simulated histograms match closely the theoretical pdfs.

6.4 Power delay angle (PDA) profile generation

In this Section the generation of a power-delay-angle profile is explained. In the generation of the PDA profile, the following parameters are assumed to be known:

- Distance between the base station and the mobile unit (D).
- Path loss exponent (n).
- Reference power (P_{ref}) and reference distance (d_o), used in the calculation of the power of the multipath component.
- Maximum multipath delay (t_{max}) or the radius of the scattering circle (R).
- Receiver and transmitter antenna gain patterns ($G_r(\theta)$ and $G_t(\theta)$).
- Number of multipaths (L).

The following are the steps involved in the generation of the PDA profile:

- Create a direct component with power $P_o = P_{ref} - 10nlog\left(\frac{d_o}{d_{ref}}\right) + G_r(0) + G_t(0)$.
- Generate L random variables for the location parameter (r) of the scatterers using the distribution $f_r(r) = \frac{2r}{R^2}$ and a uniform random variable for θ_d from 0 to 2π.
- Calculate the angle-of-arrival θ_a for the L multipaths using Eqn. 6.8.
- Based on the location of the scatterer the excess distance traveled is calculated for each multipath and then the excess delay is calculated.

Table 6.1: Simulation parameters for the PDA profile.

Parameters	Values
L	5,20 and 50
D	10 km
n	4
P_{ref}	1 W
d_o	100 m
t_{max}	5 μs
L_r	6 dB
τ_p	1 μs
θ_g	2°

- The power of the ith multipath component is given by

$$P_i = P_o - 10nlog(r_i) - L_r + G_r(\theta_a) - G_r(0) + G_t(\theta_d) - G_t(0),$$

  where L_r is the reflection loss in dB. All the quantities in the above equation are in dB.

- The PDA profile is generated assuming that the channel is sounded using a Gaussian pulse of width τ_p and a Gaussian beam antenna with a beamwidth of θ_g degrees.

Figure 6.3 shows a plot of the PDA profile generated using the parameters listed in Table 6.1 and $L = 5$. Omnidirectional receiver and transmitter antennas with 0 dB gain are assumed in this simulation. A power threshold of 20 dB below the power of the direct component was set up and components arriving below the threshold were ignored. Figures 6.4 and 6.5 are sample PDA profiles for $L = 20$ and 50.

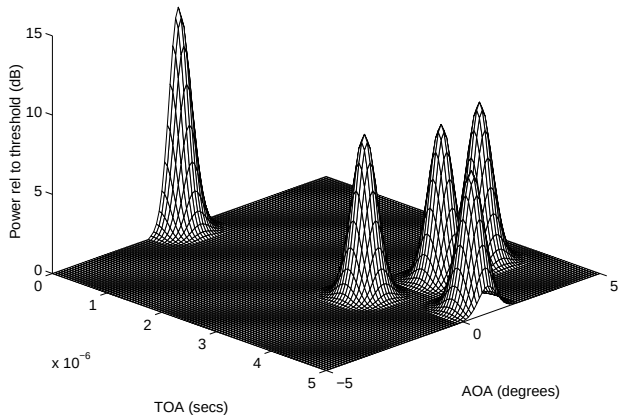

Figure 6.3: Power-delay-angle profile for a macrocell channel with 5 multipath components at the base station.

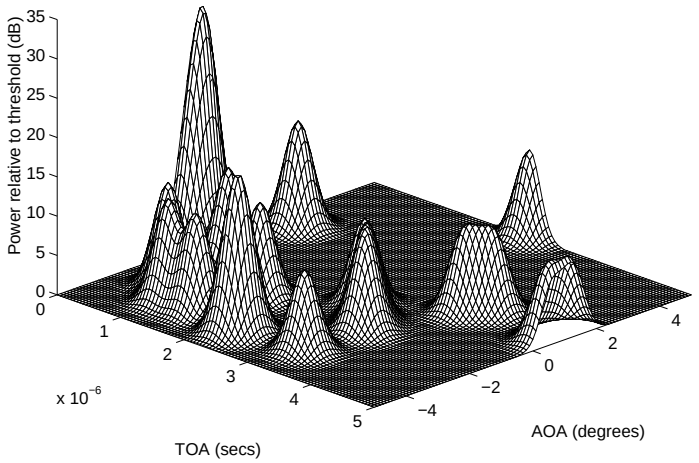

Figure 6.4: Power-delay-angle profile for a macrocell channel with 20 multipath components at the base station.

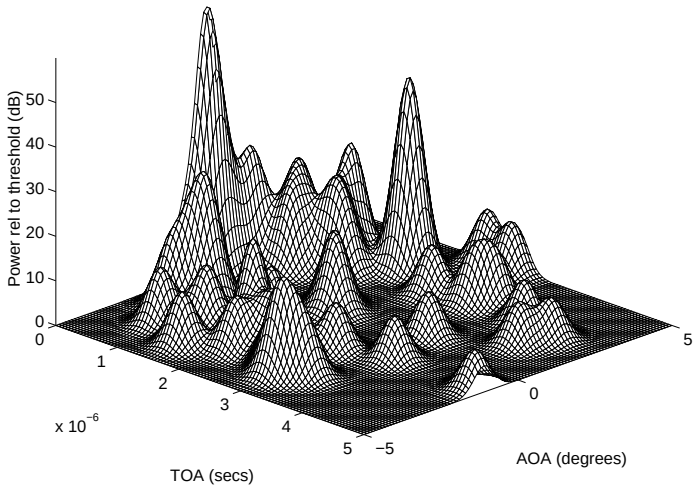

Figure 6.5: Power-delay-angle profile for a macrocell channel with 50 multipath components at the base station.

6.5 Angle Spread

The multipath components arrive at angles different from the direct component and angle spread is a measure used to determine the angular dispersion of the channel. A measure for angle spread based on the central moment is defined [66] as

$$\hat{\sigma}_{\phi} = \sqrt{\frac{\sum_{i=1}^{L-1} P_i \phi_i^2}{\sum_{i=1}^{L-1} P_i} - \left(\frac{\sum_{i=1}^{L-1} P_i \phi_i}{\sum_{i=1}^{L-1} P_i}\right)^2}. \tag{6.3}$$

Here we have not included the direct component. The angle spread based on the central moment is a measure of the spread of the multipath components (other than the direct component) and it gives a measure to which multipaths can be reduced using directional antennas.

The GBSBM model predicts that the range of AOA of the multipaths from the mobile is restricted. To eliminate the interfering multipaths at the base station directional antennas, whose beamwidths are smaller than the range of the AOA of the multipaths, are needed. A sectorized antenna of 120° may mitigate the effects of interference but not the effects of multipaths from the desired user which is caused by the local scatterers around the desired mobile unit. Finer beams are necessary at the base station to achieve multipath rejection. But a directional antenna at the mobile can significantly reduce multipath interference because the AOA of the multipaths from the base station is assumed to be arriving uniformly from all directions around the mobile.

Let us define R/D as the ratio of the radius of the scattering circle to the distance between the base station and the mobile unit. R/D can take a maximum value of 1. We then calculate the angle spread as a function of R/D. As expected, the ratio of R/D increases the angle spread also increases. Figure 6.6 is a plot of the angle spread as a function of R/D for path-loss exponents of 2,3, and 4. The number of multipath components is assumed to be 5. There is no significant difference in the angle spread as the path-loss exponent changes. Figure 6.7 shows the angle spread obtained using the GBSBM model for 50 multipath components and for path-loss exponents of 2,3, and 4. Even in this case there is no significant difference in the angle spread as the path-loss exponent changes. Figure 6.8 compares the angle spread for a path loss exponent of 4 and the number of multipaths are 5, 20, 50, and 200. The angle spread

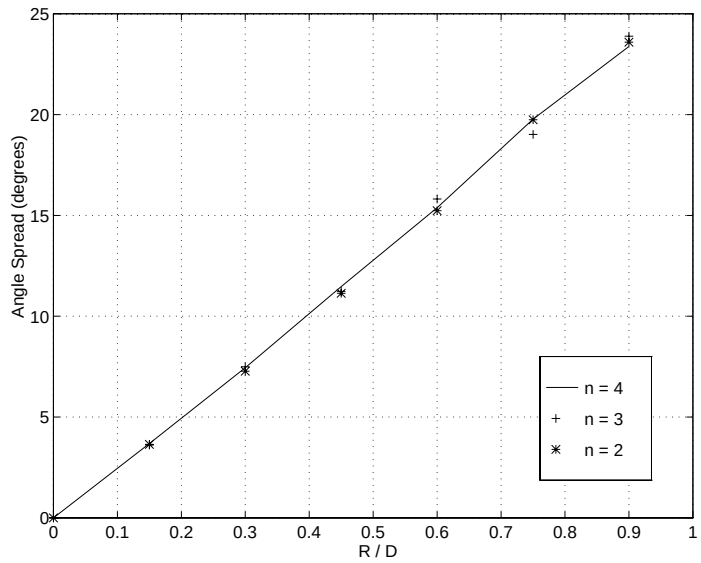

Figure 6.6: Plot of angle spread as a function of ratio of radius of the scatterer's circle to distance between the base station and the mobile unit for path-loss exponents of 2,3, and 4. The number of multipaths is equal to 5.

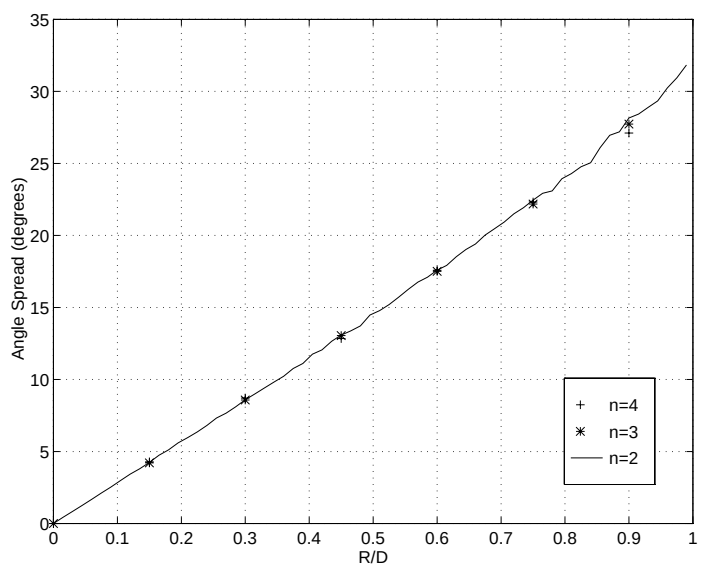

Figure 6.7: Plot of angle spread as a function of ratio of radius of the scatterer's circle to distance between the base station and the mobile unit for path-loss exponents of 2,3, and 4. The number of multipaths is equal to 50.

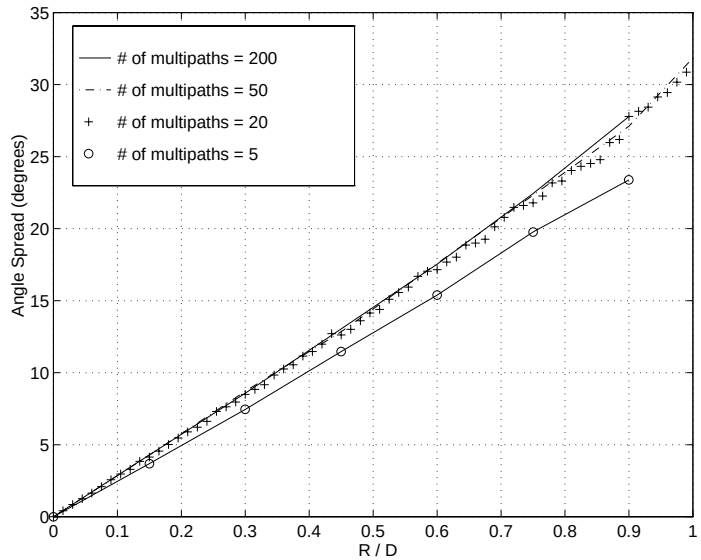

Figure 6.8: Plot of angle spread as a function of ratio of radius of the scattering circle to distance between the base station and the mobile unit for a path-loss exponent of 4. The number of multipaths are 5, 20, 50 and 200.

obtained for 20, 50, and 200 multipaths are very close to each other. The angle spread for the case where the number of multipaths is equal to 5 is smaller than the other cases.

6.6 Delay Spread

Another parameter that characterizes the channel is the delay spread. Delay spread is a measure of time dispersion of the channel. A measure based on the central moment is the square root of the second central moment of the power delay profile. It is defined as

$$\hat{\sigma}_\tau = \sqrt{\frac{\sum_{i=1}^{L-1} P_i \tau_i^2}{\sum_{i=1}^{L-1} P_i} - \left(\frac{\sum_{i=1}^{L-1} P_i \tau_i}{\sum_{i=1}^{L-1} P_i}\right)^2}. \tag{6.4}$$

The central moment delay spread is used in quantifying delay spread with measured data. But if the probability density function of the delay is known, then the delay spread is quantified by ensemble average delay spread given by

$$\sigma_\tau = \sqrt{E[\tau_i^2] - E[\tau_i]^2}. \tag{6.5}$$

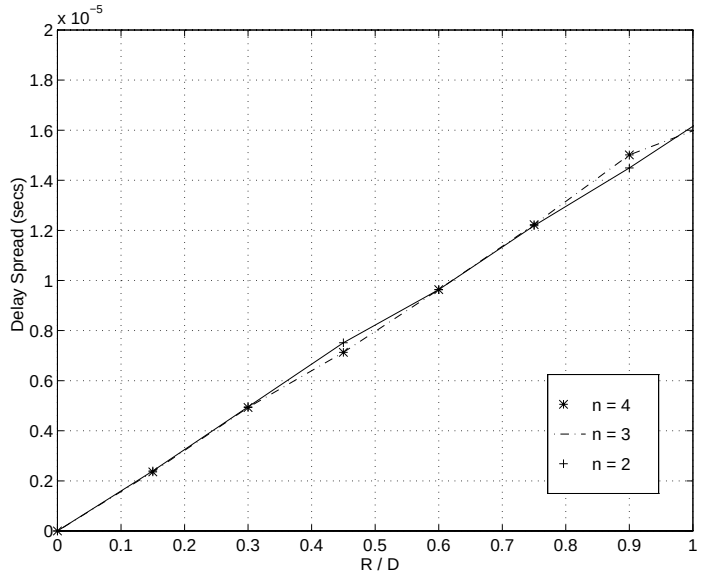

Figure 6.9: Plot of delay spread as a function of ratio of radius of the scattering circle to distance between the base station and the mobile unit for path-loss exponents of 2,3, and 4. There are 5 multipath components.

We now calculate the central moment delay spread as a function of R/D. As expected, the ratio of R/D increases the delay spread also increases. Figure 6.9 is a plot of the delay spread as a function of R/D for path-loss exponents of 2,3, and 4. The number of multipath components is assumed to be 5. There is no significant difference in the angle spread as the path-loss exponent changes. Figure 6.10 shows the delay spread obtained using the GBSBM model for 50 multipath components and for path-loss exponents of 2,3, and 4. Even in this case there is no significant difference in the delay spread as the path-loss exponent changes. Figure 6.11 compares the delay spread for a path loss exponent of 4 and the number of multipaths are 5, 20, 50, and 200. The delay spread obtained for 20, 50, and 200 multipaths are very close to each other. The delay spread for the case where the number of multipaths is equal to 5 is smaller than the other cases.

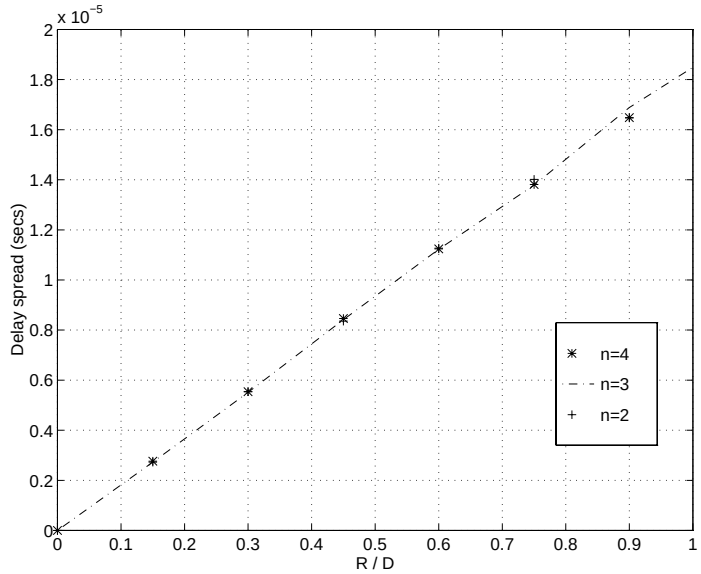

Figure 6.10: Plot of delay spread as a function of ratio of radius of the scattering circle to distance between the base station and the mobile unit for path-loss exponents of 2,3, and 4. There are 50 multipath components.

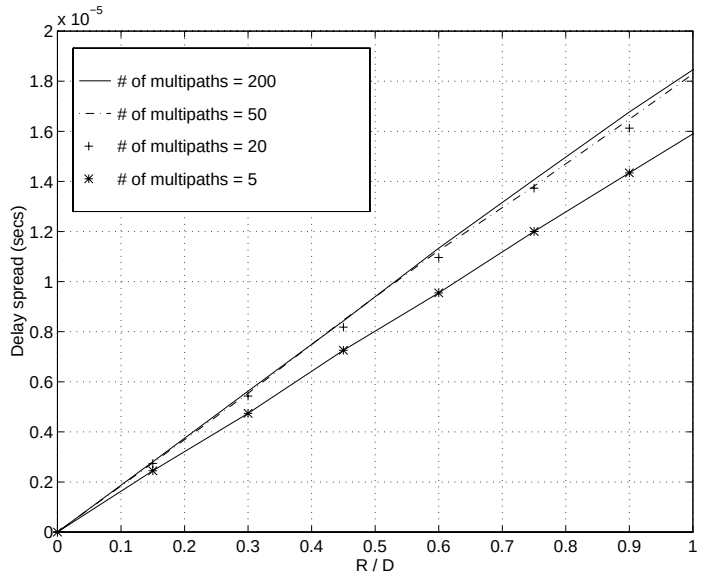

Figure 6.11: Plot of delay spread as a function of ratio of radius of the scattering circle to distance between the base station and the mobile unit for a path-loss exponent of 4. The number of multipaths are 5, 20, 50 and 200.

6.7 Effects of directional antennas at the base station on the Doppler spectrum

In this section we analyze the effect of directional antennas at the base station on the Doppler spectrum. It is important to note that the Doppler spectrum is dependent on the pdf of the AOA of the multipath components at the mobile unit and the direction of the motion of the mobile. The Doppler spectrum is a U-shaped spectrum as noted by Clark [67], only when the pdf of the AOA of the multipath components at the mobile is uniform. In the GBSBM model, we have assumed that the scatterers are uniformly around the mobile. When a narrow directional antenna is used at the base station, the beam will not illuminate the entire circle of scatterers around the mobile. Therefore the pdf of the AOA at the mobile from the base station will not be uniform, and hence the Doppler spectrum cannot be modeled using Clarke's model.

6.7.1 Characterizing the AOA of the signal at the mobile when a directional antenna is employed at the base station

Figure 6.12 illustrates the condition when a flat-top directional antenna with unity gain and beamwidth 2α is used at the base station. Since the scatterers are confined to a circle around the mobile, the AOA of the multipath components at the base station is restricted to an angular region of $2\theta_{max}$. If $\alpha \geq \theta_{max}$, then the base station antenna will illuminate all the scatterers and hence the pdf of the AOA at the mobile is uniform. But if $\alpha < \theta_{max}$, then the base station antenna will partially illuminate the scatterers and hence the pdf of the AOA of the multipath components at the mobile will not be uniform and here we derive the pdf of the AOA when a directional antenna is used at the base station and the Doppler spectrum is then derived.

In Figure 6.12, the scatterer's region EFGHIJ is illuminated by the base station antenna. Let us now derive the pdf of θ, when $\alpha < \theta_{max}$. Let us consider only the region EFGMJ, where $0 < \theta \leq \pi$, because the same holds true for the region GHIJM, where $\pi < \theta \leq 2\pi$. Let us divide the region EFGMJ into three distinct regions, JEM,

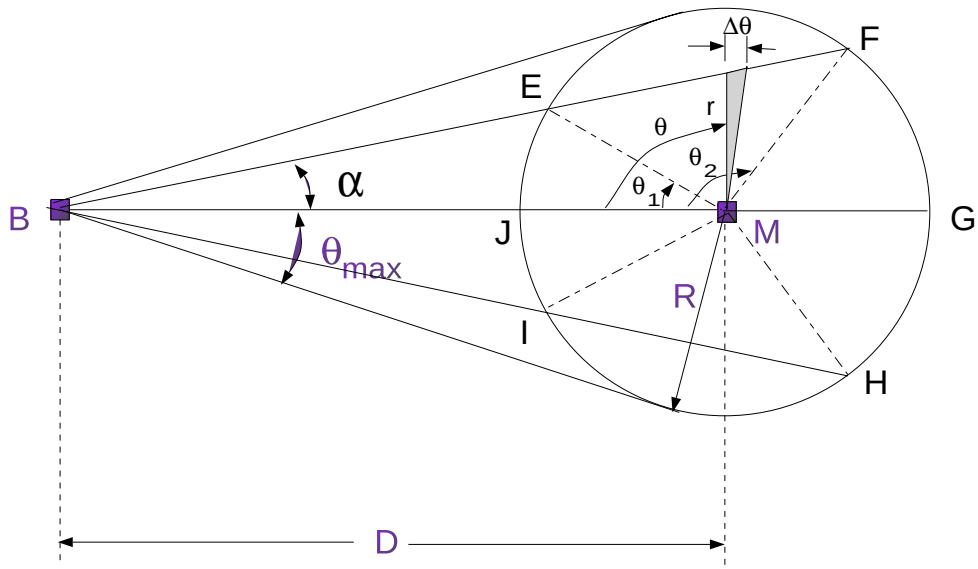

Figure 6.12: Illustration of the AOA at the mobile when a directional antenna with beamwidth of 2α. The scattering region illuminated by the base station antenna beam is the area marked by EFGHIJ.

EFM, and FGM. The value of θ_1 and θ_2 marks the three regions. The pdf of the AOA can be derived by computing the area within a thin strip (shaded region) shown in Figure 6.12. The area (A_1) within a strip (shaded region in Figure 6.12) between θ and $\theta + \Delta\theta$ can be shown using calculus to be

$$A_1 = \int_{\theta}^{\theta+\Delta\theta} \frac{1}{2} r^2 d\theta \tag{6.6}$$

where the value of r for the three regions can be shown to be

$$r = \begin{cases} R & : \quad 0 < \theta \leq \theta_1 \\ \frac{Dtan(\alpha)}{sin(\theta)+cos(\theta)tan(\alpha)} & : \quad \theta_1 < \theta \leq \theta_2 \\ R & : \quad \theta_2 < \theta \leq \pi. \end{cases} \tag{6.7}$$

Let us now calculate θ_1 and θ_2. From Figure 6.12, α and θ can be related by

$$tan(\alpha) = \frac{rsin(\theta)}{(D - rcos(\theta))}. \tag{6.8}$$

Squaring Eqn. 6.8 and solving for θ, we can express θ as

$$\theta = cos^{-1}\left[\frac{D}{r}sin^2(\alpha) \pm \frac{cos(\alpha)}{r}\sqrt{r^2 - D^2 sin^2(\alpha)}\right]. \tag{6.9}$$

Now θ_1 and θ_2 can be determined by substituting $r = R$ in Eqn. 6.9.

$$\theta_1 = cos^{-1}\left(\frac{D}{R}sin^2(\alpha) + cos(\alpha)\sqrt{1 - \left(\frac{D}{R}\right)^2 sin^2(\alpha)}\right) \tag{6.10}$$

$$\theta_2 = cos^{-1}\left(\frac{D}{R}sin^2(\alpha) - cos(\alpha)\sqrt{1 - \left(\frac{D}{R}\right)^2 sin^2(\alpha)}\right). \tag{6.11}$$

Since the scatterers are uniformly distributed within the region EFGHIJ, the density of the area within the region is the reciprocal of the area within the region. The area (A) within the region EFGHIJ can be expressed as

$$A = R^2(\pi + \theta_1 - \theta_2) + 2Dsin(\alpha)\sqrt{R^2 - D^2sin^2(\alpha)}.$$

The area density is given by

$$f_{area} = \frac{1}{R^2(\pi + \theta_1 - \theta_2) + 2Dsin(\alpha)\sqrt{R^2 - D^2sin^2(\alpha)}}. \tag{6.12}$$

Using Eqns. 6.6, 6.7, and 6.12, the cumulative distribution function (cdf) of the AOA, $F_\theta(\theta)$, for the region $\theta_1 < \theta \leq \theta_2$ can be expressed as

$$F_\theta(\theta) = \int_{-\infty}^{\theta} \frac{f_{area}}{2}\left(\frac{Dtan(\alpha)}{sin(\beta) + cos(\beta)tan(\alpha)}\right)^2 d\beta \tag{6.13}$$

where β is a dummy variable. For the regions $0 < \theta \leq \theta_1$ and $\theta_2 < \theta \leq \pi$, the cdf is given by

$$F_\theta(\theta) = \int_{-\infty}^{\theta} \frac{f_{area} \times R^2}{2} d\beta. \tag{6.14}$$

The probability density function, the derivative of the cdf, can then be expressed as

$$f_\theta(\theta) = \begin{cases} \frac{R^2}{2R^2(\pi+\theta_1-\theta_2)+2Dsin(\alpha)\sqrt{R^2-D^2sin^2(\alpha)}} & : \quad -\theta_1 < \theta \leq \theta_1 \\ \frac{(Dtan(\alpha))^2}{\left(2R^2(\pi+\theta_1-\theta_2)+2Dsin(\alpha)\sqrt{R^2-D^2sin^2(\alpha)}\right)(sin(\theta)+cos(\theta)tan(\alpha))^2} & : \quad \theta_1 < |\theta| \leq \theta_2 \\ \frac{R^2}{2R^2(\pi+\theta_1-\theta_2)+2Dsin(\alpha)\sqrt{R^2-D^2sin^2(\alpha)}} & : \quad \theta_2 < \theta \leq -\theta_2 \end{cases} \tag{6.15}$$

where θ_1 and θ_2 are given by Eqns. 6.10 and 6.11. Figure 6.13 validates the theoretical pdf developed in this section. Let us consider a test case where D = 3 kms and R = 1 km, therefore $2\theta_{max} = 38.9$ degrees. If a flat-top beam with unity gain and beamwidth

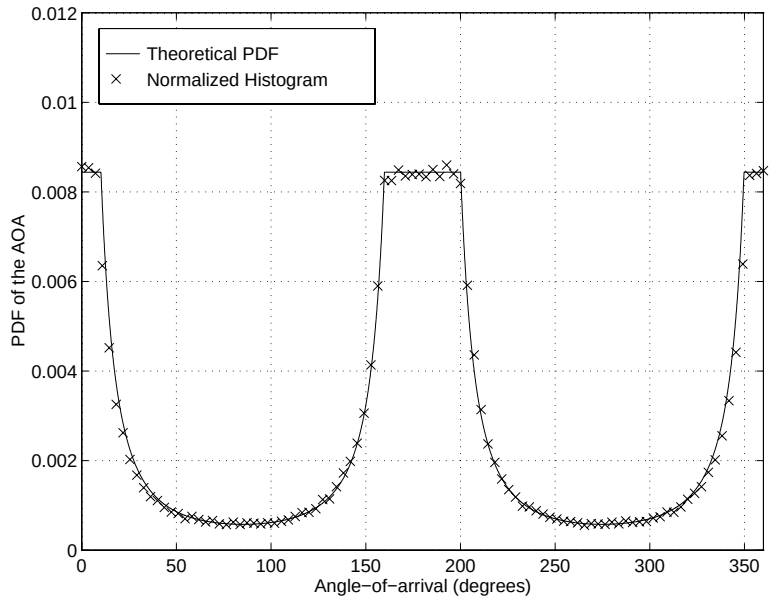

Figure 6.13: Theoretical pdf and simulated normalized histograms of the AOA at the mobile. The base station uses a directional antenna with beamwidth (2α) 10 degrees and $D/R = 3$ and $2\theta_{max} = 38.9$ degrees.

of 10 degrees is used at the base station, then the theoretical pdf is evaluated using Eqn. 6.15 and shown in Figure 6.13. To obtain the normalized simulated histogram for the AOA, scatterers are uniformly created around the mobile and the histogram of the AOA a the mobile from the scatterers that are illuminated by the beam is computed. The normalized histogram is also shown in Figure 6.13. It can be seen that simulated normalized histogram fits closely with the theoretical pdf curve.

6.7.2 Doppler spectra and fading envelope

The received signal at the mobile experiences Doppler spread because of the motion of the receiver. Figure 6.14 illustrates the condition when the mobile is moving at an angle of ϕ_v with respect to the direct line of sight (LOS) component. The ith multipath component arrives at the mobile at an angle of ϕ_i with respect to the LOS component. The multipath components at the receiver experiences Doppler shift depending on the direction of the motion of the mobile. The ith multipath

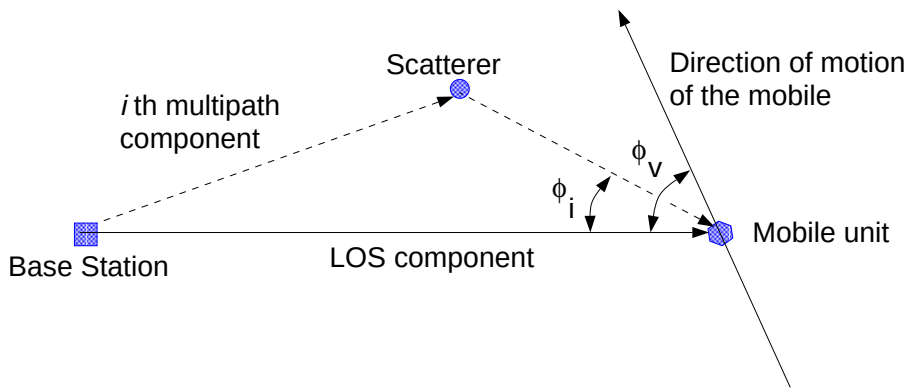

Figure 6.14: Illustration of a multipath component arriving at the mobile from the base station.

component experiences a Doppler shift v_i given by

$$v_i = f_m cos(\phi_i - \phi_v), \tag{6.16}$$

where f_m is the maximum possible Doppler shift which is given by $f_m = v/\lambda$, ϕ_i is the angle between the ith multipath component and the direct path, and ϕ_v is the angle between the direction of the motion of the vehicle and the direct path. Let the received signal be $r(t) = E_o \sum_{i=0}^{L-1} \alpha_i e^{j2\pi v_i t}$. The Doppler spectrum $S_r(f)$ was shown in [66] to be

$$S_r(f) = A_o^2 f_v(f), \tag{6.17}$$

where $A_o^2 = E_o^2/4 \sum_{i=1}^{L-1} |\alpha_i|^2$, and $f_v(f)$ is the probability density function of the distribution of the Doppler frequency. Assuming an omnidirectional antenna at the receiver, it was shown in [66] that $f_v(f)$ is given by

$$f_v(f) = \frac{f_\phi(\phi_v + |cos^{-1}(f/f_m)|)}{f_m\sqrt{1-(f/f_m)^2}} + \frac{f_\phi(\phi_v - |cos^{-1}(f/f_m)|)}{f_m\sqrt{1-(f/f_m)^2}}, |f| < f_m, \tag{6.18}$$

where $f_\phi(\phi)$ is the pdf of the AOA of the multipath components at the mobile unit. Therefore the power spectral density is given by [67]

$$S_r(f) = \frac{A_o^2}{f_m\sqrt{1-(f/f_m)^2}} \left[f_\phi(\phi_v + \left|cos^{-1}(f/f_m)\right|) + f_\phi(\phi_v - \left|cos^{-1}(f/f_m)\right|) \right], |f| < f_m. \tag{6.19}$$

If the angle-of-arrival of the signal at the mobile is uniform, then the Doppler spectrum is given by Clarke's model [67] as

$$S_r(f) = \frac{A_o^2}{\pi f_m \sqrt{1-(f/f_m)^2}}, |f| < f_m. \tag{6.20}$$

If a directional antenna is used at the base station then the pdf of the AOA of the multipath components is given by Eqn. 6.15. Substituting Eqn. 6.15 in Eqn. 6.19, the Doppler spectrum can be obtained when using a directional beam at the base station. Let us consider a test case where the mobile is traveling at a velocity of 54 kmph and the carrier frequency is 2 GHz is considered. The maximum Doppler shift is 100 Hz. The base station uses a directional antenna with 10 degrees beamwidth. Three different T-R separations are considered here: 1, 3, and 5 kms. The radius of the scattering circle is 1 km. Two different direction of motion of the mobile is considered, $\phi_v = 0^o$ and $\phi_v = 90^o$. Figures 6.15(a) and (b) show the Doppler spectrum for $\phi_v = 0^o$ and $\phi_v = 90^o$, respectively.

For $\phi_v = 0^o$, the spectrum is skewed to the right, i.e., more negative Doppler frequency components than positive frequency components. This is because, when the mobile is moving in the direction of the line-of-sight (LOS) component towards the base station (see Figure 6.16), the positive Doppler frequency components results from the scatterers located in the region marked A_1 and the negative Doppler frequency components from region A_2. Since the area of the region A_2 is larger than the area of the region A_2, there are more negative Doppler frequency components than positive frequency components in the Doppler spectrum. For $\phi_v = 90^o$, the specrum is symmetrical about the zero Doppler frequency component. This is because, when the mobile is moving perpendicular to the base station (see Figure 6.17), the positive Doppler frequency components results from the scatterers located in the region marked A_1 and the negative Doppler frequency components from region A_2. Since the area of the region A_2 is equal to the area of the region A_2, the Doppler spectrum is symmetrical about zero Doppler frequency.

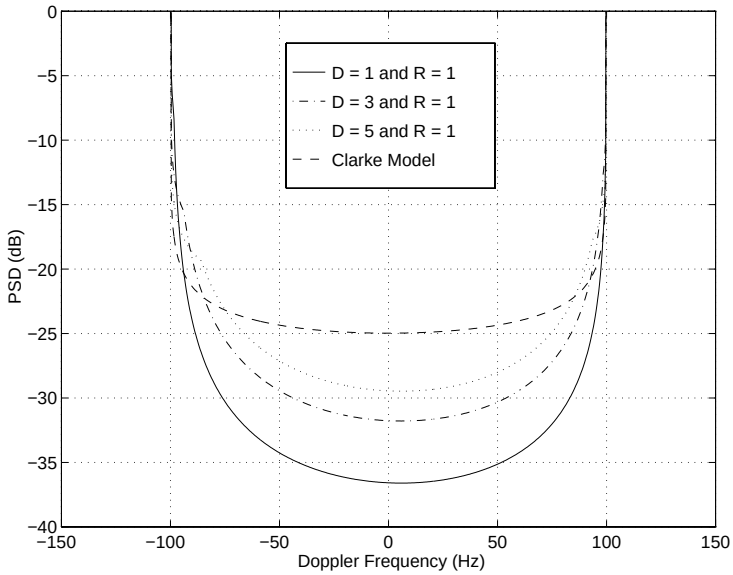

(a)

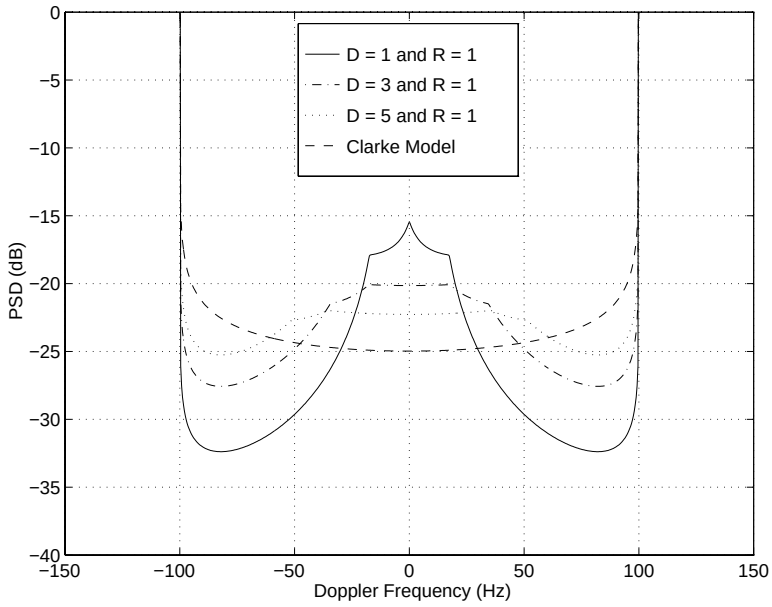

(b)

Figure 6.15: Doppler spectra when using a directional antenna at the base station is compared with the Clarke's model. The radius of the scattering circle is 1 km and the T-R separations of 1, 3, 5 kms are considered. The motion of the mobile is (a) 0 degrees and (b) 90 degrees with respect to the direct component and is traveling at 54 kmph. The carrier frequency is 2 GHz and the directional antenna uses a flat-top beam with a beamwidth of 10 degrees.

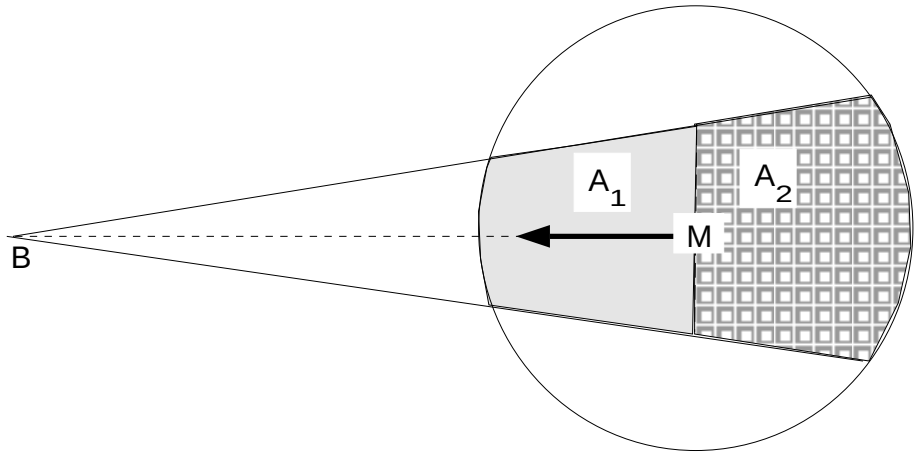

Figure 6.16: Figure illustrating the scatterers region that causes positive and negative frequency components when the mobile is moving towards the base station along the line of sight component. The scatterers in the region A_1 and A_2 cause the positive and negative Doppler frequency components, respectively.

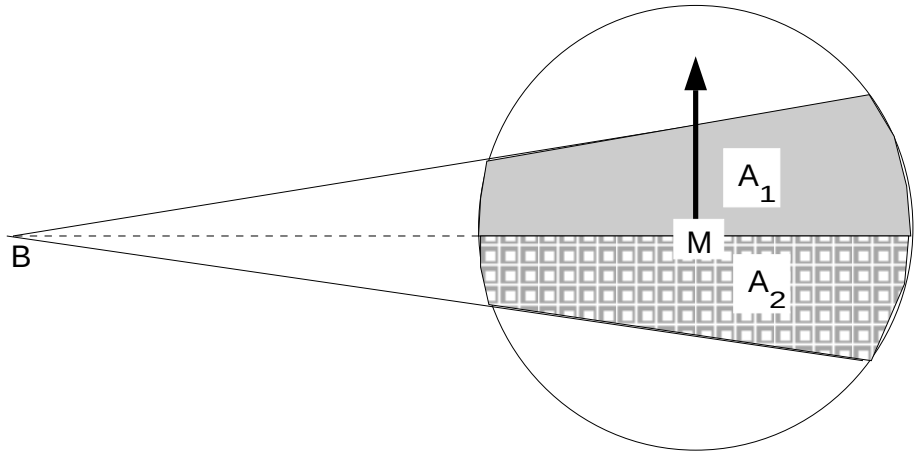

Figure 6.17: Figure illustrating the scatterers region that causes positive and negative frequency components when the mobile is moving perpendicular to the base station. The scatterers in the region A_1 and A_2 cause the positive and negative Doppler frequency components, respectively.

Figure 6.18(a) shows the Doppler spectrum for a fixed D/R ratio of 3 and the beamwidths of the antenna at the base station considered are 2, 10 and 30 degrees and $\phi_v = 0^o$. The Doppler spectrum for $\phi_v = 90^o$ is shown in Figure 6.18(b). As the beamwidth increases the Doppler spectrum tends towards the U-shaped Clarke's spectrum, because the pdf of the AOA at the mobile tends towards the uniform distribution. Figures 6.19 shows the fading envelope obtained using Clarke's model with maximum Doppler frequency of 100 Hz. The envelope is normalized by their RMS value. Figures 6.20 and 6.21 shows the fading envelope obtained when using a directional antenna with maximum Doppler frequency of 100 Hz for $\phi_v = 0$, and $\phi_v = 90^o$, respectively. The radius of the scattering circle is 1 km and the T-R separation is 3 kms. the directional antenna has a beamwidth of 2 and 30 degrees. From Figure 6.20, it can be seen that for a beamwidth of 2 degrees and $\phi_v = 0$ the envelope shows a periodic component. This is because as in Figure 6.18(a), the PSD for a beamwidth of 2 degrees shows components only in the region of maximum Doppler frequencies, i.e., around $\pm$ 100 Hz. From Figure 6.21, it can be seen that when $\phi_v = 90^o$, the envelope variation for beamwidth of 2 degrees is smaller compared to the case when the beamwidth is 30 degrees.

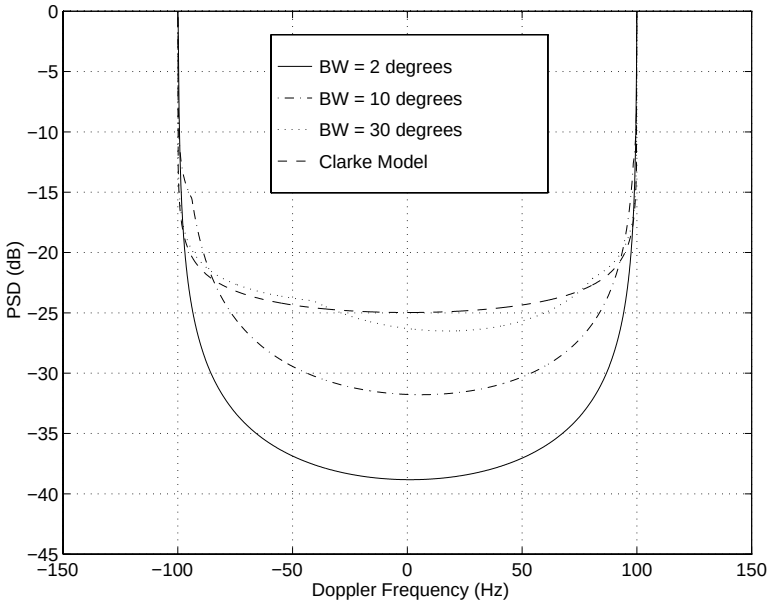

(a)

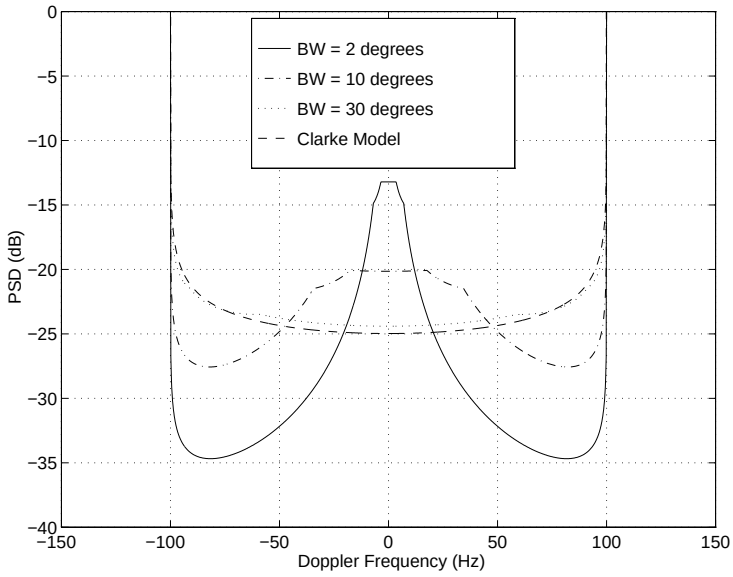

(b)

Figure 6.18: Doppler spectra when using a directional antenna at the base station is compared with the Clarke's model. The radius of the scattereing circle is 1 km and the T-R separations is 3 kms. The motion of the mobile is (a) 0 degrees and (b) 90 degrees with respect to the direct component and is traveling at 54 kmph. The carrier frequency is 2 GHz and the directional antenna uses a flat-top beam with beamwidths 2, 10, and 30 degrees.

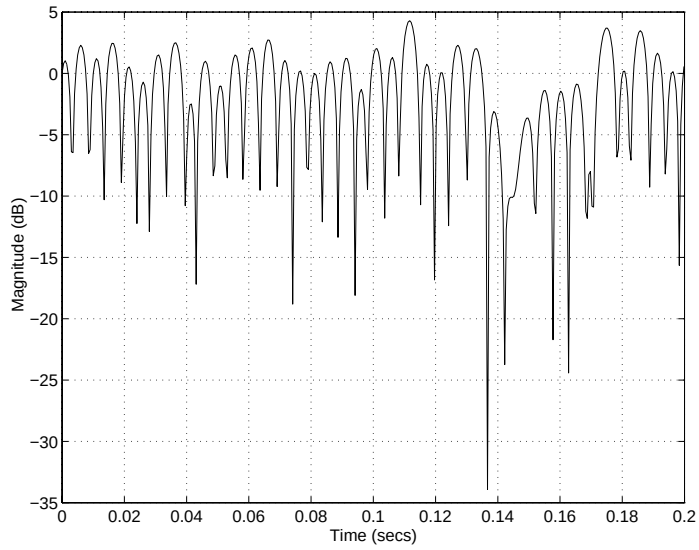

Figure 6.19: Fading envelope obtained using Clarke's model with maximum Doppler frequency of 100 Hz. The envelope is normalized by their RMS value.

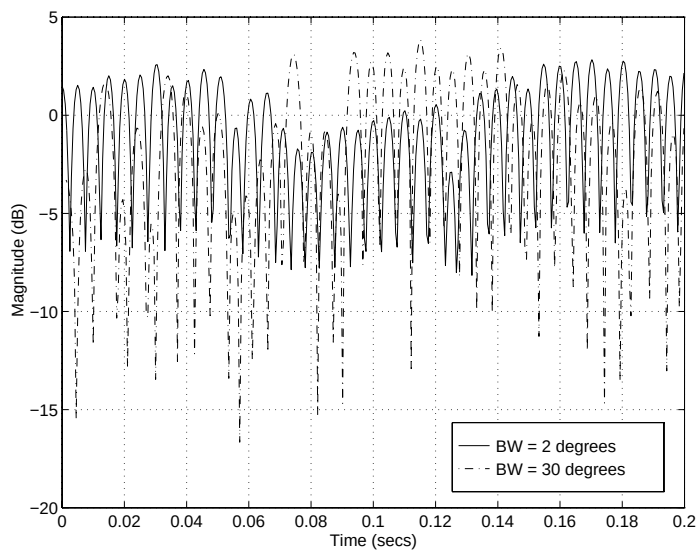

Figure 6.20: Fading envelope obtained when using a directional antenna with maximum Doppler frequency of 100 Hz. The envelope is normalized by their RMS value. The radius of the scattereing circle is 1 km and the T-R separation is 3 kms. The motion of the mobile is 0 degrees with respect to the direct component and the directional antenna has a beamwidth of 2 degrees and 30 degrees.

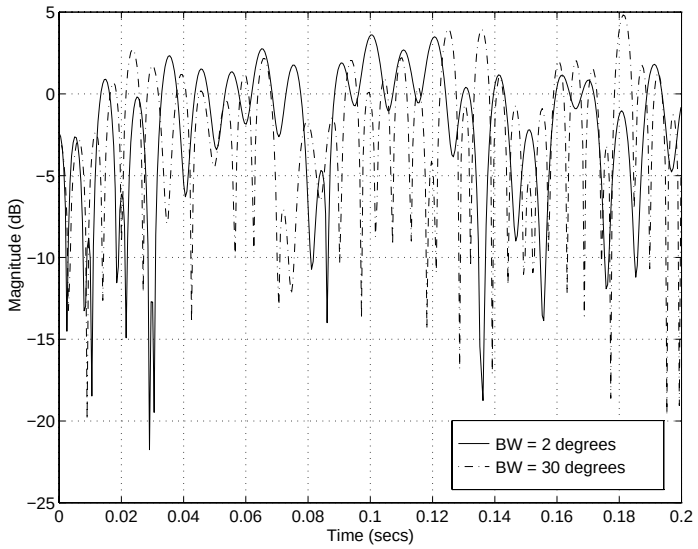

Figure 6.21: Fading envelope obtained when using a directional antenna with maximum Doppler frequency of 100 Hz. The envelope is normalized by their RMS value. The radius of the scattereing circle is 1 km and the T-R separations is 3 kms. The motion of the mobile is 90 degrees with respect to the direct component and the directional antenna has a beamwidth of 2 degrees and 30 degrees.

6.8 Summary

In this chapter, we have introduced a statistical geometric propagation model for a macrocell mobile environment. This channel model assumes that each multipath component of the mobile transmission undergoes only one bounce traveling from the transmitter to the receiver and the scatterers are located uniformly within a circle around the mobile. This Geometrically Based Single Bounce Macrocell (GBSBM) channel model provides three important parameters that characterize a channel: the power of the multipath component, the time-of-arrival (TOA) of the component, and the angle-of-arrival (AOA) of the components. This chapter presents a technique to generate such models for an arbitrary wireless system. In this chapter we have derived the power spectral density of the fading envelope when directional antennas are used at the base station.

Chapter 7

Adaptive Array Architecture and Algorithms for CDMA Signals

7.1 Introduction

Having explored the possibility of exploiting spatial diversity techniques for AMPS system, let us shift our focus to Code Division Multiple Access (CDMA) signals. CDMA is viewed by many researchers around the globe as the primary multiple access technique for the future. CDMA for cellular communication was proposed by Qualcomm, Inc. [68]. CDMA is a promising technology for future wireless systems as it provides more capacity than the conventional FDMA and TDMA techniques.

Recently there has been growing interest in applying multi-user interference cancelation techniques to further enhance the capacity (defined as the number of users/Hz/cell) of a CDMA cellular system. These techniques can be classified as nonlinear and linear techniques. The nonlinear techniques use the principle of decision feedback [69, 70, 71, 72]. In these receivers a tentative decision is made of the bits of the interferers and then the interferers are subtracted out from the received signal to estimate the desired user. These performance of these techniques rely on accurate estimation of amplitudes, phases and delays of all the users and hence suitable for AWGN channels. But in a practical cellular environment, channel imperfections hamper reliable estimation of the users' parameters.

Linear techniques [73] are easy to implement and they make fewer assumptions

about the channel. All the above techniques fall under single-channel MAIMUR techniques.

Multi-channel MAIMUR techniques use multiple spatially separated sensors. Adaptive antenna array techniques fall under this category. Adaptive array algorithms for CDMA are classified as *1) conventional algorithms 2) blind adaptive algorithms 3) channel estimation algorithms.* Conventional algorithms use the knowledge of the desired or training signal and the received signal to adapt its weights. Blind adaptive array algorithms on the other hand do not require any training signal, these algorithms use the properties of the signals (e.g., constant modulus, cyclostationarity, knowledge of the code, ...) to adapt the weights. These algorithms can save bandwidth compared to the conventional techniques, because of the reduction in overhead with transmission and offer more flexibility to the networking protocols. Channel estimation techniques use the knowledge of the special code properties of the SS signal to obtain estimates of the channel parameters. In this research, we will consider only the blind adaptive array algorithms to adapt the antenna weights.

7.2 CDMA design philosophies

There are two different philosophies in CDMA: Random CDMA (R-CDMA) and Deterministic CDMA (D-CDMA) [74]. R-CDMA uses a very long pseudo-random (PN) sequence (e.g., IS-95) and is inherently unsuitable for linear interference cancelers, which require each user to occupy unique dimension in the signal space. D-CDMA assigns a unique dimension to each user. Hence D-CDMA uses PN sequences that have a period of one bit or code sequences symbol of a user. The sequences assigned to different users are designed to have low cross-correlations.

The two aforementioned designs treat multiple access interference differently. Since R-CDMA uses a long PN sequence, MAI is treated as AWGN and also powerful error correction codes are used. Coding gains of 3-7 dB are obtained for AWGN channel and even more for fading channels, when appropriate interleavers are used. For each user to treat the interferers as AWGN, power control is necessary, otherwise near-far problem results.

D-CDMA differs from R-CDMA because it relies on the uniqueness of the dimension a signal occupies in the signal space. The signature (PN) sequences of different users are weakly correlated and hence multi-user detection techniques can be applied. Most of the D-CDMA systems don't address the issue of error control coding because at the symbol level the SNR is reduced due to coding, this will affect the speed of convergence of linear interference cancelers [74].

7.3 Parameters of the deterministic CDMA under consideration

GloMo project involves developing a modem for a D-CDMA system. The GloMo project aims at incorporating advanced signal processing techniques to enhance the capacity of a wireless network. This wireless network is applicable to a microcell and it has a base station which employs on adaptive array to separate one mobile user from the other. In addition to the adaptive array, the base station employs multi-stage interference cancelation techniques. The mobile unit employs a linear fractionally-spaced equalizer to reject interference and combine multipaths.

7.3.1 GloMo parameters

The GloMo system parameters are listed below:

- Multiple access - Direct sequence CDMA
- Modulation Scheme - BPSK
- Code-on-pulse modulation, i.e, one PN sequence fits exactly in one bit
- Number of chips per bit - 15
- Carrier frequency - 2.05 GHz
- Data rate - 128 kbps
- Chip rate - 1.92 Mcps
- Sampling rate - 7.78 MHz

7.3.2 Base station architecture

The architecture and the features of the base station are listed below.

Adaptive array

- Number of elements in the uniform linear array - 8
- Spacing between the antenna elements - $\lambda/2$
- Adaptation - Blind
- Architecture - multi-target system

Multi-stage interference canceler

- Cancellation type - parallel
- Number of stages of cancelation - 2

7.3.3 Mobile unit architecture

The mobile unit uses a 30 tap linear-fractionally spaced equalizer for interference cancelation.

7.4 Choice of processing - narrowband or wideband processing ?

In order to decide whether narrowband or wideband processing is required, we need to relate the bandwidth of the signal to the carrier frequency. If the signal bandwidth relative to the carrier frequency is small, then the propagation delay across the array must be small compared to the inverse bandwidth of the signal.

The carrier frequency (f_c) for the GloMo is 2.05 GHz and the corresponding wavelength is approximately 0.1463 m. The array is a ULA with 8-elements and has an inter-element spacing of $\lambda/2$, therefore the array aperture is $4\lambda = 0.585$ m. The maximum time (τ) necessary for the signal to propagate across the array is then

$4\lambda/c = 1.95$ nsecs, where $c = 3 \times 10^8$ m/s. The largest delays occur when the signal is coming from the end-fire of the array, and under this condition the signal undergoes a delay of 1.95 nsecs to travel across the array. If the signal is coming from the broadside, the signal will have no relative delay.

The first null-to-null signal bandwidth (B) is 3.84 MHz. Using the largest expected time delay, the highest frequency component of the signal experiences a phase shift of

$$2\pi(f_c + B/2)\tau = 2\pi(2051.92 \times 10^6)(1.95 \times 10^{-9}) = 25.140557 = 0.007815 radians,$$

while the lowest frequency component experiences a phase shift of

$$2\pi(f_c - B/2)\tau = 2\pi(2048.08 \times 10^6)(1.95 \times 10^{-9}) = 25.09350 = -0.03924 radians.$$

The difference in the phase shift between the highest and the lowest frequency component is 0.04705 rad or 2.966 degrees. Even for the worst case scenario, the difference in the phase shift is only 2.9 degrees, this is a very small deviation from the narrowband assumption, hence it will be accurate to model the GloMo signal as a narrowband signal. Hence narrowband array processing is a good choice.

7.5 Adaptive array architecture

The adaptive array is based on a multi-target system [5] which is shown in Figure 7.1. The Multi-Target Adaptive Array (MTAA) essentially performs multi-user detection at the base station. The main components of a multi-target adaptive array are:

- Sensors
- RF front end
- Signal digitization and baseband conversion
- Baseband processing

The MTAA has M spatially separated sensors which can be simple monopoles. by a RF chain also called a RF channel. Each RF chain is followed by a signal digitization

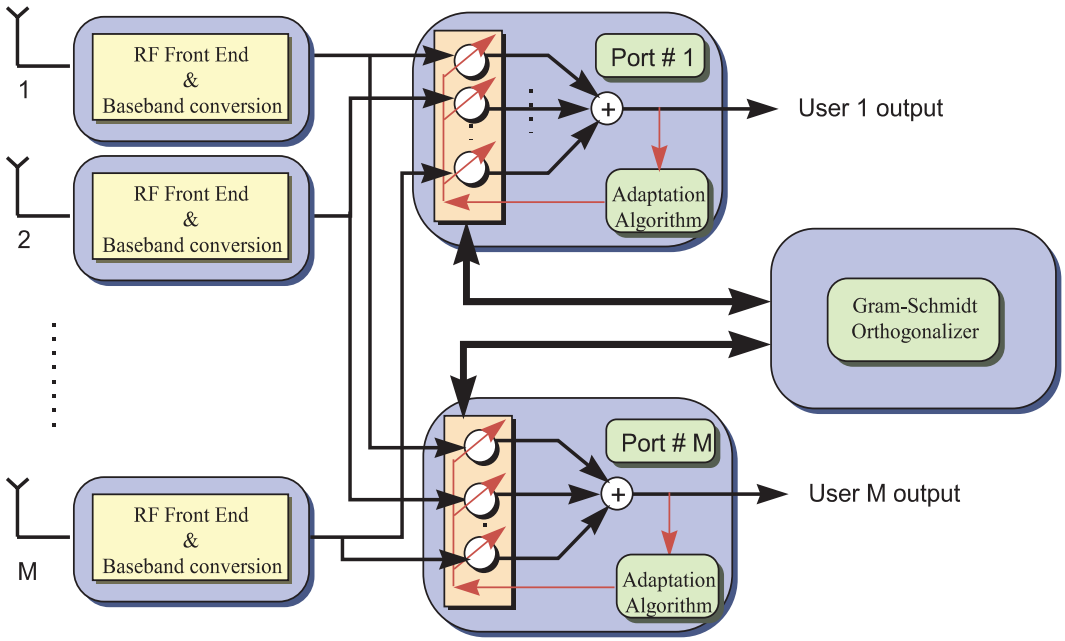

Figure 7.1: Block diagram of a multi-target adaptive array architecture for an algorithm that lacks signal-selectivity.

and a baseband conversion section. The MTAA has beamformers following the baseband conversion stage, which are also referred to as *ports*. Each port has M weights that multiply the signal from each sensor and the outputs are summed up to form the output of the port. The weights are adaptive and they are adapted by a blind algorithm.

7.6 Multi-target adaptive array framework

To do multi-user detection at the base station, the MTAA architecture is the most suitable architecture. The MTAA has parallel beamformers adapting independent of each other and the number of beamfomers in a MTAA is dependent on the algorithm that is used to adapt the weights. The MTAA architecture varies with the signal-selectivity property[1] of the algorithms.

[1] An algorithm is said to be signal-selective if it can distinguish a particular user from the rest.

7.6.1 MTAA architecture for an algorithm that lacks signal-selective property

The MTAA architecture for an algorithm that lacks signal-selectivity is shown in Figure 7.1. To prevent a signal from being captured by multiple ports, orthogonalization of the weight vectors is applied. The MTAA architecture for an algorithm that lacks signal-selectivity has two important components: adaptation algorithm and orthogonalizer. In this architecture, the maximum number of parallel beamformers in the MTAA is equal to the number of sensors in the array. Therefore if the array is *overloaded*, i.e., the number of users is more than the number of elements, then multiple users appear at the port outputs.

• Adaptation algorithm

The parallel beamformers in the MTAA are adapted using blind adaptive algorithms to maximize SINR of each user. The adaptation algorithms considered in this research fall under the constant modulus (CM) type algorithms. The Multi-Target (MT) framework is flexible to accommodate any type of adaptation algorithm. The following are the existing adaptation algorithms that lacks signal-selectivity considered in this research:

- Steepest descent multi-target decision directed array
- Least squares multi-target constant modulus array

• Orthogonalizer

Many blind algorithms, like the CM type algorithms do not have the ability to be signal-selective and hence in order to prevent a signal captured by two different ports, the beams corresponding to different beamformers have to be forced to point beams in different directions. To force the weight vectors to be independent of each other, hard orthogonalization is employed. Gram-Schmidt Orthogonalization (GSO) is the hard-orthogonalization procedure used. Figure 7.2 shows the operation of a MTAA. The weights of the beamformers are initialized to an omnidirectional beampattern and

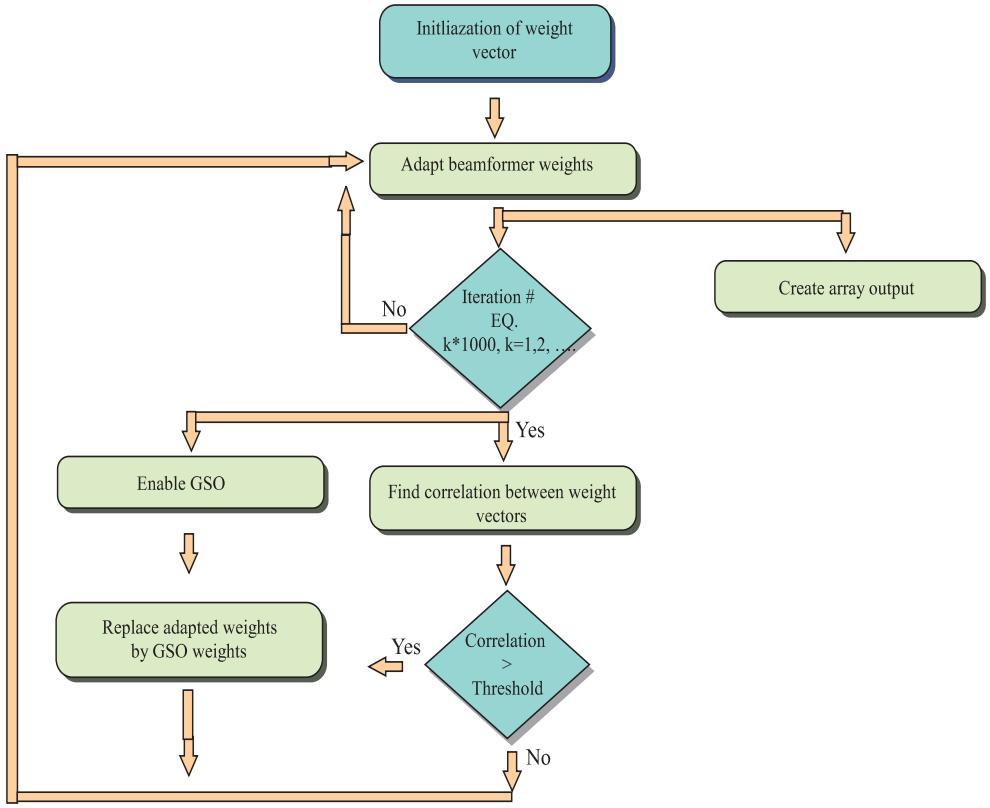

Figure 7.2: Signal flow chart of the MTAA driven by a non-signal-selective algorithm.

the CM-type adaptive algorithm is applied. After every 1000 iteration or samples, the GSO procedure is applied to the weight vectors. The weight vectors are then fed into a correlator which computes the correlation between the vectors. If the correlation between the weight vectors is higher than a threshold, the adapted weights are replaced by the GSO outputs. After this operation, the adaptation is continued and the output of the array is calculated for every input sample. It is important to note that the GSO is used only with algorithms that do not have the signal-selectivity property. As we will see in the next section, the novel algorithm that have signal-selectivity is introduced and the algorithm does not require the GSO.

- **Sorting and Classification**

MTAAs that use algorithms that lack signal-selectivity needs sorting and classification, i.e., the output of a beamformer has to be related to a particular user. To relate a particular user to the output of a port, the output of each port has to be correlated with the code of each user. Therefore the sorting and classification operation requires ${}_kC_2$[2] correlators if the correlations are done in parallel.

7.6.2 MTAA architecture for an algorithm that has signal-selective property

The MTAA architecture for an algorithm that is signal-selective is shown in Figure 7.3. Let k be the number of users in the environments and the MTAA can have a maximum of k parallel beamformers, while an MTAA structure that is driven by a non-signal-selective algorithm can have only M beamformers. This is because using an M element array, only M orthogonal weight vectors can be obtained and hence only M beamformers. On the other hand, the MTAA for a signal-selective algorithm can have k beamformers since no orthogonalization is employed. Here we consider two signal-selective algorithms:

- Least squares despread respread multi-target array (LS-DRMTA)
- Least squares despread respread multi-target constant modulus array (LS-DRMTCMA)

LS-DRMTA is well known in the literature, but the LS-DRMTCMA is a novel algorithm introduced in this research. These algorithms use the knowledge of the PN codes of the users to achieve signal separation.

7.7 Existing property restoral adaptive array algorithms

In this section, we discuss existing blind adaptive algorithms that are relevant to the CDMA problem. These algorithms lack signal-selectivity, because they are based on

[2] C is the combinatorial operator.

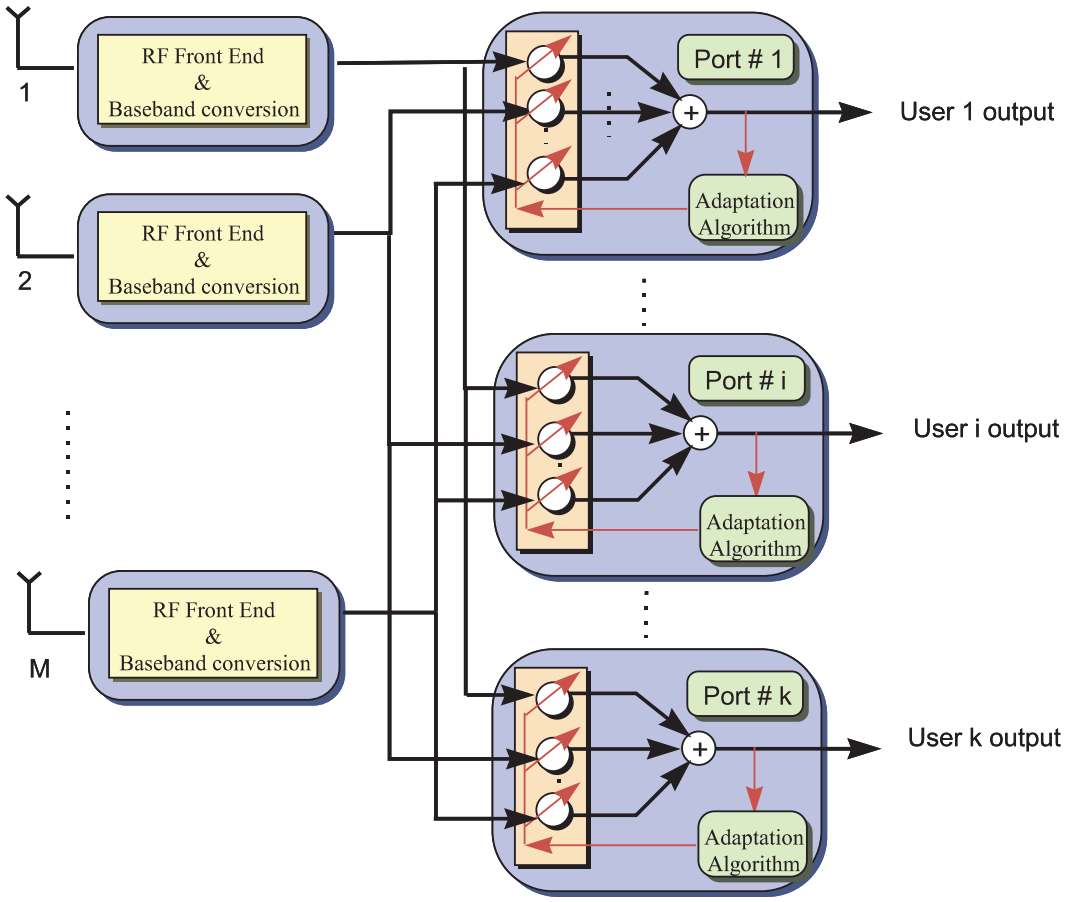

Figure 7.3: Block diagram of a multi-target adaptive array architecture for a signal-selective algorithm.

either CM or decision-directed adaptation.

7.7.1 Steepest Descent Multi-Target Decision Directed Array (SD-MTDDA)

SD-MTDDA is an MTAA based on decision directed adaptation (DDA). SD-MTDDA is used to provide a baseline comparison for other algorithms. A decision directed adaptation algorithm is usually recommended when the eye pattern of the input signal appears open. Decision directed algorithm is classified as a *bussgang algorithm* because it uses a zero-memory nonlinearity [3].

Let $\mathbf{x}(n)$ be the complex input signal vector, $\mathbf{w}(n)$ be the complex weight vector,

and *y(n)* be the complex signal at the output of the array at time n. In a decision-directed algorithm, the nonlinear operation is a threshold operation. The weight update equation for decision-directed algorithm is given by

$$\mathbf{w}_{k+1}(n) = \mathbf{w}_k(n) + \mu e^*(n)\mathbf{x}(n), \tag{7.1}$$

where $e(n) = sgn(real(y(n)) - y(n)$ and $sgn(.)$ is the signum function equal to +1 if the argument is > 0 and -1 if the argument is < 0. The decision directed algorithm for a BPSK signal projects the output from the beamformer to the closest constellation point and uses the closest constellation point as the reference signal. Naturally, if the constellation of the output of the beamformer is on the correct side of the constellation plane or the eye is open, decision directed performs like a trained algorithms. But if the constellation of the output of the beamformer is on the wrong side of the plane, wrong decisions are fedback and this results in poor performance. Suppose that the following conditions are satisfied:

1. The eye pattern is open
2. The step-size parameter μ used in the adaptation is fixed
3. The observed signal $\mathbf{x}(n)$ is ergodic in the sense that

$$\lim_{N\to\infty} \frac{1}{N} \sum_{n=1}^{N} \mathbf{x}(n)\mathbf{x}^T(n) \to E\left[\mathbf{x}(n)\mathbf{x}^T(n)\right]$$

almost surely.

Then, under these conditions, the weight vector converges to the optimum (Weiner) solution in the mean-square sense. But unfortunately if the array is overloaded the eye is not open and hence results in poor BER performance.

7.7.2 Least Squares Multi-Target Constant Modulus Array (LS-MTCMA)

The decision directed algorithm works only when the eye is open, because the algorithm inherently creates a reference signal by destroying the phase. But a CM

algorithm preserves the phase of the output of beamformer and forces the magnitude to be unity. A CM algorithm minimizes a cost function $J_{(p,q)}$ given by [23]

$$J_{(p,q)} = \langle ||y(n)|^p - 1|^q \rangle \,, \tag{7.2}$$

where p and q can take values 1 or 2 and $y(n)$ is the output of the beamformer. Least squares constant modulus algorithm (LSCMA) is a block-based algorithm which minimizes $J_{(1,2)}$ cost function. This is the fastest converging algorithm of the CMA family. The weight vector of the beamformer that minimizes the cost function in Eqn. 7.2 is given by

$$\mathbf{w} = \mathbf{R_{XX}}^{-1}\mathbf{r_{Xd}}, \tag{7.3}$$

where $\mathbf{d}$ is the reference signal, $\mathbf{R_{XX}}$ is the input spatial autocorrelation matrix and $\mathbf{r_{Xd}}$ is the cross-correlation vector of the input and the reference signal. The LSCMA is implemented as follows:

1. $\mathbf{R_{XX}}$ is computed using a block of data .
2. The weight vector $\mathbf{w}$ can be initialized so that the beamformer has an omnidirectional pattern.
3. The output vector of the beamformer is computed as $\mathbf{y} = \mathbf{w}^H\mathbf{X}$, where $\mathbf{X}$ is the input data matrix.
4. The reference signal vector is calculated as $\mathbf{d} = \mathbf{y}./\,|\mathbf{y}|$, where ./ is an element-by-element divisor.
5. The weight vector is then computed using Eqn. 7.3.
6. Steps 2 to 5 are repeated till the algorithms converges.
7. A new block of data is fetched and Steps 1 to 6 are repeated and the initial weights for the new block are the weights from the previous block.

LS-MTCMA is an MTAA that uses the LSCMA based adaptation.

7.8 Despread Respread adaptive array algorithms

The despread-respread based blind algorithms have good signal-selectivity properties. These algorithms use the PN codes which are unique to each user in the adaptation to achieve signal-selectivity. The advantages of these algorithms over the existing algorithms are

- MTAA architecture does not require GSO and sorting.
- These algorithms provide better signal-selectivity and better performance over existing algorithms.

The disadvantage of these algorithm over existing algorithms is that they require synchronization and the algorithm may suffer if proper synchronization is not achieved. On the other hand, the existing algorithms do not require synchronization for adapting the beamformer. Synchronization for the existing algorithms are done after beamforming, where the SINR is higher than at the input of the array. Synchronization issues are less critical for existing algorithms than for these algorithms.

7.8.1 Least Squares Despread Respread Multi-Target Array (LS-DRMTA)

This algorithm is based on the principle of *despread-respread*. Let us assume that we are interested in separating the signal of the ith user from the others. A block diagram of a LS-DRMTAA is shown in Figure 7.4. The figure shows the ith beamformer configure to enhance the ith user. A despread-respread technique works on the principle of despreading the signal at the output of the ith beamformer and then making a bit decision. Then the ith user's PN code C_i *re*spreads the data bit. Then the error between the respread data and the output of the array is minimized using a least-squares or a steepest descent approach. The fundamental assumption behind the despread-respread based adaptation is that the synchronization has been achieved prior to beamforming, because despreading requires synchronization. The despread-respread technique is very similar to the *demod-remod* technique, which is used to reject interference for FM signals.

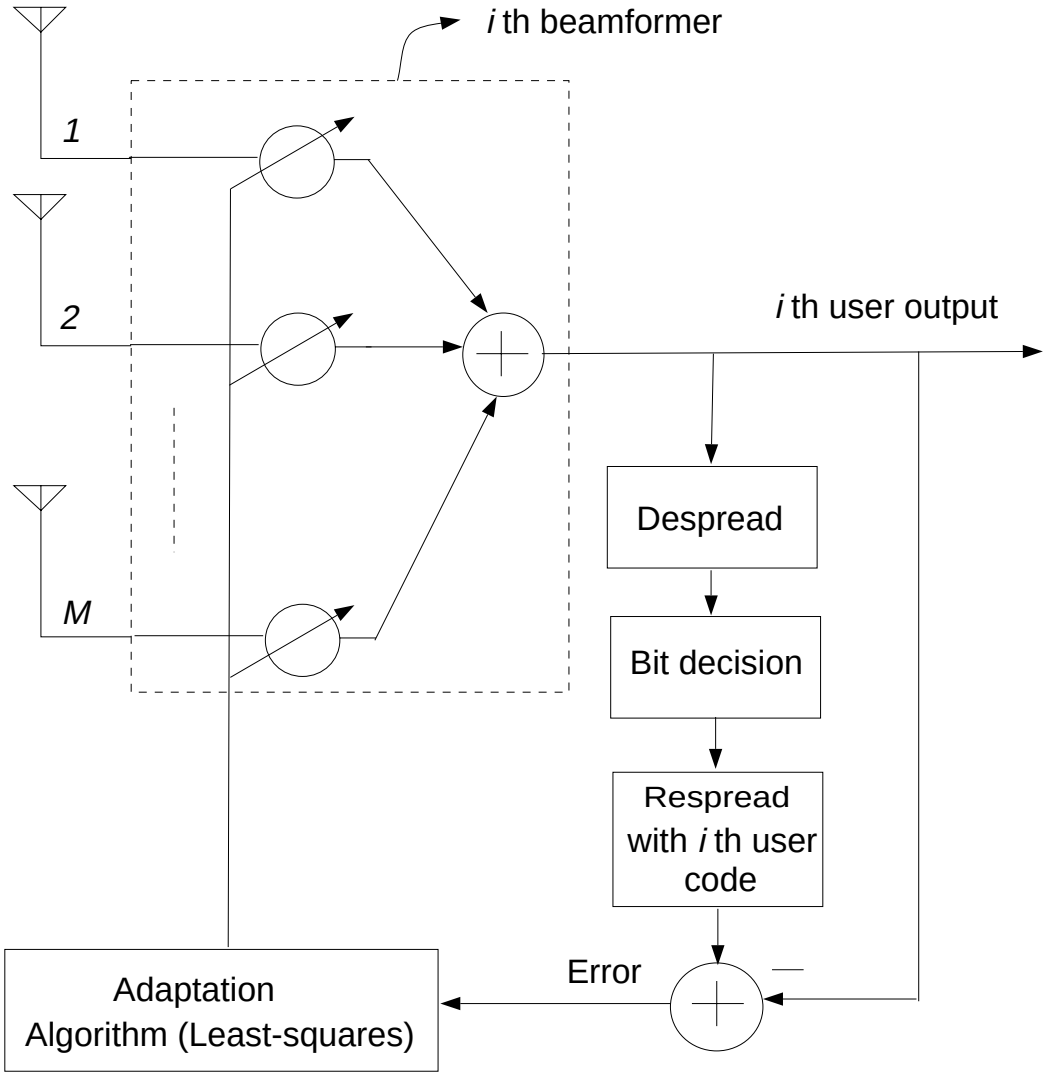

Figure 7.4: Block diagram of the LS-DRMT adaptive array.

LS-DRMTAA is an adaptive array algorithm based on despread-respread techniques. This algorithm minimizes the error between the respread data and the output of the array in the least-squares sense. Let $y_i(k)$ be the output of the ith beamformer at the time instant k. The beamformer minimizes an objective J which is defined as

$$J = \left\langle \left| C_i(p) \left(sgn \left[\sum_{j=1}^{NT_c} y_i((n-1)T_c + j) C_i(j) \right] \right) - y_i(k) \right|^2 \right\rangle, \tag{7.4}$$

where

$|.|$ is the absolute operation,
$k = (n-1)T_c + p$,
$p = 1 : NT_c$,
N is the *processing gain*,
sgn is the *signum function*,
T_c is the *chip duration*,
and $\langle . \rangle$ is the time-averaging operation as opposed to ensemble-averaging.

The weight vector that minimizes the above cost function is given by

$$\mathbf{w} = \mathbf{R_{XX}}^{-1} \mathbf{r_{Xd}}, \tag{7.5}$$

where $d = C_i(p) \left(sgn \left[\sum_{j=1}^{NT_c} y_i((n-1)T_c + j) C_i(j) \right] \right)$, $\mathbf{R_{XX}}$ is the input spatial autocorrelation matrix and $\mathbf{r_{Xd}}$ is the cross-correlation vector of the input and the output of the respreader.

7.8.2 Least Squares Despread Respread Multi-Target Constant Modulus Array (LS-DRMTCMA)

LS-DRMTCMA is also an adaptive array algorithm based on despread-respread techniques. This is a *novel* algorithm introduced in this research. This technique combines a CM-type adaptation with the despread-respread adaptation. The motivation behind combining CM-type adaptation with despread-respread type adaptation is to get better performance by using the processing gain of the system (despread-respread) and the constant modulus property of the signal. A block diagram of a LS-DRMTAA

is shown in Figure 7.5. The figure shows the ith beamformer trying to separate the ith user. In this algorithm, the reference signal is derived as the weighted sum of the respread data and the output of the array after a complex limiter operation.

The adaptation algorithm minimizes the difference between the reference signal and the output of the array in the least-squares sense. The beamformer minimizes an objective J which is defined as

$$J = \left\langle \left| k_1 C_i(p) \left(sgn \left[\sum_{j=1}^{NT_c} y_i((n-1)T_c + j) C_i(j) \right] \right) + k_2 \frac{y_i(k)}{|y_i(k)|} - y_i(k) \right|^2 \right\rangle, \quad (7.6)$$

where $|.|$ is the absolute operation. The first term in the cost function is the output of the respread block and the second term is the output of the constant modulus constraint block. k_1 and k_2 are weights given to the respread data and the output of the array after a complex limiter operation, respectively in deriving the reference signal. k_1 and k_2 are related by $k_1 + k_2 = 1$. The reference signal is given by

$$d = k_1 C_i(p) \left(sgn \left[\sum_{j=1}^{NT_c} y_i((n-1)T_c + j) C_i(j) \right] \right) + k_2 \frac{y_i(k)}{|y_i(k)|}. \quad (7.7)$$

where

$k = (n-1)T_c + p$,
$p = 1 : NT_c$,
N is the *processing gain*,
sgn is the *signum function*,
and T_c is the *chip duration*.

If $k_1 = 0$ and $k_2 = 1$, then the LS-DRMTCMA reduces to a LS-MTCMA without GSO, and if $k_1 = 1$ and $k_2 = 0$, then the LS-DRMTCMA reduces to LS-DRMTA. For the simulation study, we use $k_1 = k_2 = 0.5$. The choice of k_1 and k_2 will be justified in the simulation section.

The MTAA architecture based on the signal-selective algorithms do not suffer from the problem of *port-shuffling* which is inherent of CM-type algorithms when the array is operated in a fading environment. Port-shuffling is the problem of the signal of a particular user jumping from one port to the other. Therefore under such environments when using CM-type algorithm we need to keep track of users as they

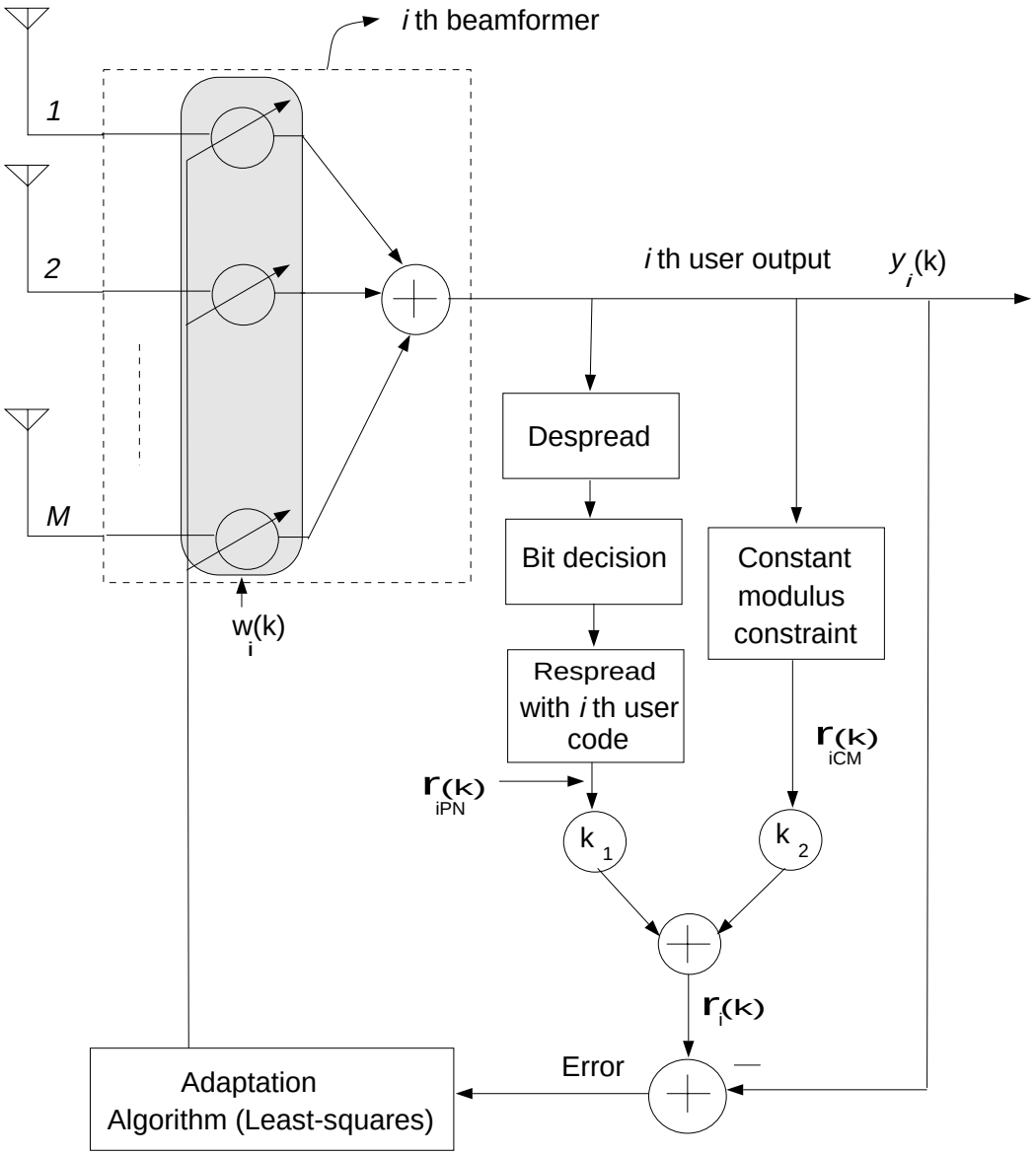

Figure 7.5: Block diagram of the LS-DRMTCM adaptive array.

jump from one port to the other. This problem does not arise if signal-selective algorithms are used.

7.9 Simulation results

In this section, the performance of all the four algorithms in different mobile communication environments are compared to a conventional receiver. In addition for the AWGN test cases, the performance of these adaptive array algorithms will be compared to a 3-stage multistage interference canceler (3-stage IC) [75]. The simulation parameters used are explained in Section 7.3. Three different channel and receiver imperfections are considered in this simulation study. The channel and receiver imperfections considered here are: 1) AWGN channel, 2) timing offsets, and 3) frequency offsets. E_b/N_o (Mean bit energy/noise density) of 4 and 8 dB are considered in this study. Under each study of either channel or receiver imperfection, we will consider two cases, one where the AOA of the users are well separated (non-crowded case) and the other where the users are not well-separated (crowded-case). The AOAs of the users for the non-crowded case are uniformly distributed from 0 to 160 degrees, while for the crowded case, the AOAs of the users are uniformly distributed from 0 to 90 degrees. In the AWGN, timing and frequency offset test cases, the power of all users are assumed to be equal.

In all the simulations random codes of length 15 are used as the PN codes. Since the 8-element beamformer is implemented at the base station, the mobile users are *asynchronous*. Random delays and phase shifts are introduced to the users' signals to model the asynchronous transmission. To obtain an estimate of the BER with small variance, the phases and the delays of all the users are changed every 100,000 bits. The PN codes are also changed every 100,000 bits to average out the correlations between the PN codes of different users. A total number of 4 million bits are considered for each BER estimate. In all the simulations, a conventional correlation receiver follows the adaptive array.

7.9.1 Performance analysis in AWGN channel

In this section, the performance of the four adaptive algorithms are compared with a conventional receiver and a 3-stage multistage interference canceler (IC). The BER performance is measured after the algorithms converge and the weights are kept fixed after convergence.

- **Choice of the weighting factors (k_1, k_2) for the LS-DRMTCMA**

Here we analyze the proportion in which the reference signals derived from the CMA constraint and the despread-respread block have to be combined to derive the overall reference signal for the LS-DRMTCMA adaptation. In this simulation study, there are 10 equal powered users in the environment and $E_b/N_o = 8$ dB. k_1 value is varied from 0 to 1 while k_2 takes values from 1 to 0. Figure 7.6 is a plot of the BER at the output of LS-DRMTCMA as a function of k_1. It can be seen from the plot that the BER reaches a minimum for values of k_1 around 0.5. It is worth-noting that the curve is not symmetrical about $k_1 = 0.5$. Therefore we can conclude that even when the proportion of the CMA constraint is small (eg., $k_1 = 0.8$ and $k_2 = 0.2$), the performance is close to the optimal. For further simulations, we use $k_1 = k_2 = 0.5$ is used.

- **Non-crowded case**

Here the channel is modeled to be an AWGN channel and there is also multiple access interference in the environment. The main source for the AWGN is the receiver front-end noise, and this noise is added before the baseband conversion section and hence for the beamformer that follows the baseband conversion section, the noise appears to have no directivity. Since the digital beamforming techniques do not use any radiating elements, the noise from the receiver front-end appears to be coming from all azimuthal directions. The AWGN channel is characterized by E_b/N_o and here we consider E_b/N_o of 8 and 4 dB. The number of users in the environment is varied from 2 to 14. It is worth noting that the maximum number of ports in the LS-MTCMA and SD-MTDDA is 8, while the number of ports in the LS-DRMTA and

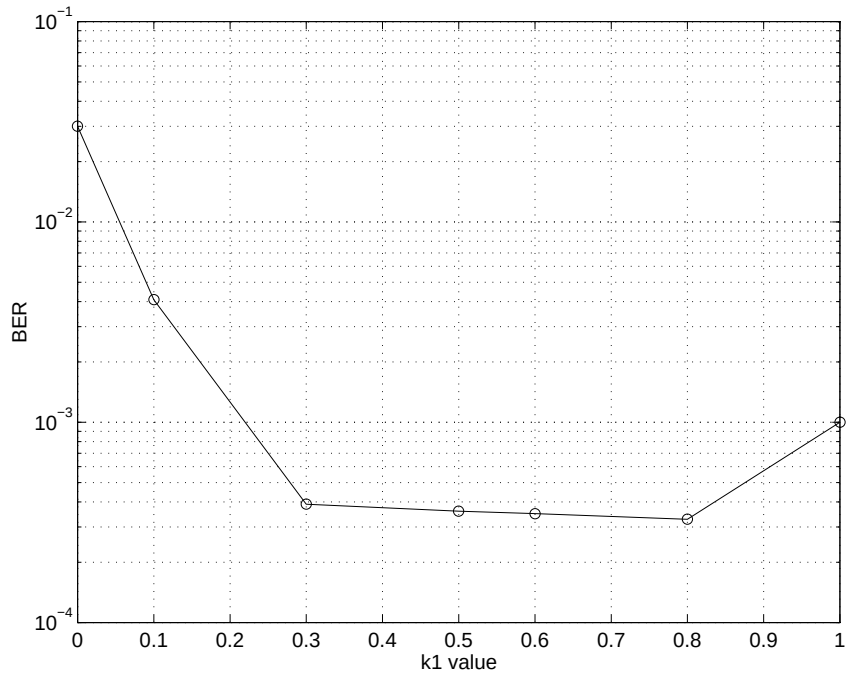

Figure 7.6: Plot of BER as a function of the weight k_1, and k_1 and k_2 are related by $k_1 + k_2 = 1$.

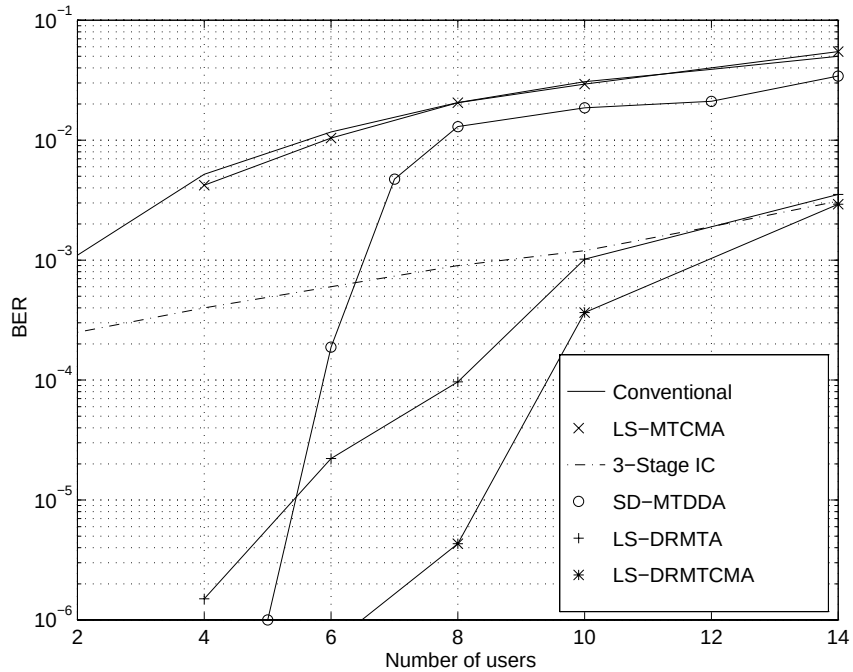

Figure 7.7: BER curves for all the techniques for the noncrowded case and $E_b/N_o =$ 8 dB.

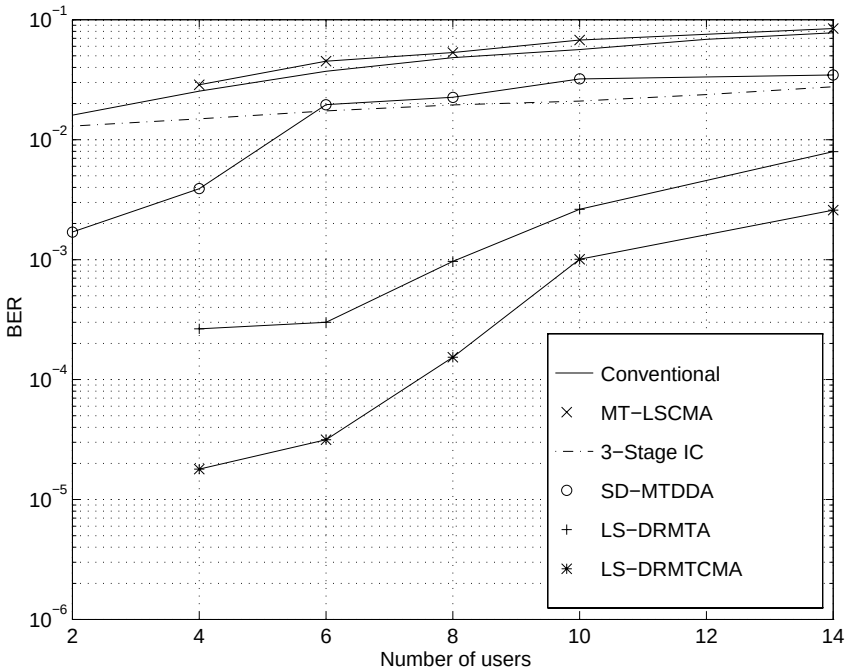

Figure 7.8: BER curves for all the techniques for the noncrowded case and $E_b/N_o =$ 4 dB.

LS-DRMTCMA is equal to the number of users. The BER results for the non-crowded case and the E_b/N_o of 8 dB are plotted in Figure 7.7.

The conventional receiver as expected performs worse than the other receiver structures. The MT-LSCMA performs worse than the other adaptive array algorithms, because of the following reasons.

- Here the users have the same power, CMA works well when the users have different powers.
- CMA is inherently not suitable for BPSK signals in the absence of frequency shift. CMA can combine 2 BPSK signals to create a QPSK signal. This is a major problem and hence it is cautioned that CMA based beamforming, though simple to implement, is potentially catastrophic when operated on BPSK signals.
- CMA performs satisfactory only when the E_b/N_o is high (e.g., 15 dB).

Therefore the LS-MTCMA performs no better than the conventional receiver. The SD-MTDDA performs far better than the LS-MTCMA for smaller number of users, but for larger number of users the DDA performs very similar to the conventional receiver. This is because DDA is guaranteed to perform well only when the eye is open which is the case when the number of users is small.

The performance of the 3-stage IC degrades gracefully as the number of users increases. The IC performs better than the SD-MTDDA for number of users greater than 6, therefore for the overloaded case the IC performs better than the MTAA based on non-signal selective blind algorithms. For number of users smaller than 6, the SD-MTDDA performs better because the SD-MTDDA not only increases the CIR but also reduces noise in the receiver. But an IC at its best can only remove interference but cannot eliminate noise.

LS-DRMTA, the MTAA that exploits the knowledge of the spreading code of the users, performs better than all the above discussed algorithms. It performs similar to the 3-stage IC for larger number of users and for smaller number of users the LS-DRMTA performs similar to the SD-MTDDA.

LS-DRMTCMA which uses not only the knowledge of the spreading code but also forces the output of the array to be a constant. This algorithm outperforms all other algorithms. If the acceptable BER is 10^{-3}, the LS-DRMTCMA is able to accommodate 6 times the number of users compared to a conventional receiver. It should be noted that the LS-DRMTA and LS-DRMTCMA assume synchronization which is also the assumption made in implementing the IC.

Results for $E_b/N_o = 4$ dB is shown in Figure 7.9, it can be seen that the performance of the 3-stage IC and the SD-MTDDA degrade significantly as the E_b/N_o decreases from 8 to 4 dB. The 3-stage IC eliminates interference but cannot reject noise, and therefore the IC cannot have a BER lower than 1.25×10^{-2}, which is the BER for the single user case, i.e., $Q(\sqrt{2E_b/N_o}) = 1.25 \times 10^{-2}$. The SD-MTDDA does not perform well because, for this noise dominated test case, the eye remains closed even for lower number of users. The LS-DRMTA and LS-DRMTCMA outperform other algorithms because these algorithms uses a better reference signal and these algorithms not only eliminate interference but also reduces the noise due to the array

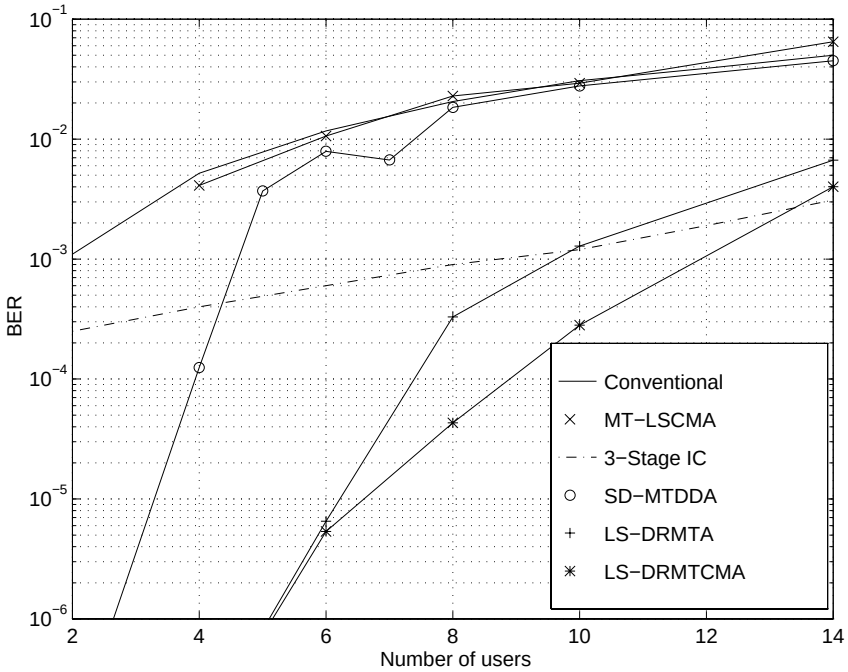

Figure 7.9: BER curves for all the techniques for the crowded case and $E_b/N_o = 8$ dB.

gain.

- **Crowded case**

In the crowded test case, all the users are concentrated in a 90 degree sector. The results for $E_b/N_o = 8$ dB are shown in Figure 7.9. The 3-stage IC and the conventional receiver are not affected by the location of the users and hence the performance of these receivers in the crowded and the non-crowded cases are similar. SD-MTDDA for the crowded case performs worse than the noncrowded case. If the acceptable BER is 10^{-3}, then using the SD-MTDDA two users are lost as the users concentrate within a 90 degree sector. This is obvious because for the crowded case the angular separation between the users is small for the array to resolve.

From Figure 7.9, it can be seen that the LS-DRMTA and LS-DRMTCMA perform better than the other receiver structures. The LS-DRMTA and LS-DRMTCMA perform close to optimal performance. This can be shown as follows. Let us consider the case where the number of users is 14 and the angular separation between

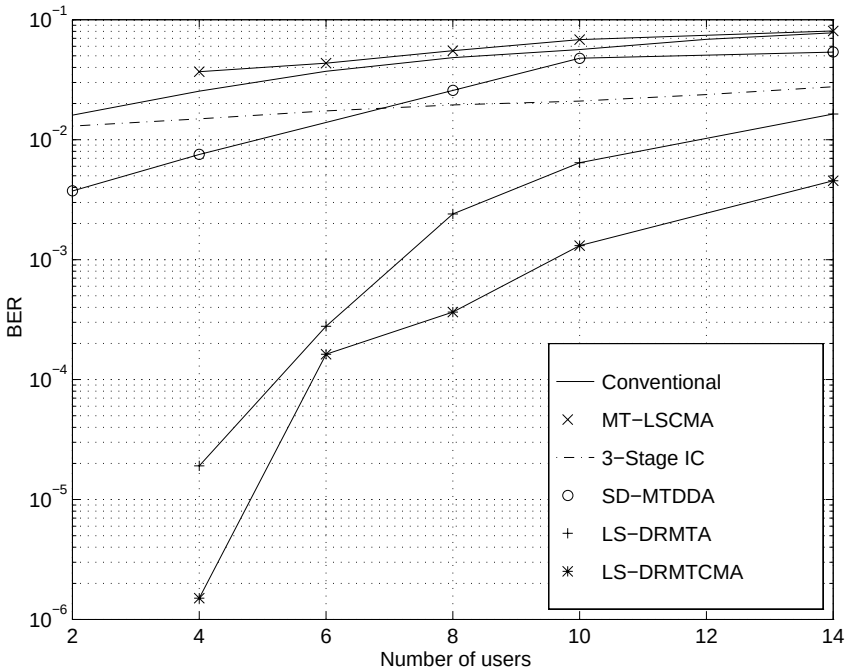

Figure 7.10: BER curves for all the techniques for the crowded case and $E_b/N_o = 4$ dB.

the users is approximately 6 degrees. An adaptive array with 8 elements can form a 15 degrees beam in the broadside and a 30 degrees beam along the endfire. On an average, there will be 4 users in each beam if the users are distributed in a sector of 90 degrees from the endfire to the broadside of the array. Therefore the array can reject 14 (number of users in the environment) - 4 (number of users in the beam) = 10 users in the environment for the crowded case. Therefore the BER performance of the LS-DRMTA and LS-DRMTCMA are close to the conventional receiver in the presence of 4 users.

Figure 7.10 shows the BER results for the crowded case and the $E_b/N_o = 4$ dB. The LS-DRMTA and LS-DRMTCMA perform better than other algorithms and the same trend is seen in this case the case when the $E_b/N_o = 8$ dB.

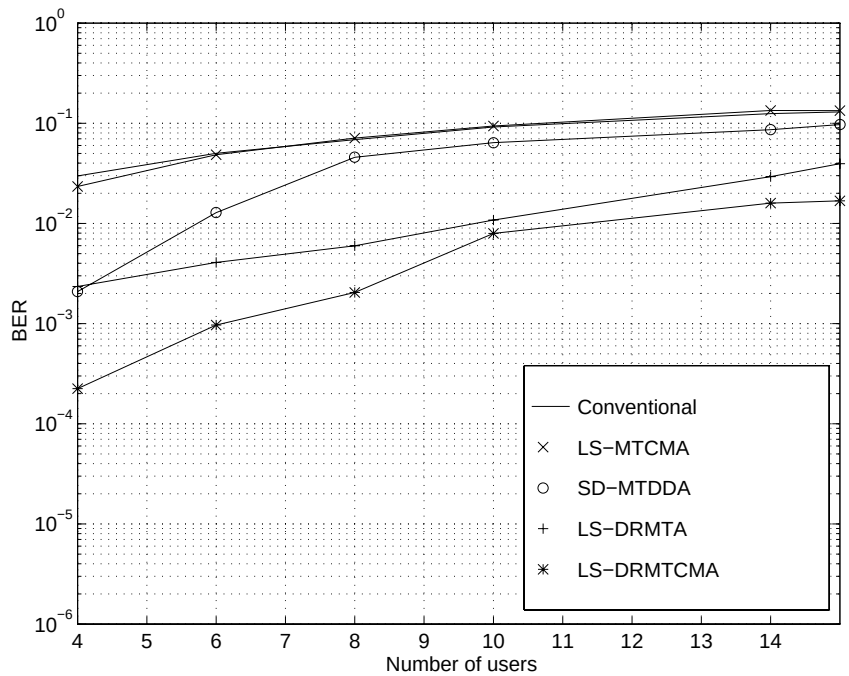

Figure 7.11: BER curves for all the techniques for the non-crowded case with a timing offset of 1/4 of the chip period and $E_b/N_o = 8$ dB.

7.9.2 Performance analysis in the presence of timing offset

Timing offset occurs when the locally generated PN sequence is not properly synchronized to the incoming signal. In this section, we analyze the performance of the algorithms in the presence of this receiver imperfection.

- **Non-crowded case**

Let us assume that the users are in the non-crowded fashion and the timing offset is 1/4 of the chip duration. The E_b/N_o is 8 dB. The BER performance of the various adaptive array receivers and the conventional receiver are shown in Figure 7.11. As seen is other test cases, LS-DRMTA and LS-DRMTCMA perform better than SD-MTDDA and the LS-MTCMA performs no better than the conventional receiver. If the acceptable BER is 10^{-2}, then the LS-DRMTA and LS-DRMTCMA can provide 5 to 6 times the capacity compared to a conventional receiver.

Figure 7.12 is a plot of the BER performance of the various receiver structures when the timing offset is 1/2 of the chip duration. The E_b/N_o is 8 dB. All the

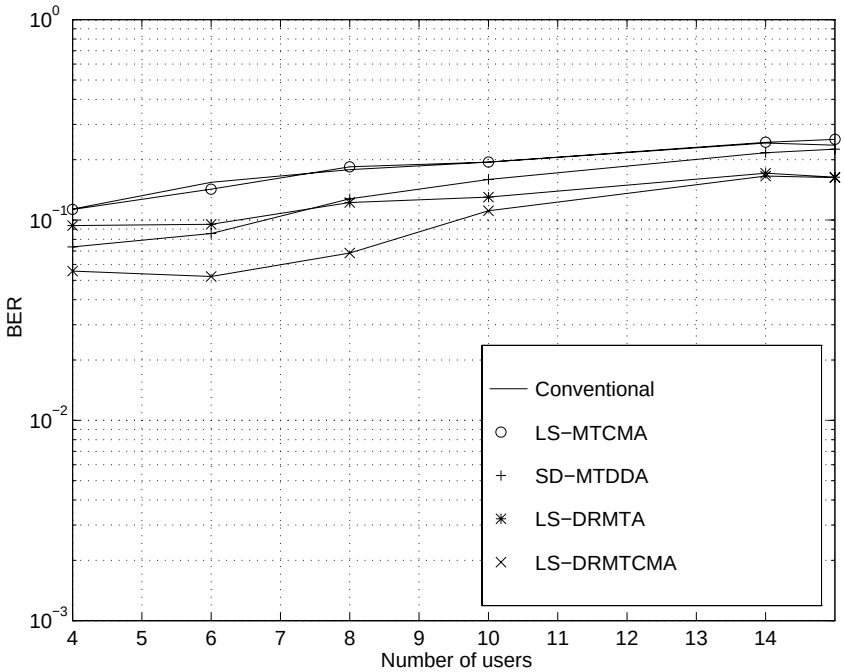

Figure 7.12: BER curves for all the techniques for the non-crowded case with a timing offset of 1/2 of the chip period and $E_b/N_o = 8$ dB.

receivers fail when the timing offset is 1/2 of the chip duration. The BER curves remain flat irrespective of the number of users. Figure 7.13 is a plot of the the BER performance as a function of timing offset for the noncrowded case. The E_b/N_o is 8 dB and the number of users in the environment is 10. The timing offset is varied from 0 to 1 chip duration. It can be seen that the performance of the LS-DRMTA and the LS-DRMTCMA does not degrade gracefully while the other receivers degrade gracefully. If the acceptable BER is 10^{-2}, then the LS-DRMTA and LS-DRMTCMA are the only receivers that can support users even when the offset is 1/4 of the chip duration. LS-DRMTA and LS-DRMTCMA are more robust to timing offset than the other receiver structures.

- **Crowded case**

Figures 7.14 and 7.15 are the BER performance curves for all the receivers for the crowded case for an E_b/N_o of 8 dB and the timing offsets are 1/4 and 1/2 of the chip

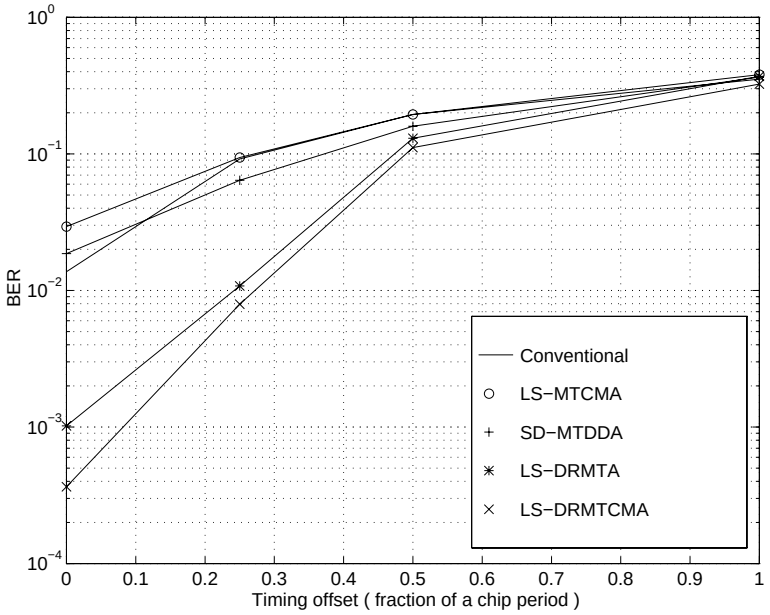

Figure 7.13: BER curves for all the techniques for the non-crowded case as a function of the timing offset and $E_b/N_o = 8$ dB.

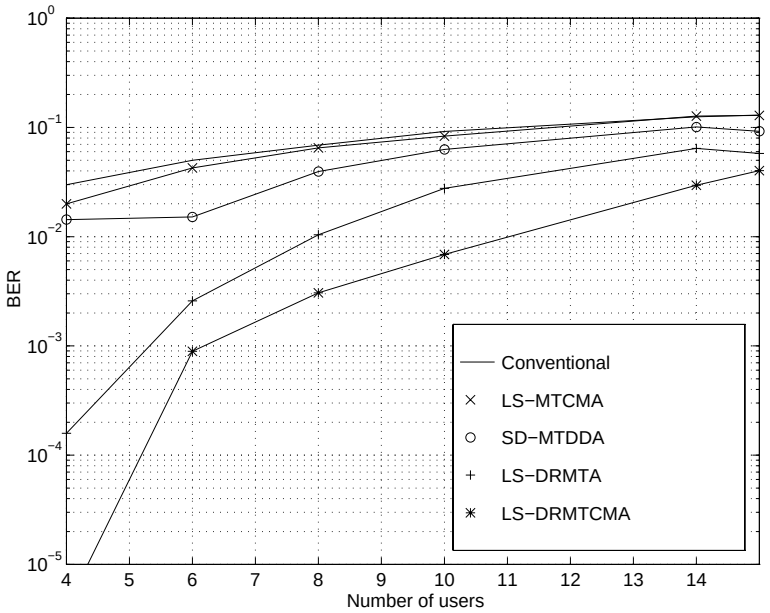

Figure 7.14: BER curves for all the techniques for the crowded case with a timing offset of 1/4 of the chip period and $E_b/N_o = 8$ dB.

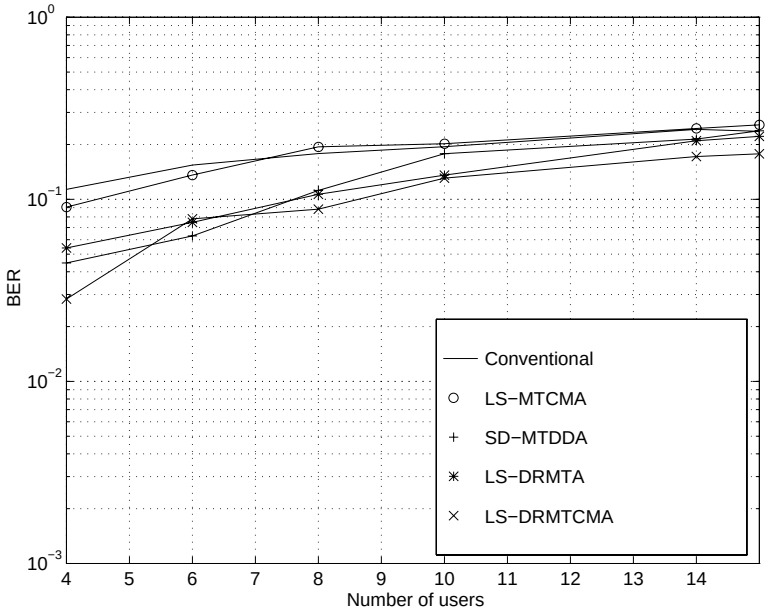

Figure 7.15: BER curves for all the techniques for the crowded case with a timing offset of 1/2 of the chip period and $E_b/N_o = 4$ dB.

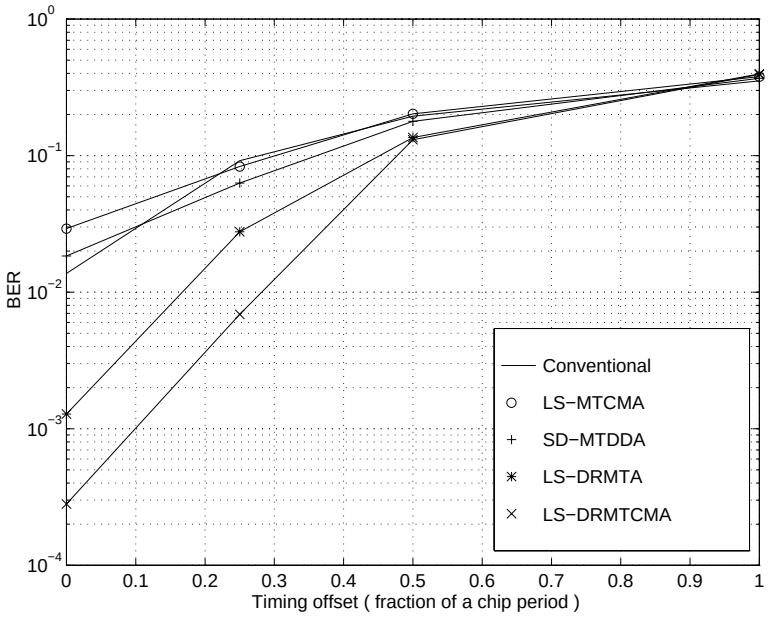

Figure 7.16: BER curves for all the techniques for the crowded case as a function of the timing offset and $E_b/N_o = 8$ dB

duration, respectively. The BER performance of the various receivers are very similar to the non-crowded case, but the performance of the receivers in the overloaded and crowded case is worse than the overloaded and non-crowded case. Figure 7.16 is a plot of the BER performance of the receivers as a function of timing offset for the crowded case.

7.9.3 Performance analysis in the presence of frequency offset

Frequency offset in the down-converted signal arises due to improper carrier tracking, therefore any difference in frequency between the local carrier and the incoming signal appears as the frequency offset in the baseband signal. The residual carrier can severely degrade the BER performance depending on the amount of frequency offset. The BPSK constellation spins around the unit circle due to the frequency offset, which can be viewed as a continuous phase shift to the constellation points. A chip error occurs when the constellation points crosses the imaginary line, if hard decision is applied to the chips.

For the frequency offset case, the adaptive array algorithms are allowed to converge and once the algorithm converges, the weights are *not* kept fixed, instead they are updated frequently depending on the frequency shift. Here we assume that we know the frequency of the residual carrier component in the baseband signal.

• Effect of the update rate of the algorithms on the performance in the presence of frequency offset

In this section, we will analyze the adaptation rate as a function of frequency offset to result in a satisfactory BER performance. Let us consider the LS-DRMTA and LS-DRMTCMA for this analysis, because these algorithms perform better than the others. Since frequency shift results in the constant spinning of the constellation points, the adaptive array algorithms has to updated fast enough to track the rotating phase. Let us first consider the LS-DRMTA in the presence of frequency offsets of 100 and 500 Hz. Figure 7.17 shows the BER performance of the LS-DRMTA as a function of maximum phase shift allowed before the adaptation is applied. Intuitively,

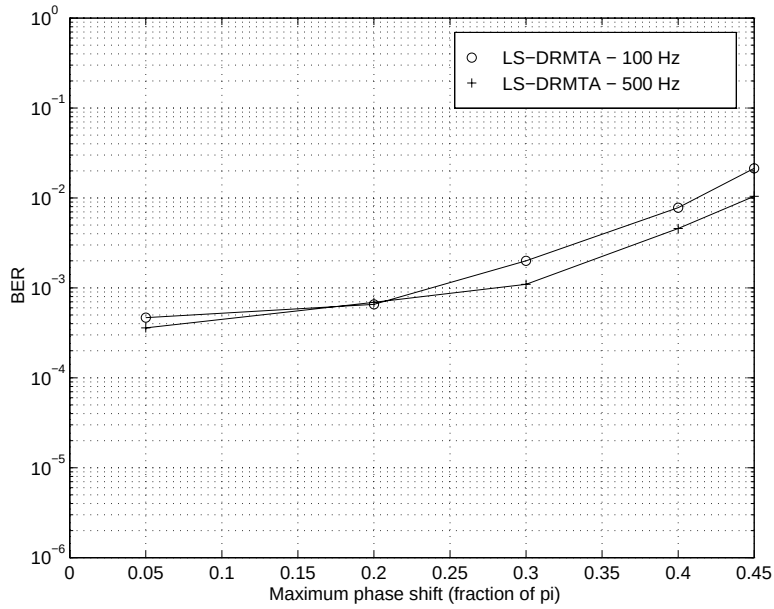

Figure 7.17: BER curves for the LS-DRMTA techniques as a function of maximum phase shift allowed before the update is carried out for the non-crowded case and $E_b/N_o = 8$ dB. Two different frequency offset conditions, 100 and 500 Hz are considered.

as long as the phase shift is less than $\pi/2$ and no noise is present, there should not be any error introduced in the chips but the energy along the real axis is close to zero as the phase shift approaches $\pi/2$. It can be seen from Figure 7.17 that the BER performance does not differ significantly as long as the maximum phase shift is less than 0.2π. For the 500 Hz case, the BER degradation is slightly steeper than 100 Hz. We can conclude that to obtain satisfactory performance, the adaptation rate has to be fast enough to allow only a maximum phase shift of 0.2π. But we can also see that there is no improvement in reducing the maximum phase shift allowed from 0.2π to 0.05π. Therefore there is no need to update faster as long as the maximum phase shift is less than 0.2π. If the carrier offset is 500 Hz and a maximum phase shift of 0.2π is allowed, then the adaptation rate has to be at least 5000 Hz.

Figure 7.18 is the BER performance curve plot as a function of the maximum allowed phase shift for the LS-DRMTCMA. The BER performance trend is the same as the LS-DRMTA. The LS-DRMTCMA is able to achieve lower BER than the LS-DRMTCMA. Therefore, for further simulations the maximum allowed phase shift will

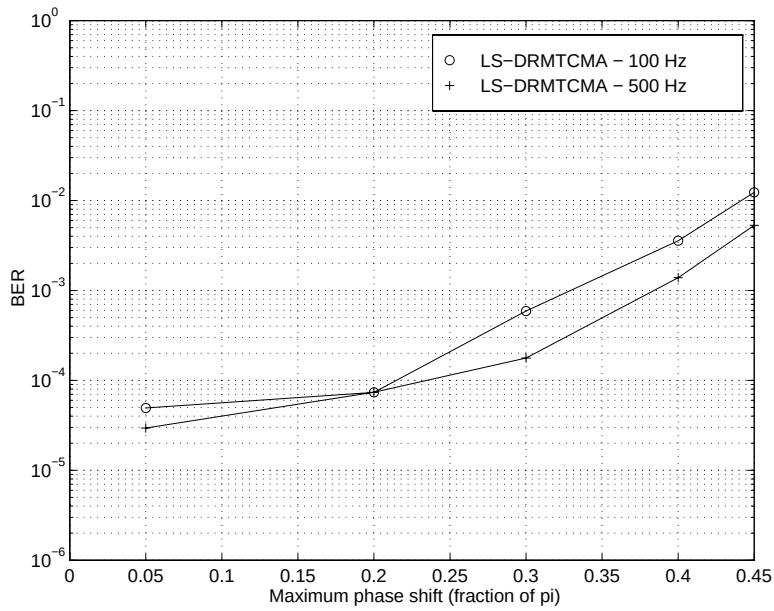

Figure 7.18: BER curves for the LS-DRMTCMA techniques as a function of maximum phase shift allowed before the update is carried out for the non-crowded case and $E_b/N_o = 8$ dB. Two different frequency offset conditions, 100 and 500 Hz are considered.

be 0.2π.

- **Non-crowded case**

Let us first consider the non-crowded case, $E_b/N_o = 8$ dB and the frequency offset between the locally generated carrier and the incoming carrier is 100 Hz. The BER performance curves as a function of number of users is shown in Figure 7.19. It can be seen that the LS-MTCMA and SD-MTDDA fail like the conventional receiver. These algorithms fail because these algorithms do not converge during the orthogonalization period and hence result in a BER of 0.5. The LS-DRMTA and the LS-DRMTCMA does not suffer from BER degradation due to frequency offset, because these algorithms assume that synchronization has been achieved and hence with the help of the reference signal, the DR algorithms are able to undo the phase shift and bring the constellation back to the real axis. As seen in other test cases, the LS-DRMTA performs better than the LS-DRMTCMA. Under frequency offset

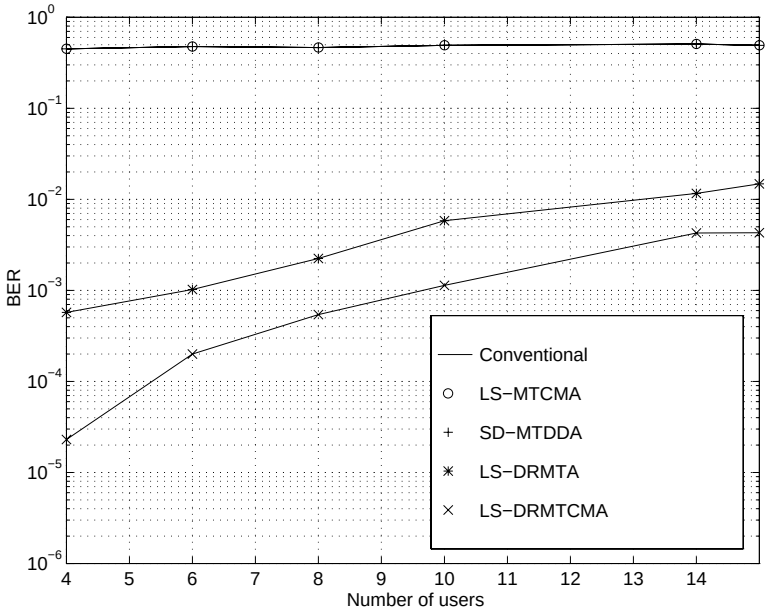

Figure 7.19: BER curves for all the techniques for the non-crowded case with a frequency offset of 100 Hz and $E_b/N_o = 8$ dB.

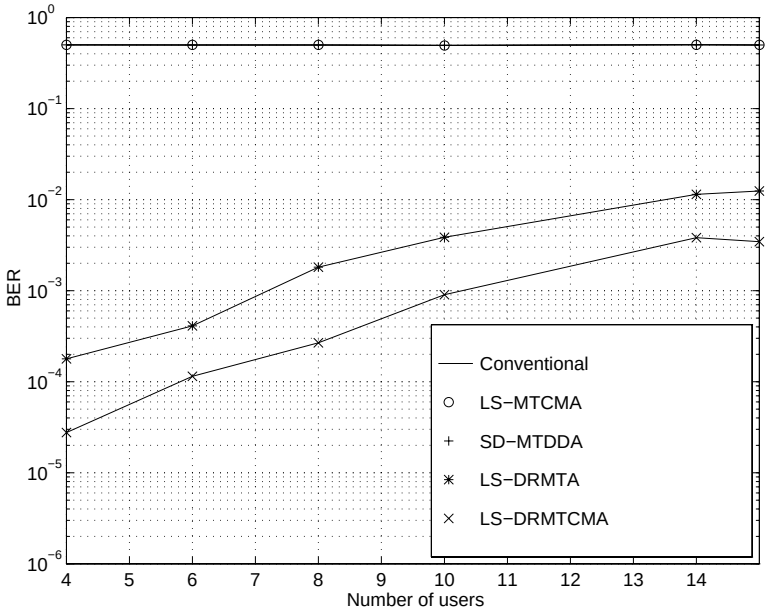

Figure 7.20: BER curves for all the techniques for the non-crowded case with a frequency offset of 500 Hz and $E_b/N_o = 8$ dB.

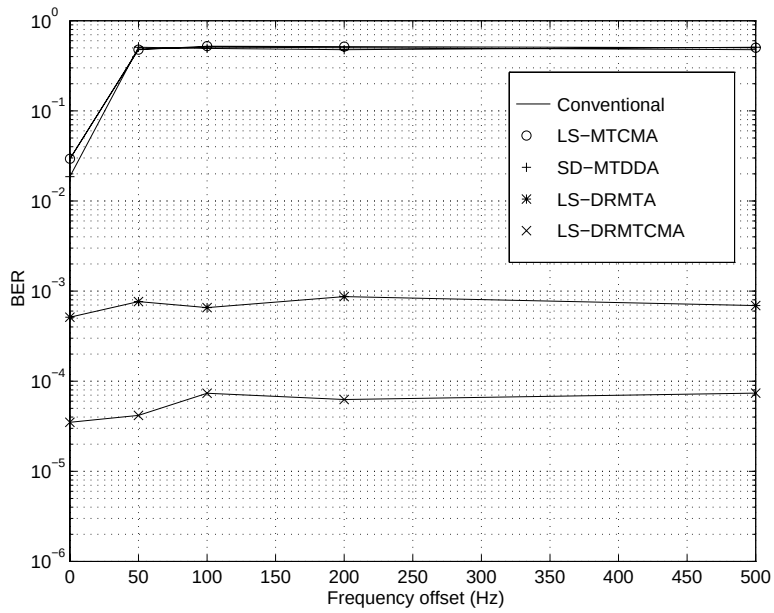

Figure 7.21: BER curves for all the techniques as a function of frequency offset for $E_b/N_o = 8$ dB. There are 4 equal powered users in the environment and the users are located within the sector of 30 to 150 degrees.

conditions, the LS-DRMTA and LS-DRMTCMA perform very similar to the AWGN case for larger number of users, but for smaller number of users the BER performance under frequency offset conditions is worse than the AWGN case.

Figure 7.20 is a plot of the BER performance curves for a frequency offset of 500 Hz. The performance curves for the 500 Hz offset case is very similar to the 100 Hz offset case.

Therefore, we study next the minimum BER that can be achieved using the various algorithms under a range of frequency offset conditions. There are 4 equal powered users in the environment and the users are located within the sector of 30 to 150 degrees. Figure 7.21 is a plot of the BER performance of all the algorithms and the conventional receiver as a function of residual carrier frequency. It can be seen that the LS-MTCMA and the SD-MTDDA degrade significantly as the frequency offset increases to 50 Hz from 0 Hz and remains flat at 0.5 for higher frequency offsets. But the BER curves for LS-DRMTA and the LS-DRMTCMA remain flat and is insensitive to change in the carrier offset as long as the adaptation is carried

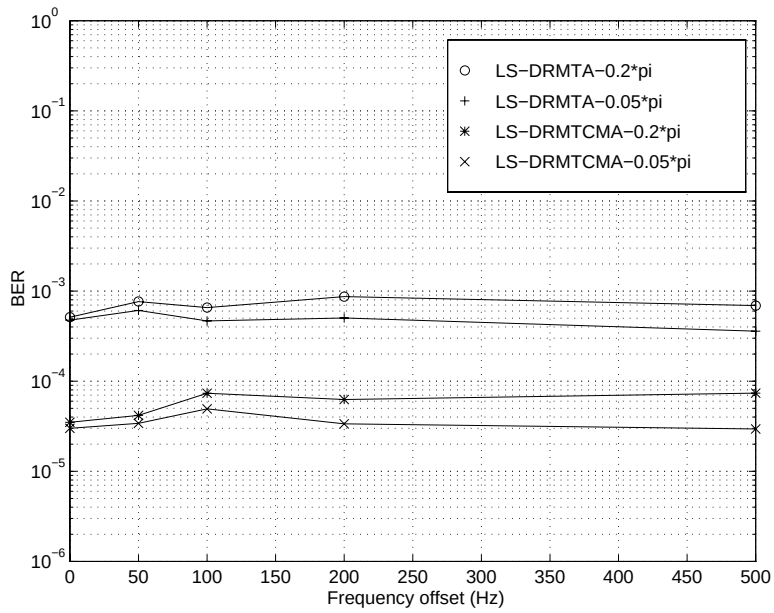

Figure 7.22: BER curves for the despread and respread techniques as a function of frequency offset for the non-crowded case and $E_b/N_o = 8$ dB. Two different update rates are considered, one for every rotation of $0.2 \times \pi$ and $0.05 \times \pi$.

to allow only a maximum phase shift of 0.2π. The higher the carrier offset the higher is the adaptation rate required to achieve good BER performance. Therefore, there is a trade-off between performance and complexity.

Figure 7.22 is a plot of the BER performance of the LS-DRMTA and LS-DRMTCMA as a function of frequency for two different adaptation rates whose maximum allowable phase shifts are 0.2π and 0.05π. It can be seen that there is insignificant performance gain as the adaptation rate is reduced over a range of frequency offset.

- **Crowded case**

Let us now consider the crowded frequency offset case. Again, we consider frequency offsets of 100 and 500 Hz. Figures 7.23 and 7.24 are BER plots as a function of number of users for 100 and 500 Hz frequency offsets, respectively. The performance curves show the same trend as the non-crowded case but with a slight degradation.

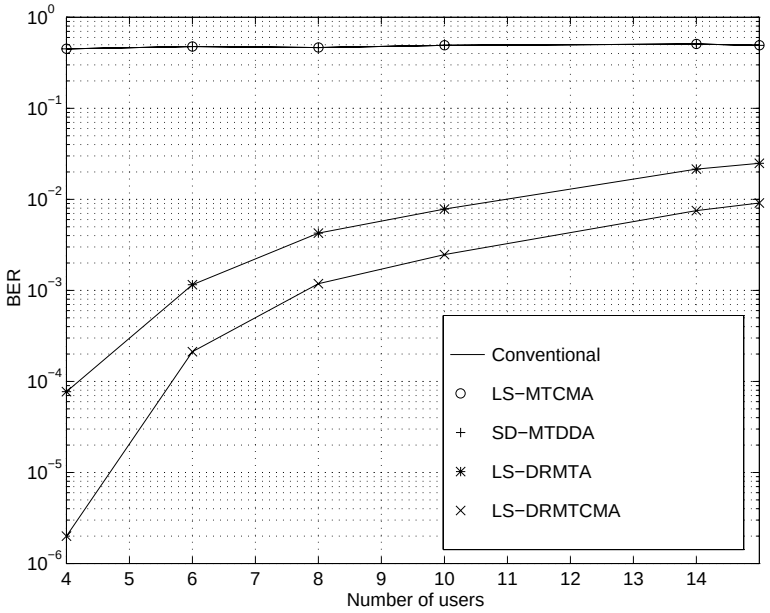

Figure 7.23: BER curves for all the techniques for the crowded case with a frequency offset of 100 Hz and $E_b/N_o = 8$ dB.

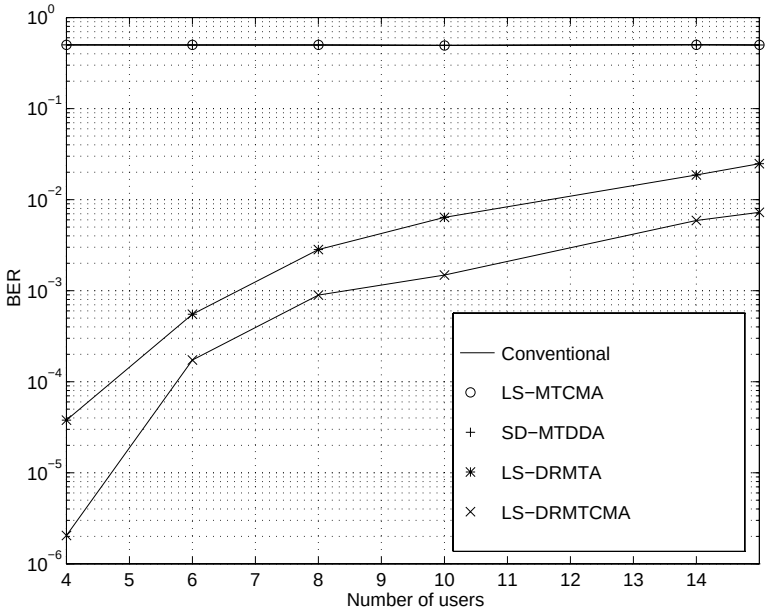

Figure 7.24: BER curves for all the techniques for the crowded case with a frequency offset of 500 Hz and $E_b/N_o = 8$ dB.

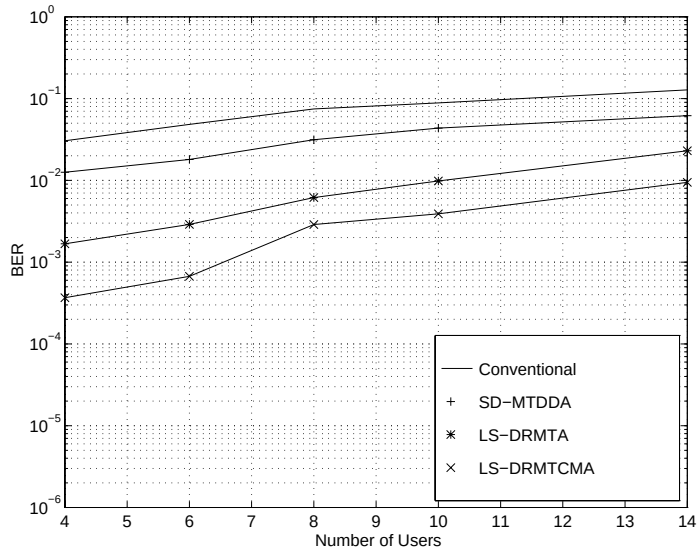

Figure 7.25: BER curves for all the techniques in a 2-ray multipath channel. The reflected component is delayed by 0.5 the chip duration and is 6 dB below the main component. The difference in the AOA between the components is 10 degrees, and the E_b/N_o is 8 dB.

7.9.4 Performance analysis in multipath channels

The multipath channel considered here has two paths, a direct and a reflected path. There are two scenarios considered here. In the first scenario, the second component arrives with a delay of 1/2 the chip duration, and the angular separation between the direct and the delayed component is 10 degrees and the average amplitude of the delayed component is 6 dB below the direct component. In the second scenario, the second component arrives with a delay of 1.5 the chip duration, and the angular separation between the direct and the delayed component is 20 degrees and the average amplitude of the delayed component is 10 dB below the direct component. The multipath in the first case is *correlated* with the main component, while in the second case the delayed component is *uncorrelated*. In both these cases, the users are uniformly located in a sector of 0 to 160 degrees. The E_b/N_o for all these test cases is 8 dB.

LS-DRMTCMA is not considered here because LS-DRMTCMA does not work for low E_b/N_o. The BER performance comparison curves for the first scenario is shown in Figure 7.25. In the first test case, the delayed path is correlated with the direct

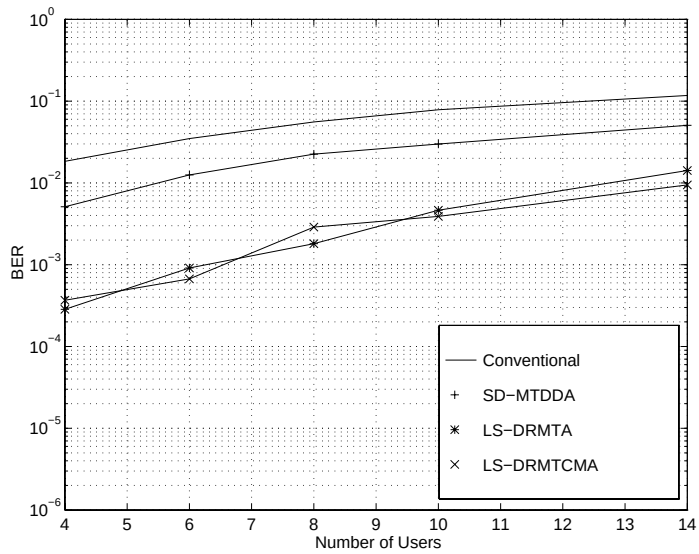

Figure 7.26: BER curves for all the techniques in a 2-ray multipath channel. The reflected component is delayed by 1.5 the chip duration and is 10 dB below the main component. The difference in the AOA between the components is 20 degrees, and the E_b/N_o is 8 dB.

path and therefore the multipath is an *interference* that degrades the performance of a conventional receiver. Also the delay between the components is only 0.25 μs and hence the AOA of the second arriving component is close to the AOA of the first arriving component. Therefore, the array does not have the ability to separate two closely arriving components. But in the second test case, the delay between the components is 0.75 μs and is uncorrelated with the main component and it has an AOA which is larger than the first case.

From Figure 7.25, it can be seen that the correlated multipath causes severe degradation in BER performance. If we consider the number of users to be 8, LS-DRMTA in an AWGN channel for an E_b/N_o maintains a BER of 10^{-4} while in a correlated multipath channel, LS-DRMTA maintains only a BER of 6×10^{-3}. Similarly, the BER of LS-DRMTCMA increases from 4×10^{-6} to 3×10^{-3}. As expected, the BER performance in the presence of uncorrelated multipath interference is better than in correlated multipaths. This is because of three reasons:

- The multipath component arrives after a chip so the correlation with the main

component is small.

- The power of the multipath component in the uncorrelated case tends to be smaller than the correlated case because the multipath component in the uncorrelated case has traveled a larger distance.

- The angular separation between the multipath component and the main component tends to be larger in the uncorrelated case than in the correlated case.

7.9.5 Near-far problem

Near-far problem is an inherent problem of CDMA systems, and it is a major factor that limits the capacity of a cellular system [76]. Near-far problem occurs, when a base station receives signals of unequal power from mobile units (in the reverse link). The mobile unit which is closer to the base station masks the mobile units which are far away from the base station. This problem is overcome by power control. There are two types of power control, one is the *open-loop power control*,and the other is the *closed-loop power control*. In the open-loop power control, the mobile units adjust the power of the transmitted signal depending on the power of the received signal. In the closed-loop power control, the base station acts as a centralized control, and it instructs the mobile units to adjust the power of their transmitted signals.

Power control was proposed by QUALCOMM Inc. to fight the near-far problem [68]. Power control is used to compensate for fading on the received signal. The transmitter transmits with enough power to overcome fading and keep a constant level of received power over all time. In practice, there are limitations to how fast the power control algorithms can respond and so there is not an ideal compensation for this problem. The use of power control has benefits other than just improving capacity. A major result of using power control is that the mobile transmits with only enough power to maintain the required E_b/N_o . This means that a mobile will only have to transmit at peak power levels in harsh environments. Therefore, battery life is extended (or smaller batteries can be used) since less power is expended over a period of time. power control can also be used on the forward channel to improve performance.

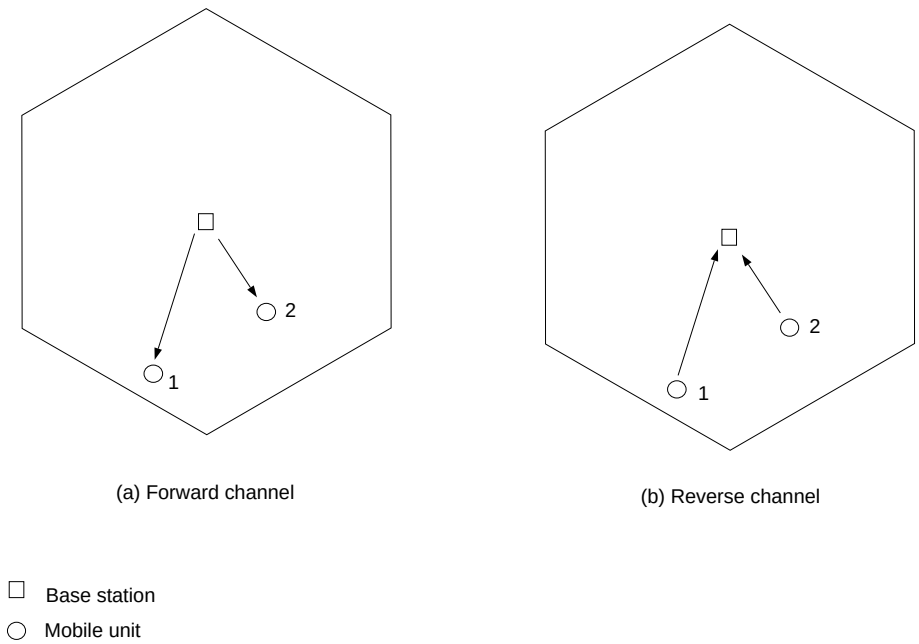

Figure 7.27: Illustration of near-far problem.

From Figure 7.27 it can be seen that without power control, the base station will receive the stronger signal from mobile # 2 than from the mobile # 1. Although mobile # 2's signal can be decoded properly, this will cause a large amount of interference to user # 1 (and all other users in the cell). Therefore, it is desirable to have mobile # 2 transmit with less power (or have mobile # 1 transmit more power) so that the received power at the base station is the same for all signals. In the forward channel, shown in Figure 7.27, there is only one transmitter at the base station. Therefore, a mobile will receive all transmitted signals at the same power level. Therefore, the need for power control is not based on the near-far problem. Instead, power control is used to provide more power to mobile units in a difficult environment, while providing less for those with strong signal receptions. A mobile unit may have a strong signal if it is stationary, experiencing little multipath fading, close to the station, or experiencing little interference from the other users. Therefore, this mobile does not need as much power to maintain an acceptable bit error rate (BER) as does a mobile that is not receiving a strong signal due to interference or fading. The goal is to keep all mobiles within an acceptable range for BER.

- **Open-loop power control**

In the open loop technique, mobile unit varies its power inversely with the received power from all the cell site. The open loop control mechanism for the reverse link is an analog system and can respond within several microseconds. The dynamic range is 85 dB. In the U.S. cellular system, the forward and reverse links differ in frequency 45 MHz. Due to this wide frequency difference and the frequency selective nature of multipath fading, the multipath fading over the reverse and forward channels is not correlated. Therefore, the open loop technique is not effective for fast fading but only for slow fading. However, if the channel changes suddenly, such as when a mobile moves and is no longer shadowed by a large object, the power control can respond quickly to adjust the mobile's transmit power.

- **Closed-loop power control**

In the closed loop technique on the reverse link, the cell measures the received power from the mobile and instructs the mobile to adjust its power based on this measurement. The decision to have the mobile increase or decrease the power is made every 1.25 ms. Fields tests have shown that this rate of updates is fast enough to counteract the Rayleigh fading that occurs on the incoming path. The closed loop estimate is used to make corrections to the open loop estimate due to different multipath fading on the forward and reverse links. It is important that the power control can react very quickly, otherwise the fading may have changed significantly by the time the transmit power update is received, and the mobile will not be able to react quickly enough to the rapidly changing channel. Power control schemes are necessary because of the vulnerability of conventional receiver to near-far problem. It is desirable to have receivers that are resistant to near-far problem, therefore avoiding the implementation of complex power control schemes.

7.9.6 Performance analysis in Near-Far channels

So far we compared the performance of the conventional receiver with the adaptive array algorithms in perfect power control. However, one of the major drawbacks of

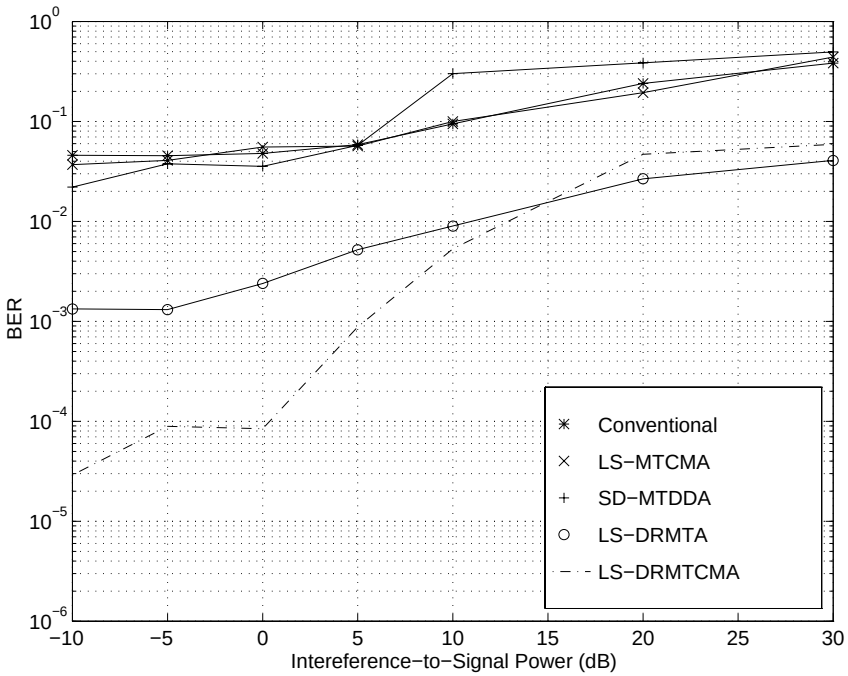

Figure 7.28: BER performance curves of various adaptive array algorithms in a near-far channel.

the conventional receiver is its vulnerability to near-far problem. Here we examine the performance of the adaptive array algorithms in near-far channels and compare the performance with the conventional receiver. The simulation setup is as follows. There are 10 users in the environment and the array is overloaded. The $E_b/N_o = 5$ dB and the users are located uniformly in a 160 degrees sector. Nine out of ten users have the same power while one of the user's power (P_{int}) is varied. The ratio of P_{int} to the average power of the other users is varied from -10 dB to 30 dB and the BER performance of the users with equal power is calculated and plotted in Figure 7.28.

SD-MTDDA and LS-MTCMA perform no better than the conventional receiver, this is because of the high noise level. LS-DRMTA and LS-DRMTCMA perform far better than the conventional receiver, but the BER performance of the equal-powered users degrade significantly as P_{int} increases. If 10^{-2} is the acceptable BER, then DR algorithms can support all the users in the system as long as P_{int} is less than 10 dB. It is worth noting that the DR algorithms suffer from near-far problem because they use a conventional receiver to estimate the data bits.

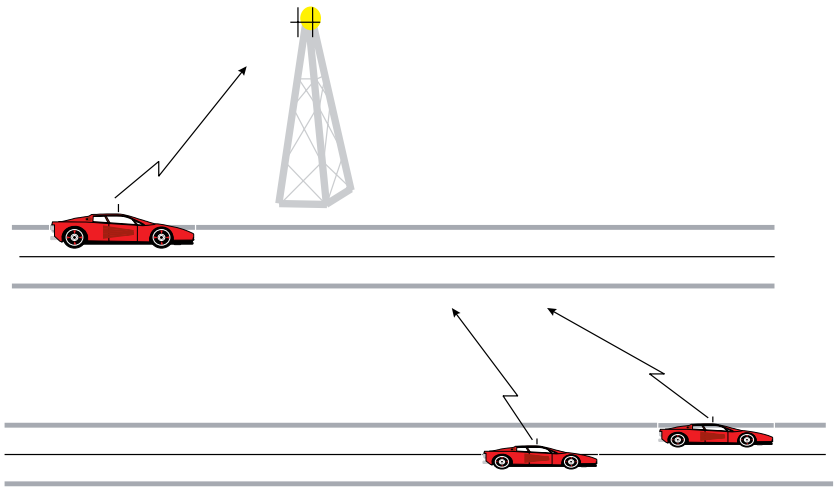

Figure 7.29: Figure illustrating the simulation setup for the near-far channel.

7.10 Synchronization issues for Despread Respread algorithms

For proper demodulation of CDMA signals, bit and chip synchronization have to be achieved prior to despreading the CDMA signal. In Subsection 7.9.2, we discussed the effect of timing offset on the performance of the adaptive array algorithms. If perfect synchronization has not been achieved, then timing offset exists between the receiver PN generator and the transmitter PN generator. It was shown in Figure 7.13 that the DR algorithms are more robust than the other algorithms in the presence of timing offsets. It can be seen that the DR algorithms can perform an order of magnitude better than the other algorithms even when the timing offset is 25% of the chip duration. All the algorithms perform very similar to the conventional receiver when the timing offset is 50% of the chip duration. In this section, we demonstrate the advantage of boot-strapping the beamforming operation with synchronization. When using a DR algorithm the adaptation of the weights and the synchronization process can be carried out in a boot-strap fashion. A synchronization circuit is operated at the output of the array and even if perfect synchronization has not been achieved, the beamforming operation can be carried out. Any increase in the SINR at the output of the array aids the synchronization process, resulting in smaller timing offset and

thus better beamforming.

Since the DR algorithms are tolerant to timing offsets, let us consider the initial condition where the timing offset is 25% of the chip duration. We want to show here that since the DR algorithms are tolerant to a timing offset of 25% of the chip duration, a synchronization circuit at the output of the adaptive array should be able to achieve better synchronization since the SINR at the output is higher than the SINR at the input of the adaptive array. In this discussion, we assume that we use a simple matched filter (MF) acquisition technique. We will also look into ways of improving synchronization.

We use two performance metrics to quantify acquisition, *probability of false alarm* (POF) and the *mean acquisition time* (MAT) [75]. Probability of false alarm is the probability that we lock onto the wrong code phase, this is measured by fixing a certain threshold and looking for correlation peaks that exceed the threshold. If the peak that exceeds the threshold does not occur for the true phase, then a false alarm has occurred. Mean acquisition time is the time required to achieve three consecutive true peaks and is measured in terms of dwell periods. Dwell period is the integration time which is a bit duration in this case.

In addition to the matched filter acquisition technique, we employ an enhanced matched filter (EMF) [75], a cascade of the matched filter and a single tap IIR filter with a delay of a bit duration and is shown in Figure 7.30 to serve as an exponential weighting function. b_o or the pole of the IIR filter decides the amount of memory in the system. Thus we can sum consecutive peaks resulting in a higher peak-to-sidelobe ratio provided that

1. the peak doesn't shift over the time considered, and

2. the sidelobes tend to have large values at different places each bit interval.

The output of the matched filter is normalized by the number of samples (NN_s) per bit and the output of the EMF is normalized by $NN_s/(1-b_o)$. Here let us assume $b_o = 0.9$. Such a scheme assumes that the channel is static over a time interval of $1/(1-b_o)$ bit intervals.

Let us consider a condition where there are ten users in the environment with equal power and a LS-DRMTCMA is employed at the base station. Initially we

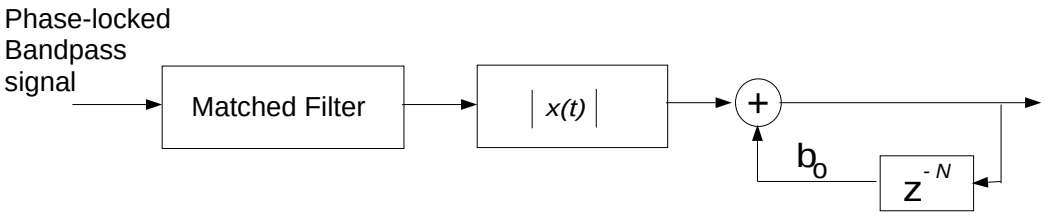

Figure 7.30: Block diagram of the enhanced matched filter (EMF)

assume the timing offset is 25% of the chip duration and the array is adapted. A MF and an EMF are implemented at the input and at the output of the array. The correlation plots are shown in Figure 7.31. Comparing the correlation peaks obtained from the MF applied to the input and at the output of the array, it can be seen that the increase in SINR has eliminated a large number of false peaks. From the outputs of the EMF, it can be seen that the location of true peaks are enhanced and therefore the EMF will perform better than the MF. Also, the EMF at the array output performs better than the one at the array input, which can be seen in terms of the ratio of the mainlobe to sidelobe levels. This ratio at the array output is higher than at the array input.

7.10.1 Probability of false alarm

Here we compare the POF at the input and at the output of the array using a MF and an EMF. The threshold is varied from 0 to 2 and the probabilities of false alarm are plotted in Figure 7.32. Therefore the higher the threshold we choose the lower the POF. But we cannot choose a threshold based on the POF alone, because a high threshold might take an excessive time to acquire the true code phase.

7.10.2 Acquisition time

POF by itself does not give a sufficient information. In other words, POF cannot be used as the main criterion to decide the threshold. Instead the acquisition time is a better criterion. Acquisition is said to be achieved if three consecutive correlation peaks occur at the true code phases. Every time a false peak is detected, a penalty

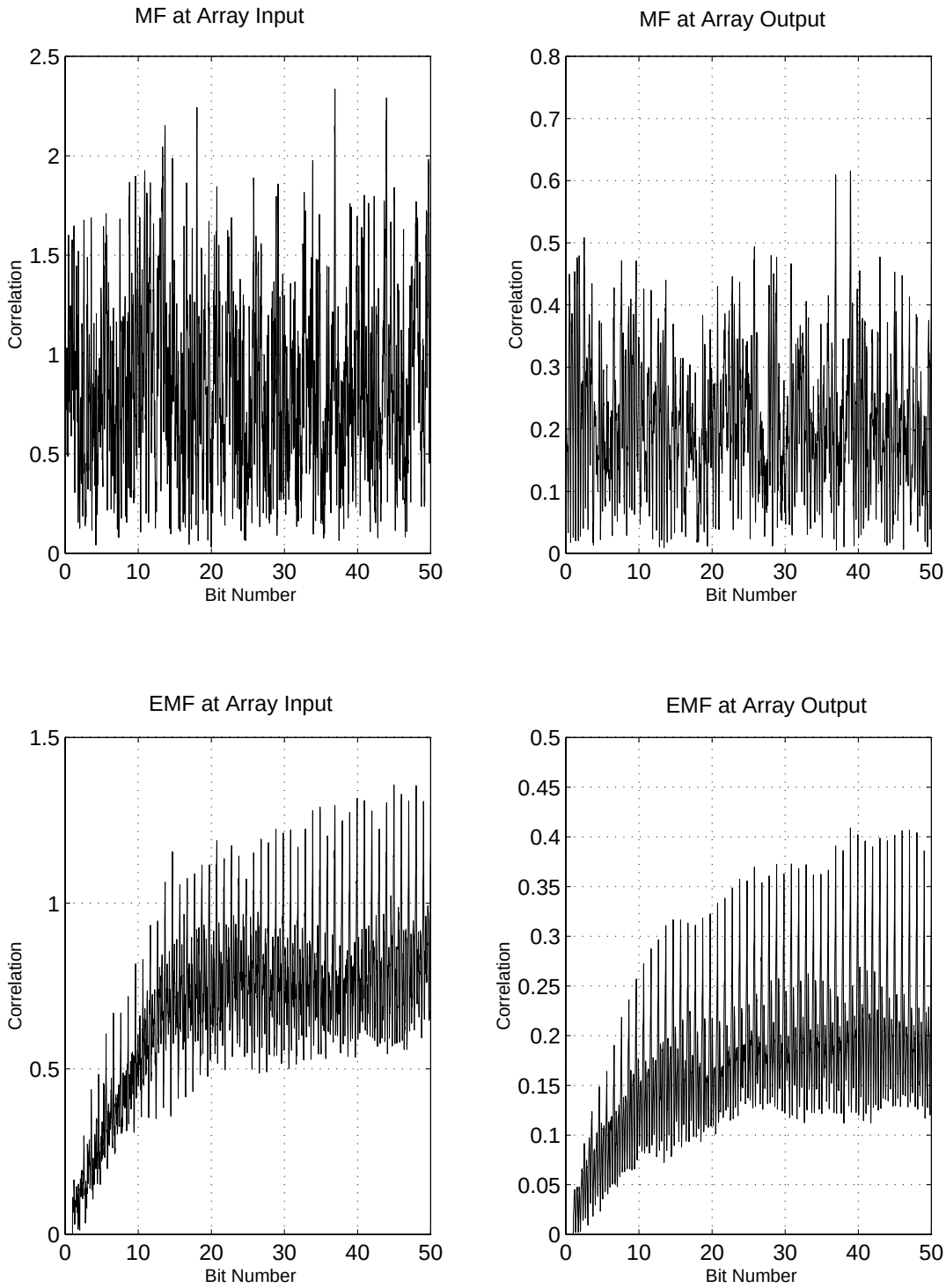

Figure 7.31: Plots show the correlation peaks obtained from the MF and EMF applied to the input and at the output of the array.

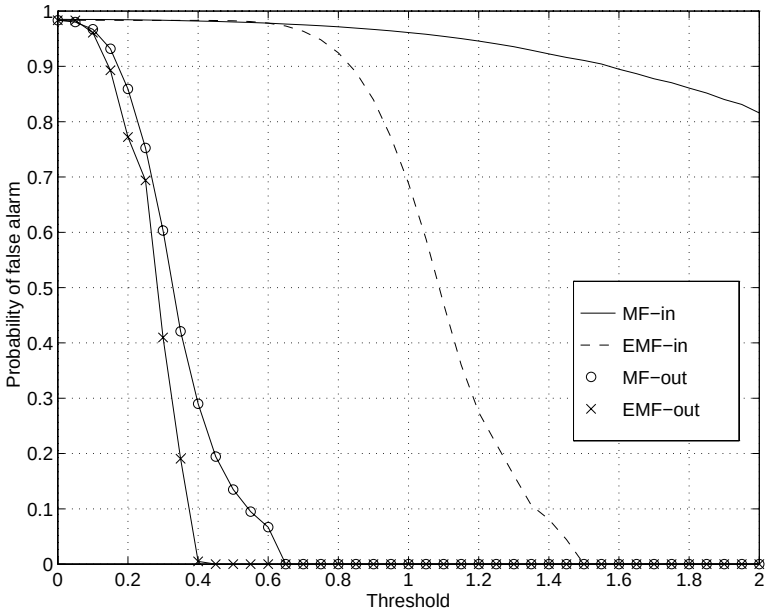

Figure 7.32: Plot of the probability of false alarm as a function of threshold for the matched filter and the enhanced matched filter at the input and at the output of the array. (*MF-in* - MF at the input of the array, *MF-out* - MF at the output of the array, *EMF-in* - EMF at the input of the array, *EMF-out* - EMF at the output of the array)

of 3 dwell periods is applied. For the IIR filter, a fixed penalty of 20 dwell periods is added to the acquisition time to account for the transient period of the filter.

Figure 7.33 shows a plot of MAT in terms of dwell periods as a function of threshold for the MF at the array input and the array output of the adaptive array. The channel conditions are the same as above. It can be seen that the MF at the output is able to lock onto the true phase faster than the MF at the input. An optimum threshold of 0.41 is required at the output to achieve a MAT of 90 dwell periods and at the input an optimum threshold of 1.18 achieves a MAT of 175 dwell periods. Figure 7.34 shows a plot of MAT in terms of dwell periods as a function of threshold for the EMF at the input and the output of the adaptive array. An optimum threshold of 0.35 is required at the output to achieve a MAT of 22 dwell periods and at the input an optimum threshold of 1.2 achieves a MAT of 35 dwell periods. Let us now determine the POF for each threshold. Fixing the threshold based on the

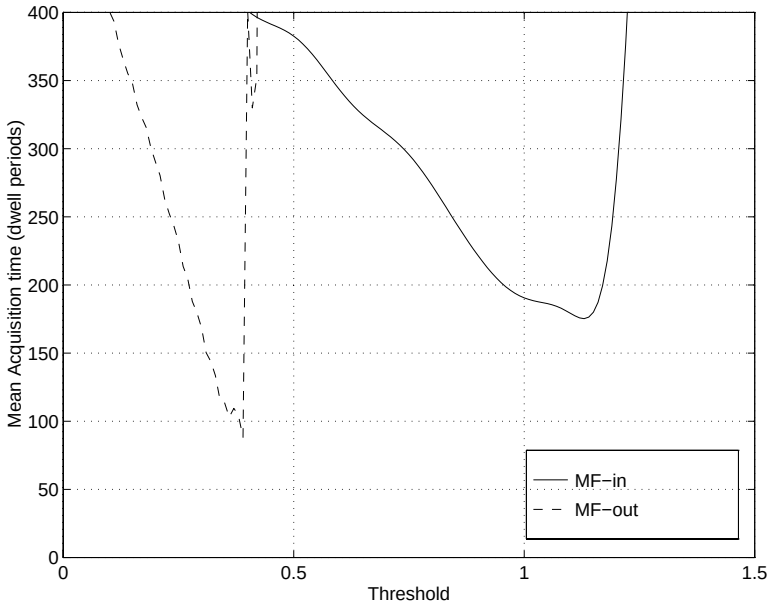

Figure 7.33: Plot of the mean acquisition time (in dwell periods) as a function of threshold for the matched filter at the input and at the output of the array. (*MF-in* - MF at the input of the array, *MF-out* - MF at the output of the array)

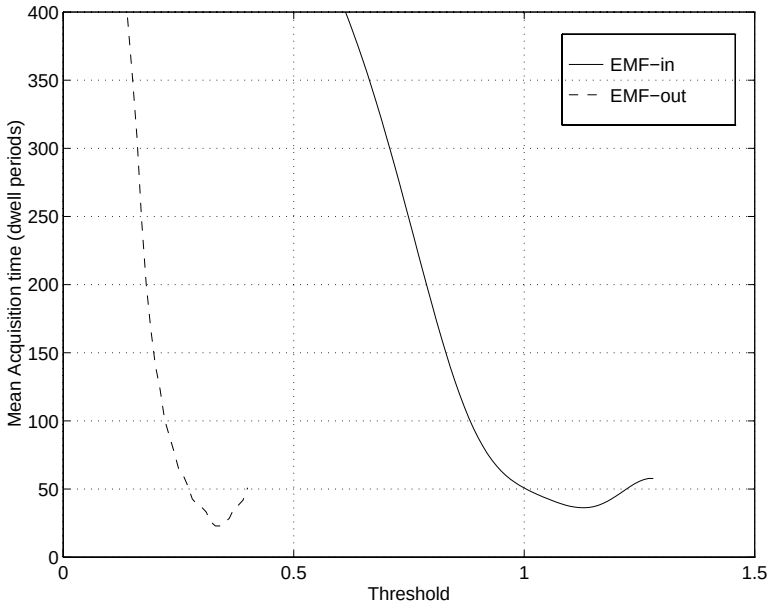

Figure 7.34: Plot of the mean acquisition time (in dwell periods) as a function of threshold for the enhanced matched filter at the input and at the output of the array. (*EMF-in* - EMF at the input of the array, *EMF-out* - EMF at the output of the array)

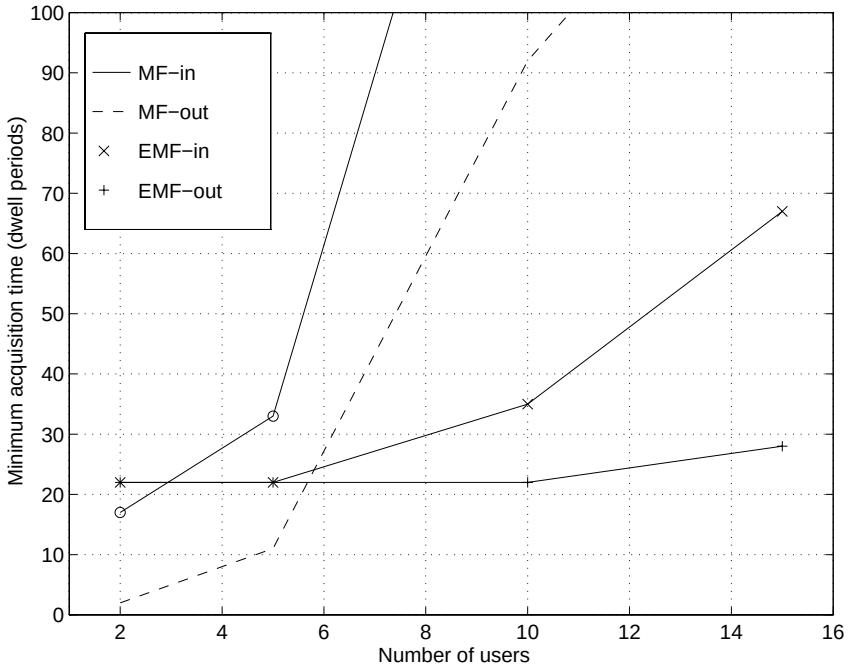

Figure 7.35: Plot of the minimum acquisition time (in dwell periods) as a function of number of users in the system for the matched filter and the enhanced matched filter at the input and at the output of the array. (*MF-in* - MF at the input of the array, *MF-out* - MF at the output of the array, *EMF-in* - EMF at the input of the array, *EMF-out* - EMF at the output of the array)

Table 7.1: Probability of false alarm for the optimum threshold

	Acquisition structure	Probability of false alarm (POF)
Input	Matched filter	0.94
	Matched filter	0.26
Output	Enhanced matched filter	0.28
	Enhanced matched filter	0.19

minimum acquisition time, the POFs results are summarized in Table 7.1. It can be seen that the POF for the MF at the input of the array is very high compared to the POF for the MF at the output of the array. POF at the input reduces drastically if an EMF is employed. The EMF at the output is able to achieve the lowest MAT and the lowest POF.

Minimum MAT is the MAT obtained using the optimal threshold. Figure 7.35 is a plot of the minimum MAT as a function of number of users. It can be seen that minimum MAT shoots up exponentially as the number of users increases for the matched filter at the input and at the output of the array. But the performance of the EMF degrades gracefully as the number of users increase. The performance of the EMF at the output of the array is insensitive to the number of users. It is important to note that the EMF is able to achieve only a minimum MAT of 22 dwell periods, this is because of the fixed penalty period for the IIR (20 dwell periods) and the wait period before a decision is made (2 dwell periods). Therefore for lower number of users, an EMF is not recommended.

7.11 Conclusions

Application of adaptive arrays to CDMA systems has been studied in this chapter. A brief description of the GloMo parameters and its system architecture have been provided in this chapter. A multitarget adaptive array architecture is used to perform multiuser detection at the base station. The multitarget architecture is classified based on the signal selective property of the algorithm. Three existing blind algorithms are compared with a new adaptive array algorithm. The novel algorithm has

good signal selective property. The BER performance of all the above algorithms has been compared in the presence of various channel and receiver imperfections. The DR algorithms outperformed the conventional algorithms, but they assume that synchronization has been achieved before beamforming which the conventional algorithms do not require.

Chapter 8

Implementation of an Adaptive Antenna Array for CDMA systems

8.1 Introduction

In this chapter, the issues involved in building an adaptive array are investigated. As mentioned earlier, the goal is to build an 8-element adaptive array. The investigation begins with examining the DSP hardware suitable for the application. The issues involved in the implementation of the adaptive array algorithms on the DSP will be examined followed by calculations of the computation complexity of the algorithms and an assessment of the DSP hardware.

8.2 Choice of the digital signal processor and its features

With the development phases and algorithms in hand, we must now decide upon the hardware and software which will best suit the project. The main piece of hardware required is a DSP processor. Due to the large dynamic range provided by floating point processing, we do not consider fixed point DSPs. The discussion will be limited to 32-bit floating point processors. When comparing DSP processors there

are several issues to consider. Among these are processor speed, on-chip memory, ease of programming, development tools available, support, external interface ease, and multi-processing ability. A further consideration in this case is experience. It is important, when time is a consideration, to consider the experience with different processors of the personnel in the lab. The more experience available, the more favorable the DSP becomes since it will require less time to traverse the chip's learning curve. We will look at each of these categories in turn.

8.2.1 Speed

Several speed measures for the four considered DSP processors are given in Table 8.1. (The four chips considered were the best chips available from each of the major DSP manufacturers.) While MFLOPS is the often quoted measure of processor speed, it can be deceiving. This is because a MFLOP rate is normally a peak rate based on instructions which perform the largest number of operations. Typically, these are not the most common instructions used, and the sustained number of operations per second can be significantly less than the advertised maximum rate. Thus, we also look at the instruction cycle of each of the chips as well as the 1024-point complex FFT time. The instruction cycle is determined from the clock speed and the number of clock cycles required to perform an instruction. From Table 8.1, we can see that the ADSP2106x is the fastest processor, with a 25 ns cycle time, the highest FLOP rating and the best FFT time [77]. With the large number of operations required by MTAA, speed becomes an extremely important consideration.

8.2.2 Multiprocessing

As mentioned, the receiver structure presented here is extremely computationally intensive. While a fast processor will be sufficient for early phases of the development, at later phases when tracking and synchronization add significantly to the computation total, a single processor will simply be inadequate. Thus, multiprocessing is a significant consideration. Table 8.2 shows the I/O ports for interprocessor communications for each chip. It is seen that only the ADSP2106x and the TMS320C40 can truly be considered multi-processor oriented.

8.2.3 Memory

On-chip memory is another important consideration. If data must be retrieved from off-chip, either time must be sacrificed (slow external memory) or money must be sacrificed (fast external memory). It is thus desirable to have a large amount of on-chip program and data memory. The memory available for each of the chips considered is displayed in Table 8.2. The ADSP2106x has a significantly larger amount of on-chip memory available with as much as 4 Mbits of SRAM.

8.2.4 Software

Development tools are also a significant consideration. Of high importance are hardware emulators, software simulators, and C language compilers. These tools will make a big impact on the speed of implementation. Fortunately, each of the chips considered thus far have these development tools available. Another development tool to consider is a block diagram oriented software tool. One such tool is available by converting SPW [78] simulation code to assembly language. Software is currently available to convert SPW code to DSP96002 assembly language. Further, software is being developed to do the same for Analog Devices chips. A similar development tool is Hypersignal for Windows by Hyperception, Inc [79]. This software allows block diagram oriented development for Analog Devices chips including the 2106x. Also of great importance is the availability of a development board for the chip. Each of the

Table 8.1: Comparison of the speed of different processors

Manufacturer	Chip	Clock speed	Clock cycles per Instruction cycle	Rating	1024 FFT
Analog Devices	ADSP21060x	25 ns	1	120 MFLOPS	0.46 ms
AT&T	AT&T32C/3210	20 ns	4	25 MFLOPS	3.2 ms
Motorola	DSP96002	25 ns	2	60 MFLOPS	1.04 ms
TI	TMS320C40	20 ns	2	50 MFLOPS	1.93 ms

Table 8.2: Comparison of I/O and memory of different processors

Manufacturer	Chip	I/O	Memory
Analog Devices	ADSP21060x	one 240 Mbytes/s six 20 Mbytes/s	120 Kword data 80 kword program
AT&T	AT&T32C/3210	one serial (16 bit) one parallel (32 bit)	1.5 kwords
Motorola	DSP96002	none dedicated	1 kword data 2 Kword program
TI	TMS320C40	six 20 Mbytes/s	2 kwords

chips considered is available on a DSP development board.

8.2.5 Other Considerations

Some considerations are somewhat subjective, including ease of programming, support, and experience. From the comments made by several involved in DSP development in our lab, it was found that Analog Devices has the most straightforward assembly language. Texas Instruments on the other hand is recognized as the industry leader and Analog Devices is making significant progress with the introduction of the DSP2106x. Finally, experience is a key factor. While the author have limited amount of DSP experience, the lab as a whole has significant experience with both Motorola and Analog Devices chips.

Based on the previous discussion, it has become apparent that the Analog Devices 2106x (SHARC) is the best choice for this project. It is the fastest chip, has by far the most on-chip memory at 4Mbits, and is most readily applied to multiprocessing with 240 Mbytes of I/O bandwidth. At present Bittware and Analog Devices both offer PC plug-in boards with a single SHARC processor. Further, both boards allow expansion to multiple processor configurations through SHARCPAC expansion modules available from Bittware. LSI is also in the process of creating development boards based on the SHARC.

8.3 Description of the transmitter architecture

8.3.1 Transmitter RF front end

The transmitter radio frequency (RF) front end implements a single upconversion scheme where the binary phase shift keying (BPSK) modulated signal at the low intermediate frequency (IF) of 21.4 MHz (as provided by the baseband modulator) is upconverted, filtered, power amplified and transmitted using a monopole.

8.3.2 Transmitter baseband processing

A block diagram of the transmitter architecture is shown in Figure 8.1. The transmit section of the baseband system comprises a fourth-order linear feedback shift register (LFSR) pseudo-noise (PN) generator, a variable-order (maximum order = 30) LFSR PN data generator, associated clock circuitry and a baseband modulator to modulate the PN code and the data. The initial states of the two PN generators, and the initiation of the code and data generation is controlled by the ADSP21020. The data modulated PN code sequence is then sent to a general purpose modulator module, the STEL1375 [80] for BPSK modulation. The STEL1375 was chosen as it allows the generation of a wide variety of modulation formats such as M-ary PSK, BFSK and CPFSK (with up to 12 bits of phase modulation resolution). The STEL1375 can generate an IF modulated signal up to frequencies of 35 MHz. It is initially programmed by the ADSP21020 to the desired transmit IF frequency and an initial phase.

8.4 Hardware architecture of the adaptive array

The hardware architecture for MTAA is shown in Figure 8.1. The main components of the the hardware architecture are

- RF front end
- Signal digitization
- Baseband processing

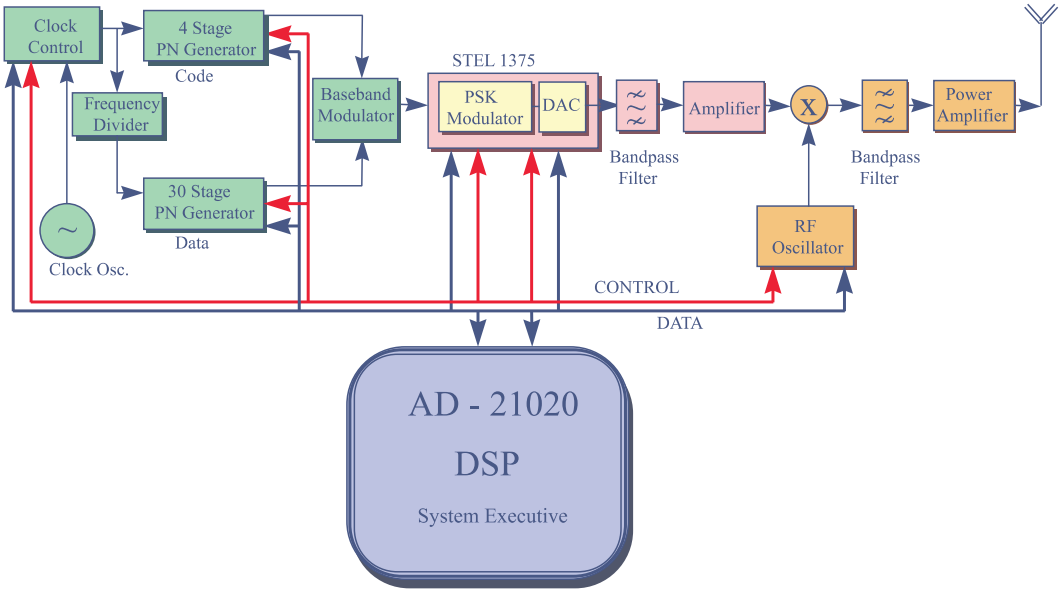

Figure 8.1: The hardware architecture of the transmitter.

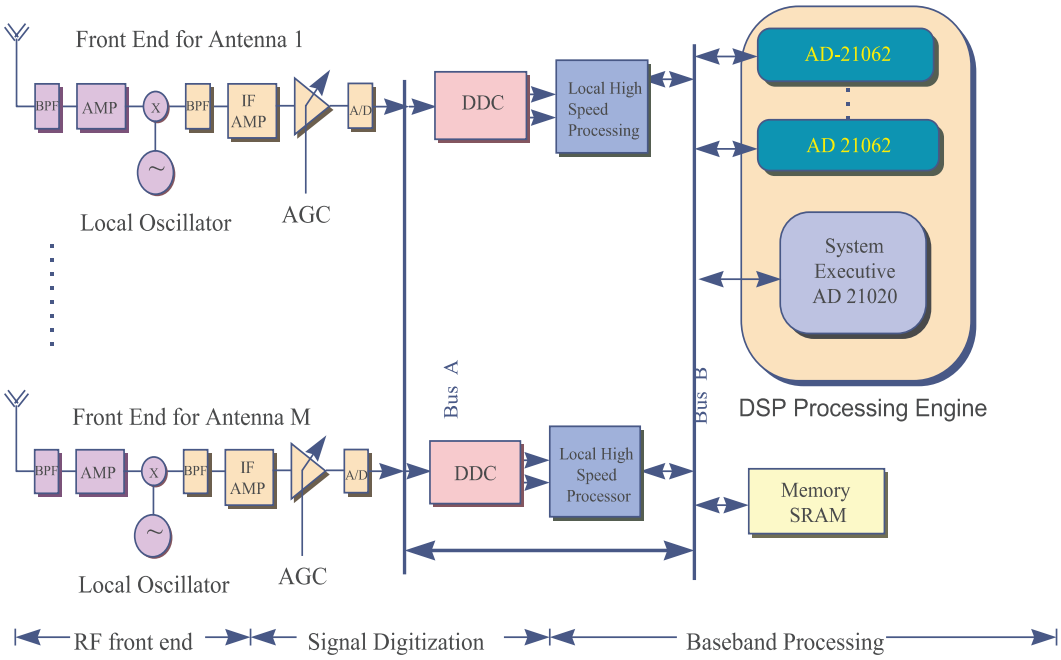

Figure 8.2: Hardware architecture of the multi-target adaptive array.

8.4.1 Receiver RF front end

Ideally, the receiver RF front end would consist of a perfectly linear, passive tunable bandpass filter followed by automatic gain control (AGC) and detection functions. The RF front end should have the following characteristics:

1. Sufficient linearity to avoid the generation of intermodulation products by high level signals. This is particularly important for the base station receiver because of the near-far situation that could exist on the uplink. Intermodulation products generated by the nonlinearities in the RF chain by high power users can easily swamp out weak users and make the near-far problem even worse. This means that front end amplifier and mixer should have a high degree of linearity. In addition, the first local oscillator should have a high degree of spectral purity to avoid adding excessive spectral spread.

2. Sufficient channel filter discrimination to reject high power adjacent channel interferers.

3. A large dynamic range. This is especially important at the base station due to the near- far problem.

Generally, there are two RF front end architectures:

1. The conventional superheterodyne arrangement which typically involves two stages of mixing and filtering.

2. Direct conversion to either baseband or a low IF frequency.

The use of a superheterodyne or a direct conversion receiver is governed by a number of factors such as the availability of inexpensive, linear low-noise amplifiers, highly stable oscillators, etc. Another important factor is the signal digitization scheme to be employed, which is discussed in detail in the following section.

8.4.2 Signal digitization

Ideally, signal digitization should occur as close as possible to the antenna. This not only reduces the noise introduced by the analog mixers, filters and amplifiers (that are

no longer required), but also extends software control as close to the antenna as possible [81]. This is important because software control provides more flexibility than hardware control. Two types of digitization techniques are used [82]: lowpass digitization and bandpass digitization. Lowpass digitization performed at a rate greater than or equal to twice the highest frequency component. This kind of sampling is associated with lowpass signals. For communication bandpass signals, digitization at twice the highest bandpass frequency component is often not feasible due to the high frequencies involved. In such situations, the bandpass version of the Nyquist sampling theorem can be used to sample the signal at a rate commensurate with the bandwidth of the signal and not with respect to the highest frequency component. The sampling process creates images of the bandpass signal at integer multiples of the sampling frequency, and hence downconversion is achieved by selecting the appropriate spectral replica of the original bandpass signal. A system which employs bandpass digitization can thus do away with the last downconversion stage. There are two important factors in IF bandpass digitization that affect the cost/performance ratio of the technique:

1. Although the analog-to-digital converter (ADC) operates at a rate slower than the highest frequency component, it must still be able to effectively operate on the highest frequency component of the signal. This calls for the use of high speed ADCs. High speed ADCs are usually expensive in terms of both cost and power consumption, which is very critical in the design of the mobile receiver.

2. Since a bandpass digitization technique would usually use only one downconversion stage, frequency-offset tracking and compensation must be done at the local oscillator which usually operates in the microwave region. Because of the very high frequency of operation, very good frequency tracking has to be performed. This could be avoided by having another stage of downconversion so that frequency tracking may be performed at a much lower IF frequency. Alternatively by increasing the bandwidth of the IF filtering in the single stage architecture the same objective could be achieved, although this would result in a reduction of the signal-to-noise ratio.

Some of the critical issues in the choice of an ADC are [83]:

1. Dynamic range: When multiple signals are present, each signal level must be considerably less than the full scale of the converter. One signal alone may use the full- scale range of the converter, but when two signals are present, each of equal power, each signal must be of half the amplitude (-6 dB), to prevent output clipping, as the signals add together at their peaks. Each doubling of the number of signals requires individual levels to be reduced by 6 dB. This means that the ADC must have enough dynamic range to prevent nonlinear distortion during digitization. In addition, a 3-15 dB reserve is kept at the top of the ADC range to prevent clipping that comes from inevitably high incoming peak-to-RMS ratios and saturation as additional users come online.

2. SNR specification for the ADC: The SNR specification for an ADC specifies the amount of quantization noise, random noise and nonlinear distortion present at the output of the ADC.

3. Spurious Free Dynamic Range (SFDR): The SFDR is a parameter that allows us to assess how well an ADC can simultaneously detect a very small signal in the presence of a very large signal. This specification is critical for ADCs at the base station receiver because of the existence of the near-far problem.

4. Full power analog input bandwidth: This specification is important in a band-pass sampling application where the maximum input signal frequency is higher than one half the sampling frequency.

• Configurations proposed

Two configurations have been designed and will be evaluated from a cost/performance tradeoff aspect. The block diagrams of the two configurations are shown in Figures 8.3 and 8.4. Figure 8.3 shows a superheterodyne RF front end with the second local oscillator being a numerically controlled oscillator (NCO) controlled by the frequency offset compensation subsystem. A novel scheme is used to generate the I-Q samples using a single ADC. In a conventional scheme, the analog input signal is split into two signals which are then quadrature downconverted all the way to baseband and then digitized. This scheme requires two ADCs, one each for the I and Q arms.

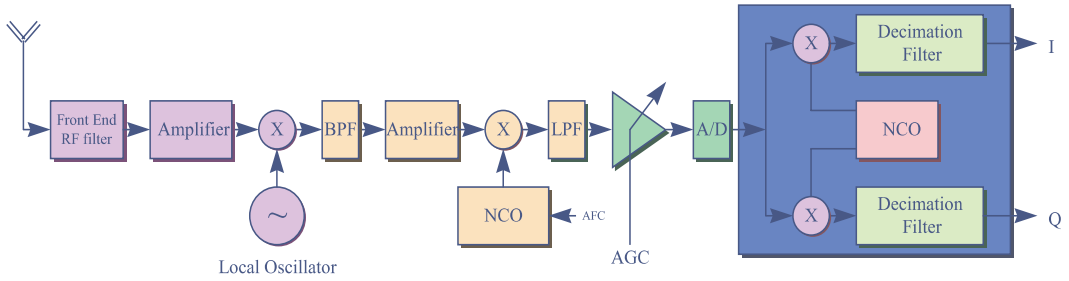

Figure 8.3: RF front end and signal digitization schemes (lowpass sampling).

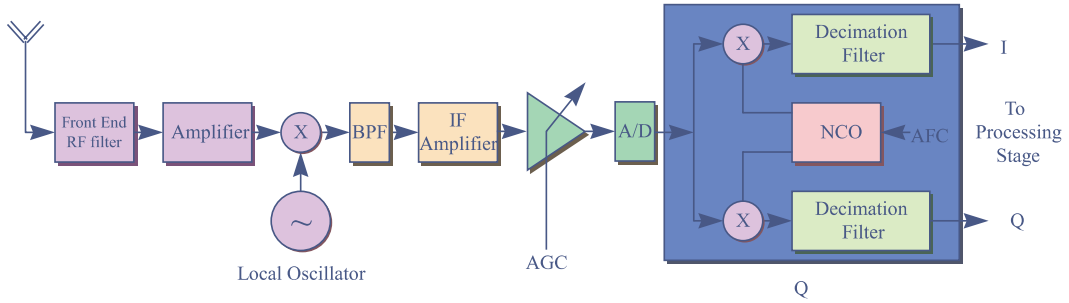

Figure 8.4: RF front end and signal digitization schemes (bandpass sampling).

In the proposed scheme, the input analog signal frequency is downconverted by the NCO not all the way down to baseband, but to a very low IF equal to the chip rate. In this situation, the highest frequency component of the signal is the same as the (null-to-null) bandwidth of the signal. This signal is then digitized and the I-Q samples are generated by having the quadrature outputs of the NCO in the digital downconversion (DDC) block multiply the ADC samples. The ADC used is a 12-bit Comlinear CLC949 [84]. Dedicated DDC application-specific integrated circuits (ASICs), such as the HSP50110 [85] are used.

The second configuration shown in Figure 8.4 is a classic bandpass digitization scheme with a single downconversion stage. The bandpass IF signal is then digitized by a high performance ADC such as the AD9032, which is a 12-bit 25 Msps ADC with an analog input bandwidth of 150 MHz [77]. The ADC output is then sent to the DDC ASIC for final downconversion to baseband and I-Q generation.

8.4.3 The DSP based baseband processing sub-system

This section describes the innovative aspects of the transceiver that is designed to act as a flexible testbed for testing the theoretical concepts and algorithms that are being developed. The transceiver architecture designed and currently being implemented is based on the concept of the software radio. The software radio architecture under development centers on the use of wideband ADCs and digital-to-analog converters as close to the antenna as possible, with as much radio functionality as possible defined and controlled by software. In this application, the transmit segment of the proposed transceiver does not merely transmit, it also performs the following operations: characterizes the RF channels available, probes the propagation path, selects the appropriate power level, and then transmits. Similarly, the receive segment characterizes the energy distribution in the channel, uses adaptive beamforming (at the base station), carries out adaptive interference suppression, estimates multipath, and combines the multipath to demodulate the signal with the lowest possible bit error rate. Finally, the proposed software radio supports future upgrades and service enhancements since it is based on a canonical open systems hardware and software architecture.

The radio architecture is split into two segments: the RF segment and the (baseband) processing stage. The following paragraphs address the design of the two segments of the architecture. The stages in the RF segment, such as upconversion; power amplification; and filtering at the transmitter; and RF amplification; filtering; and downconversion (to a suitable IF frequency) at the receiver are implemented using off-the-shelf mixers, filters and amplifiers available from manufacturers such as Mini-Circuits. The processing stage is custom designed and is based on the use of a mix of dedicated ASICs and high-performance DSP processors. The DSP processors used are the ADSP21020 and the ADSP21062, which are 32-bit floating point DSP processors from Analog Devices [86, 87]. These DSPs were chosen because of their high performance, high I/O bandwidth (eliminating communication bottlenecks), modular interface and ease of assembly programming (higher level cross-compiled code is not an option because of the high processing demand). Some of the heavy computational loads such as correlation at the sample rate are beyond the capability of the DSPs,

and in such cases, use is made of dedicated application-specific integrated circuits to off-load some of the processing from the DSPs. Multiple DSPs are used to handle the processing as required. A single ADSP21020 acting as the system executive and two ADSP21062s which implement the adaptive interference suppression and demodulation/despreading are found to be adequate for the mobile unit. For the implementation of the MTAA at the base station, multiple ADSP21062 are to be used. Again, some processing is off-loaded to ASICs to reduce the computational load on the DSPs, since ASICs can operate at higher speeds to perform many of the fixed tasks of the MTAA (such as transversal filter calculations, etc.). A single ADSP21020 again acts as the system executive.

The DSPs and the other ASICs are connected via bi-directional links (when appropriate) to the ADSP21020s data and address buses. All inter-processor communication (for the scheduling and synchronization tasks), and data transfers (between subsystems) is through this high bandwidth bus structure. All the subsystems and their interfaces are modular in nature so that future modifications can be made seamlessly without affecting the other systems. In addition, this modular multiprocessor architecture allows the major functions to be organized in any processing sequence dictated by the tasks required. To make this a reality, a built-in software diagnostic tool is being developed. This software module, which will be activated whenever the radio initially comes on-line, is being designed so that the system executive (the ADSP21020) automatically determines the functionality of all the subsystems connected to and under its purview. The system executive will automatically configure the radio architecture, allocate resources, and carry out the processing required.

8.5 Implementation of the MT adaptive array on ADSP21020/62 and computational complexity issues

An MTAA that employs a non-signal selective algorithm has been implemented in the assembly language on ADSP21020/62. Two steepest-descent based blind algorithms, the constant modulus and the decision directed algorithms are implemented on the

MTAA platform. Initially, the algorithms implemented on the DSP are tested using data files generated by MATLAB and the results are stored in memory. The algorithms are also implemented with MATLAB and the results from the ADSP are then compared with the results obtained from running the algorithms implemented with MATLAB. In the implementation of the algorithms, *pipelining* of the instructions is used to efficiently use the processor. In an ADSP21020/62, multiple instructions can be executed in one clock cycle. In a clock cycle, a maximum of 4 instructions can be executed using the ADSP processor. The 4 instructions include 1 multiplication, 1 addition, and 2 fetches, one from the program and the other from data memory.

The memory space in ADSP21020/62 is divided into *program* and *data memory*. The data stored in these memory spaces can be accessed simultaneously because they have different buses. Therefore simultaneous loading/fetching to/from the data and program memory are possible. Since the data used is represented in the complex envelope form, the processing is also done in the complex domain. Implementation of algorithms in the complex domain is costly, e.g., a complex multiplication requires 4 multiplications and 2 additions as opposed to a real multiplication which requires only 1 multiplication. To efficiently use the resources in the ADSP, the real parts of all the complex quantities are stored in the data memory and the imaginary parts of all the complex quantities are stored in the program memory. Therefore, we are able to fetch the real and imaginary parts of a complex quantity in a single clock cycle.

MTAA structure implementation

The signal flow graph for the basic MTAA structure is shown in Figure 8.5. The real and the imaginary parts of the input from the antenna elements are generated from MATLAB and fed as data files to the ADSP assembly routine. The initial weight vectors of the M beamformers in the MTAA are all initialized to an omnidirectional pattern and this data is also generated by MATLAB and fed into the assembly routine. ADSP21020/62 has 16 floating and fixed point registers to store intermediate values using the execution of a routine. These registers are usually global to all the routines. The adaptation step-size μ used in the steepest-descent approach is stored in a floating point register.

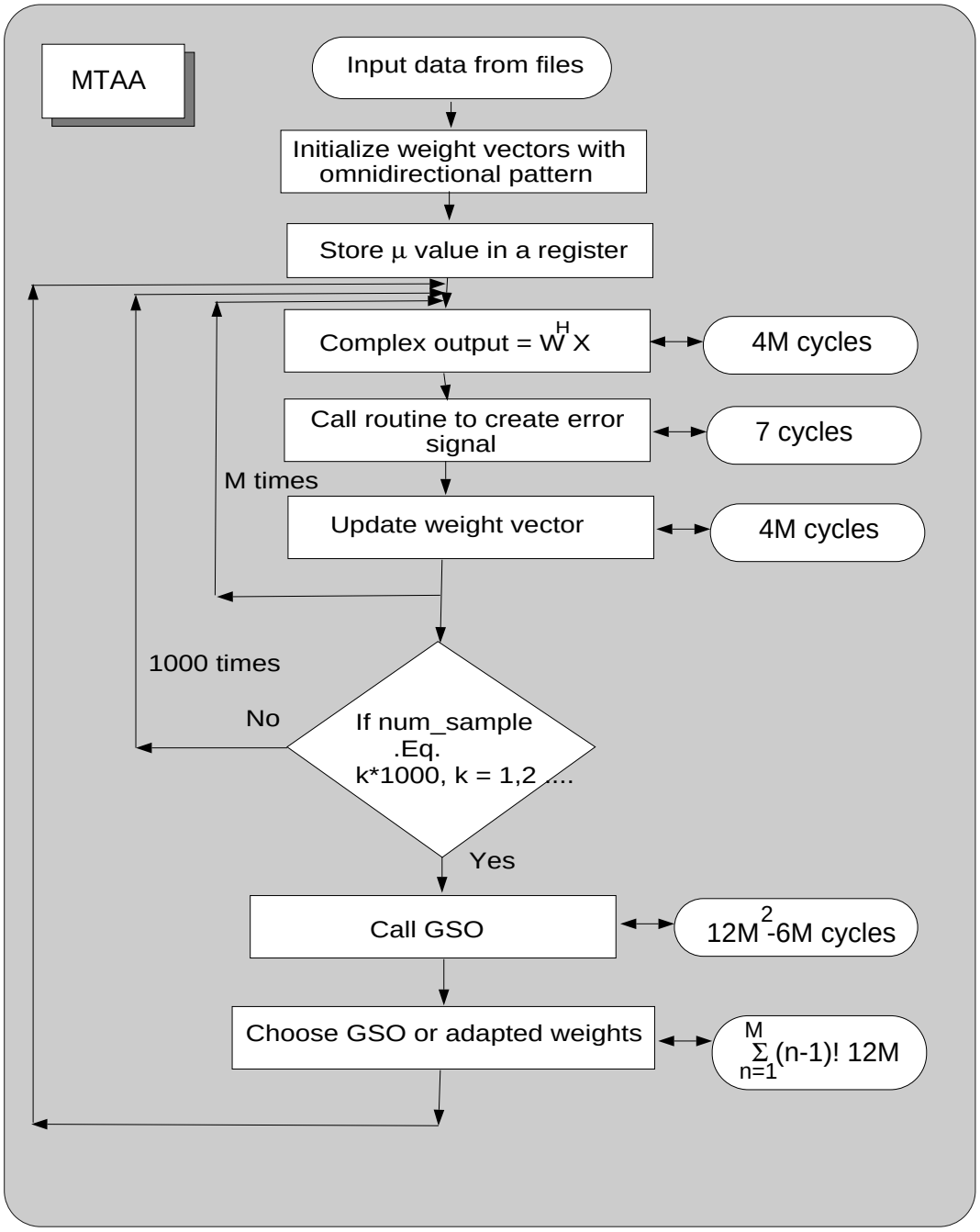

Figure 8.5: Signal flow chart of the MTAA.

• Output signal generation

For each port, a complex output ($y = \mathbf{w}^H\mathbf{x}$) is computed for every sample that enters the processor. The weight vector $\mathbf{w}$ is a $M \times 1$ vector and this complex vector inner product can be computed in $4M$ instruction cycles, where M is the number of antenna elements. The computed output is then fed into the routine that computes the error signal.

• Error signal generation

The input to the routine that creates the error is the output of the beamformer y as shown in Figure 8.6. Depending on the algorithm being used, the reference signal is either $y./|y|$ (CMA) or $sign(real(y))$ (DDA). To create the reference signal for the CMA, a division is required. Division is costly and hence we use a function that approximates the reciprocal-square root operation. The reference signal is given by

$$d = \frac{y}{|y|} = \frac{y_r + jy_i}{\sqrt{y_r^2 + y_i^2}}, \tag{8.1}$$

where y_r and y_i are the real and the imaginary parts of y. The function RSQRTS in the ADSP assembly language performs the reciprocal-square root operation in 1 clock cycle. The syntax is F_n =RSQRTS F_x, where $F_x = y_r^2 + y_i^2$ in this case. RSQRTS creates a 4-bit accurate seed for $1/\sqrt{F_x}$. The mantissa of the seed is determined from a read-only-memory (ROM) table using the least significant bit (LSB) of the biased exponent of F_x concatenated with the 6 most significant bits (MSBs) of the mantissa of F_x (excluding the hidden bit). The unbiased exponent of the seed is calculated as the *two*s complement of the unbiased F_x unbiased exponent, shifted to the right by one bit and decremented by one, i.e., if e is the unbiased exponent of F_x, then the unbiased exponent of F_n = -INT$[e/2] - 1$. The sign of the seed is the sign of the input. To perform division with full accuracy (32 bit precision) requires 13 clock cycles as opposed to 1 clock cycle if RSQRTS is used.

If DDA is used for adaptation, there is no need for division because it involves a signum operation of the real part of the output to create the reference signal. Finally the error is created by subtracting the reference signal from the output.

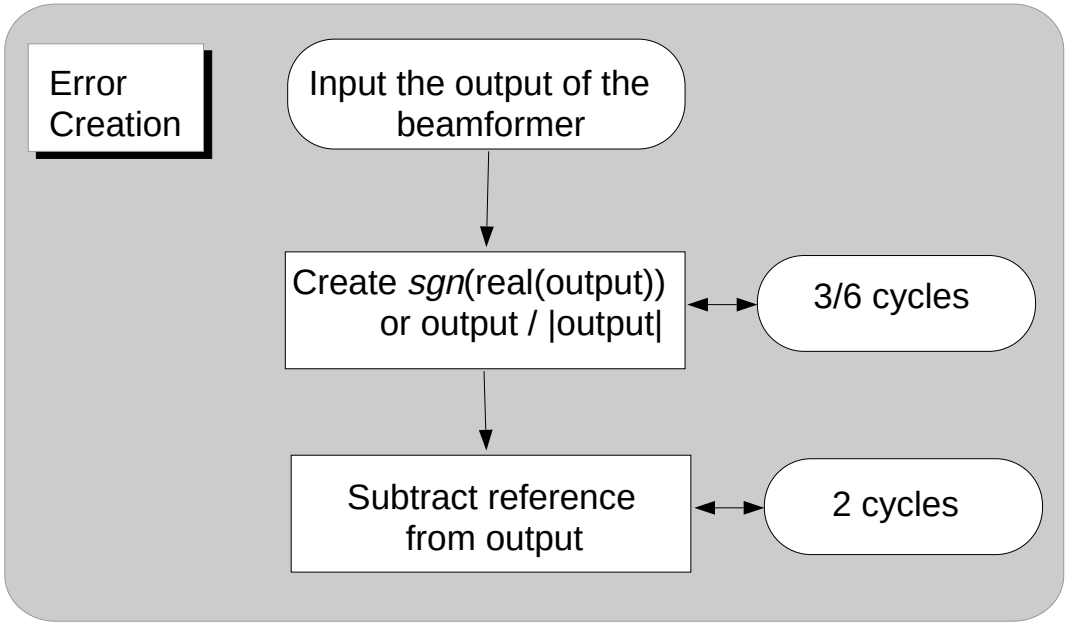

Figure 8.6: Signal flow chart of the macro that creates the error signal.

• Weight vector adaptation

The adaptation of weight vector is based on steepest-descent approach, to implement the following update

$$\mathbf{w}_{k+1} = \mathbf{w}_k + \mu e_k^* \mathbf{x}_k, \tag{8.2}$$

requires $4M$ clock cycles at any time instant k.

The output calculation, error signal generation and the weight vector adaptation are carried out M times, as there are M ports. For every 1000 samples, the GSO operation is carried out.

• Gram-Schmidt orthogonalization

The GSO operation is the most computationally intensive operation in the MTAA implementation. The GSO involves two main components, 1) normalization of the weight vectors and 2) orthogonalization of the weight vectors. The signal flow graph for the GSO is shown in Figure 8.7. The GSO operation involves two normalization

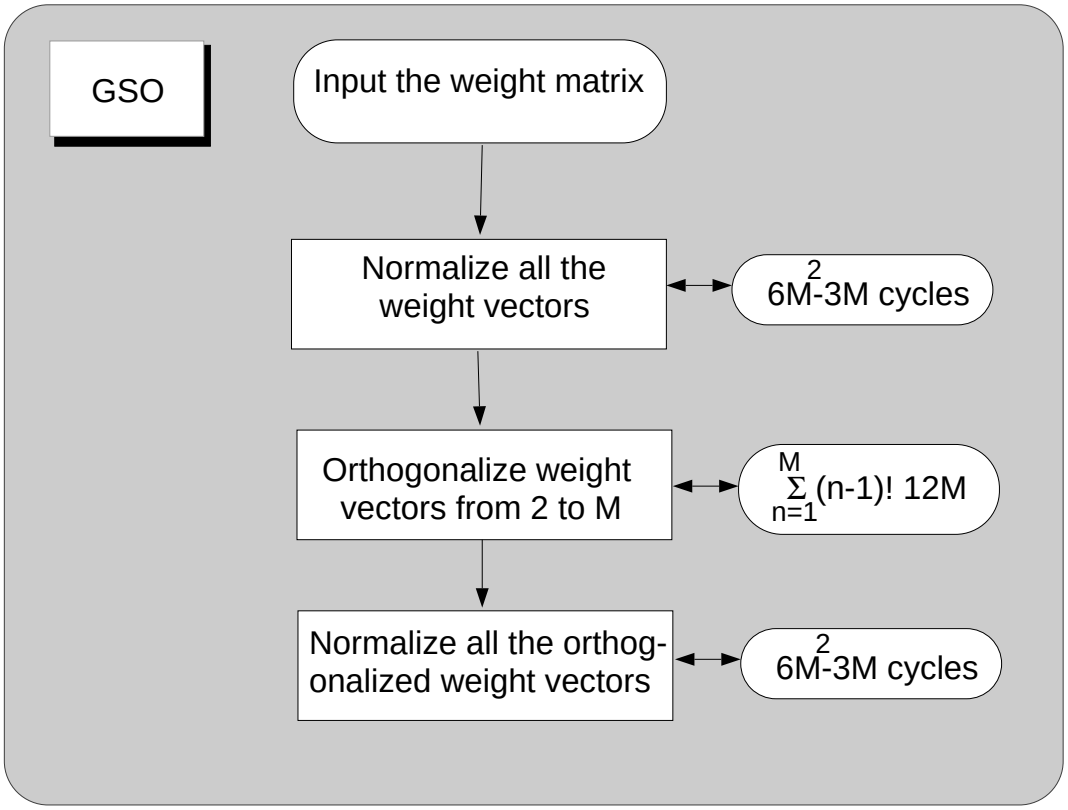

Figure 8.7: Signal flow chart of the GSO.

steps, one before the orthogonalization and one after it. The weight vectors are normalized before the orthogonalization, because the correlation between the adapted weight vectors has to estimated and compared to a threshold to determine if the adapted beam weights of two different ports point towards the same user. The normalization after the orthogonalization is required to make the *norm*[1] of the weight vector equal to unity.

- The normalization operations requires approximately $12M^2$ - $6M$ clock cycles.
- The orthogonalization requires $\sum_{n=1}^{M}(n-1)!12M$ clock cycles.

[1] $norm(\mathbf{w}) = \|\mathbf{w}\|_2 = \sqrt{\sum_{i=1}^{M} |w_i|^2}$

• Correlation and selection of weight vectors

The next operation is the correlation of the normalized adapted weight vectors and checking if the correlation between the weight vectors is higher than a threshold (threshold of 0.9 was found to be satisfactory). If the threshold is exceeded, then the GSO weights replace the adapted weights. For an M-element array, a total number of $\sum_{n=1}^{M}(n-1)!$ correlations is required. Each correlation operation requires approximately $4M+7$ clock cycles. After this operation, the weight vectors are used to create the output and operation continues.

8.6 Development phases and current status

The development of an 8-element MTAA for the GloMo specifications is underway currently. The development is divided into two phases: 1) algorithm implementation on the ADSP21020/62, 2) implementation of the RF front-end and signal digitization sections of the adaptive array.

• Phase 1

The first phase involves the implementation of the MTAA on the ADSP21020/62 and the MTAA can be configured to use either the CMA or the DDA. This phase involved implementing the algorithms both with MATLAB and both in the assembly language of ADSP21020/62. The algorithms were first tested in the ADSP simulator using data files that have been generated by MATLAB. Then the ADSP assembly code is ported into the chip to test the algorithms. The assembly code has been tested and found to function satisfactorily. The author has developed the assembly codes for the MTAA based on CMA and DD, and has tested the algorithm.

• Phase 2

The second phase involves the implementation of the RF front end and the signal digitization sections. This phase involves phase tracking, RF and IF filtering, and digitization. It is anticipated that this phase will prove to be most challenging.

Commercial Analog-to-Digital Converters (ADCs), mixers, filters may be used for the RF front end or a fully developed RF front end section may be employed. This phase of development will not be carried out by the author, but instead will be a part of a continuing research effort.

8.7 Conclusions

Implementation of an adaptive array is a challenging task and in this chapter many issues involved in the implementation are addressed. The architectures for the transmitter and the receiver are discussed. The choice of the processor is an issue that has been addressed in depth. Analog Devices DSP is used to implement the baseband section of the radio. Finally, efficient implementation of an MTAA on the DSP hardware is discussed.

Chapter 9

Link Analysis of a CDMA-AMPS Overlay System Employing Beamformers

9.1 Introduction

To cope with the demand for increased capacity in a cellular system, conventional analog (AMPS) systems are gradually being replaced by digital systems (TDMA and CDMA). Digital systems can provide increased capacity over the analog systems while maintaining the same signal quality. CDMA systems hold promise for increasing the capacity multifold [88] over AMPS systems. In areas with cellular coverage, CDMA systems are overlayed on existing AMPS systems as a strategy for gradual replacement of the analog system. In an overlay system, the CDMA users occupying a 1.25 MHz bandwidth are overlayed in all the AMPS cells. Due to overlay, AMPS and CDMA signals interfere with each other. Therefore the number of CDMA users that can be accommodated in the system depends on the total interference caused by these CDMA users to the AMPS users and vice versa. The AMPS users are required to have an input CIR $>$ 18 dB. So there is a bound to the number of CDMA users that can be accommodated if conventional receivers are used.

CDMA signals are vulnerable to narrowband interference from AMPS signals. Narrowband interference rejection techniques have been proposed [89] in the past to

facilitate the co-existence of narrowband systems with wideband systems. In [90], the author derived the frequency reuse efficiency of a CDMA system and has analyzed the effect of CDMA users on AMPS signals. Furthermore in [91], a thorough analysis of the forward and reverse links is presented in a system where CDMA signals are overlayed on AMPS signals.

Though narrowband interference rejection techniques help the performance of the CDMA users, the performance of the AMPS system degrades as the number of CDMA users increases. Hence signal processing techniques are needed to mitigate the effect of CDMA interference seen by the AMPS users and vice versa. Adaptive arrays are as a viable solution to this problem. The adaptive array at the base station can significantly reduce interference seen by both AMPS and CDMA users by forming beams in the directions of the users. To obtain comparable performance on both forward and reverse links, forward and reverse link beamforming must be performed. In this chapter, we analyze the link performance of both the AMPS and the CDMA systems when an ideal beamformer forward and reverse link beamforming are employed at the base station.

Notation used in the chapter is introduced in Section 9.2. Section 9.3 discusses the concentric cellular geometry, which forms the basis for the analysis in this chapter. Section 9.4 presents the reverse link analysis for an AMPS system. Section 9.5 presents the reverse link analysis for CDMA systems. Sections 9.6 and 9.7 deal with the forward link analysis for the AMPS and the CDMA systems, respectively. Sections 9.8 and 9.9 present the numerical results for AMPS and CDMA system capacity, respectively. Finally the conclusions are discussed in Section 9.11.

9.2 Notation variable definitions

The following are the notations used in this chapter:

P_c - Power of a CDMA user

P_f - Power of an AMPS user

D - Reuse distance

R - Radius of a cell

G - Gain of the array

B - Bandwidth of the AMPS channel

W_{ss} - Bandwidth of the CDMA signal

N - Reuse factor for AMPS system

N_1 - Number of CDMA users in a cell

α - Voice activity factor

$\Delta\theta$ - Beamwidth of the beamformer

r_d - Data rate

9.3 Concentric cell geometry

For the link analysis we use the concentric cell geometry instead of a hexagonal geometry for convenience. The concentric cell geometry is shown in Figure 9.1. There are six cochannel first tier CDMA users in the circular geometry as with the hexagonal geometry[1]. The radius of the home cell is R. The area within each cell is the same and is equal to πR^2. Therefore the radius of the second tier of cells is $\sqrt{7}R$. In the second tier of cochannel cells, there are 12 cochannel CDMA cells and the radius of the third tier of cells is $\sqrt{19}R$. The cells are marked with a number which represents the set of AMPS channels used by a particular cell. The CDMA base station in the first tier is separated from the home base station by a distance $1.82R$, while the distance between the home base station and the one in the second tier is $3.50R$. In the analysis, we consider only the first two tiers of CDMA cells and the first tier of AMPS cells.

9.4 Reverse link analysis for AMPS system

Let us first analyze the reverse link for the AMPS systems when there are interfering AMPS and CDMA users. The 30 kHz AMPS signal occupies the same spectrum as a 1.25 MHz CDMA signal. An AMPS user hence suffers from two types of cochannel

[1]Strictly speaking the first tier of CDMA signals is the home cell, but to be consistent with the description for AMPS cells, we call the cells surrounding the home cell as the first tier of CDMA cells.

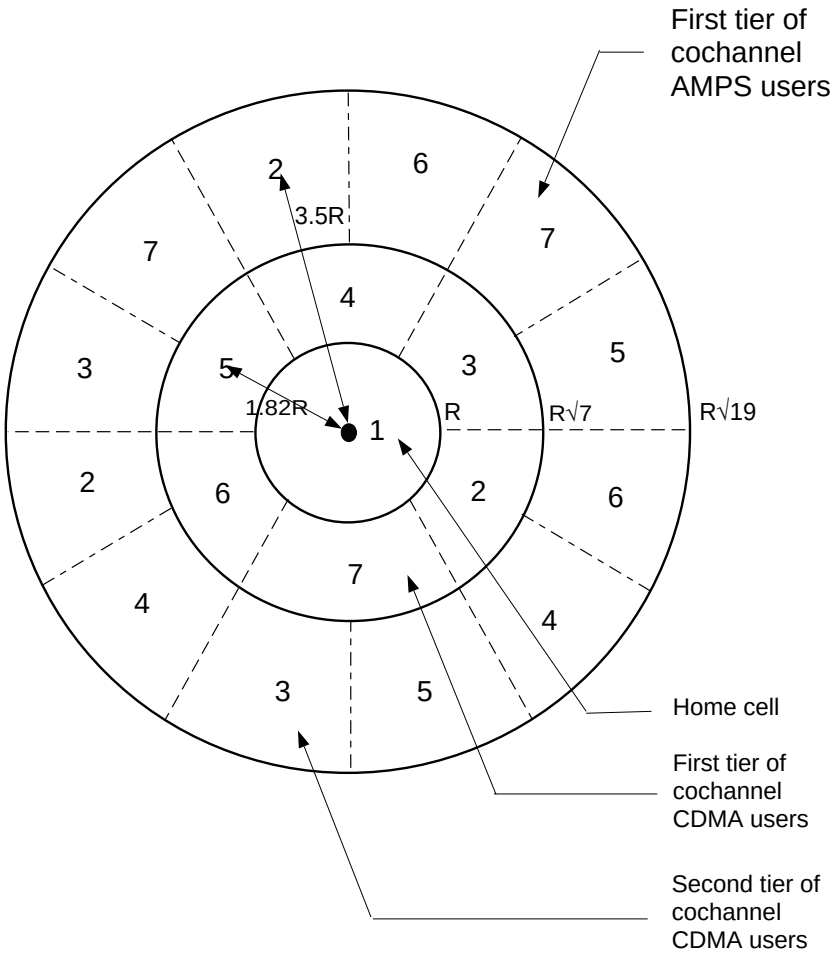

Figure 9.1: Concentric cellular geometry.

signals: one is the interference from AMPS signals from the neighboring clusters and the other is the interference from CDMA signals of all the cells including the home cell. The amount of interference from the cochannel AMPS users depends on the reuse distance D, while the amount of interference from the CDMA users depends on the relative bandwidth of the AMPS signal to the CDMA signal and the number of CDMA users sharing the spectrum.

Let us define the interference from the cochannel AMPS signals as I_a and from the CDMA signals as I_c. The total interference I is given by

$$I = I_a + I_c. \tag{9.1}$$

Let us assume that the beamformer at the base station of the home cell points in the direction of the desired AMPS user. The beamformer receives not only the desired AMPS signal but also the signal from the AMPS cochannel users in the first tier of AMPS cells, CDMA users within the home cell, CDMA users from the first and the second tier cells. This interference emanates from the same direction as the desired AMPS user. Let us consider the worst-case scenario where the desired AMPS mobile is at the edge of the home cell, hence the power of the desired AMPS signal is given by

$$I_d = GP_f R^{-4}. \tag{9.2}$$

If the beamformer has a beamwidth $\Delta\theta \leq 60°$, then there is a high probability that only one or less AMPS interferer lies within the beam since we consider only the first tier of AMPS cochannel signals for the analysis. Therefore the power of the interfering AMPS signal is given by

$$I_a = GP_f D^{-4}. \tag{9.3}$$

Let us assume that the CDMA users are uniformly distributed within each cell. Figure 9.2 illustrates the regions illuminated by the beamformer. Now let us calculate the amount of CDMA interference received at the base station. The following is the calculation of number of CDMA users that lie within the beam in the home cell, first tier and the second tier of cells.

Home cell:

$$\text{Number of CDMA users in an angular region of } \Delta\theta = N_1 \left(\frac{\Delta\theta}{360}\right).$$

First tier:

$$\text{Area within the first tier illuminated by the beam} = \frac{1}{2}\int_0^{\Delta\theta} (r_2^2 - r_1^2) d\theta \tag{9.4}$$

where $r_1 = R$ and $r_2 = \sqrt{7}R$. Therefore the illuminated area $= 3R^2\Delta\theta$. Given this illuminated area, the number of CDMA users illuminated in the first tier $= 6N_1 \left(\frac{\Delta\theta}{360}\right)$.

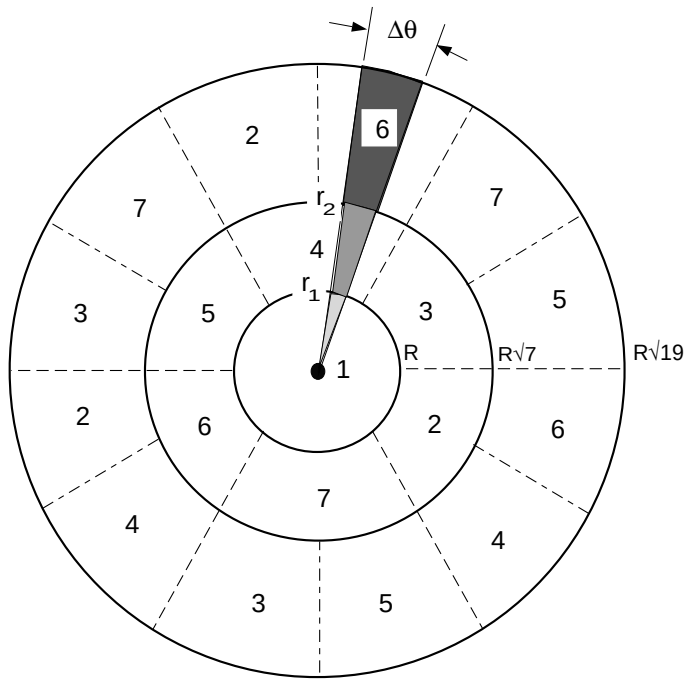

Figure 9.2: Figure illustrating the regions illuminated by a beamformer with a beamwidth of $\Delta\theta$ at the base station of the home cell #1. Regions illuminated in different tiers are shaded differently.

Second tier:

Similarly the number of CDMA users illuminated in the second tier $= 12N_1 \left(\frac{\Delta\theta}{360}\right)$.

The total CDMA interference, $I_c = I_{c\circ} + I_{c1} + I_{c2}$, where $I_{c\circ}$, I_{c1}, I_{c2} are the total CDMA interference from the home cell, first tier of cells, and second tier of cells, respectively.

Let us now calculate the average distances between the CDMA users from the home base station (cell #1) in the home cell, first tier cell and the second tier cell. Figure 9.3 illustrates the calculation of the average distance, r, between the CDMA users and the base station for the home cell. The shaded areas are the regions illuminated by the base station beam. The average T-R separation for a CDMA user within the home cell is calculated by finding the value of r that makes the area

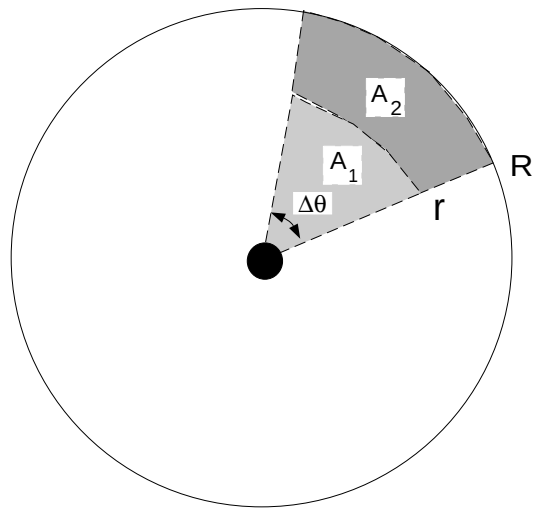

Figure 9.3: Figure illustrating the calculation of the average distance between the CDMA users and the base station.

A_1 equal to A_2, i.e., the number of users on both sides of the boundary is equal.

$$A_1 = \frac{\Delta\theta}{2} r^2$$

while

$$A_2 = \frac{\Delta\theta}{2}(R^2 - r^2).$$

By setting A_1 equal to A_2, r is given by

$$r = \frac{R}{\sqrt{2}}.$$

Similarly for the first tier of cells, the average distance of separation between the CDMA users in the first tier and the home base station is equal to $2R$, while for the second tier of cells it is equal to $\sqrt{13}R$. Therefore the total CDMA interference, I_c, is the sum of interference power of the CDMA users in the home cell, first tier, and the second tier with average distances of $R/\sqrt{2}$, $2R$, and $\sqrt{13}R$, respectively.

$$\begin{aligned} I_c &= G\left(\frac{B}{W_{ss}}\right)\left(\frac{\Delta\theta}{360}\right)\left[N_1\alpha P_c\left(\frac{R}{\sqrt{2}}\right)^{-4} + 6N_1\alpha P_c(2R)^{-4}\right. \\ &\qquad \left. +12N_1\alpha P_c(\sqrt{13}R)^{-4}\right] \\ &= 4.446N_1 G\alpha P_c\left(\frac{B}{W_{ss}}\right)\left(\frac{\Delta\theta}{360}\right)R^{-4}. \end{aligned} \tag{9.5}$$

Therefore the carrier-to-interference ratio (CIR) is given by

$$\text{CIR} = \frac{I_d}{I_a + I_c} \tag{9.6}$$

where I_d, I_a, and I_c are given by Eqns. 9.2, 9.3, and 9.5, respectively.

$$\begin{aligned} \text{CIR} &= \left[\frac{GP_f R^{-4}}{GP_f D^{-4} + 4.446 N_1 G\alpha P_c \left(\frac{B}{W_{ss}}\right)\left(\frac{\Delta\theta}{360}\right) R^{-4}} \right] \\ &= \left[\frac{1}{K_1 \left(\frac{D}{R}\right)^{-4} + 4.446 N_1 \alpha \left(\frac{P_c}{P_f}\right)\left(\frac{B}{W_{ss}}\right)\left(\frac{\Delta\theta}{360}\right)} \right]. \end{aligned} \tag{9.7}$$

The value of K_1 is 1 for $\Delta\theta \leq 60°$. For the concentric cell geometry, the ratio of the distance between the base stations in the Kth CDMA tier and the home cell, D, to the radius of the cell, R, can be shown to be

$$\left(\frac{D}{R}\right)_K = \frac{1}{2}\left[\left(\sqrt{\sum_{k=1}^{K} 6k+1}\right) + \left(\sqrt{\sum_{k=1}^{K-1} 6k+1}\right)\right]. \tag{9.8}$$

The first term within the bracket is the distance between the home cell and the boundary of the Kth CDMA tier while the second term is the distance between the home cell and the boundary of the $(K-1)$th CDMA tier. The term $\sum_{k=1}^{K} 6k+1$ corresponds to the number of cells within K tiers of CDMA cells. Since the base station is assumed to be at the middle of the cell, the D/R is the average distance between the $(K-1)$th and the Kth CDMA tiers from the home cell base station. The AMPS system uses a reuse factor of 7 and hence $K = 3$, therefore $\frac{D}{R} = 5.2208$. For an omnidirectional antenna, $K_1 = 6$ and hence the CIR is given by

$$\text{CIR} = \left[\frac{1}{6\left(\frac{D}{R}\right)^{-4} + 4.446 N_1 \alpha \left(\frac{P_c}{P_f}\right)\left(\frac{B}{W_{ss}}\right)} \right]. \tag{9.9}$$

9.5 Reverse link analysis for CDMA system

We now study the reverse link performance of the CDMA system, i.e., the effects of AMPS interferers on the CDMA signals. Here we look at the worse-case scenario when the desired CDMA user is at the boundary of the cell, while the other CDMA

and AMPS users are uniformly distributed within the cell. The CIR is related to the despread $E_b/I_\circ$ by the following relationship:

$$\text{CIR} = \left(\frac{E_b}{I_\circ}\right)\left(\frac{2r_d}{W_{ss}}\right) \tag{9.10}$$

where r_d is the data rate, E_b is the bit energy, and $I_\circ$ is the interference energy. A CDMA user suffers interference from $(N_1 - 1)$ CDMA users in the home cell, N_1 CDMA users from each of the other cells, and the AMPS users occupying the 1.25 MHz band. The number of AMPS users in a 1.25 MHz bandwidth $= 1.25 \times 10^6/(N \times 30 \times 10^3)$, where N is the reuse factor. If $N = 7$, then there can be 5 or 6 AMPS users in a 1.25 MHz bandwidth,

Let us now calculate $E_b/I_\circ$. The desired CDMA user power after despreading is given by

$$I_d = \alpha G P_c R^{-4}. \tag{9.11}$$

The total CDMA interference after despreading is (similar to Eqn. 9.5)

$$I_c = (4.446N_1 - 1)G\alpha P_c R^{-4}\left(\frac{2r_d}{W_{ss}}\right)\left(\frac{\Delta\theta}{360}\right). \tag{9.12}$$

The AMPS interferers are independent and orthogonal in frequency. It was shown in [91], the total received power from the kth AMPS interferer after despreading, with frequency offset equal to $k \times B$ Hz from the CDMA center frequency, where k is an integer, is given by

$$P(kB) = p(k)\left[\frac{L+1}{L^2}\sum_{-N_1, n\neq 0}^{N_1} \text{sinc}^2\left(\frac{n}{L}\right)\cdot\phi_{B,r_d}\left(kB + \frac{n}{LT_c}\right) + \frac{1}{L^2}\phi_{B,r_d}(kB)\right] \tag{9.13}$$

where L is the length of the PN sequence, $L = 2^l - 1$, l is an integer. $p(k)$ in Eqn. 9.13 is the kth AMPS power spectral density and is approximated by a constant P_f/B. $\phi_{B,r_d}(x)$ is defined as

$$\phi_{B,r_d}(x) = \int_{-r}^{r} \text{rect}\left(\frac{f-x}{B}\right) dx$$

for $B > 2r_d$

$$\phi_{B,r_d}(x) = \begin{cases} 0 & : \quad |x| > r_d + \frac{B}{2} \\ r_d + \frac{B}{2} - |x| & : \quad \frac{B}{2} - r_d < |x| < \frac{B}{2+r_d} \\ 2r_d & : \quad \frac{B}{2} - r_d > x > -\frac{B}{2-r_d} \end{cases}. \tag{9.14}$$

Table 9.1: Coefficients of total interfering power of each cell ($C_k = P(kB)$)

Users/Cell	C_1	C_2	C_3	C_4	C_5	C_6	C_7
6 users	2.0764	2.0754	2.0886	2.0886	2.0754	2.0764	1.9537
5 users	1.3104	1.3265	1.3628	1.3628	1.3265	1.3104	1.3068

If $x = kB$, k is an integer, then

$$\phi_{B,r_d}(x) = \begin{cases} 2r_d & : \quad k = 0 \\ 0 & : \quad k \neq 0 \end{cases} \tag{9.15}$$

For $B = 30$ kHz, $W_{ss} = 1.25$ MHz, then

$$x = 30k + \frac{1250}{2L}n.$$

The value of L is assumed to be 127 for further calculations. From [91], the coefficients of total interfering power of each cell is given by the following table. As shown in Figure 9.1, each cell is assigned a set of frequencies and are marked by a number from 1 to 7. The home cell is marked 1. The AMPS interferer within the home cell is separated from the base station by an average distance of $R/\sqrt{2}$, while the AMPS users in the first tier and the second tier are separated from the home base station by distances of $2R$ and $\sqrt{13}R$, respectively. The total AMPS interference is given by

$$\begin{aligned} I_f &= \left[\sum_{k=1} P(kB)\left(\frac{R}{\sqrt{2}}\right)^{-4}\left(\frac{\Delta\theta}{360}\right) + \sum_{k=2,3,4,5,6,7} P(kB)\,(2R)^{-4}\left(\frac{\Delta\theta}{360}\right) + \right. \\ &\quad \left. 2 \times \sum_{k=2,3,4,5,6,7} P(kB)\left(\sqrt{13R}\right)^{-4}\left(\frac{\Delta\theta}{360}\right)\right] G\left(\frac{P_f}{30}\right) \end{aligned} \tag{9.16}$$

If there are 6 AMPS users in a 1.25 MHz spectrum, then

$$I_f = 0.3075\left(\frac{\Delta\theta}{360}\right) G P_f R^{-4}. \tag{9.17}$$

Now $E_b/I_\circ$ can be written as

$$\left(\frac{E_b}{I_\circ}\right) = \frac{I_d}{I_c + I_f}. \tag{9.18}$$

where I_d, I_c, and I_f are given by Eqns. 9.11, 9.12, and 9.17, respectively. Now substituting $E_b/I_\circ$ in Eqn. 9.10, CIR is given by

$$\text{CIR} = \left[\frac{\alpha G P_c R^{-4}\left(\frac{2r_d}{W_{ss}}\right)}{0.3075G\left(\frac{\Delta\theta}{360}\right)P_f R^{-4} + (4.446N_1 - 1)G\alpha P_c R^{-4}\left(\frac{2r_d}{W_{ss}}\right)\left(\frac{\Delta\theta}{360}\right)}\right]$$

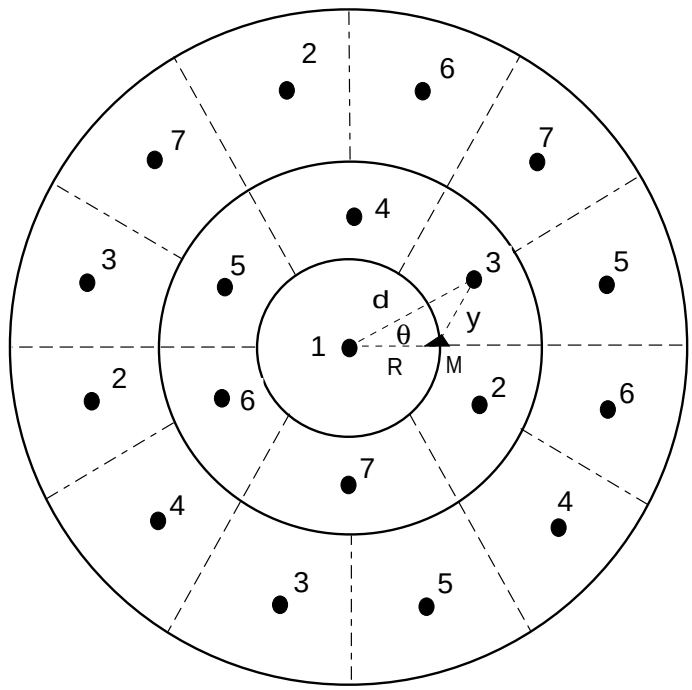

Figure 9.4: Figure illustrating the calculation of the distance between the AMPS mobile at the home cell boundary and the interfering base stations. The mobile is marked "M" and the shaded circles are the base stations.

$$= \left[\frac{1}{\frac{0.3075}{\alpha}\left(\frac{P_f}{P_c}\right)\left(\frac{\Delta\theta}{360}\right)\left(\frac{W_{ss}}{2r_d}\right) + (4.446N_1 - 1)\left(\frac{\Delta\theta}{360}\right)} \right] \tag{9.19}$$

9.6 Forward link analysis for AMPS system

Let us now analyze the performance of the AMPS system forward link. Let us consider the worst-case scenario when the mobile is at the edge of the cell as illustrated in Figure 9.4. Here we assume that the mobile unit employs an omnidirectional antenna and receives signals from all directions in the azimuth. Let us calculate the distance between the desired mobile and the base stations that transmit CDMA signals and interfere with the desired AMPS signal. The distance, y, between the mobile at the edge of the cell and any base station which is separated from the home base station by a distance d, and makes an angle of θ degrees with respect to the mobile, M, is given by

$$y = \left[\sqrt{d^2 + 1 - 2d\cos\theta}\right] R. \tag{9.20}$$

Table 9.2: Distance between the mobile and the base stations in the first tier

Angle in degrees	$\theta = \pm 30°$	$\theta = \pm 90°$	$\theta = \pm 150°$
Distance	1.077R	2.076R	2.732R

Table 9.3: Distance between the mobile and the base stations in the second tier

Angle in degrees	$\theta = \pm 15°$	$\pm 45°$	$\pm 75°$	$\theta = \pm 105°$	$\pm 135°$	$\pm 165°$
Distance	2.547R	2.881R	3.38R	3.88R	4.266R	4.473R

If the base station is in the first tier, then $d = 1.82R$, and for the second tier $d = 3.5R$. Based on Eqn. 9.20, the distance between the mobile and the base stations in the first tier and the second are listed in Tables 9.2 and 9.3, respectively. The signal from the desired base station to the mobile is given by

$$I_d = GP_f R^{-4}. \tag{9.21}$$

Since each base station employs a beamformer, the number of cochannel AMPS base stations interfering with the desired mobile depends on the width of the beam. In the worst-case, all the six cochannel AMPS base stations can interfere with the desired mobile and hence I_a is given by

$$I_a \approx 6GP_f D^{-4}. \tag{9.22}$$

Figure 9.5 illustrates the scenario when the base station of each AMPS cell uses a beamformer. The base stations are marked B and the mobiles by M. Since the mobile uses an omnidirectional antenna, it collects signal from all directions and hence there is a nonzero probability that all the six base stations might interfere with the desired mobile unit. If we assume that the mobiles are equally likely to be anywhere within their home cell, the probability that K_2 cochannel AMPS base stations interfering

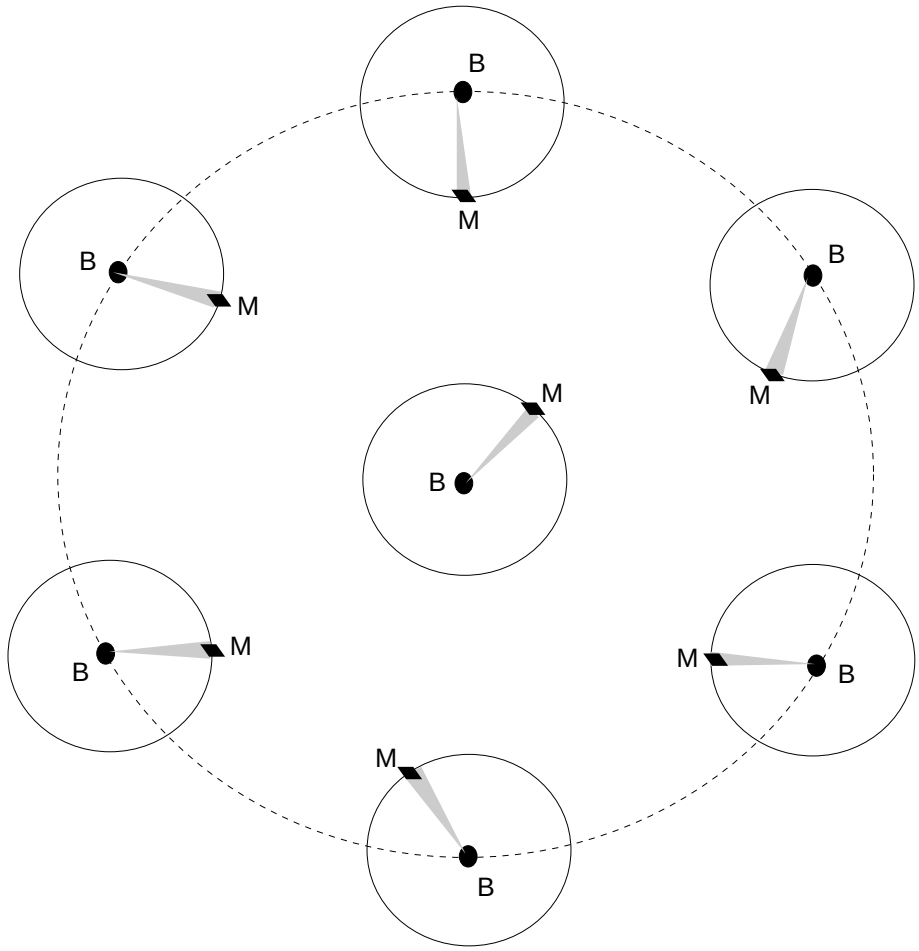

Figure 9.5: Illustration of the scenario when each base station uses a beamformer and the mobile uses an omnidirectional antenna. The beams are shown as shaded regions.

with the desired mobile user, $P(K_2)$, is given by the binomial distribution as follows:

$$P(K_2 = i) = \begin{cases} \left(1 - \frac{\Delta\theta}{360}\right)^6 & : \quad i = 0 \\ 6\left(\frac{\Delta\theta}{360}\right)\left(1 - \frac{\Delta\theta}{360}\right)^5 & : \quad i = 1 \\ 15\left(\frac{\Delta\theta}{360}\right)^2\left(1 - \frac{\Delta\theta}{360}\right)^4 & : \quad i = 2 \\ 20\left(\frac{\Delta\theta}{360}\right)^3\left(1 - \frac{\Delta\theta}{360}\right)^3 & : \quad i = 3 \\ 15\left(\frac{\Delta\theta}{360}\right)^4\left(1 - \frac{\Delta\theta}{360}\right)^2 & : \quad i = 4 \\ 6\left(\frac{\Delta\theta}{360}\right)^5\left(1 - \frac{\Delta\theta}{360}\right) & : \quad i = 5 \\ \left(\frac{\Delta\theta}{360}\right)^6 & : \quad i = 6 \end{cases} \tag{9.23}$$

If the beamwidth $\leq 30°$, then $K_2 \leq 2$ for 99% of the time.

The total CDMA interference is given by (similar to Eqn. 9.5)

$$\begin{aligned} I_c &= \alpha G N_1 P_c \left(\frac{\Delta\theta}{360}\right)\left(\frac{B}{W_{ss}}\right)\Big[1 + 2(1.077^{-4} + 2.076^{-4} + 2.732^{-4}) + \\ &\quad 2(2.547^{-4} + 2.8816^{-4} + 3.38^{-4} + 3.88^{-4} + 4.266^{-4} + 4.473^{-4})\Big] R^{-4} \\ &= 2.7418 R^{-4} \alpha G N_1 P_c \left(\frac{\Delta\theta}{360}\right)\left(\frac{B}{W_{ss}}\right). \end{aligned} \tag{9.24}$$

Therefore the CIR is given by

$$\text{CIR} = \left[\frac{1}{K_2\left(\frac{D}{R}\right)^{-4} + 2.7418\alpha N_1\left(\frac{P_c}{P_f}\right)\left(\frac{B}{W_{ss}}\right)\left(\frac{\Delta\theta}{360}\right)}\right] \tag{9.25}$$

For beamwidths $\leq 30°$, K_2 is equal to 2 for 99% of the time.

9.7 Forward link analysis for CDMA system

Following the same analysis as the reverse link, presented in the Section 9.5. In the forward link all the mobiles have omnidirectional antennas and hence receive interference energy from all directions. So capacity increase can be achieved by reducing the interference energy focused on the mobile. The carrier power on the forward link is given by

$$I_d = \alpha G P_c R^{-4}\left(\frac{2r_d}{W_{ss}}\right). \tag{9.26}$$

The total CDMA interference can be shown to be (similar to Eqn. 9.12)

$$I_c = (2.7418N_1 - 1) G\alpha P_c R^{-4}\left(\frac{2r_d}{W_{ss}}\right)\left(\frac{\Delta\theta}{360}\right). \tag{9.27}$$

If there are 6 AMPS users in a 1.25 MHz spectrum, then the total AMPS interference can be shown to be (similar to Eqn. 9.17)

$$I_f = 0.1897 G\left(\frac{\Delta\theta}{360}\right) P_f R^{-4}. \tag{9.28}$$

Therefore CIR is given by

$$\text{CIR} = \left[\frac{1}{\frac{0.1897}{\alpha}\left(\frac{P_f}{P_c}\right)\left(\frac{\Delta\theta}{360}\right)\left(\frac{W_{ss}}{2r_d}\right) + (2.7418N_1 - 1)\left(\frac{\Delta\theta}{360}\right)}\right] \tag{9.29}$$

9.8 Comparison of results for forward and reverse links analysis for AMPS system

Using the analysis presented in the Sections 9.4 and 9.6, we compute the CIR of the forward and the reverse links for the AMPS system. Figures 9.6(a) and (b) show the CIR performance of the AMPS system as a function of number of CDMA users for beamformers with beamwidths 10, 20, 30 and 360 degrees (omnidirectional). Figure 9.6(a) and (b) are the performance curves for the forward and the reverse links, respectively for a power ratio (P_c/P_f) of -10 dB. It is important to observe for lower number of CDMA users, the forward link performs worse than the reverse link. This is due to the fact that in the reverse link the base station restricts the signal reception to a narrow angular region. In the forward link even though the base station transmits using directivity, the mobile employs an omnidirectional antenna and hence it receives more interference than the reverse link. Furthermore the rate at which the performance degrades as the number of CDMA users increases is higher for the reverse link than the forward link. In the forward link, when the mobile is at the edge of the base station, as the number of CDMA users increase, the distance traveled by both the AMPS and the CDMA signals is equal to R. But in the reverse link, when the mobile is at the edge of the cell, the CDMA users are uniformly distributed within the cell and hence the desired signal travels a distance of R, while the interferers on the average travels a distance of $R/\sqrt{2}$. Therefore, as the number of CDMA users increases, the performance in the reverse link degrades faster than the forward link. Let us assume that a minimum CIR of 18 dB is necessary, then a beamformer with 20 degrees beamwidth can support 100 CDMA users in the forward link and 60 users in the reverse link. Therefore the reverse link limits the performance of the whole system.

Figures 9.7(a) and (b) are performance curves for a -20 dB power ratio. The performance trend is the same as the -10 dB power ratio case. For -20 dB power ratio case, the forward and the reverse links can accommodate more than 100 CDMA users in the system with a beamformer of beamwidth 30°.

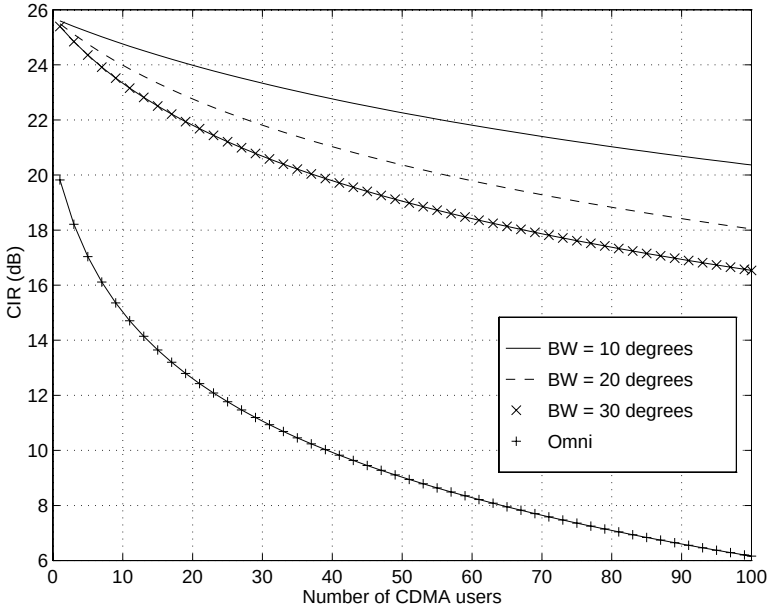

(a)

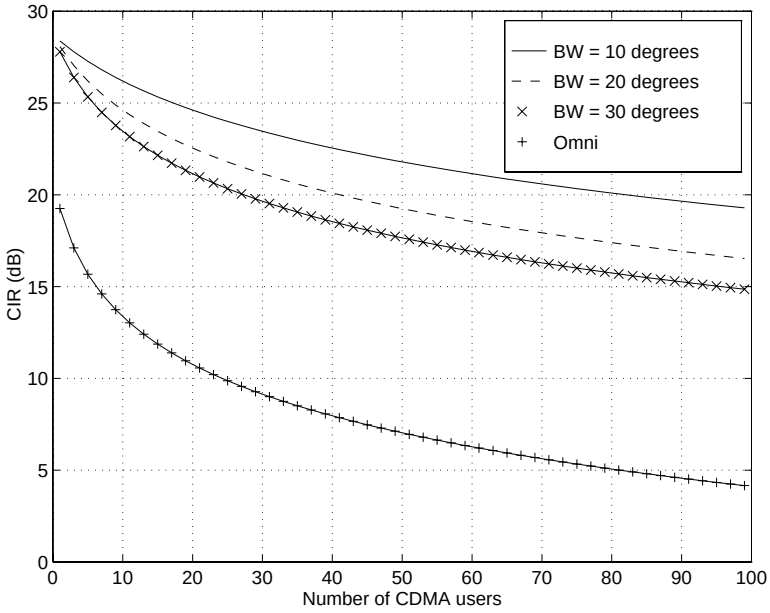

(b)

Figure 9.6: CIR plots for the AMPS signal in (a) the forward and (b) the reverse links for a power ratio of -10 dB.

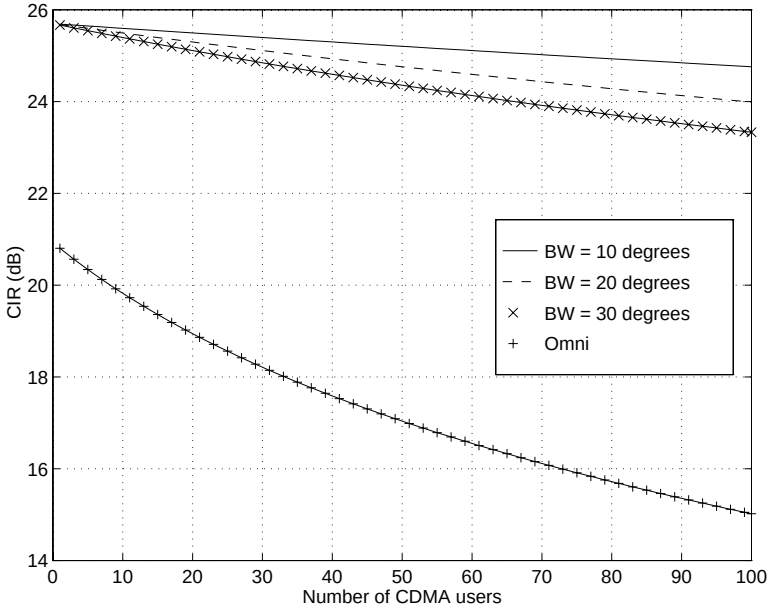

(a)

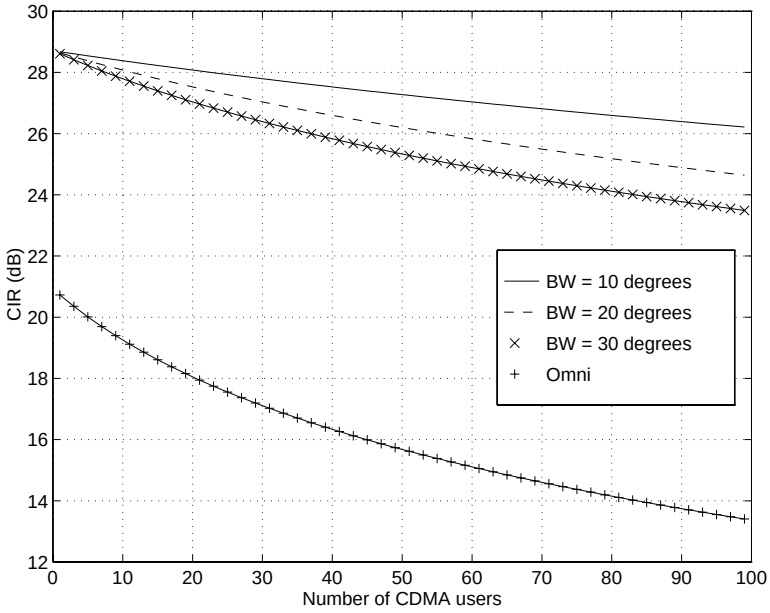

(b)

Figure 9.7: CIR plots for the AMPS signal in (a) the forward and (b) the reverse links for a power ratio of -20 dB.

9.9 Comparison of results for forward and reverse links analysis for CDMA system

The performance curves for the CDMA system are shown in Figures 9.8 and 9.9. Figure 9.8 shows the CIR curves for both the forward and the reverse link for a power ratio of 0 dB, while Figure 9.9 is for a power ratio of -5 dB. It can be seen that the forward link performs better than the reverse link, therefore the reverse link limits the capacity of the system under the worst case scenario when the desired mobile is at the edge of the cell while the other users are uniformly distributed within the cell. Comparing Figures 9.8 and 9.9, the performance of the CDMA system for a power ratio of -5 dB is worse than 0 dB, as expected. A beamformer with a beamwidth of 10° can perform 15 dB better than the omnidirectional antenna, while 20° and 30° beamformers can perform 12 dB and 10 dB better than the omnidirectional antenna, respectively.

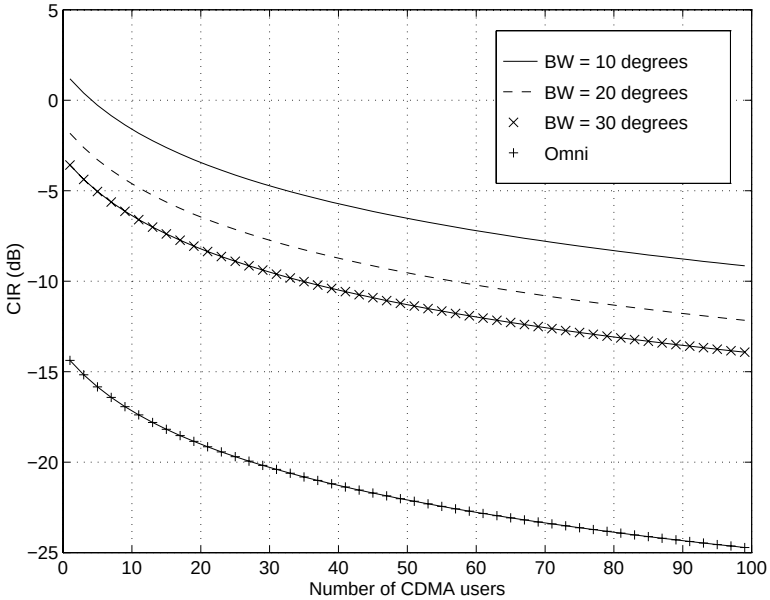

(a)

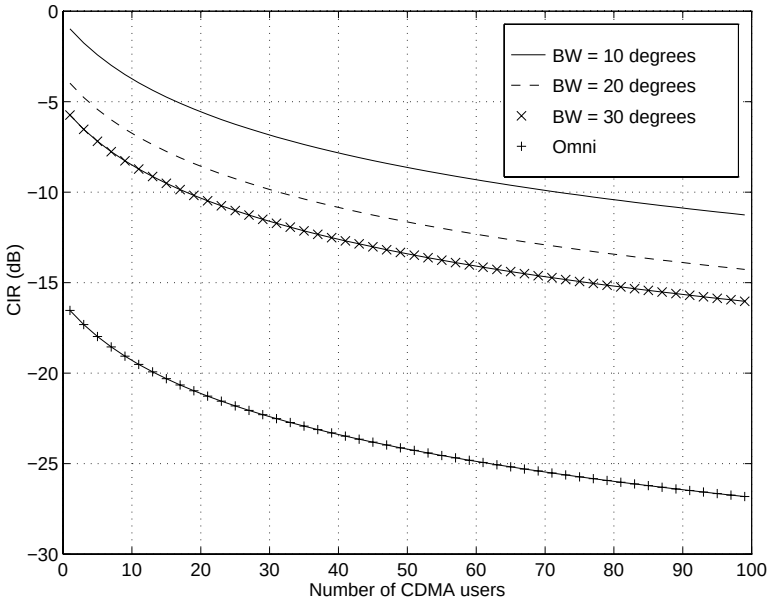

(b)

Figure 9.8: CIR plots for the CDMA signal in (a) the forward and (b) the reverse links for a power ratio of 0 dB.

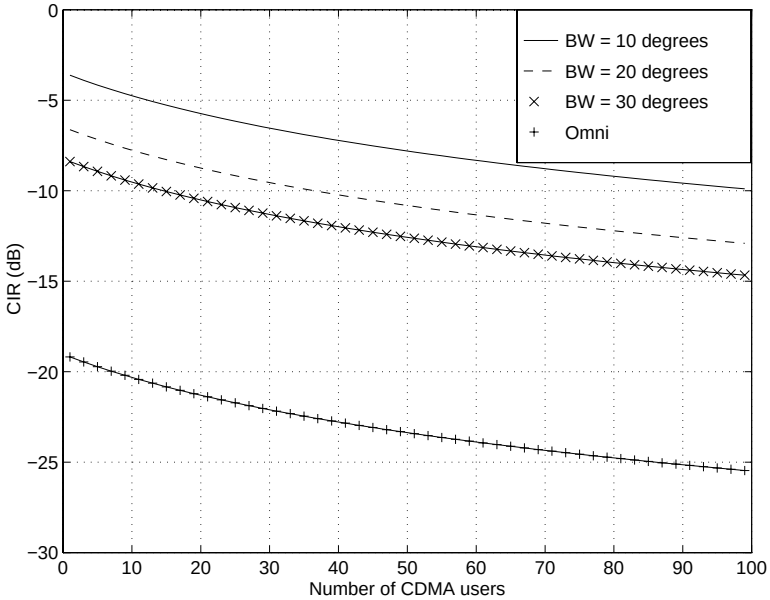

(a)

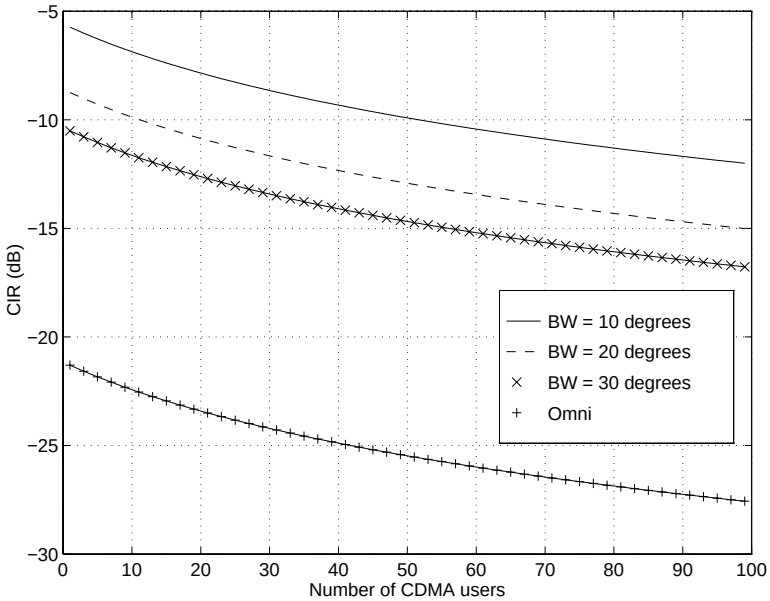

(b)

Figure 9.9: CIR plots for the CDMA signal in (a) the forward and (b) the reverse links for a power ratio of -5 dB.

9.10 Performance dependence on path loss exponent

In this section we will investigate the effect of path loss exponent on the CIR performance of the AMPS system. Let us consider 3 different path loss exponent, 2, 3, and 4. A path loss exponent of 2 corresponds to free space environment, while a path loss exponent of 3 is for urban regions, and a path loss exponent of 4 corresponds to a shadowed urban region. The analysis presented in the previous sections assumes a path loss exponent of 4. The results of the CIR performance of the AMPS system for the different path loss exponents are presented in Figures 9.10(a) and (b) for a power ratio of -10 dB and the beamwidth is set equal to 20°. The CIR performance of the beamformer is compared with an omnidirectional antenna. The effects of change in path loss exponent on both the links are dramatic. Severe degradation in the CIR performance results due to the decrease in the path loss exponent. As the path loss exponent decreases so is the propagation loss, therefore the power of the interferers are significantly higher for lower path loss exponents compared to the higher ones. In the forward link, the improvement due to the beamformer over an omnidirectional antenna is larger for $n = 4$ than $n = 3$ or $n = 2$, while the effects are reversed for the reverse link.

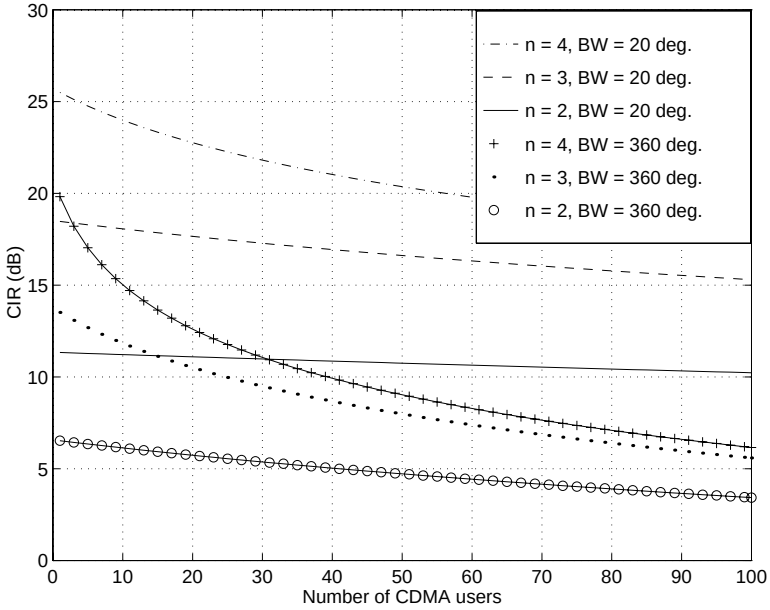

(a)

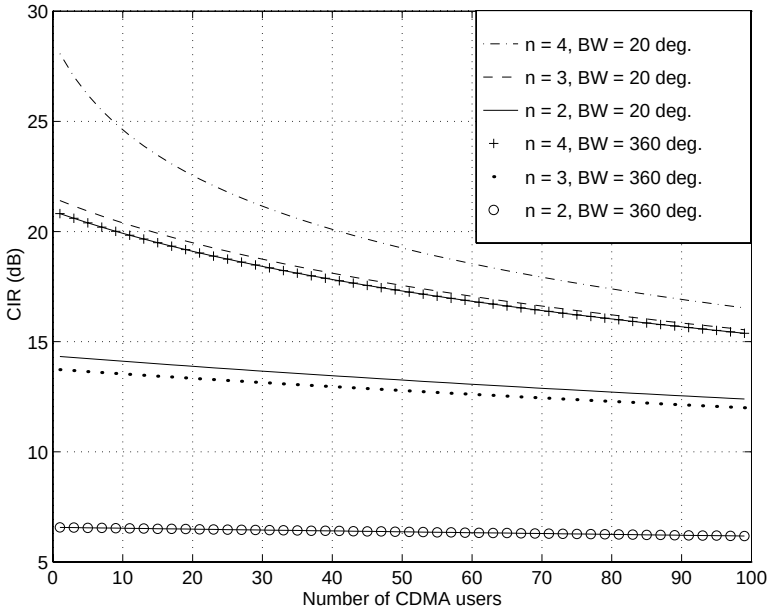

(b)

Figure 9.10: CIR plots for the AMPS signal in (a) the forward and (b) the reverse links for a power ratio of -10 dB. The beamwidth is set equal to 20° and 360°.

9.11 Conclusions

In this chapter, we have analyzed the performance of a CDMA over AMPS overlay system which employs a beamformer. The CIR performance of both the forward and the reverse links for AMPS and the CDMA systems are studied. A circular cell geometry is assumed in the analysis. Here we have presented the worst case scenario where the desired user is assumed to be at the edge of the cell. The analysis shows that the performance of both the AMPS and the CDMA systems are limited by the reverse links for the worst-case scenario. Also we have analyzed the effect of path loss exponent on the performance of the system.

Chapter 10

Novel Cellular System Exploiting Spatial Filters

10.1 Introduction

Adaptive arrays for cellular systems can significantly enhance capacity. Most of the current adaptive array efforts [7, 92, 93] involve developing adaptive algorithms to suit existing standards. Because of the constraint involved in the development of the adaptive algorithms to suit existing signal standards, adaptive arrays are not exploited to the full extent. Future cellular or wireless local loop systems should be designed to exploit adaptive arrays, because of the many advantages that can be provided by exploiting the spatial dimension. Adaptive antennas can increase the coverage range through antenna gain and interference rejection. Coverage range can be extended by a factor of $M^{1/n}$ for noise-limited environments, where M is the number of elements and n is the pass loss exponent [94]. This means that the cell size is larger and hence fewer base stations are needed to cover a given area. The interference rejection capability of the adaptive arrays can directly translate to increase in capacity by enabling system designers to reduce the reuse factor. The transmitted power by the base station and by the mobile can be significantly reduced using an antenna array. The maximum Effective Isotropic Radiated Power (EIRP) at the base station can be reduced by $10\log M$ dB over an omnidirectional antenna. Similarly the power radiated at the mobile can be reduced by at least $10\log M$ dB [94] when using adaptive arrays

at the base station.

To maximize the benefits from a base station that employs adaptive arrays, changes have to be made in the physical layer of the communication link. For example, most of the cellular systems use frequency division duplexing (FDD) and hence the forward and the reverse links' spectrum are typically separated by 45 MHz. The frequency separation between the links poses a big problem in using the weights obtained from reverse link beamforming for forward link beamforming, because of the lack of reciprocity of the channel. Techniques [95, 96, 97] have been proposed in the past to perform forward link beamforming for a FDD system. In [95], estimates of the spatial signatures of each user are used to calculate the AOA of each user and then forward link beamforming is performed. In [96], a feedback technique has been proposed. In this approach, the base station sends out a probe signal and each mobile in the cell measures its own response to the probing signal and reports back to the base station. Based on the responses, the base station derives the downlink weights.

On the other hand if time division duplexing (TDD) is employed, the weights obtained from the reverse link can be readily used for forward link beamforming. So if one has to design a new signal standard, then to exploit adaptive arrays, the standard should employ TDD. The Space/Time/Frequency Division Multiple Access (STFDMA) technique [98] is a FDMA technique designed to exploit adaptive arrays. This promising technique enhances capacity multifold compared to existing standards. The only disadvantage with this technique is it employs a 63-element circular adaptive array to achieve a capacity gain of 128 over an AMPS system.

In this chapter we introduce a new multiple access scheme called the Spatial Code Division Multiple Access (SCDMA) scheme. This scheme is designed to take maximum advantage of the adaptive arrays and CDMA. This scheme is superior than STFDMA and it can achieve capacity gains equal to STFDMA with half the number of elements. This scheme employs short spreading codes to enable the adaptive array to exploit the knowledge of the code by despreading the signal at the output of the array and use it as the reference signal. The chapter is organized as follows: Section 10.2 describes briefly the features of the STFDMA scheme. Section 10.3 discusses the new SCDMA scheme followed by the Section 10.4 which presents the BER performance

of the SCDMA system. Section 10.5 presents the comparison of capacity offered by FDMA, TDMA, CDMA, STFDMA, and SCDMA. Handoff in a SCDMA system is an important issue which is discussed in Section 10.6 and the conclusions are presented in Section 10.7.

10.2 Space/Time/Frequency Division Multiple Access (STFDMA) system

STFDMA is a multiple access technique which is a hybrid of FDMA and SDMA employing TDD [98]. STFDMA uses a circular adaptive antenna array at the base station and since it employs TDD, weights computed in the reverse link are used for the forward link beamforming. Therefore the performance of both the forward and the reverse links are comparable.

Each user occupies a bandwidth of 30 kHz and they are stacked in frequency with a carrier separation of 1 kHz. The adaptive array at the base station employs the SCORE [6] algorithm to separate users whose signals are spectrally and temporally overlapping. The STFDMA system uses 63-element adaptive array to separate signals with carrier separation of 1 kHz. STFDMA provides approximately 6 times the capacity offered by the existing IS-95 CDMA technique. The only disadvantage of the STFDMA system is the requirement for 63 elements in the circular array. A 63-element adaptive array at the base station can prove to be expensive and therefore here we propose a multiple access technique called the SCDMA, which is a hybrid of SDMA and CDMA. SCDMA can achieve the same capacity gain as STFDMA with half the number of array elements.

10.3 Spatial Code Division Multiple Access (SCDMA) system

SCDMA is a deterministic CDMA [74] system which employs uniformly spaced linear adaptive arrays (ULA). The configuration of the array is shown in Figure 10.1. The

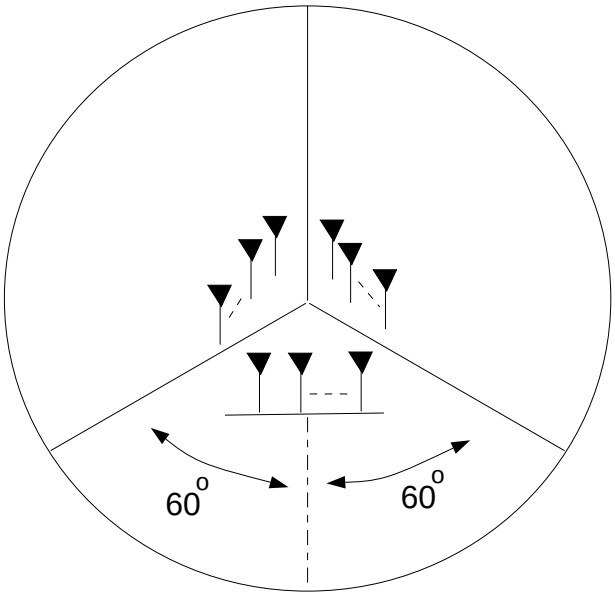

Figure 10.1: Figure illustrating the configuration of adaptive arrays in a SCDMA system.

base station employs a three-sectored configuration[1] where each sector has an M-element uniform linear array (ULA), and so the system as a whole uses $T = 3M$ array elements. This technique uses 120 degrees sectorized antennas in addition to the ULA, because the sectorized antennas are useful for handoff purposes.

The SCDMA system employs TDD and is illustrated in Figure 10.2. The duration of the frame from base to mobile and back is 2.5 ms, and the time frames are separated by a guard time of 5μs. In a time frame of 2.5 ms, 600 chips (or 40 bits) are transmitted. A TDD duplexing technique is adopted to allow beamforming on the forward link using the conjugate of the weights obtained from the reverse link beamforming. This assures that both the forward and the reverse links provide comparable BER performance. A frame length of 2.5 ms is chosen so that the channel will be stationary in fading with a Doppler frequency as high as 200 Hz. For a Doppler frequency of 200 Hz, the channel appears stationary for a duration of 5 ms and hence the weights obtained from the reverse link can be used for forward link beamforming.

[1]Three sectored approach is used at the base station because, SCDMA can be easily implemented if it has to be overlayed over existing AMPS or TDMA system.

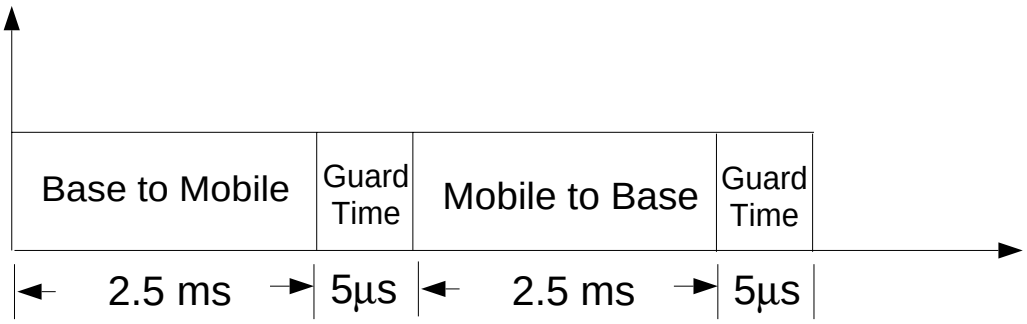

Figure 10.2: Figure illustrating time division duplex (TDD) in a SCDMA system.

The SCDMA technique uses a reuse factor of 1 and typically the multiple access interference from outside the cell is approximately half the multiple access interference from within the cell (the ratio is called the *spillover ratio*) [99, 100].

The SCDMA system assumes a vocoder rate of 8 kbps. The SCDMA system uses a short spreading code of length 15 and uses code-on-pulse modulation. But since TDD is adopted, the actual channel rate has to be 16 kbps. Therefore the chip rate is $16 \times 15 = 240$ kcps. SCDMA employs BPSK modulation and therefore the null-to-null bandwidth of the SCDMA signal is 480 kHz. Figure 10.3 shows the spectrum allocation of the signals in a SCDMA technique. There are N users occupying the same frequency band each with a random spreading code of length 15. The value of N depends on the number of array elements used, because the number of elements is going to decide the width of the beam and hence the interference rejection capability of the array. We investigate this issue in Section 10.4.

The adaptive array used at the base station is a Least Squares Despread Respread Multi-target Adaptive Array (LSDRMTA) introduced in Chapter 7. The salient features of SCDMA are as follows:

- TDD enables forward and reverse link beamforming and hence achieve superior performance as compared to a Frequency Division Duplex (FDD) scheme.

- A short spreading code is used for two reasons. The first reason is, a matched filter can be used to despread the CDMA signal and hence LS-DRMTCMA can be easily implemented. The second reason is, synchronization can be achieved

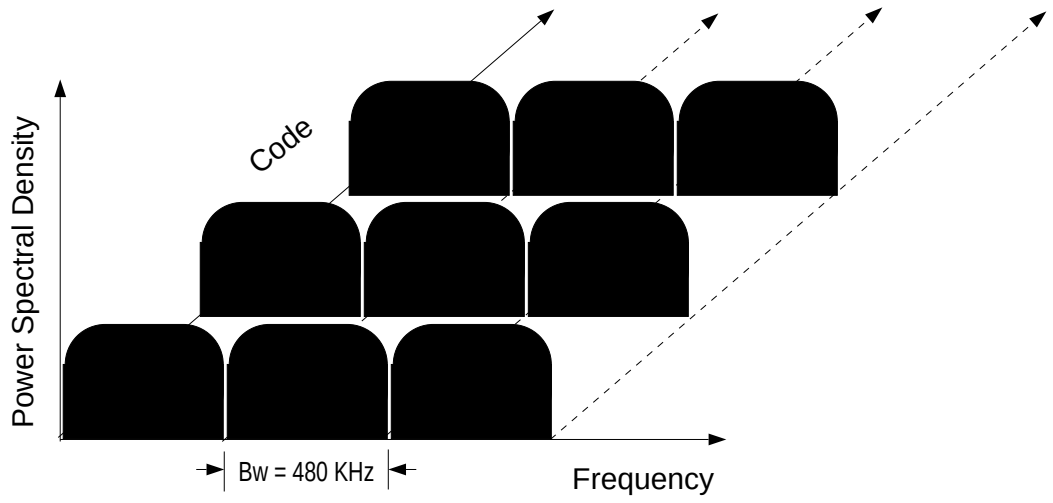

Figure 10.3: Figure illustrating the spectrum allocation in a SCDMA system.

using a fixed matched filter approach.

- SCDMA combines the best features of SDMA and CDMA.
- The main advantage of SCDMA scheme is to exploit FDMA to certain extent in addition to the CDMA features. In the SCDMA scheme if there are users not spatially separated, then the users in the beam can be dynamically allocated to a different channel and hence can significantly reduce the multiple access interference.

10.4 Performance of the SCDMA system

In this section, we analyze the BER performance of the SCDMA technique and the number of users it can support in a bandwidth of 480 kHz. In the performance evaluation of the ULA, only one sector is considered and the users are uniformly placed within an angular region bounded by $+60°$ and $-60°$ with respect to the broadside of the array. The ratio of mean bit-energy to noise density (E_b/N_o) is maintained at 12 dB and the number of simultaneous users is varied from 2 to 60. The performance of the adaptive array which employs LSDRMTCMA is evaluated

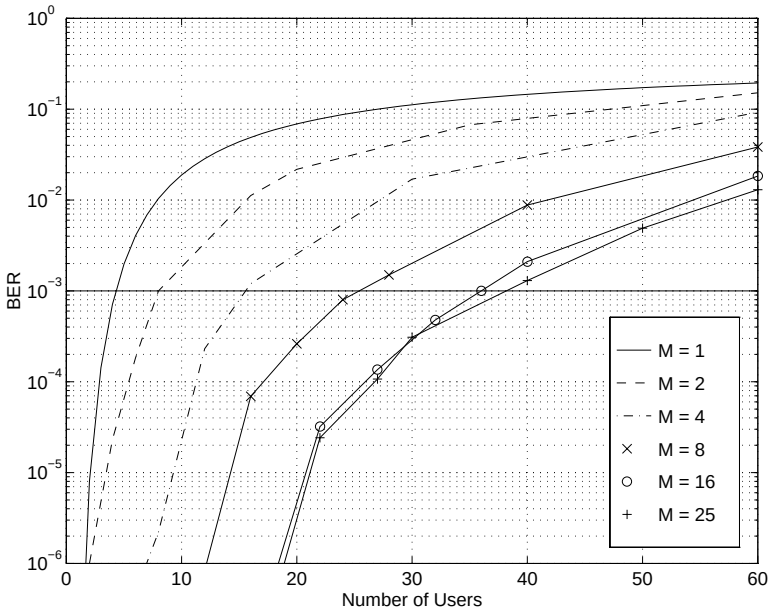

Figure 10.4: Bit error rate curves for LS-DRMTCMA array is compared with an omnidirectional antenna and the users are located uniformly within a sector of -60 to 60 degrees with respect to the broadside of the array.

using Monte Carlo simulations. The array is adapted for 10,000 bits using the blind algorithm and after convergence the weights are kept fixed for the BER calculation. In these simulations, the chip is sampled four times and the users are assumed to be asynchronous. The PN sequences used are random sequences, delays and carrier phases are randomly attributed to each user. The delays, carrier phases, and the PN codes of each user are changed frequently to estimate the average BER. The LSDRMTCMA uses a block size of 60, equal to the number of samples per bit. Also all the users are assumed to have equal power.

The performance of the array with 2, 4, 8, 16, and 25 elements is compared with a conventional receiver ($M = 1$). Figure 10.4 is a plot of BER curves for different number of array elements as a function of number of users. If the acceptable BER $= 10^{-3}$, then the number of users that can be accommodated in the system is plotted as a function of number of elements/sector in Figure 10.5. The number of users that can be accommodated in a sector increases almost linearly as the number of array elements increase from 2 to 10 and then curves for higher number of elements. .

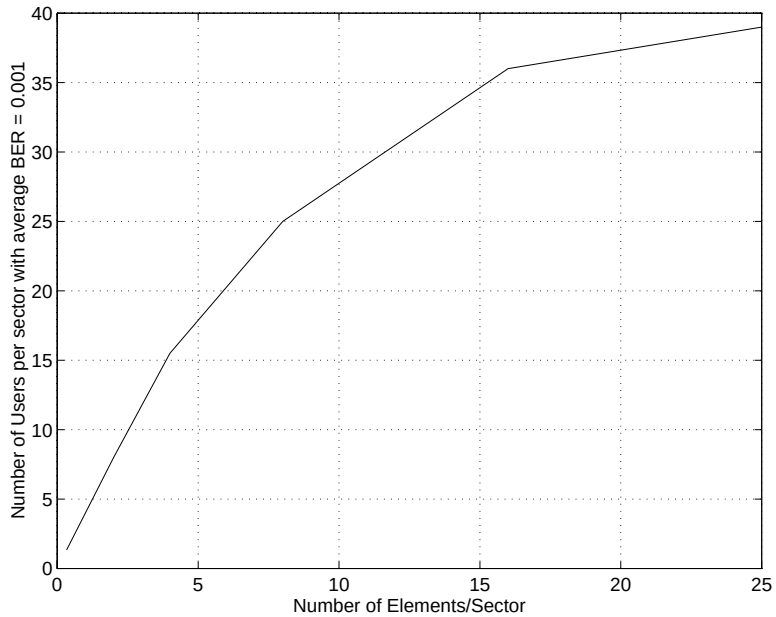

Figure 10.5: Figure showing the number of active users that can be accommodated in a sector with a BER of 10^{-3} as a function of number of elements per sector. The channel bandwidth is 480 kHz.

10.5 Capacity calculations

In this section, we will compare the capacity offered by SCDMA with FDMA, TDMA, CDMA, and STFDMA. For all the calculations we will assume the total available bandwidth to be 1.25 MHz and all capacity figures are in terms of number of users that can be supported in a bandwidth of 1.25 MHz.

• FDMA

An FM-FDMA system like AMPS uses a bandwidth of 30 kHz and a reuse factor of 7. FDMA/FDD systems use 2 channels of 30 kHz bandwidth to complete a communication loop. The number of users/cell in a FM-FDMA system is given by

$$\text{Number of users/cell} = \frac{B_t}{r \times B_{ch} \times 2}$$

where

B_t - Total available bandwidth

r - reuse factor

B_{ch} - Channel bandwidth

Example:

Let us consider $B_t = 1.25$ MHz, $B_{ch} = 30$ kHz, and $r = 7$. The number of users/cell that can be supported by the FDMA system is 3.

• TDMA

A TDMA system like IS-136 system uses a reuse factor of 7 and a channel bandwidth of 30 kHz. Three users share a bandwidth of 30 kHz and the capacity in a TDMA system is given by

$$\text{Number of users/cell} = \frac{B_t}{r \times B_{ch} \times 2} \times N_u$$

where N_u is the number of users sharing the 30 kHz bandwidth.

Example:

Let us consider $B_t = 1.25$ MHz, $B_{ch} = 30$ kHz, $N_u = 3$, and $r = 7$. A TDMA system can support 9 users per cell.

• CDMA

For a CDMA system like IS-95 system, the channel bandwidth is 1.25 MHz and uses 120 degrees sectorized antennas. A reuse factor of 1 is employed and the capacity of a CDMA is system is given by [101]

$$\text{Number of users/cell} = \frac{m \times B_t}{r \times B_{ch} \times 2 \times v_f} \times G_s$$

where

m - number of channels/cell

v_f - voice activity factor

G_s - gain due to sectorization.

Example:

Let us consider B_t = 1.25 MHz, B_{ch} = 1.25 MHz, $r = 1$, $m = 13$, $v_f = 3/8$, and $G_s = 3$. A CDMA system can support 52 users per cell.

• STFDMA

The capacity of STFDMA is dependent on the frequency separation between the channels. The frequency separation decides the number of elements required in the adaptive array. The capacity of a STFDMA system is given by [98]

$$\text{Number of users/cell} = \frac{(B_t/r - B_{ch})}{f_{sep}} + 1$$

where f_{sep} is the frequency separation between the channels. The number of antenna elements (T) required to separate the users is lower bounded by the number of users (K), and $T > K = 2(B_{ch}/f_{sep} - 1)$.

Example:

Let us consider B_t = 1.25 MHz, B_{ch} = 32 kHz, $r = 3$, and f_{sep} = 1 kHz. The STFDMA system can support 385 users/cell and it employs a 64 element array.

• SCDMA

Let us calculate the capacity in terms of number of users/cell for a SCDMA system which employs 8-element ULA per sector. Each CDMA signal in a SCDMA technique occupies a bandwidth of 480 kHz. From Section 10.4, we can find out the number of users an M-element ULA can support and maintain an average BER of 10^{-3} in a sector. In a typical CDMA system with reuse factor of 1, if we neglect background noise, the total interference in the system is given by

$$\begin{aligned} I &= \text{MAI}_{\text{in-cell}} + \text{MAI}_{\text{out-of-cell}} \\ &= \text{MAI}_{\text{in-cell}}(1 + f) \end{aligned}$$

where $\text{MAI}_{\text{in-cell}}$ is the multiple access interference (MAI) within the cell, $\text{MAI}_{\text{out-of-cell}}$ is the MAI outside the cell, and f is called the *spillover ratio*, which is the ratio of

out-of-cell MAI to in-cell MAI. The total number of users in a SCDMA system is then given by

$$\text{Number of users/cell} = N \times \frac{B_t}{r \times B_{ch}} \times \frac{N_s}{v_f} \times \frac{1}{1+f}$$

where

N - number of users per sector supported by an M-element ULA

B_t - total available bandwidth

r - reuse factor

B_{ch} - channel bandwidth

N_s - number of sectors per cell

v_f - voice activity factor

f - spillover ratio.

Example:

Let us consider $B_t = 1.25$ MHz, $B_{ch} = 480$ kHz, and $N_s = 3$. The SCDMA system uses a reuse factor of 1. If an 8-element ULA is used in a sector, the array can support 25 equal-powered users (N) at $E_b/N_o = 12$dB. In typical cellular systems, extensive studies [102] have shown that the voice activity factor is 3/8, and $f = 0.55$ [100]. Therefore a SCDMA system which employs 24 elements (8 elements/sector) can support 335 users in a cell.

Table 10.1 summarizes the capacity that can be offered by all the different multiple access techniques. It can be seen that the SCDMA is more spectrally efficient than STFDMA and other existing systems. SCDMA can provide the same capacity (385 users/cell) as STFDMA, but SCDMA uses only half the number of array elements required by STFDMA. SCDMA can provide an increase of 30% capacity over

Table 10.1: Comparison of capacity of different multiple access techniques

System	FDMA	TDMA	CDMA	STFDMA	SCDMA	
				T = 64	T = 30	T = 64
Number of users/cell	3	9	52	385	385	513
Relative efficiency	1	3	17	128	128	171

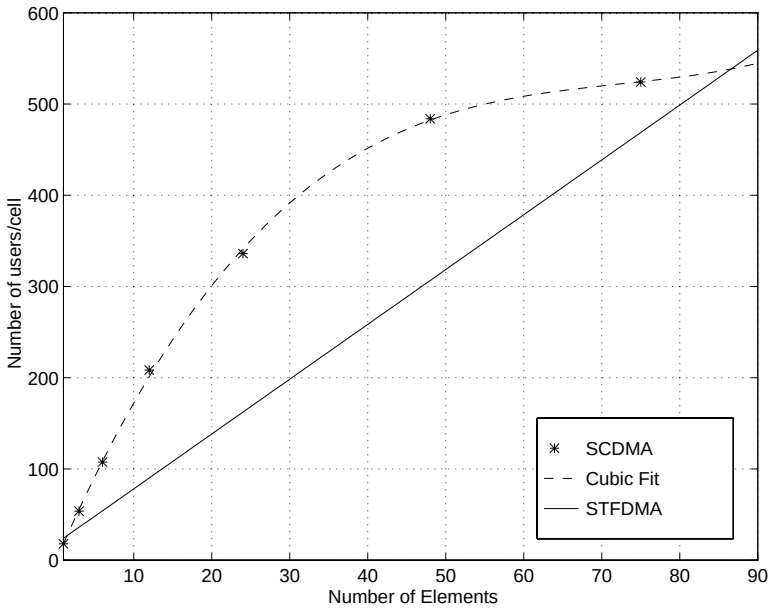

Figure 10.6: Figure comparing the number of users that can be accommodated in a cell by the SCDMA system, the cubic fit, and the STFDMA system. In this calculation, voice activity factor of 3/8 is assumed and spillover factor = 0.55.

STFDMA if both the systems use 64 elements. Figure 10.6 is a comparison plot of the capacity that is offered by the SCDMA and the STFDMA system as a function of number of array elements. The star marks in the plot are true capacity offered by the SCDMA system and the dashed line is a cubic fit to the true capacity values. Figure 10.7 is a plot that shows the ratio of the capacity offered by a SCDMA system to the capacity offered by a STFDMA system as a function of number of array elements obtained using the cubic fit. Due to space and the cost limitations at the base station, commercial systems may use typically use around 8 array elements per sector. It can be seen from Figure 10.7 that the SCDMA is spectrally more efficient than STFDMA for systems with number of array elements between 2 and 85.

Due to space and the cost limitations at the base station, commercial systems may use around 10 array elements per sector. It can be seen from Figure 10.7 that the SCDMA is spectrally efficient than STFDMA for antenna arrays which are feasible for commercial systems.

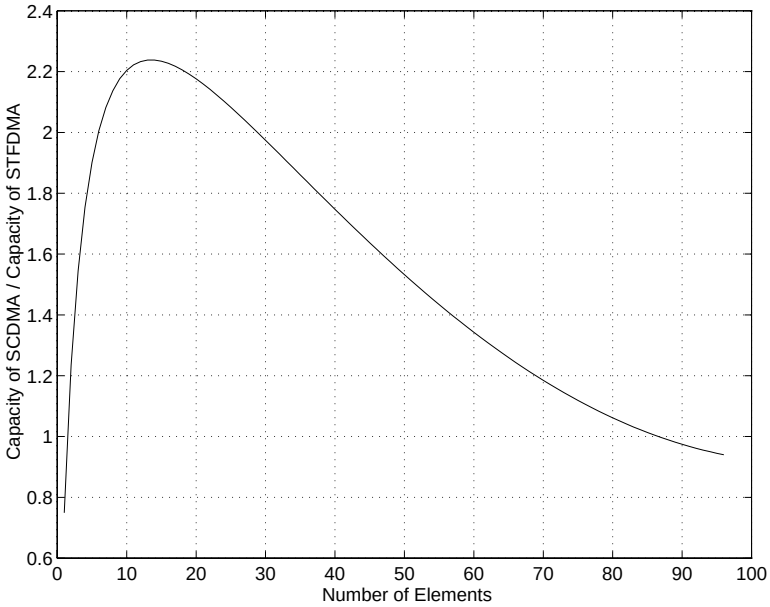

Figure 10.7: Plot showing the improvement in capacity that can be achieved by the SCDMA system over the STFDMA system as a function of number of elements.

10.6 Handoff in a SCDMA system

Handoff is an important issue when an adaptive array is employed at the base station of a cell. In a CDMA system cellular system since the reuse factor is 1, the mobile unit may not have to switch frequencies when being handed-off from one base station to the other. The SCDMA system employs a combination of base station and mobile assisted soft handoff.

10.6.1 Base station and mobile assisted soft handoff (BMSHO)

In a system which employs a sectorized antennas, there are two types of soft handoffs: intercell and intracell handoffs. Intracell handoff is the handoff from one sector to the other in the same cell, while the intercell handoff is the handoff between cells. Here we use two measures to effectively carry out handoff. The first measure is the strength of the base station signal, α, at the mobile, and the second one is the estimate of the angle-of-arrival (AOA), β, of the signal from the mobile. The value of α gives an idea of the distance between the base station and the mobile. The AOA, β, can be

estimated from the spatial signatures obtained from the beamformer.

In the BMSHO, the base station instructs the mobile to monitor which cell site/sector based on the AOA information. The base stations are identified by their pilot carriers, each base station transmits pilot carriers with different spread spectrum code phase offset. Therefore when a call is initiated, the mobile does not have to monitor all the pilot carriers from neighboring cells, but only those specified by the cell site it is communicating with. If the signal strength from a neighboring cell/sector is above a certain threshold T, then the mobile combines signals from multiple sectors/base stations using maximum ratio combining [103]. The mobile maintains connection with the old base station until the signal from the old base station is below a certain value specified by $T - \delta$, where δ is the hysteresis region. This is also true for the reverse link.

10.6.2 Intracell and intracell soft handoffs

Figure 10.8 illustrates the intracell handoff between sectors marked A_1 and A_2, while Figure 10.9 illustrates the intercell handoff between sectors marked A_1 and C_1. In the intracell handoff, the mobile monitors signals from a different sector and from different cells, while in the intercell handoff, it monitors only different base stations as instructed by the current base station it is communicating with.

In an intracell handoff, soft handoff between sectors is called *softer handoff* [104]. If the value of $|\beta| > 50^o$, then the base station instructs the mobile to not only monitor the closest base stations but also the closest sector. The base station knows which sector the mobile has to be monitor from the β value. In an intercell handoff, as shown in Figure 10.9, if $10^o \leq |\beta| \leq 50^o$ (i.e., in the shaded region) then the base station A_1 instructs the mobile (M) to monitor the code phase of the base station C_1 or B_1 and sense if the power from the base station is above a certain threshold to decide if it is within the coverage area of the new cell. Once the mobile detects the new cell site signal to be strong, intercell soft handoff occurs with the help of the systems controller. If $-10^o \leq \beta \leq 10^o$, then the base station A_1 instructs the mobile to monitor the code phase corresponding to the base stations B_1 and C_1 and then use signals from three different cell sites. Thus handoff in a SCDMA system makes use

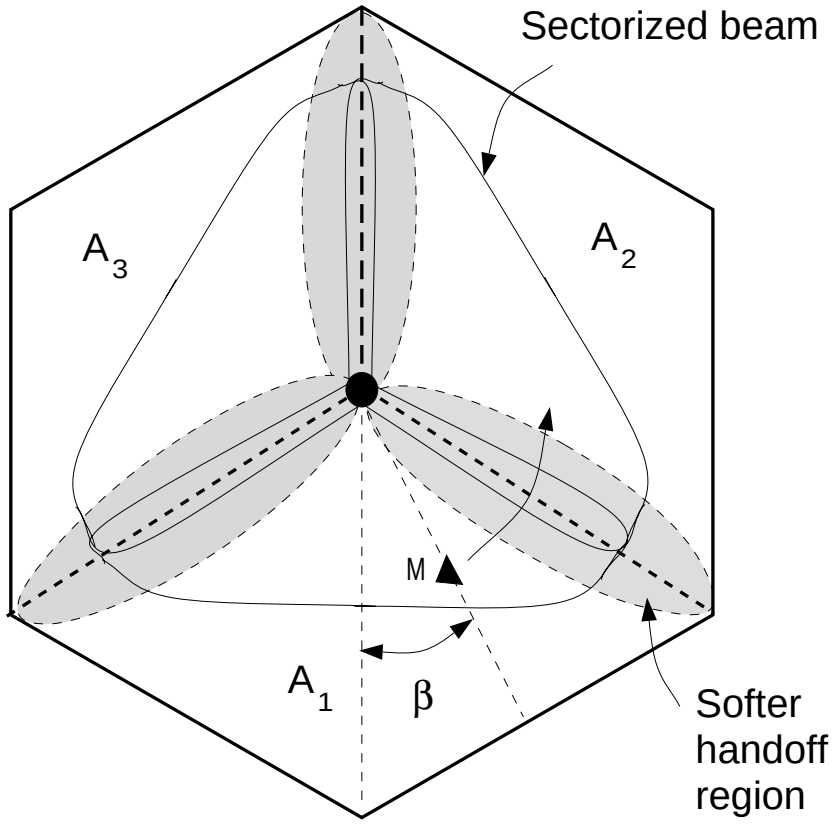

Figure 10.8: Figure illustrating the intracell handoff between one sector and the other. A_1, A_2, and A_3 are the three sectors, M is the mobile, and β is the angle between the signal from the mobile and the broadside of the array.

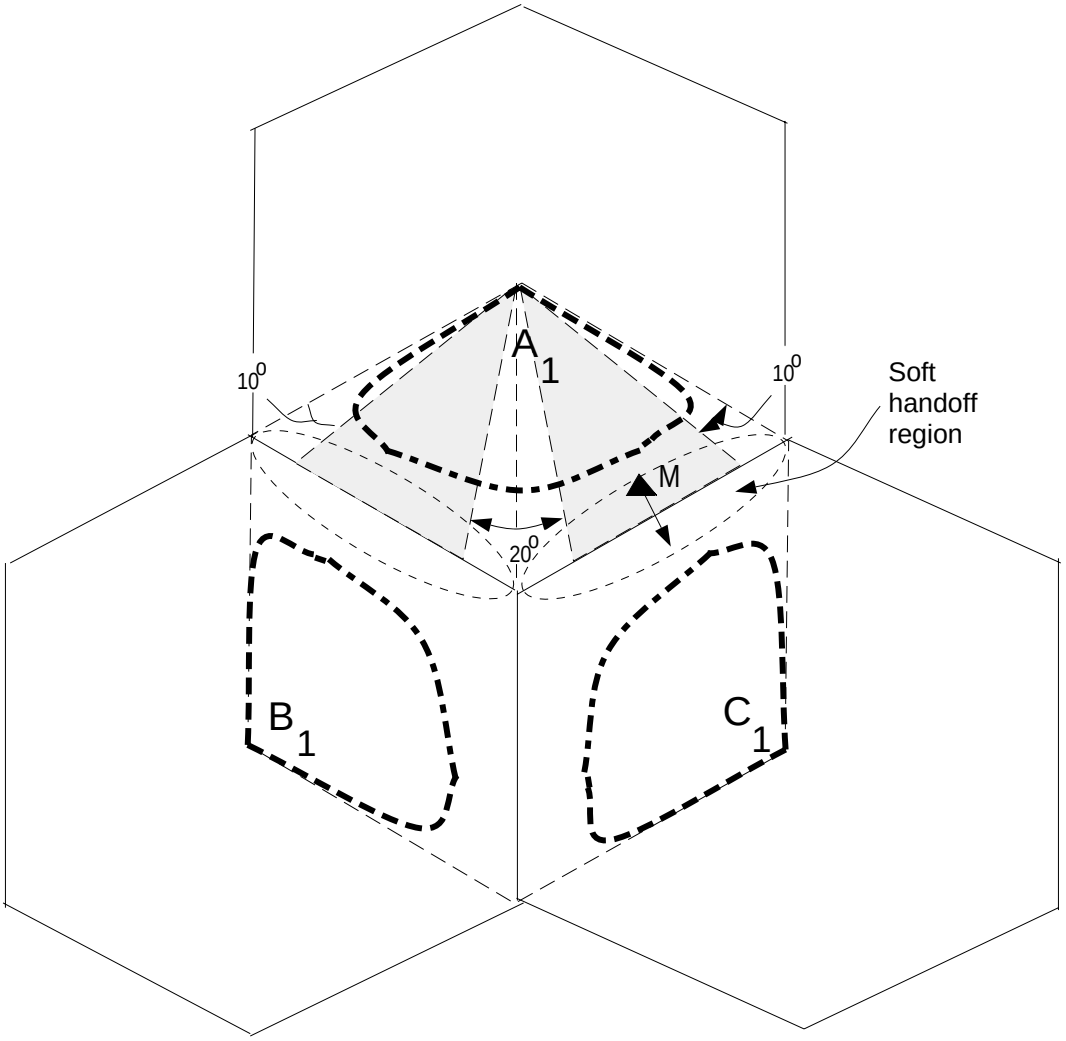

Figure 10.9: Figure illustrates the intercell handoff. If mobile is in the shadowed region then the mobile unit (M) has to measure power only from two base stations (A_1 and C_1), otherwise it will measure signal power from three base stations.

of the knowledge of the AOA in reducing the number of base stations the mobile has to monitor. By reducing the number of base stations to be monitored, the new call blocking probability and the amount of interference can be reduced. In practice, the cells are not hexagonal but the knowledge of the locations of the base stations can be used to reduce the number of base stations to be monitored.

10.6.3 Estimation of AOA from the beamformer weights

To estimate the AOA of the signal from the mobile, we need to estimate the spatial signatures of each user and then apply a combination of smoothing and subspace techniques to estimate the AOA of each user. The multi-target array driven by LS-DRMTCMA separates each user's signal and they appear as the output of each port. Since the base station has the knowledge of all the PN codes of all the users, it can easily estimate the number of users in the system by using a bank of correlators or matched filters. Let us assume that there are N users in the system and M elements in the array. Let x be the input and y be the output of the array. Once the array weights have converged, the spatial signatures of each user can be estimated as follows:

$$\begin{aligned} \hat{\mathbf{A}} &= \hat{\mathbf{R}}_{xy}\hat{\mathbf{R}}_{yy}^{-1} \\ &= \hat{\mathbf{R}}_{xx}\mathbf{W}(\mathbf{W}^H\hat{\mathbf{R}}_{xx}\mathbf{W})^{-1} \end{aligned} \tag{10.1}$$

where $\hat{\mathbf{A}}$ is a $(M \times N)$ matrix which contains the estimate of the spatial signature of all users, $\mathbf{W}$ is a $(M \times N)$ weight matrix, $\hat{\mathbf{R}}_{xx}$ is the estimate of the input correlation matrix, and $\hat{\mathbf{R}}_{xy}$ is the estimate of the cross-correlation matrix.

As proposed in [95], the AOA of the direct and the multipath components can be estimated by a combination of forward/backward smoothing technique and subspace technique. The following are the steps involved in the estimation of the AOA of multipath components of user j from the spatial signature matrix.

1. Construct the spatial signatures of user j from Eqn. 10.1.

2. Apply the standard forward/backward smoothing techniques [105] to spatial signatures to obtain a smoothed spatial signature covariance matrix

$$\mathbf{R}_{fb}(K) = \mathbf{R}_f(K) + \mathbf{J}\mathbf{R}_f^*(K)\mathbf{J}$$

where $\mathbf{J}$ is the permutation matrix with all zeros except ones in the anti-diagonal elements, K is the smoothing factor (number of subarrays) and

$$\mathbf{R}_f(K) = \sum_{i=1}^{K} (\hat{\mathbf{a}}(i : M - K + i)\hat{\mathbf{a}}(i : M - K + i)^H)$$

where $\hat{\mathbf{a}}$ is the spatial signature vector for user j, which is the jth column of $\hat{\mathbf{A}}$.

3. Now apply MUSIC [106] or ESPRIT [107] on the smoothed spatial signature covariance matrix to estimate the AOA of the multipath components.

The method described above is one method to estimate the AOA, other methods do exist. The information about the AOA of the mobile user can also be used for locating the positions of the mobile within the cell to track E-911 calls and other services. The estimate of the AOA of the user can be combined with time difference of arrival (TDOA) techniques to effectively estimate the position of the mobile.

10.7 Conclusions

In this chapter, a novel cellular system called Spatial Code Division Multiple Access (SCDMA), that exploits spatial and code division multiple access, is presented. SCDMA employs time division duplexing and hence forward and reverse link beamforming are feasible. This enables the system to provide comparable performance both in the forward and the reverse link. The capacity offered by SCDMA is compared with the STFDMA system introduced in [98], and was found to provide at least 100% more capacity than STFDMA if the number of elements is between 8 and 30. Handoff issues in an SCDMA system has been analyzed and techniques for handling inter and intra-cell handoff have been introduced.

Chapter 11

Conclusions and Future Work

This research has focused on the application of adaptive arrays for the current AMPS and the future CDMA cellular systems. The following are the reasons why AMPS system is considered in this research. AMPS system is expected to survive at least another 5 to 10 years and the cellular companies[1] are interested in increasing the capacity and hence resort to adaptive arrays. Also, AMPS system is able to provide good speech quality and hence it can survive for years to come in North America. CDMA is also considered in this research because CDMA is projected as the multiple access technique for future cellular and PCS systems.

11.1 Summary of the work

In this dissertation, new adaptive array algorithms have been developed and analyzed for both AMPS and CDMA systems. Capacity improvement offered by employing a beamformer at the base station is addressed in this research. The contributions in this research are listed below in the same order as they were presented in this report. Chapter 3 proposes and analyzes a new method of adaptive beamforming for AMPS signals which exploits the cyclostationary nature of the desired signal created by the supervisory audio tone (SAT) in the AMPS signal. The basic idea behind this beamformer is derived from the least-squares SCORE. This array exploits spatial,

[1] ArrayComm, Nortel, Bell Atlantic, Bell South, Airtouch, Southwestern Bell, Motorola and many more wireless companies are developing adaptive arrays for the current wireless systems.

temporal and spectral diversities to separate the SOI from the SNOI. This beamformer has a tapped delay line following each array element, and it shapes the input signal to enhance the SOI components and reduce the SNOI components. The mean squared error analysis of the SCDA is presented in this Chapter and the performance of the SCDA algorithm is evaluated using simulations. The SCDA is able to provide improvements in SINR of typically 15-25 dB in static multipath environments.

The focus of Chapter 4 is evaluation of the outage probability due to cochannel interference for the existing AMPS cellular system when a beamformer is employed. Two beamformers are considered in this research, an ideal and a flat-top beamformer. The performance of the beamformers is compared with the performance obtained using an omnidirectional antenna. In this Chapter, we characterize the angle-of-arrival (AOA) of a cochannel interferer at the base station of the desired cell. Outage calculation for an ideal beamformer and a flat-top beamformer are discussed. Numerical results for improvement in outage probability based on exploiting spatial dimension are presented. Chapter 5 uses the analysis presented in Chapter 4 to come up with the actual number of elements required in an array to achieve reuse factors lesser than 7. The analysis shows that a reuse of 4 can be achieved by a 5 element ULA with inter-element spacings of $\lambda/2$ and a reuse factor of 3 with an 8 element array.

In Chapter 6, we developed a statistical channel model for macrocells called the Geometrically Based Single Bounce Macrocell (GBSBM) channel model that assumes that the multipath reflection is caused by scatterers which are located closer to the mobile. The GBSBM model assumes that the plane waves reaching the base station travel horizontally and then it calculates the probability density function of the AOA of the multipath components along the azimuth. The effect of directional antennas at the base station on the Doppler spectrum is investigated and the results show that the Doppler spread reduces as the beamwidth of the antenna is decreased. Using the model, we can predict the Doppler frequency components if the direction of motion of the mobile, the velocity of the mobile, and the radius of the scattering circle are known. This is one of the first AOA models which combines the knowledge of the geometric structure of the multipath environment and the statistical aspect of the fading channel.

Chapter 7 discussed the development of blind adaptive array algorithms for CDMA that exploit the knowledge of the code and the constant modulus property of the CDMA signal. Two new algorithms, the least squares despread respread multi-target and the least squares despread respread multitarget constant modulus arrays, are introduced in this Chapter 7. Simulation results show that these two algorithms perform better than the constant modulus and the decision directed algorithms under all channel and receiver impairments.

In Chapter 8, the issues involved in implementing an adaptive array are investigated. As mentioned earlier, the goal is to build an 8-element adaptive array operating at a carrier frequency of 2.05 GHz. We have investigated the DSP hardware suitable for the application. The issues involved in the implementation of the adaptive array algorithms on the DSP are addressed in Chapter 8. A baseband version of the multi-target constant modulus adaptive array has been implemented on the Analog Devices ADSP-21020 platform.

In Chapter 9, we analyzed the forward and reverse link performance of both AMPS and the CDMA systems when an ideal beamformer is employed at the base station, assuming both reverse and forward link beamforming are achievable. A concentric cellular geometry is assumed for the link analysis. Both forward and reverse link analysis are presented for both AMPS and CDMA systems. Here we have presented the worst case scenario where the desired user is assumed to be at the edge of the cell. The analysis shows that the performance of both the AMPS and the CDMA systems are limited by the reverse links.

In Chapter 10, we introduced a new multiple access scheme called the Spatial Code Division Multiple Access (SCDMA) scheme. This scheme is designed to take maximum advantage of the adaptive arrays and CDMA. This scheme is superior than Space/Time/Frequency Division Multiple Access (STFDMA), introduced in [42], and it can achieve capacity gains equal to STFDMA with half the number of elements. This scheme employs short spreading codes to enable the adaptive array to exploit the knowledge of the code by despreading the signal at the output of the array and use it as the reference signal. Handoff in a SCDMA system is an important issue which is addressed in this Chapter. This system is based on a cellular concept and

can be applied to wireless local loop systems.

11.2 Future Work

Topics that can be explored in future are listed below:

1. The Geometrically Based Statistical Single Bounce Macrocell (GBSBM) channel model, introduced in Chapter 5, assumes that the scatterers are restricted to be within a circle. The model can be extended to include scatterers outside the circle. For example, we can assume the scatterers to be located uniformly within a circle and an exponentially decaying distribution for scatterers outside the circle.

2. The next logical step is the validation of channel model. The adaptive array under development will lend itself well to this segment of research. Using the array, we can collect data and validate the channel model. If site-specific information is known about a certain area, the area can be characterized in terms of the parameters of the model and predictions can be made. The predictions about the channel can be compared to the actual measurements.

3. The knowledge of the channel statistics, i.e., the AOA statistics, can be used in the development of Maximum Likelihood (ML) based algorithms. The algorithm can make use of the channel statistics in its adaptation criterion and in the rate of adaptation needed to combat the channel impairments.

4. On the implementation side, the baseband array implemented on ADSP-21020 employs a Constant Modulus Algorithm. Future work can involve testing the Despread Respread (DR) algorithms introduced in Chapter 7. The DR algorithms require synchronization to be performed prior to beamforming.

Bibliography

[1] W. L. Stutzman and G. A. Thiele, *Antenna Theory and Design.* John Wiley & Sons, New York, 1981.

[2] F. R. Hampel, E. M. Ronchetti, P. J.Rousseeuw, and W. A. Stahel, *Robust Statistics: The Approach Based on Influence Functions.* John Wiley & Sons, New York, 1986.

[3] S. Haykin, *Adaptive Filter Theory.* Prentice Hall, 2 ed., 1986.

[4] R. Gooch and J. Lundell, "The CM array: An adaptive beamformer for consant modulus signals," in *Proc. of ICASSP '86*, pp. 2523–2526, April 1986. Tokyo, Japan.

[5] B. G. Agee, "Blind separation and capture of communication signals using a multitarget constant modulus beamformer," in *Proc. MILCOM*, pp. 340–346, May 1989.

[6] B. G. Agee, S. V. Schell, and W. A. Gardner, "Spectral self-coherence restoral: A new approach to blind adaptive signal extraction," in *Proc. IEEE*, vol. 78, pp. 753–767, April 1990.

[7] P. Petrus and J. H. Reed, "AMPS cochannel interference rejection using spectral correlation properties and an adaptive array," in *Proc. of IEEE Veh. Tech. Conference*, vol. 1, pp. 300-305, July 1995.

[8] P. Petrus and J. H. Reed, "Time dependent adaptive arrays," in *IEEE Signal Processing Letters*, pp. 219–222, Dec. 1995.

[9] W. A. Gardner, *Cyclostationarity in communications and signal processing.* IEEE Press, 1 ed., 1994.

[10] D. Gerlach, "Base station array receivers in cellular CDMA," in *Proc. of IEEE Asilomar Conf.*, pp. 646–650, 1992.

[11] B. H. Khalaj, A. Paulraj, and T. Kailath, "2D RAKE receiver for CDMA cellular systems," in *Proc. of IEEE Globecom Conf.*, pp. 400–404, 1994.

[12] B. Suard, A. F. Naguib, G. Xu, and A. Paulraj, "Performance of CDMA mobile communication systems using antenna arrays," in *Proc. of IEEE Int. Conf. Acoust., Speech, Signal Proc.*, vol. 4, pp. 153–156, 1993.

[13] A. F. Naguib, A. Paulraj, and T. Kailath, "Capacity improvement of base-station antenna arrays cellular CDMA," in *Proc. of IEEE Asilomar Conf.*, pp. 1437–1441, 1993.

[14] A. F. Naguib and A. Paulraj, "Effects of multipath and base-station antenna arrays on uplink capacity of cellular CDMA," in *Proc. of IEEE Globecom Conf.*, pp. 395–399, 1994.

[15] B. Widrow et al., "Adaptive antenna systems," in *Proc. of IEEE*, vol. 55, pp. 2143–2159, Dec. 1967.

[16] Y. Sato, "A method of self-recovering equalization for multilevel amplitude-modulation systems," in *IEEE Trans. Comm.*, pp. 679–682, June 1975.

[17] D. M. Godard, "Self-recovering equalization and carrier tracking in two-dimensional data communication," in *IEEE Trans. Comm.*, vol. 28(11), pp. 1867–1875, Nov. 1980.

[18] J. R. Treichler and B. G. Agee, "A new approach to multipath correction of constant modulus signals," in *IEEE Trans. on Acoustics, Speech, and Signal Proc.*, vol. ASSP-31, pp. 459–472, 1983.

[19] J. R. Treichler and M. G. Larimore, "Convergence rates for the constant modulus algorithm with sinusoidal inputs," in *Proc. of ICASSP*, pp. 1157–1160, March 1985.

[20] J. R. Treichler and M. G. Larimore, "The tone capture properties of CMA-based interference suppressors," in *IEEE Trans. on Acoustics, Speech, and Signal Proc.*, vol. ASSP-33, pp. 946–9580, August 1985.

[21] M. G. Larimore and J. R. Treichler, "The capture properties of cma-based interference cancellers," in *Proc. Asilomar Conf. Signals, Syst., Comput.*, pp. 49–52, 1984.

[22] M. G. Larimore and J. R. Treichler, "Noise capture properties of the constant-modulus algorithm," in *Proc. of ICASSP*, pp. 1165–1168, March 1985.

[23] B. G. Agee, "The least-squares CMA: A new technique for rapid correction of constant modulus signals," in *Proc. of ICASSP*, pp. 953–956, April 1986.

[24] J. E. R. Ferrera, "A method for cancelling interference from a constant envelope signal," in *IEEE Trans. on ASSP.*, vol. ASSP-33, pp. 316–319, Feb. 1985.

[25] K. D. Kammeyer et al., "A modified adaptive FIR equalizer for multipath echo-cancellation in FM transmission," in *IEEE Trans. J. Selected Areas of Comm.*, vol. SAC-5, pp. 236–237, Feb. 1987.

[26] C. K. Chan and J. J. Shynk, "Stationary points of the constant modulus algorithm for real Gaussian signals," in *IEEE Trans. ASSP.*, vol. ASSP-38, pp. 2176–2181, Dec. 1990.

[27] N. J. Bershad and S. Roy, "Performance of the 2-2 constant modulus adaptive algorithm for rayleigh fading sinusoids in gaussian noise," in *Proc. of ICASSP*, pp. 1675–1678, April 1990.

[28] T. Ohgane, "Characteristics of CMA adaptive array for selective fading compensation in digital land mobile radio communications," in *Electronics and Communications in Japan*, vol. 74, 1991. Part 1, No. 9.

[29] T. Ohgane et. al., "An implementation of a CMA adaptive array for high speed GMSK transmission in mobile communications," in *IEEE Trans. on Veh. Tech.*, vol. 42, August 1993. No. 3.

[30] O. W. Kwon et. al., "Performance of constant modulus adaptive digital filters for interference cancellers," in *Signal Processing*, vol. 26, Feb. 1992. No. 2.

[31] J. K. Tugnait and R. Swaminathan, "On improving the convergence of CMA adaptive filters," in *Proc. of ICASSP*, pp. 340–343, 1993.

[32] N. Kikuma et al., "Performance of CMA adaptive array optimized by the marquardt method for suppressing multipath waves," in *Electronics and Communications in Japan*, vol. 75, March 1992. Part -1.

[33] B. G. Agee, "Convergent behavior of modulus restoring adaptive arrays in gaussian interference environments," in *Proc. of the 22nd Asilomar Conf. on Signals, Systems and Computers*, Nov. 1988.

[34] B. Agee, K. Cohen, J. Reed, and T. Hsia, "Simulation performance of a blind adaptive array for realistic channels," in *Proc. IEEE Veh. Tech. Conf.*, vol. 1, pp. 97–100, 1993.

[35] S. Mayrargue, "Spatial equalization of a radio-mobile channel without beamforming using the constant-modulus algorithm," in *Proc. of ICASSP*, pp. 344–347, 1993.

[36] S. Talwar, M. Viberg, and A. Paulraj, "Blind estimation of multiple cochannel digital signals usign antenna arrays," in *IEEE Signal Proc. Letters*, vol. 1, No. 2, pp. 29–31, Feb. 1994.

[37] I. Parra, "Improved constant modulus algorithm for smart anrenna systems," in *Masters Thesis, University of Texas, Austin*, May 1995.

[38] A. Van der Veen and A. Paulraj, "An analytical constant modulus algorithm," in *IEEE Trans. on Sig. Proc.*, vol. 44, No. 5, May 1996.

[39] Y. Li and K. J. R. Liu, "Blind adaptive spatial-temporal equalization algorithms using antenna arrays," in *IEEE Comm. Letters*, vol. 1, No. 1, pp. 25–27, Jan. 1997.

[40] W. A. Gardner, "The spectral correlation theory of cyclostationary time-series," in *Signal Processing*, vol. 11, July 1986. No. 1.

[41] W. A. Gardner, "Exploitation of spectral redundancy in cyclostationary signals," in *IEEE Signal Processing Magazine*, vol. 11, April 1991.

[42] W. A. Gardner, S. V. Schell, and P. A. Murphy, "Multiplication of cellular radio capacity by blind adaptive spatial filtering," in *Proc. IEEE Int'l. Conf. on Selected Topics in Wireless Comm*, pp. 102–106, June 1992.

[43] S. V. Schell and W. A. Gardner, "Maximum likelihood and common factor analysis-based blind adaptive spatial filtering for cyclostationary signals," in *Proc. of ICASSP*, pp. 292–295, 1993.

[44] Luis Castedo et al., "A new cost function for adaptive beamforming using cyclostationary signal properties," in *Proc. of ICASSP*, pp. 284–287, 1993.

[45] S. Shamsunder, "Exploiting cyclostationarity for range and bearing estimation," in *Proc. of ICASSP*, pp. 280–283, 1993.

[46] S. V. Schell, "Blind adaptive spatiotemporal filtering for wide-band cyclostationary signals," in *IEEE Trans. on Signal Processing*, vol. 41, May 1993. No. 5.

[47] S. V. Schell and B. G. Agee, "Application of the score algorithm and score extension to sorting to the rank-L spectral self-coherence environment," in *Proc. of 22nd Asilomar Conf. on Signals, Systems, and Computers*, pp. 274–278, Nov. 1988.

[48] B. G. Agee and D. L. Young, "Blind capture and geolocation of general spatially self-coherent waveforms using multiplatform SCORE," in *Proc. 24th Asilomar Conf. on Signals, Systems, and Computers*, pp. 33–38, Nov. 1990.

[49] R. P. Gooch and B. J. Sublett, "Joint spatial and temporal equalization in a decision-directed adaptive antenna system," in *Proc. 22nd Asilomar Conf. on Signals, Systems, and Computers*, pp. 255–259, Nov. 1988.

[50] G. Picchi and G. Prati, "Blind equalization and carrier recovery using a "Stop-and-Go" decision directed algorithm," in *IEEE Trans. on Comm.*, vol. com-35, Sept. 1987.

[51] R. C. V. Macario, *Cellular radio principles and design.* McGraw-Hill, Inc., 1 ed., 1993.

[52] F. A. Cassara, H. Schachter, and G. H. Simowitz, "Acquisition behavior of the cross-coupled phase-locked FM demodulator," in *IEEE Trans. Comm.*, vol. COM-32, pp. 195–199, Feb. 1984.

[53] Z. D. Stojanovic, M. L. Dukic, and I. S. Stojanovic, "A new demodulation method improving FM system interference immunity," in *IEEE Trans. Comm.*, vol. COM-29, no. 7, pp. 1001–1010, July 1984.

[54] Y. Bar-Ness and H. Bunin, "Cochannel interference cancellation and signal separation method," in *Proc. IEEE Int. Conf. Comm.*, June 1988, Philadelphia, PA.

[55] H. W. Hawkes, "Study of adjacent and co-channel FM interference reduction," in *IEE Proceedings-I*, vol. 138, no. 4, pp. 319–326, Aug. 1991.

[56] D. A. Rich, S. Bo, and F. A. Cassara, "Cochannel FM interference suppression using adaptive notch filters," in *IEEE Trans. Comm.*, vol. COM-42, no. 2, pp. 2384–2389, July 1994.

[57] R. He and J. H. Reed, "Spectral correlation of AMPS signals and its application to interference rejection," in *Proc. MILCOM Conf.*, vol. 3, pp. 1007 – 1011, Oct. 1994.

[58] L. Castedo and A. R. Figueiras-Vidal, "An adaptive beamforming technique based on cyclostationary signal properties," in *IEEE Trans. on Signal Processing*, vol. 43, no. 7, pp. 1637–1650, July 1995.

[59] R. H. Clarke, "A statistical theory of mobile-radio reception," in *Bell Syst. Tech. J.*, vol. 47, No. 6, pp. 957–1000, July-Aug 1968.

[60] R. Muammar and S. C. Gupta, "Cochannel interference in high-capacity mobile radio systems," in *IEEE Trans. Comm.*, vol. COM-30, pp. 1973–1978, Aug. 1982.

[61] Y. S. Yeh and S. C. Schwartz, "Outage probability in mobile telephony due to mulitple lognormal interferers," in *IEEE Trans. Comm.*, vol. COM-32, pp. 380–387, April 1984.

[62] K. W. Sowerby and A. G. Williamson, "Outage probability calculation for multiple cochannel interferers in cellular mobile radio," in *IEE Proc.*, vol. 135(3), pp. 208–215, June 1988. Part F.

[63] S. Heeralall and C. J. Hughes, "High capacity cellular patterns land mobile radio systems using directional antennas," in *IEE Proc.*, vol. 136(1), Feb. 1989. Part 1.

[64] T. S. Rappaport, *Wireless communications: Principles and Practice.* Prentice Hall, 1 ed., 1995.

[65] T. Aulin, "A modified model for the fading signal at a mobile radio channel," in *IEEE Trans. Veh. Tech.*, vol. 28, No. 3, pp. 182–203, 1979.

[66] J. C. Liberti and T. S. Rappaport, "A geometrically based model for line-of-sight multipath radio channels," in *Proc. of IEEE Veh. Tech. Conf.*, pp. 844–848, April 1996.

[67] W. C. Jakes, *Microwave Mobile Communication.* New York: Wiley, 1974.

[68] Telecommunications Industry Association, *TIA/EIA Interim standard, mobile station - base station compatiblity standard for dual-mode wideband spread spectrum cellular system, TIA/EIA/IS-95.* Telecommunications Industry Association, Washington, D.C., July 1993.

[69] A. J. Viterbi, "Very low rate convolutional codes for maximum theretical performance of spread spectrum multiple access channels," in *IEEE Journal on Selected Areas of Comm.*, pp. 641–649, May 1990.

[70] M. K. Varnasi and B. Aazhang, "Multistage detection in asynchronous code-division multiple access systems," in *IEEE Trans. on Comm.*, vol. 38, pp. 509–519, April 1990.

[71] D. Divsalar and M. K. Simon, "Improved CDMA performance using parallel interference cancellation," in *JPL Publication 95-21*, Oct 1995. Pasadena, CA.

[72] A. Kaul and B. D. Woerner, "Analysis of multistage inteference cancellation for CDMA," in *submitted to IEEE Trans. on Comm.*, vol. 41, Dec. 1994.

[73] M. L. Honig, U. Madhow, and S. Verdu, "Blind adaptative multiuser detection," in *IEEE Trans. on Inf. Theory*, vol. 41, pp. 944–960, July 1995.

[74] S. Vembu and A. J. Viterbi, "Two different philosophies in CDMA - a comparison," in *Proc. of IEEE Veh. Tech. Conf.*, pp. 869–873, April 1996.

[75] R. M. Buehrer, "The application of multiuser detection to cellular CDMA," in *Dissertation, Virginia Tech.*, July 1996.

[76] R. Cameron and B. Woerner, "An analysis of CDMA with imperfect power control," in *Proc. of Veh. Tech. Conf.*, pp. 977–980, May 1992.

[77] Analog Devices, Data Converter Reference Manual vol. 2, 1992.

[78] **SPW - The DSP Framework,** Comdisco Systems, Inc., version 3.1, March 94.

[79] Hypersignal for windows by Hyperception, Inc.

[80] Stanford Telecom, The DDS Databook 1994.

[81] J. Mitola, "The software radio architecture," in *IEEE Communications Magazine*, vol. 33, 95.

[82] J. A. Wepman, "Analog to digital converters and their application in radio receivers," in *IEEE Communications Magazine*, pp. 39–45, May 1995.

[83] B. Brannon, "Wideband radios need wide dynamic range converters," in *Analog Dialogue*, vol. 29, pp. 11–12, 1995.

[84] Comlinear CL949 Data Manual 1994.

[85] Harris Semiconsuctor, Digital Signal Processing Databook 1994.

[86] Analog Devices, ADSP21020 Users' Manual 1994.

[87] Analog Devices, ADSP21062 Users' Manual 1994.

[88] K. S. Gilhousen et al. , "On the capacity of a cellular CDMA systems," in *IEEE Trans. on Veh. Tech.*, vol. 40, no.1, pp. 303–312, May 1991.

[89] L. Milstein and P. Das, "An analysis of a real-time transform domain filtering digital communications system–Part I: Narrow-band interference rejection," in *IEEE Trans. on Comm.*, vol. COM-30, No. 6, June 1980.

[90] K. I. Kim, "CDMA cellular engineering issues," in *IEEE Trans. on Veh. Tech.*, vol. 42, No. 3, pp. 345–350, Aug. 1993.

[91] H. H. Hmimy and S. C. Gupta, "Overlay of cellular CDMA on AMPS forward and reverse link analysis," in *IEEE Trans. on Veh. Tech.*, vol. 45, No. 1, pp. 51–56, Feb. 1996.

[92] J. H. Winters, "Signal acquisition and tracking with adaptive arrays in the digital mobile radio system IS-54 with flat fading," in *IEEE Trans. Veh. Tech.*, vol. VT-42, Nov. 1993.

[93] J. C. Liberti and T. S. Rappaport, "Analytical results for capacity improvements in CDMA," in *IEEE Trans. on Veh. Tech.*, vol. 43, no. 3, pp. 680–690, 1994.

[94] J. Litva and T. K.-Y. Lo, *Digital beamforming in wireless communications.* Artech House Publishers, Mobile Communication Series, 1 ed., 1996.

[95] G. Xu and H. Lui, "An effective transmission beamforming scheme for frequency division duplex digital wireless communications systems," in *Proc. of ICASSP*, pp. 1729–1732, 1995.

[96] D. Gerlach and A. Paulraj, "Base station transmitting antenna arrays with mobile to base feedback," in *Proc. of IEEE Asilomar Conf.*, pp. 1432–1436, Nov. 1993.

[97] C. Farsakh and J. A. Nossek, "Channel allocation and downlink beamforming in an SDMA mobile radio systems," in *Proc. of Sixth IEEE Intl. Symposium on PIMRC*, pp. 687–691, Sept. 1995.

[98] S. V. Schell, W. A. Gardner, and P. A. Murphy, "Blind adaptive antenna arrays in cellular communications for increased capacity," in *Third Virginia Tech Symposium on Wireless Personal Communications*, pp. 6.1–6.12, June 1993.

[99] R. L. Pickholtz, L. B. Milstein, and D. L. Schilling, "Spread spectrum for mobile communications," in *IEEE Trans. on Veh. Tech.*, vol. 40, No. 2, May 1991.

[100] A. J. Viterbi, "The orthogonal-random waveform dichotomy for digital mobile personal communications," in *IEEE Pers. Comm.*, pp. 18–24, 1st qtr 1994.

[101] W. C. Y. Lee, "Overview of cellular CDMA," in *IEEE Trans. on Veh. Tech.*, vol. 40, no. 2, pp. 291–302, May 1991.

[102] P. T. Brady, "A statistical analysis of on-off patterns in 16 conversations," in *Bell Syst. Tech. Journal*, vol. 47, pp. 73–91, 1968.

[103] C. M. Simmonds and M. A. Beach, "Network planning aspects of DS-CDMA with particular emphasis on soft handoff," in *Proc. of 43rd Veh. Tech. Conf.*, pp. 846–849, 1993.

[104] S. W. Wang and I. Wang, "Effects of soft handoff, frequency reuse and non-ideal antenna sectorization on CDMA system capacity," in *Proc. of 43rd Veh. Tech. Conf.*, pp. 850–854, 1993.

[105] S. U. Pillai and B. H. Kwon, "Forward/backward spatial smoothing techniques for coherent signal identification," in *IEEE Trans. Acoustics, Speech and Signal Processing*, vol. ASSP-37, pp. 8–15, Jan. 1989.

[106] R. O. Schmidt, "A signal subspace approach to multipath emitter location and spectral estimation," in *Ph. D. Thesis*, Nov. 1981. Stanford University, Stanford, CA.

[107] A. Paulraj, R. Roy, and T. Kailath, "A subspace rotation approach to signal parameter estimation," in *Proc. IEEE*, vol. 74(7), pp. 1044–1045, July 1986.

Vita

Paul Petrus was born in Pondicherry, India, on August 6, 1970. He received his B. Tech. degree from the Pondicherry University in 1991. He was awarded the Gold medal by the Pondicherry University for the best outgoing student for the class of '91. He received the M.S. degree from Virginia Polytechnic Institute and State University, Blacksburg, in 1994. From Fall of '94, he has been pursuing the Ph.D. degree at Virginia Tech. He is a Graduate research assistant working with the Mobile and Portable Radio Research Group (MPRG). In the summer of 1995, he worked with AT&T Bell Laboratories, where he was involved in the performance comparison of noncoherent detection schemes for IS-136 systems. His research interests are statistical signal processing, robust filtering, noncoherent detection techniques and array signal processing for mobile communications.

His research at Bell labs has resulted in two pending patents and a Journal paper has been submitted on this topic. His research at MPRG has resulted in 3 published/accepted Journal papers, 7 published Conference papers, and 7 Journal papers currently under review.